Small regulatory RNAs promoting the oxidative stress response and adaptive metabolic changes in *Rhodobacter sphaeroides*

Inauguraldissertation zur Erlangung des

Doktorgrades der Naturwissenschaften

- Dr. rer. nat. -

vorgelegt von

M.Sc.-Biol. Katrin Monika Hedwig Müller

aus Friedberg (Hessen)

angefertigt am Institut für Mikrobiologie und Molekularbiologie

Fachbereich Biologie und Chemie Justus-Liebig-Universität Gießen

Die vorliegende Arbeit wurde am Institut für Mikrobiologie und Molekularbiologie des Fachbereiches 08 der Justus-Liebig-Universität Gießen in der Zeit von November 2012 bis Novemeber 2016 unter der Leitung von Prof. Dr. Gabriele Klug angefertigt.

1. Gutachterin: Prof. Dr. Gabriele Klug

Institut für Mikro- and Molekularbiologie,
Justus-Liebig-Universität, Gießen

2. Gutachter: Prof. Dr. Roland K. Hartmann

Institut für Pharmazeutische Chemie,
Philipps Universität, Marburg

Erklärung

Ich habe die vorgelegte Dissertation selbständig und ohne unerlaubte fremde Hilfe und nur mit den Hilfen angefertigt, die ich in der Dissertation angegeben habe.

Alle Textstellen, die wörtlich oder sinngemäß aus veröffentlichten Schriften entnommen sind, und alle Angaben die auf mündlichen Auskünften beruhen, sind als solche kenntlich gemacht. Ich stimme einer eventuellen Überprüfung meiner Dissertation durch eine Antiplagiat-Software zu. Bei den von mir durchgeführten und in der Dissertation erwähnten Untersuchungen habe ich die Grundsätze guter wissenschaftlicher Praxis, wie sie in der „Satzung der Justus-Liebig-Universität Gießen zur Sicherung guter wissenschaftlicher Praxis“ niedergelegt sind, eingehalten.

Gießen, den 9. November 2016

Katrin Müller

Table of Contents

Particular abbreviations

ad	fill up to
APS	Ammonium persulphate
BChl	Bacteriochlorphyll
bp	base pair
BSA	Bovine serum albumin
Ci	Curie
ddH_2O	double-distilled water
DEPC	Diethylpyrocarbonate
DTT	Dithiothreitol
EDTA	Ethylenediaminetetraacetic acid
et al.	and others (*et altera*)
[Fe-S]	iron-sulphur
GSH	Glutathione
IGR	Intergenic region
IPTG	Isopropyl β-D-1-thiogalactopyranoside
kb	kilobase
kDa	kilodalton
λ	wavelength
LHC	light harvesting complex
MU	Miller Unit
MOPS	3-(N-morpholino) propanesulfonic acid
nt	nucleotide
NADH	Nicotinamide adenine dinucleotide
NADPH	Nicotinamide adenine dinucleotide phosphate
OD	optical density
ONPG	ortho-Nitrophenyl-β-galactoside
PAA	Polyacrylamide
PAGE	Polyacrylamide gel electrophoresis
PBS	Phosphate buffered saline
PMSF	Phenylmethanesulphonyl fluoride
RÄ	Rhodobacter Äpfelsäure (malate medium)
RC	Reaction centre
ROS	reactive oxygen species
RT	room temperature
SDS	Sodium dodecyl sulphate
TAE	Tris actetae EDTA
TBE	Tris borate EDTA
TB	Tris borate
TBS	Tris buffered saline
TEMED	Tetramethylethylenediamine
wt	wild-type

1. Introduction

In all habitats, organisms need strategies to sense and respond to their environment and adapt to it. Especially microorganisms, which are not able to change their habitat quickly and exhibit a large surface-to-volume ratio, need sophisticated ways to respond to changes in their surrounding. Changes can be biotic factors, such as competition for nutrients, commensalism, and parasitism, or abiotic factors. Regarding the latter availability of oxygen and light but also oxidative stress, pH, and temperature can strongly influence the quality of a habitat. Microorganisms have evolved various mechanisms to sense these properties of their environment, to respond to these changes (signalling) and to change their gene expression accordingly (regulation).

The signalling is achieved by different signal transduction systems. They can consist of multifunctional receptor molecules that include both sensor domains specifically recognising external signals and effector domains converting these signals into adequate cell response (Shpakov and Pertseva, 2008). The receptors sensing environmental stimuli can be roughly divided into extracellular and intracellular receptors. Extracellular, also called membrane receptors, can bind signalling molecules outside the cell while intracellular receptors typically bind signalling molecules that are able to pass through the membrane, such as gases. The signal transduction is generally composed of three different steps: binding of the signal molecule with the sensor domain, resulting in a conformational change of the effector domain, which triggers intracellular signalling cascades. Dimerization or oligomerization is one of the main conformational changes known for the effector domains.

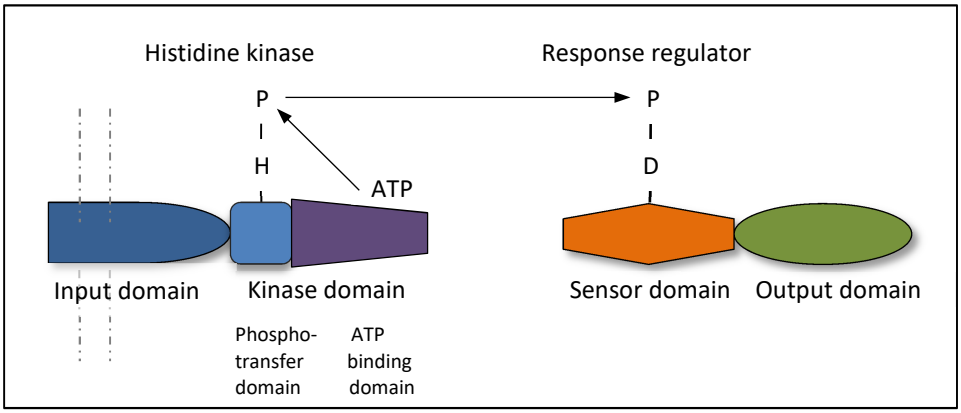

Figure 1: Scheme of a two component system. A two-component signal transduction system typically consists of a histidine kinase and a response regulator. Signal sensing by the input domain (dark blue) causes activation of the autokinase domain (light blue and purple), which results in phosphorylation of a specific histidine residue (H) in the phosphotransfer subdomain of the autokinase. The phosphoryl group is transferred to an aspartate residue (D) in the sensor domain (orange) of the cognate response regulator protein, which results in modulation of the function of the linked output domain (green) and thereby further signal transduction. Since many histidine kinases contain a transmembrane domain coupled to the autokinase domain, a membrane is implied by the dotted grey line. Adapted from Jensen *et al*., 2002.

Besides these typical receptor proteins, two component systems frequently act as signalling factors in prokaryotes. The first player of a two-component system (Fig. 1) is usually a histidine kinase, which can be membrane bound or soluble. The histidine kinase harbours at least two domains: a quite variable input domain and a cytoplasmic transmitter, the kinase domain (Parkinson and Kofoid, 1992). The former displays the sensor part detecting environmental stimuli either directly or indirectly, the latter by interaction with an upstream receptor. The signal is transduced to the second player, the response regulator via phosphorylation. The response regulator receiver domain (N-terminus) catalyses the transfer of the phosphoryl group from the histidine of the sensor kinase to one of its conserved aspartate residues. Upon phosphorylation, the receiver changes the activity of its C-terminal output domain, which starts a further downstream signal cascade or acts a transcriptional regulator, adapting the cell response to the sensed stimuli (reviewed in Appleby *et al*., 1996).

The regulation entailed by the signalling takes place on various levels. On the transcriptional level, genes can be regulated by transcription factors and alternative sigma factors. Especially the latter can be seen as eminent for regulated expression in response to changing environmental conditions. As variable subunits of the RNA polymerase (RNAP), alternative sigma factors allow binding and transcription from explicit promoter motifs. For instance, the alternative sigma factor sigma E (σ^E) from the class of ExtraCytoplasmic Function (ECF) sigma factors is known to activate various genes in the stress response of different organisms, such as the photo-oxidative stress response in *R. sphaeroides* and envelope stress in *E. coli* (reviewed in Paget, 2015). Commonly alternative sigma factors are sequestered by anti-sigma factors and some activation mechanisms (release from anti-sigma factors) also involve direct sensing of signal molecules (signalling). In the σ^R-RsrA system of *Streptomyces coelicolor,* RsrA forms an intramolecular disulphide bond between two cysteines in response to oxidative stress, stabilising a RsrA form unable to bind and thereby releasing σ^R (Li *et al.,* 2003). Also, signalling receptors themselves can directly influence the gene expression by binding to the DNA and repressing or inducing the transcription. A well-known member of this receptor protein type is LuxR from *Vibrio fisheri*, an autoinducer-binding transcriptional regulator involved in quorum sensing (Dunlap, 1999). The gene expression and subsequent protein synthesis can also be regulated post-transcriptionally on the mRNA level. The susceptibility to RNases, accessibility for the ribosome and stability of an mRNA can be influenced through protein binding (Van Assche *et al*., 2015), RNA structure (Condon, 2007) (1.1) or small regulatory RNAs (sRNAs; 1.1.) (Desnoyers *et al*., 2013). A remarkable example of posttranscriptional regulation is displayed by the sRNA RybB from *Salmonella*. RybB inhibits the synthesis of outer membrane proteins, such as *ompN*, during envelope stress by pairing with the mRNAs 5' coding region (Papenfort *et al*., 2006). Moreover, so-called riboswitches (1.1.3) as part of an mRNA can directly affect the translation rate (Waters and Storz,

2009) and moreover, translation can be affected positively or negatively at the ribosome itself (Deana and Belasco, 2005).

The exact and fast regulation of gene expression is especially important to adjust the energy metabolism to changing environmental conditions and resources, and to protect the cells against toxic conditions by inducing stress responses. One can imagine that the more changes can impact an organism, the more versatile adaption mechanisms will evolve. This idea is supported by findings that microorganisms living in relatively constant habitats show genomes encoding only a few transcriptional regulators and are largely devoid of two-component histidine kinases. Examples can be found in the phylum Chlorobi, living in the anaerobic zones of lakes, having little need to respond to their environment which changes only slightly (Frigaard *et al*., 2003).

The following chapters will, amongst others, discuss oxygen and light as environmental signals and source for cell damage, as well as the cellular signalling and regulation entailed by them.

1.1 RNA regulators

1.1.1 Small RNAs

As mentioned above, various RNA molecules and structures can affect the gene expression. One quite heterogeneous group of investigated regulators in bacterial gene expression, which is growing since its discovery in 1981 (Stougaard *et al*.), consists of sRNAs. They are known to be involved in manifold cellular processes such as virulence, stress response, and regulation of metabolic pathways by either repression or stimulation of gene expression. Since the synthesis of an RNA is faster than that of a protein, sRNAs could display an opportunity for more rapid and possibly more direct regulation in contrast to regulatory proteins (Shimoni *et al*., 2007). Overall, sRNAs can be classified as cis- and trans-encoded sRNAs (Fig. 2 and 3) known to interact with one or multiple RNA targets (base pairing sRNAs) or proteins.

As the classification implies, the cis-encoded sRNA type is located antisense to its target gene and thereby exhibits a region of complete complementarity to its target mRNA (Fig. 2). In contrast to that, trans-encoded sRNAs can be encoded somewhere, also distant, from their target(s) in the genome and do not interact by perfect base pairing (Fig. 3). Many of the so far described antisense sRNAs (asRNAs) reside on plasmids or other mobile genetic elements, even though the number of genome-encoded asRNAs is increasing. The asRNAs are for example known for being able to maintain the copy number of their origin plasmid or bacteriophage (reviewed in Brantl, 2007). Furthermore, they can often be associated with toxin-antitoxin systems, such as the asRNA SR5 that displays the antitoxin of the RNA-toxin BsrE in *B. subtilis* (Müller, P. *et al*., 2016). More antitoxin sRNAs, namely

IstR1 and OhsC, can be found in *E. coli* which, although not being true asRNAs, are at least located adjacent to the corresponding toxin gene (Wagner and Unsons, 2012; Fozo, 2012). In other known cases, asRNAs are encoded complementary to coding or intergenic regions (IGRs) of an operon. Thus an sRNA-mRNA pairing can lead to intra-operon transcription termination or mRNA cleavage (Fig. 2). As an example, the sRNA IsrR (iron-stress repressed RNA) in *Synechocystis* binds within the coding region of *isiA* of the *isiAB* transcript, leading to reduced *isiA* transcript levels (Dühring *et al*., 2006). Not only the interaction of an asRNA with a target mRNA can result in gene regulation, but also the transcription of an asRNA harbours a regulatory potential (Fig. 2). This becomes obvious in the S1136 asRNA case from *B. subtilis*, where the expression from the S1136 promoter upon ethanol stress leads to reduced transcription of the *rpsD* gene on the opposite strand (Mars *et al*., 2015).

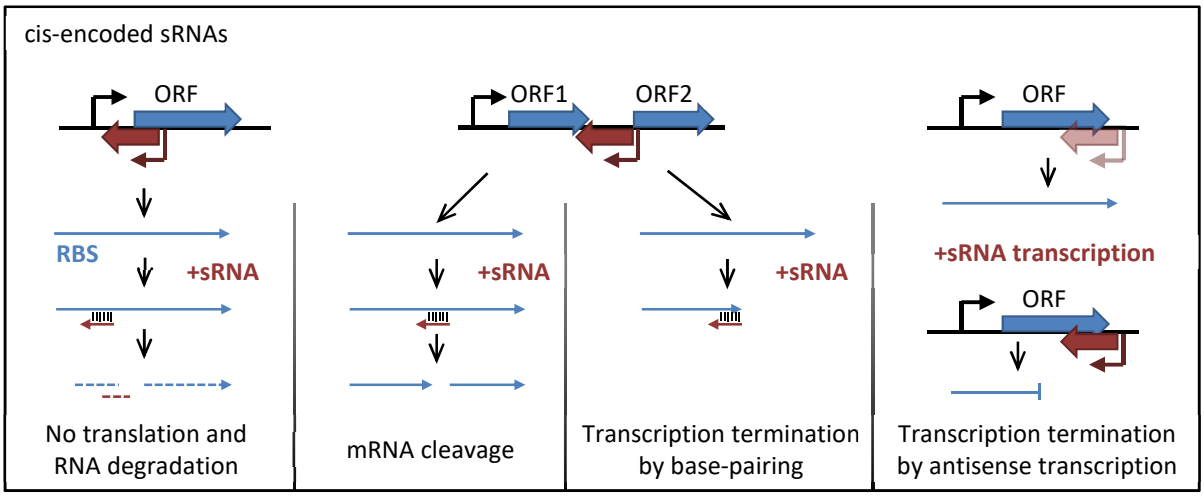

Figure 2: Possible gene arrangments of cis-encoded RNAs (red; asRNAs) and their mRNA targets (blue). An asRNA encoded opposite of the 5' UTR of its target mRNA (left) inhibits ribosome binding by base-pairing. An asRNA encoded antisense to an intergenic region in an operon (middle two) can cause mRNA cleavage or transcription inhibition by base-pairing. When the asRNA is encoded antisense to the 3'UTR or coding region (ORF) of its target (right) the transcription from the antisense promoter (red) can block the transcription from the target promoter (black). Less active promoter indicated in pale red. Modified from Waters and Storz, 2009.

Trans-encoded sRNAs can be found in IGRs, expressed from an own promoter, as well as in 5' and 3' UTRs of protein coding genes (Tsai *et al*., 2015; Kawano *et al*., 2005). Regarding sRNAs derived from UTRs, those from 3' UTRs seem to be more abundant (Kawano *et al*., 2005). They can be distinguished into two major types: those which are expressed independently of the overlapping mRNA from a promoter inside the mRNA coding sequence (Type I) and those originating from processing of the paternal mRNA (Type II) (Miyakoshi *et al*., 2015). As already mentioned, the genomic localisation of a trans-encoded sRNA and its mRNA target does not necessarily correlate with each other, and trans-encoded sRNAs typically show interaction with multiple mRNA targets (Papenfort and Vogel, 2009; Gottesman, 2005). The base-pairing between an sRNA and its mRNA target can inherently lead to modulation of translation, mRNA stabilisation or mRNA degradation

(reviewed in Lalaouna *et al*., 2013) (Fig. 3). Examples for translational modulation can be found in both directions: positively and negatively. An example of the former is RNAIII from *Staphylococcus aureus,* which can resolve a secondary structure in the 5'-leader of the *hla* mRNA which otherwise occludes the RBS (Toledo-Arana *et al*., 2007). A well-studied sRNA known to negatively affect the translation of its mRNA target is MicF from *E. coli*. MicF forms a ~20 bp imperfect RNA duplex with the translation-initiation region of the *ompF* mRNA and thereby negatively regulates its expression at the post-transcriptional level (Schmidt *et al*., 1995). Also, the stability of an mRNA can be affected positively or negatively by sRNA binding. An mRNA susceptible towards a ssRNA specific RNase can be protected by sRNA binding, while the formation of an mRNA-sRNA duplex can allow degradation via a dsRNA-specific RNase (Fig. 3). RatA (RNA antitoxin A), an untranslated sRNA from *B. subtilis*, was indicated to bind the *txpA* mRNA via overlapping 3' UTRs leading to degradation of the RNA duplex and thereby avoiding the formation of the TxpA toxin (Silvaggi *et al.,* 2005). Then again sRNAs are known to stabilise an mRNA target, such as GadY in *E. coli* that is suggested to stabilise the *gadX* mRNA encoding a transcriptional activator of the acid response system by interaction with the mRNAs 3' UTR (Opdyke *et al*., 2004). Overall most known trans-encoded sRNAs negatively affect the expression of their target (Gottesman, 2005).

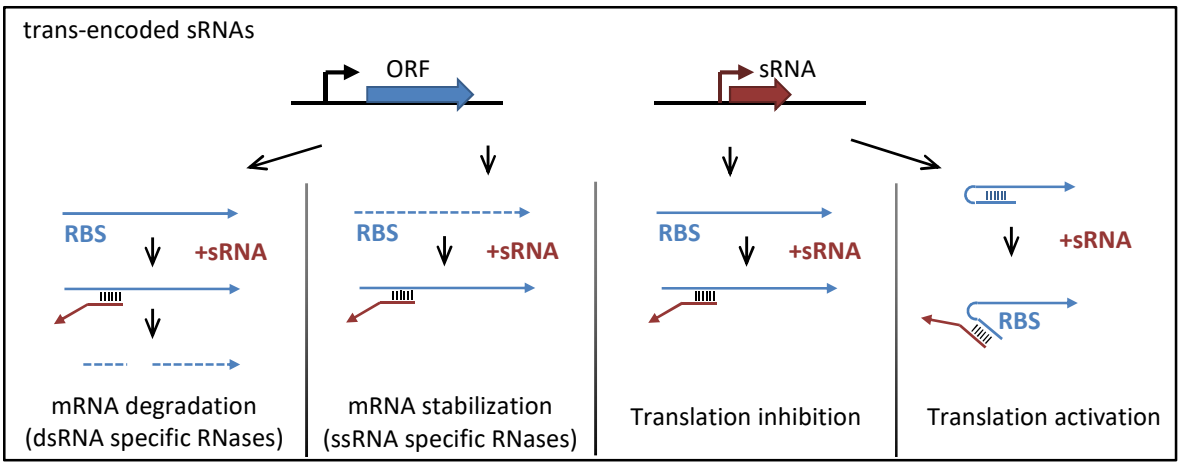

Figure 3: Regulatory functions of trans-encoded sRNAs. Base-pairing of a trans-encoded sRNA (red) with its mRNA target (blue) can lead to enhanced degradation or stability of the mRNA (two left). As well was inhibition or enabling of translation (two right). Modified from Waters and Storz, 2009.

Many of the studied bacterial sRNAs were shown to be dependent on the chaperon Hfq (host factor of bacteriophage Qß in *E. coli*) (Franze de Fernandez *et al*., 1986) for the binding of their mRNA targets (Vogel and Luisi, 2011). The phylogenetically widespread Hfq is found in many bacterial as well as in some archaeal taxa, but all so far sequenced ε-proteobacteria and microorganisms showing an intracellular lifestyle (e.g. *Rickettsia* and *Chlamydia*) lack Hfq (Sobrero and Valverde, 2012). Hfq belongs to the family of RNA-binding proteins and shows homology to Sm and Sm-like (LSm) proteins found throughout all three domains of life. These proteins are known to assemble into ring-shaped

complexes, facilitating a variety of RNA-RNA and RNA-protein interactions (Wilusz and Wilusz, 2005). In prokaryotes, the binding of the homohexameric apo-Hfq, which seems to be a quiet heterogeneous process (Sobero and Valverde, 2012), can stabilise an sRNA and promote its interaction with an mRNA target and thereby subsequently alters the stability or translation (reviewed in Vogel and Luisi, 2011). The binding of sRNAs to Hfq was identified to occur to all four exposed regions of the protein: the proximal and the distal face, the rim and the C-terminal tail (reviewed in Sobrero and Valverde, 2012). After it had become evident that the interplay of Hfq with different sRNAs can mediate gene regulation, the physiological role of Hfq was the subject of various studies in several model organisms. In the majority of the described cases an *hfq* deletion led to pleiotropic phenotypes, including increased stress sensitivity (Berghoff *et al*., 2011; Geng *et al*., 2009) and reduced virulence (Sousa *et al*., 2010; Fantappie *et al*., 2009), arguing for a global role of Hfq in bacterial physiology. Recent findings support the idea that Hfq acts on multiple steps in the sRNA-mRNA interaction: changing the structure of RNAs, bringing RNAs in proximity, neutralising the negative charge of the pairing RNAs, stimulating the nucleation of the first base pairs, and facilitating the further annealing of the two RNA strands (reviewed in Updegrove *et al*., 2016). Despite all this knowledge on Hfq, for a long time, it remained elusive how Hfq "finds" distinct RNAs in the cell to act in the short timeframes known for stress responses involving sRNAs. Over the last three years, more and more data was generated trying to answer this question. Three distinct states of Hfq with different diffusion rates were found by single-molecule monitoring: free unbound Hfq (fastest diffusion), Hfq bound to RNA, and/or other proteins (intermediate diffusion) and Hfq bound to RNA during transcription in the transcription complex (slowest diffusion) (Persson *et al*., 2013). Moreover, modelling studies indicated that the maximum sRNA-dependent regulation occurs at a specific Hfq concentration, which varies for each RNA pair and can be affected by competition for Hfq with other sRNAs, mRNA levels, and so-called sponge RNAs (unspecific binding to Hfq by e.g. unprocessed tRNA fragments) (Sagawa *et al*., 2015). Taken together, Hfq represents an effective and flexible RNA-chaperone involved in manifold sRNA-dependent processes, with binding surfaces and mechanisms varying profoundly between different organisms.

Interestingly, besides sRNAs acting as "classical" RNA regulators, some sRNAs are found which in addition to their regulatory function encode small functional peptides. So far the function of only a very few sRNA-encoded peptides has been elucidated. One of these so-called dual-function sRNAs is SgrS studied in *E. coli*. SgrS negatively affects the *ptsG* mRNA, encoding a major glucose transporter, via base-pairing. Translation of SgrS produces the SgrT protein, which additionally reinforces the negative effect of SgrS on the glucose uptake by direct or indirect inhibition of the PtsG transporter (Wadler and Vanderpool, 2007). A second example can be found in *Staphylococcus aureus*, where the RNAIII sRNA, acting as a central virulence factor by increasing the synthesis of secreted factors, encodes the δ-hemolysin. The later being characterised before the RNAIII base-pairing activity was

uncovered (reviewed in Vanderpool *et al*., 2011). A very recently described example of a dual-function sRNA can be found in *B. subtilis*. The peptide SR1P promotes binding of RNase J1 over RNase Y to the metabolic enzyme GapA and is encoded within the sRNA SR1 (Gimpel and Brantl, 2016). Taken together sRNAs can comprise additional sORFs encoding functional peptides and a riboregulatory function of so far appointed mRNAs can not be ruled out.

1.1.2 Protein-interacting sRNAs

Besides the sRNAs interacting with an mRNA as a target, some sRNA molecules are described to interact with and regulate the activity of proteins. Three well-characterised examples for protein-antagonising sRNAs are GlmY, CsrB, and the 6S RNA.

GlmY, known from *E. coli*, *Shigella flexneri*, *Yersinia pestis,* and *Salmonella* species, acts as an anti-adaptor sequestering RapZ (RNase adaptor protein for sRNA GlmZ). By sequestering RapZ GlmY preserves GlmZ from degradation by RNase E and in turn GlmZ can activate the translation of *glmS* encoding glucosamine-6-phosphate synthase (Göpel *et al*., 2014). Another example is the CsrB sRNA in *E. coli*, which is bound by the CsrA protein with a higher affinity than the untranslated leader regions of CsrA's regular target mRNAs. Thereby CsrB acts as antagonist of CsrA, limiting the mRNA binding and subsequent post-transcriptional regulation of CsrA (Vakulskas *et al*., 2016; Liu *et al*., 1997). The 6S RNA, also studied e.g. in *E.coli*, is present in a wide range of bacterial species and antagonises the housekeeping σ70-containing RNA polymerase while it mimics an open promoter structure (reviewed in Wassarman, 2007). The 6S RNA is especially abundant in stationary phase; nevertheless, it does not bind to the stationary phase σS form of the RNAP (Trotochaud and Wassarman, 2005) but leads to increased activation of certain stationary phase dependent promoters by weakening the competition between housekeeping and stationary phase RNAP. When bound to the RNAP, the 6S RNA acts as a template for short so-called product RNAs (pRNAs). The pRNAs can lead to a structural RNA-rearrangement upon reaching a certain length; this will release the RNAP which thus can recover to DNA promoters. In *B. subtilis* two 6S RNA paralogs, the 6S-1 RNA and the 6S-2 RNA are known. Regarding the 6S-2 RNA, it was only recently shown that it serves as pRNA template (Hoch *et al*., 2016). For both 6S RNAs, an overlapping function was predicted by phenotypic characterisation of deletion mutants of each gene (Hoch *et al*., 2015).

1.1.3 Riboswitches and ribozymes

In addition to sRNAs as trans-regulatory factors, an mRNA itself can harbour cis-regulatory elements. The so-called riboswitches can be located at the 5' and, less frequently, at the 3' UTR of an mRNA. They consist of a specific ligand-binding domain coupled to an expression platform; the latter undergoes structural changes upon binding of a ligand to the former. Known riboswitch ligands are small metabolites and ions such as metals, ATP, ci-d-GMP, amino acids, and S-adenosylmethionine

(SAM), but also physical factors such as temperature and pH are known to affect the riboswitch conformation. The structural change in a riboswitch can lead to transcriptional control when the newly formed structure serves as an intrinsic terminator or anti-terminator, while translational control occurs when the structural change exposes or masks an RBS (reviewed in Serganov and Nudler, 2013). Additionally, riboswitches were identified to promote or sequester binding of additional protein factors, such as the Rho termination factor (Hollands *et al*., 2012) or RNase E (Caron *et al*., 2012) respectively, regulating their parental mRNA. Ligand binding by riboswitches is typically found in mRNAs encoding functions in the biogenesis or transport of the same ligand, such as the cobalamin riboswitches in the upstream region of the *cob* (cobalamin biosynthesis) and *btuB* (outer membrane protein transporting cobalamin) genes (Nahvi *et al*., 2004). Moreover, it is known that riboswitches not only occur as single elements but also as tandem-riboswitches, either exhibiting the same or two different ligand specificities (reviewed in Serganov and Nudler, 2013). Besides acting in cis on their origin-mRNA, there is growing evidence that riboswitches can act in trans as sRNA. The SAM riboswitches SreA and SreB of *Listeria monocytogenes* pair with the 5' UTR and downregulate the expression of the PfrA mRNA, after the SAM-dependent transcription termination of their own mRNA (Loh *et al*., 2009). Another mechanism found to be coupled to riboswitches is the self-splicing or ribozyme activity. The already mentioned mRNA *glmS* (1.1.2), found in Gram-positive bacteria, is cleaved within the riboswitch sequence upon binding of glucosamine-6-phosphate (GlcN6P) and other related chemical compounds (Winkler *et al*., 2004). Ribozymes themselves display a functional group of regulatory RNA molecules whose catalytic activity is not yet fully understood. They are found in eukaryotes, prokaryotes, and viroids and their biological roles include self-cleavage during replication of RNA genomes, co-transcriptional processing, and metabolite-dependent gene regulation, as mentioned above (reviewed in Jimenez *et al*., 2015).

1.2 Oxygen – friend and foe

Oxygen (O_2) appeared in significant amounts in the Earth's atmosphere over 2.2 billion years ago. Since cyanobacteria evolved to use light energy from the sun to split water gaining reducing power, tonnes of the reactions' by-product O_2 pollutes the atmosphere (Lane, 2002). Nowadays O_2 is the third most abundant element on earth (Morgan and Anders, 1980). Except for some anaerobic and aerotolerant species, all organisms require O_2 for efficient production of energy by use of electron transport chains that ultimately donate electrons to O_2 (Halliwell and Gutteridge, 2006). With its high redox potential O_2 is an excellent electron acceptor in aerobic respiration and also in chemolithotrophic metabolic pathways. The sensing of O_2 availability can occur through manifold processes; most abundant is the sensing of the surrounding and intracellular redox potential via

redox sensor proteins (see 1.4 for details).

Molecular O_2, also called triplet oxygen, occurs in its inert ground state. In this ground state two unpaired electrons are present in separate molecular orbits (Fig. 4). An electron arrangement that makes molecular oxygen quite susceptible to radical formation. Since redox enzymes are notoriously nonspecific, they transfer electrons to any good acceptor with which they make electronic contact and molecular O_2 is small enough to penetrate all but the most shielded reaction sites (Imlay, 2003). So leakage of single electrons from redox reactions in the bacterial respiratory chain can lead to univalent reduction of molecular O_2. A potential reason for the electron leakage from the respiratory chain is that the respiratory dehydrogenase uses flavin cofactors to accept hydride anions from organic substrates. When these reduced flavins subsequently transfer the electrons one at a time onto secondary redox moieties, O_2 can collide with the reduced flavin before it passes the electrons to the next carrier and an electron can hop off the $NADH_2$ (Cabiscol *et al.*, 2000). The sequential reduction of O_2 through the addition of electrons leads to the formation of a number of reactive oxygen species (ROS) including superoxide ($O_2^{\bullet -}$), hydrogen peroxide (H_2O_2) and hydroxyl radical (•OH; Fig. 4) (Seaver and Imlay, 2004).

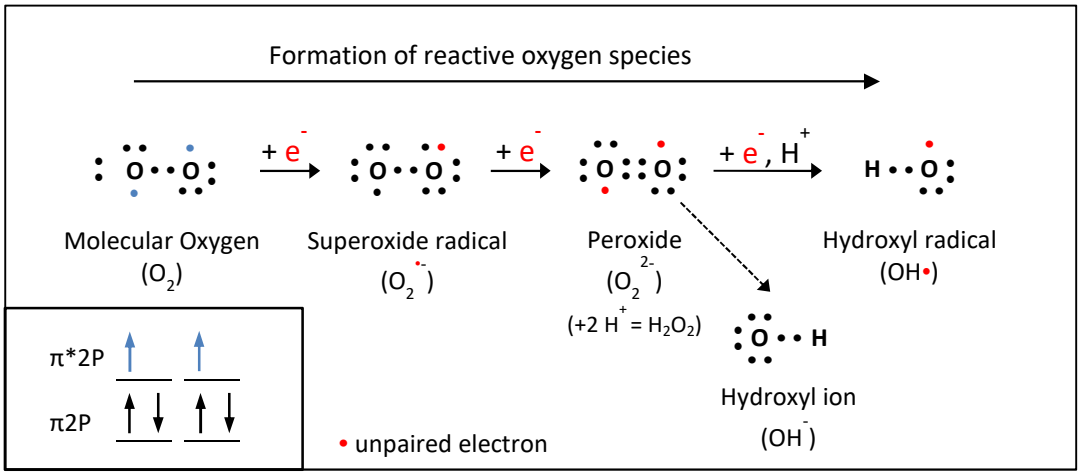

Figure 4: Formation of ROS by sequential reduction of O_2 trough the addition of electrons. In its inert ground state molecular O_2 appears with two unpaired electrons (blue) in its separate outer orbitals (lower left panel). The univalent reduction (addition of electrons: red) of O_2 leads to the formation of a number of ROS including superoxide (O_2•-), hydrogen peroxide (H_2O_2), hydroxyl radical (•OH) and hydroxyl ion (OH-).

The singlet oxygen ($^1O_2$) differs in its formation from the described ROS since it depends on energy rather than electron transfer. The $^1O_2$ generation in biological systems occurs by two different routes - photo-excitation reactions (light reactions) and chemiexcitation reactions (dark reactions) (reviewed in Devasagayam and Kamat, 2002). A major route for the former process is the type II photosensitisation which results in energy transfer to ground state molecular oxygen and thereby a spin conversion in the outer two molecular orbits (Fig. 5). In this type II reaction, the excited sensitiser transfers its excess energy to ground state molecular O_2, producing excited state $^1O_2$, and

regenerating the ground state sensitiser (Oleinick, 2011) (Fig. 5). Examples for known naturally occurring sensitisers are porphyrins, bilirubin, and bacteriochlorophyll (Roeder, 1990).

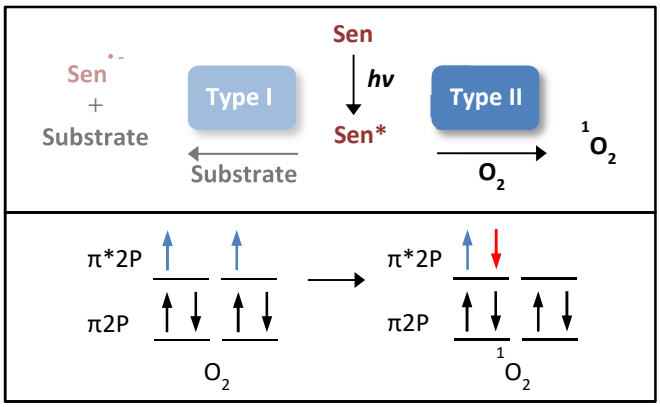

Figure 5: Photosensitisation reaction I and II. A photosensitiser is excited by absorption of light energy (hv). In the type I reaction (left) the excited sensitiser (Sen*) directly reacts with a substrate. In the Type II reaction (right), the excited sensitiser transfers its excess energy to ground-state molecular oxygen (O_2), producing excited state singlet oxygen ($^1O_2$), and regenerating the ground-state sensitiser. Adapted from Oleinick, 2011.

An additional source for ROS formation can be found in iron metabolism. While a basal iron level is essential for almost all living organisms (1.8), an excess of iron can trigger ROS formation in the Fenton reaction (Fenton, 1894). The Fenton reaction (Fig. 6) is driven by the inadvertent production of H_2O_2 and $O_2^{\bullet-}$ during aerobic respiration (Lemire *et al.*, 2013). Reduced iron (Fe^{2+}), present in the cell, can be oxidised by H_2O_2 to ferric iron (Fe^{3+}), producing a hydroxyl radical (•OH) and hydroxide ion (OH^-; Fig. 6). In the next step $O_2^{\bullet-}$ can reduce ferric iron (Fe^{3+}) to ferrous iron (Fe^{2+}) and water. In addition, the H_2O_2 and $O_2^{\bullet-}$ can interact to generate •OH in the Haber Weiss reaction (Kehrer, 2000) (Fig. 6). In this fashion, the reaction can occur over and over again. The Fenton chemistry is not limited to iron but can be provoked by other metal ions such as copper and nickel as well (Lloyd and Philips, 1999).

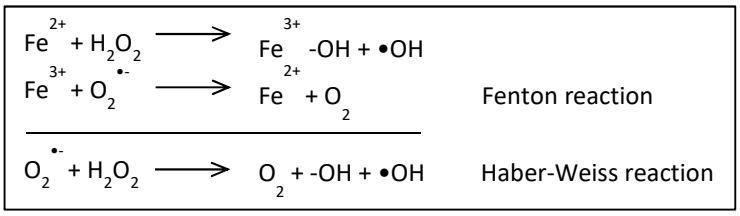

Figure 6: Fenton and Haber-Weiss reaction. The mildly reactive one- and two-electron reduction products of oxygen H_2O_2 and O_2•- (Fig. 4) react with iron to generate the highly reactive •OH.

Besides intracellular sources, exogenous sources of ROS are also widespread. ROS can be for example generated during the oxidative burst of macrophages (Imlay, 2003) or by light excitation of dissolved organic matter, especially humic matter, in surface waters of aquatic ecosystems (Zepp *et al.*, 1977). Moreover, bacteria have to cope with many other redox-active compounds, including reactive nitrogen species (RNS) (Zhart and Deretic, 2002), antimicrobials, antibiotics and environmental xenobiotics which can act as reactive electrophilic species (RES) and affect the cellular redox status (Jacobs and Marnett, 2010).

1.3 Damage due to oxidative stress

The damage to the cell that can be caused by oxidative stress shows quite some diversity and will be pictured in this chapter.

$O_2^{\bullet-}$ anions, for example, are electrostatically attracted to the catalytic iron atoms in iron-sulphur (Fe-S) clusters present in many proteins (Imlay, 2003). Upon binding, the $O_2^{\bullet-}$ univalently oxidises the cluster which gets unstable and degrades, losing the catalytic iron atom (Flint *et al*., 1993) and thereby the protein's function or enzymatic activity. Also, H_2O_2 directly affects proteins by oxidation of cysteinyl residues, creating sulphenic acid adducts that can either form disulphide cross-links with other cysteines or be oxidised further to sulphinic acid moieties (Imlay, 2003). The highly reactive •OH is considered the main contributing reactive oxygen species in endogenous oxidation and damage of cellular DNA (Cadet *et al*., 1999). At least, five main classes of •OH mediated oxidative DNA damage are known to be generated. They include oxidised bases, abasic sites, DNA–DNA intrastrand adducts (Lloyd *et al*., 1997; Randerath *et al*., 1996), DNA strand breaks and DNA–protein cross-links (Cadet *et al*., 1997; Cadet, 1994). Regarding $^1O_2$, *in vitro* studies revealed that it oxidises many organic molecules, including membrane lipid, protein, amino acids, nucleic acids, nucleotides, pyridine nucleotides, carbohydrates and thiols (Straight and Spikes, 1985). Products of the so-called indirect photo-oxidation of proteins by $^1O_2$ comprise tryptophan, tyrosine, and histidine peroxides as well as methionine sulphoxides and disulphides formed from cysteines (Pattison *et al*., 2011).

Even though research articles are available discussing the potential productive use of ROS as well (Poljsak *et al*. 2011; De Grey and Rae, 2007; Rhee, 1999), oxidative stress as described displays a major source of cell damage. Therefore mechanisms sensing the redox state (1.4), altering the metabolism in accordance with the given environment, and detoxifying ROS (1.7) play a crucial role in cell survival.

1.4 Redox sensing

The cellular redox state, also called reduction/ oxidation potential, can be defined as the result of the balance of the levels of oxidised and reduced species of redox couples (Martinovich *et al*., 2005). Oxidative stress disturbs the natural redox state of the cell, hence sensing the redox state is a key component in the oxidative stress response. In response to the redox imbalance, new metabolic pathways are initiated, the repair or bypassing of damaged cellular components is coordinated, and systems that protect the cell from further damage are induced (Green and Paget, 2004). Factors and their moieties responsible for this sensing and responding in bacteria will be described in more detail below.

1.4.1a Iron-sulphur cluster redox sensors

Many known redox sensing factors contain one or multiple Fe-S clusters, heme or mononuclear iron as co-factor. By virtue of its unique electrochemical properties, iron makes an ideal redox active co-factor for many biologic processes (Outten and Theil, 2009). Fe-S clusters are known to be integrated into proteins through coordination of the iron ions by cysteine or histidine residues, yet alternative ligands such as aspartate and arginine are known (Lill, 2009). One mechanism how iron co-factors can transduce the redox signal to their protein partner is a change of coordination number or ligand specificity upon reduction or oxidation.

A well-studied Fe-S cluster redox sensor is the transcription factor FNR (fumarate nitrate reduction) from *E. coli*, known for involvement in switching from aerobic to anaerobic respiration. Under O_2-limiting conditions, FNR binds a $[4Fe\text{-}4S]^{2+}$ cluster (cubane form; Fig. 7) and acts in its transcriptionally active dimer form. When O_2 is present, the cluster is converted to its $[2Fe\text{-}2S]^{2+}$ (rhombic form; Fig. 7) form, leading to dissociation of the protein into inactive monomers and thus the loss of the DNA-binding ability (Crack *et al*., 2014).

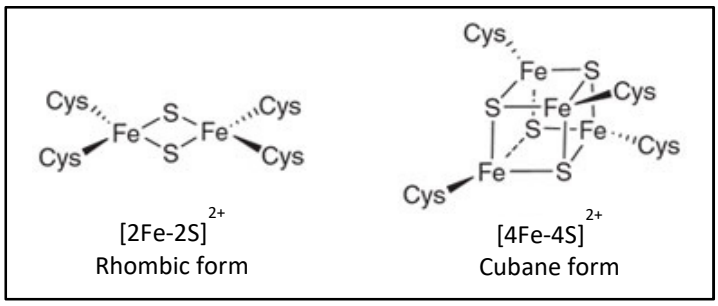

Figure 7: Rhombic and cubane form of Fe-S cluster. The cysteine residues coordinating the cluster binding to the protein are indicated (Cys).

1.4.1b Heme-based redox sensors

Besides the iron-sulphur cluster, a second iron containing co-factor is important for redox sensing proteins: heme (Fig. 8), consisting of a ferrous iron ion (Fe^{2+}) contained in the centre of a porphyrin ring. Heme-proteins (hemoproteins) can be divided into different classes, of which one is called heme-based sensors. In these enzymes, the ligand (for example O_2) association or dissociation from the heme iron leads to protein conformational changes, which transmits signals to a second domain where they initiate catalytic functions or DNA binding (Sasakura *et al*., 2002). The FixL protein, from the FixL-J two-component system in *Sinorhizobium meliloti*, controlling the expression of nitrogen fixation genes in response to O_2, is a well-known member of this group (Tuckerman *et al*.,

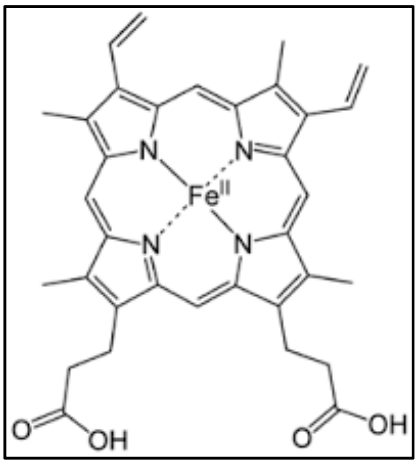

Figure 8: Sructure of heme – a ferrous iron ion (Fe^{2+}) contained in the centre of a porphyrin ring.

2001). A more recently described member is the AppA protein from *Rhodobacter sphaeroides* (Han *et al.,* 2007; Moskvin *et al*., 2007). It contains a C-terminal, 120 AA long SCHIC (Sensor Containing Heme Instead of Cobalmin) domain, binding heme as co-factor for redox-sensing. Moreover, AppA contains a blue-light sensing BLUF (Blue Light Using FAD) domain and uses flavin as a chromophore (Yin *et al*., 2013) (details in 1.6). AppA was shown to act as anti-repressor to the repressor protein PpsR, which is a homolog to *R. capsulatus* CrtJ (1.4.2).

1.4.2 Cysteine-based redox sensors

Besides the named iron-based co-factors, reactive thiol groups of cysteines are known to be sensitive to redox state changes. The thiol groups can be targeted by ROS leading to oxidation or chemical modification of these sensor thiols. This results in a change in protein activity and signal transduction in response to redox fluctuations. For example, post-transcriptional thiol modifications in redox sensing transcription factors lead to conformational changes and activate or inactivate the transcriptional regulator (Hillion and Antelmann, 2015). As a result, specific detoxification pathways are upregulated to destroy the reactive species or to repair the resulting damage and to maintain the thiol homoeostasis (Antelmann and Helmann, 2011).

A prominent member of the group of thiol-based redox sensing transcriptional factors is the OxyR protein. OxyR from *Salmonella typhimurium*, a LysR type DNA binding protein, was the first transcription factor described with a dedicated role in sensing ROS (Zheng *et al*., 1998). OxyR is known to be conserved among Gram-negative and Gram-positive bacteria (Hillion and Antelmann, 2015) and to use cysteine residues for ROS sensing (Antelmann and Helmann, 2011). OxyR binds to the DNA as a tetramer varying in its binding site-dependent on its redox state (Toledano *et al*., 1994). In *E. coli* OxyR is known to induce a set of antioxidant genes, such as *katG* (hydroperoxidase), *ahpCF* (alkyl hydroperoxide reductase), *oxyS* (a regulatory RNA), *dps* (a non-specific DNA-binding protein), *fur* (ferric uptake regulation), *gorA* (glutathione reductase), and *grxA* (glutaredoxin), in response to elevated H_2O_2 levels (Zheng and Storz, 2000). Another cysteine-based redox-sensor is displayed by CrtJ, a redox-regulated DNA binding protein. Dependent on the oxidation of a conserved cysteine (C420) located in the DNA binding motif CrtJ binds to specific promoter regions (Cheng *et al.,* 2012). CrtJ from *Rhodobacter capsulatus*, for example, is known as a major regulator of genes coding for enzymes involved in the biosynthesis of heme, bacteriochlorophyll and carotenoids, as well as structural proteins of the light harvesting-II complex (Ponnampalan *et al.,* 1995) (1.9.2).

1.5 The Bacterial photosynthetic apparatus and anoxygenic photosynthesis

Besides O_2, light is a crucial factor for energy income in various microorganisms. Light-dependent metabolic pathways can be separated into phototrophy and photosynthesis, the former displaying conversion of light energy into chemical energy for growth, while the latter can be defined as the reduction of carbon dioxide (CO_2) into biomass (oxygenic photosynthesis) using energy derived from light (Bryant and Frigaard, 2006). Phototrophy can be, for example, based on bacteriorhodopsin, an energy-conserving transmembrane proton pump (reviewed in Lanyi, 2004). During photosynthesis light energy can be either used in oxygenic, O_2 generating, or anoxygenic, non O_2 generating, photosynthesis. The former is mainly performed by eukaryotic organisms, like plants and algae, as well as cyanobacteria while the latter is used by purple bacteria, green sulphur, and non-sulphur bacteria, as well as heliobacteria and the acidobacteria (Macalady *et al*., 2013). The decisive feature of anoxygenic photosynthesis is the usage of an alternative electron donor (H_2, H_2S, or other certain organic compounds) instead of H_2O, and thereby not resulting in the production of O_2. Key elements in bacterial photosynthesis are photochemical reaction centres (RCs) which are divided into two types. Type I RCs use homodimeric or heterodimeric cores with [4Fe-4S] clusters as their terminal electron acceptor and are found in cyanobacteria, green sulphur bacteria, and heliobacteria. Different from that, Type II RCs have heterodimeric cores with quinones as the terminal electron acceptor; they are also found in cyanobacteria and additionally in purple bacteria and filamentous anoxygenic bacteria (reviewed in Bryant and Frigaard, 2006). While Type I RCs produce weak oxidants and strong reductants, Type II RC reactions result in the opposite outcome. As it is of importance for the presented work, the following section will describe the anoxygenic photosynthesis in purple non-sulphur bacteria in more detail.

Photosynthetic bacteria found in the group of green and purple bacteria commonly share the ability to perform anoxygenic photosynthesis on the basis of bacteriochlorophyll mediated processes. They can contain a variety of bacteriochlorophylls (BChls) and carotenoids, which are not only important for the transformation of light into chemical energy but are also responsible for their colouring. In many purple phototrophs, such as *Rhodobacter*, the cyclic electron transport driven by the anoxygenic photosynthesis requires three membrane-bound complexes: the RC-light harvesting I (LH I) core complex, the LH II, and the cytochrome bc_1 (cytbc_1) complex. In *R. sphaeroides* the formerly named core complex occurs in monomeric or dimeric form (Fig. 9 and 12), where each half of a dimer complex consists of an RC surrounded by 14 LH I αβ subunits, with two BChls, sandwiched between each αβ pair of transmembrane helices (Olsen *et al.,* 2014).

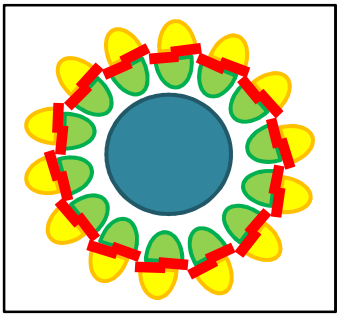

Figure 9: Scheme of a monomeric RC-LHC I core complex.
The RC is shown in blue, while the α- and β-subunits of the LHC I are depicted in yellow and green, respectively. Sandwiched between the LHC I transmembrane helices two BChls are shown in red.

The peripheral LH II complex, absorbing and transferring excitation energy to the LH I complex surrounding the RC, is not essential and can lack in other purple phototrophs (Cartron *et al*., 2014). While the amount of LHC II in *R. sphaeroides* is dependent on various factors such as light intensity and oxygen tension, the LHC I is synthesised in determined stoichiometric amounts together with the RCs (Drews and Golecki, 1995). Most purple non-sulphur phototrophs are facultative anaerobes (McEwan *et al.,* 1994) and only when the surrounding oxygen tension drops below a species-specific threshold the photosynthesis genes are triggered. The latter is also true when no light is present (reviewed in Gregor and Klug, 1999), since in natural habitats the bacteria "expect" light to occur after a period of darkness. The formation of the pigment-protein complexes for photosynthesis is accompanied by invagination of the cytoplasmic membrane and formation of intracytoplasmic membranes carrying the photosynthetic complexes as already described in 1972 by Oelze and Drews. The genes encoding the components of the photosynthetic complexes in *Rhodobacter* are mostly arranged in the so-called photosynthetic gene clusters, depicted schematically in figure 10. These gene loci contain the genes for the carotenoid synthesis (*crt*), bacteriochlorophyll synthesis (*bch*) and the genes for structure proteins of LHC I (*pufBA*) and LHC II (*puc*), RCs (*pufLM*, *puhA*) and the scaffolding protein PufX enhancing LHCI/RC dimerisation (Fig. 10) (Comayras *et al*., 2005; Choudhary and Kaplan, 2000). Due to its role in the presented work PufX will be further discussed in 1.5.1. Additionally, genes encoding photosynthesis gene regulators, such as PpsR and PpaA, are located in this cluster.

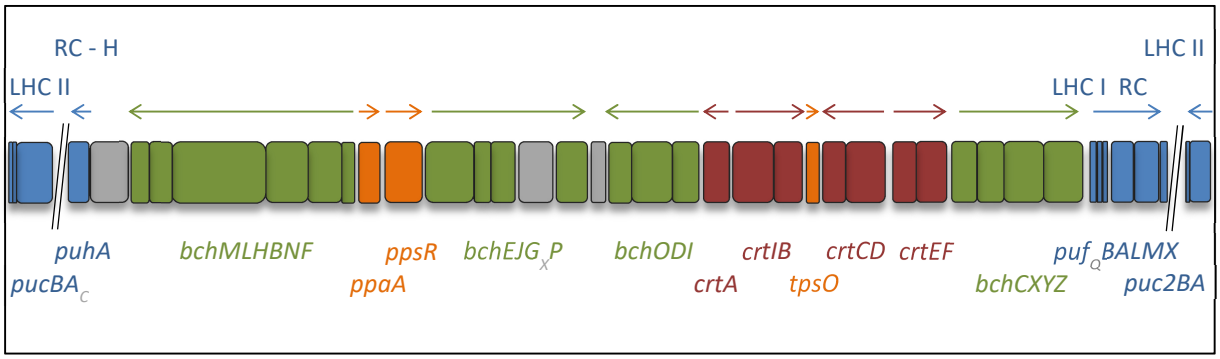

Figure 10: Scheme of the photosynthesis gene cluster arrangement in *R. sphaeroides*. The genes are depicted as coloured boxes, the width corresponding to their length and the arrows indicating the transcriptional orientation. Genes whose products belong to functional groups are coloured alike, displaying the following: blue – structural proteins; green – BChl synthesis components; red – carotenoid synthesis proteins; orange – regulatory proteins (PpaA: photopigment and *puc* activation; PpsR: photopigment suppression; TpsO: tryptophan-rich sensory protein). Modified from Roh *et al*., 2004 and Choudhary and Kaplan, 2000.

During the anoxygenic photosynthesis taking place at the described photosynthetic apparatus in *R. sphaeroides* (Fig. 11), a photon is captured by LHC I or II. Carotenoids in the LHCs can enhance the range of wavelengths of light that can be utilised. The excitation energy is directed to a BChl special pair, triggering the displacement of an electron. The electron is passed to a primary ubiquinone acceptor (Q_A) and subsequently to a second ubiquinone acceptor (Q_B) in the RC. A second photon can

be captured, triggering the electron transfer again. This leads to the complete reduction and subsequent double-protonation of the ubiquinone with protons from the cytoplasm to form ubiquinol (QH_2). The ubiquinol is replaced by an oxidised ubiquinone (Q_{AB}), is released into the membrane lipid phase, and passes its electrons to the next redox component in the cyclic electron transport path: the cytochrome *b/c1* complex. From the cytochrome c_1, the electron is transferred to a soluble cytochrome c_2 that is the physiological electron donor to the oxidised BChl. This cyclic mechanism of redox reactions acts as a proton pumping system, moving protons from the cytoplasmic to the periplasmic space. The formed H^+ gradient is the driving force for the synthesis of ATP that is used to power the metabolic reactions in the cell. The mechanism of anoxygenic photosynthesis is summarised from the detailed description in Scheuring (2006), Okamura *et al.* (2000) and Crofts and Wraight (1983).

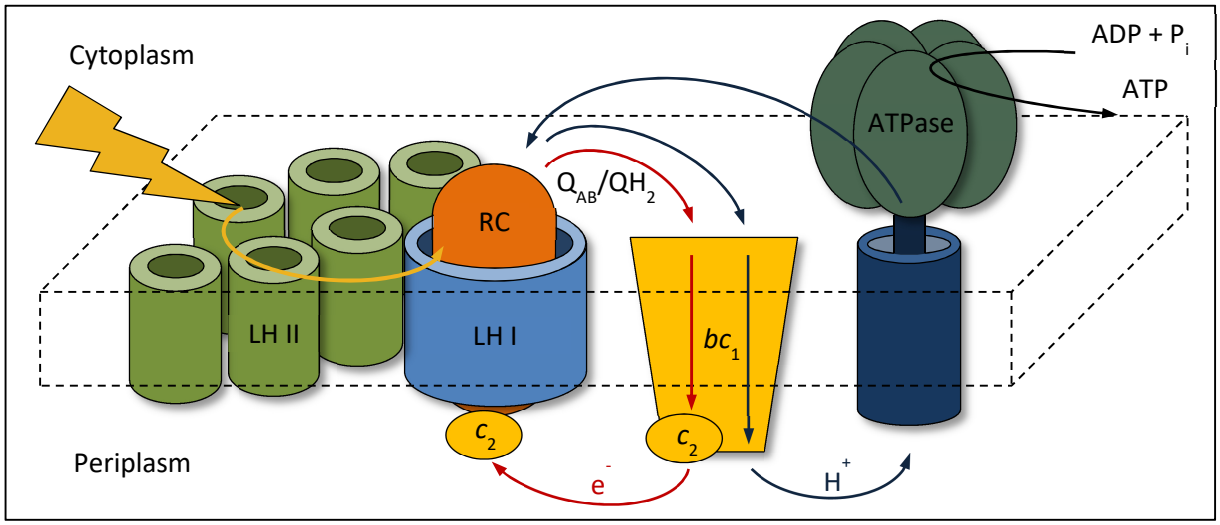

Figure 11: Schematic representation of the photo-induced cyclic electron transfer chain in purple photosynthetic bacteria, and the protein complexes involved. After absorption of a photon by peripheral LH II, the excitation reaches over LH I, to the reaction centre where charge separation occurs. An electron is transferred to quinone (Q_{AB}). After two turnovers, the quinol (QH_2) formed is oxidised by cyt c_2, a reaction catalysed by the cytochrome bc_1 complex that releases two H^+ to the periplasmic space. The cyclic electron transfer is completed by the reduction of the photo-oxidised RC by cyt c_2. The resulting H^+-gradient is used by the ATP-synthetase (ATPase) to form ATP from ADP and inorganic phosphate (P_i). The yellow arrow represents excitation-transfer; the red arrows electron (e^-) transfer and the blue arrows correspond to proton (H^+) transfer. Dashed lines indicate the plane of the membrane. The core complex, comprising LHI subunits (light blue) and the RC (orange) is alone sufficient to perform light capture and generation of an electron-membrane potential. Adapted from Scheuring, 2006.

As described above (1.2) the photosynthetic apparatus, precisely the bacteriochlorophyll, can promote the formation of $^1O_2$ in a photo-sensitisation reaction when oxygen is around. The excited, triplet state bacteriochlorophyll can lead to the formation of $^1O_2$ by energy transfer to molecular oxygen (Fig. 5). Since light is pivotal for this energy transfer, $^1O_2$ stress is often referred to as photo-oxidative stress. The photo-oxidative stress displays one reason to regulate the photosynthesis genes tightly in the presence of oxygen, while the second reason can be found in the energy balance: when

oxygen is present, there is no need for the photosynthetic apparatus since respiration is the favoured energy source. Besides the already described mechanisms to sense the oxygen tension (1.4) cells harbour various factors to sense light as well. The latter will be presented in chapter 1.6, while the role of both sensing types in the regulation of the photosynthesis genes is described in 1.9.2.

1.5.1 PufX in *Rhodobacter sphaeroides*

The ORF encoding *pufX* as the last gene of the *puf* operon in *Rhodobacter* was first identified in 1984 (Youvan *et al*., 1984). Since then PufX was shown to be required for photosynthetic growth of *R. sphaeroides* (Farchaus *et al*., 1992) and *R. capsulatus* (Lilburn *et al*., 1992). Later PufX was identified as a potential player in the supramolecular structure of the LH I/RC core complex, where it is found in a 1:1 ratio with the RC (Francia *et al*., 1999).

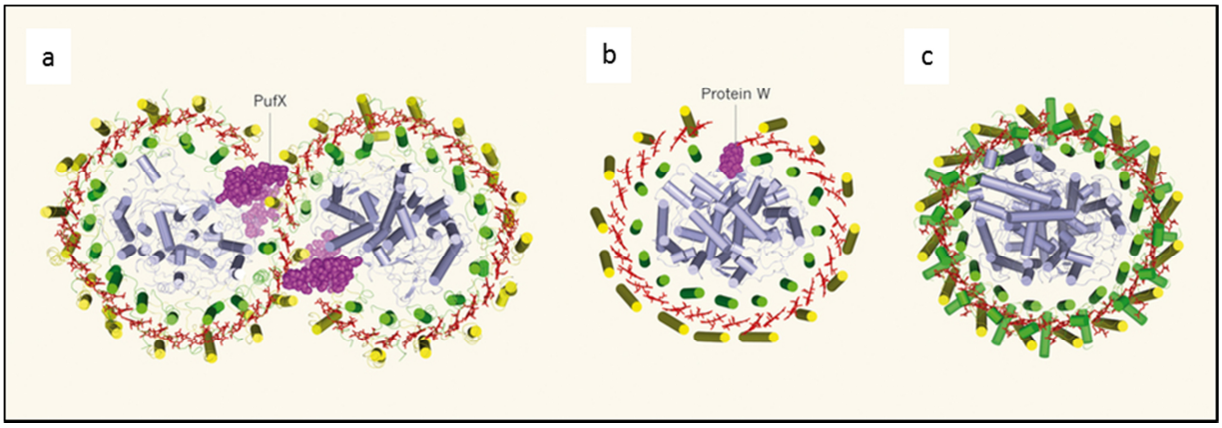

Figure 12: Overview of X-ray crystal structures of monomeric and dimeric LH I/RC complexes with and without gap described in chapter 1.5. **a:** A model of the dimeric RC/LH I/PufX complex from *Rhodobacter sphaeroides* (8 Å resolution; Qian *et al*., 2013), in which PufX proteins create gaps in the LH I rings. Yellow and green cylinders represent helical portions of protein subunits of LH I (α- and β-apoproteins, respectively); blue cylinders are helices of the RC. Non-helical portions of protein chains are shown as thin coils. BChl pigments of the LH I complex are shown in red. No LH I carotenoid pigments or RC cofactors are shown, for clarity. **b**: A model of the monomeric RC/LH I/protein W complex from *Rhodopseudomonas palustris* (4.8 Å resolution; Roszak *et al*., 2003). Here, protein W creates a gap in the LH I ring. **c**: The 3 Å model of the monomeric RC/LH I complex from *Thermochromatium tepidum* (Niwa *et al*., 2014). In the absence of a protein such as PufX or protein W, there is no visible break in the LH I ring. Adopted from Cogdell and Roszak, 2014.

Soon it became evident that in many photosynthetic bacteria, such as *Thermochromatium tepidum* (Niwa *et al*., 2014), the LH I forms a closed ring around the RC, while in *R. sphaeroides* the additional polypeptide PufX creates a gap in the ring around the RC (Comayras *et al*., 2005; Fig. 12) and promotes core complex dimerisation. A similar case is known from *Rhodopseudomonas palustris*, where the polypeptide W is responsible for the gap in the monomeric LH I/RC complex (Roszak *et al*., 2003). Presumably also bacteria from other genera could contain PufX-like proteins not yet identified due to a very low sequence identity (Holden-Dye *et al*., 2008). Later on, the role of PufX in core complex dimerisation could be narrowed to its cytoplasmically exposed N-terminal domain (Ratcliffe *et al*., 2011) and LH I/RC/PufX complexes were shown to adopt a bent configuration imposing the

curvature of the membrane bilayer (Qian *et al*., 2008). Recent discoveries achieved with X-ray crystallography (Qian *et al*., 2013) gave insight to the structural arrangement of the LH I/RC/PufX complex: each PufX is positioned adjacent to an RC Q_B site by attachment of its N-terminal region to the cytoplasmic extrinsic domain of RC-H. Both the N- and C-terminal extrinsic regions of PufX promote dimerisation by interacting with an LH I β polypeptide from the other half of the complex. The architecture of the complex creates a channel, allowing Q/QH_2 molecules to cross the LH I barrier and to internally migrate between the two halves of the dimer structure. The X-ray crystal structures of the three described LH I/RC complex types are summarised in figure 12 (adopted from Codgell and Roszak, 2014).

1.6 Sensing of light

Sensing light as an environmental factor was shown to be of importance for photosynthetic as well as non-photosynthetic bacteria. While for the former the importance of light-sensing is self-evident, examples of the latter are found more seldom; such as in the genus *Brucella*, in which a functional photoreceptor, here a histidine kinase, could be directly related to survival and replication within macrophages (Swartz *et al*., 2007). Not only to sense the presence of light but also to sense its intensity is detrimental for many microorganisms to avoid damage by UV radiation (reviewed in Carstenholz and Garcia-Pichel, 2000). Moreover, the retention of a circadian rhythm can depend on light perception (Emery *et al*., 1998).

The key components for light sensing are, as implied, photoreceptors. Photoreceptors can be defined as proteins carrying a light-sensitive co-factor, the chromophore. The chromophores absorb certain wavelengths and thereby get excited, often causing conformational changes. These changes lead to activation of the photoreceptor and subsequent signal transduction. Typical chromophores are known to be flavins and tetrapyrroles. Only very recently, besides chlorophyll, also the tetrapyrrole cobalamin (vitamin B_{12}) was recognised as potential light-dependent co-factor, for example of the transcriptional regulator CarH in *Myxococcus xanthus* (Pérez-Marín *et al.*, 2008) and PpaA (1.5) in *R. sphaeroides* (Vermeulen and Bauer, 2015). The so far studied photoreceptors can be classified into different types: phytochromes, sensory rhodopsins, cryptochromes, photoactive yellow proteins (PYP), Light Oxygen Voltage (LOV) domain proteins, and Blue Light Using Flavin (BLUF) light receptors. The last three are commonly known to bind flavins as co-factors. All in all the photoreceptors can differ in how they respond to light, in which wavelength and what response they trigger. The best-described group so far is represented by the phytochromes, absorbing red light (650-750 nm) and being well known for affecting plant development and growth (reviewed in Casal, 2013). The first bacterial phytochrome was not described until 1997 (Yeh *et al*.; Hughes *et al*.). Blue and green light (380 -575 nm) can be absorbed by rhodopsins, binding retinal (vitamin A aldehyde) as

chromophore co-factor. A bacterial representative of this group is the proteorhodopsin found in γ-proteobacteria, also binding retinal as chromophore (Béjà *et al*., 2000). The remaining four types of photoreceptors can by classified as blue light sensing photoreceptors (380-490 nm), a group known to be dominant in bacteria. Cryptochromes, one member of this group, are flavoproteins also defined as photolyase-like blue light receptors, found in microbes including bacteria, archaea and yeast (Lin, 2002). Besides cryptochromes proteins from the phototropin family, representing the main photoreceptors for phototropism in plants (Briggs *et al.,* 2001) and carrying an LOV domain, are known for blue light sensing. In 2002 there was the first evidence that a phototropin, namely YtvA from *B. subtilis*, also functions in prokaryotes in blue light sensing (Losi *et al*., 2002). A further, in prokaryotes also more recently described, sensor type are the BLUF domain proteins. They were simultaneously described in *R. sphaeroides* (Gomelsky and Klug) and *Euglen gracilis* (Iseki *et al.*) as blue light sensors, again in 2002. The PYP was already described in 1985 (Meyer) as a photoreceptor in the purple sulphur bacterium *Ectothiorhodospira* (*Halorhodospira*) *halophile,* where it has been proposed to be responsible for the bacterium's negative photo-response; which is swimming away from blue light (Sprenger *et al*., 1993). Although, the photocycle kinetics (overview in Cho *et al*., 2016) and already since 1989 the crystal structure (McRee *et al.*, 1989) of PYP have been studied in great detail its exact function remains elusive.

1.7 Defence against reactive oxygen species

Oxidative stress reflects a disturbance in the balance between the production of ROS and the opposing antioxidant defences (Betteridge, 2000), more precise an imbalance towards the pro-oxidative state. Besides the avoidance of oxidative stress promoting components, such as BChl, there are several additional ways to defend the cell against oxidative stress. The defence can be composed out of various factors and occurs as the elimination of the ROS, as repair of the damage caused by the ROS and keeping the cellular environment reduced. Overall these factors can be divided into enzymatic and non-enzymatic antioxidants.

The enzymatic antioxidants eliminating ROS are catalases, peroxidases, and superoxide dismutases (SODs). Catalases are common enzymes found in almost all organisms exposed to O_2 and catalyse the decomposition of H_2O_2 to water and O_2. Peroxidases can detoxify H_2O_2 using an intracellular reductant. Other than their beneficial role in ROS detoxification peroxidases are also known to be involved in ROS production in plants (Kim *et al.,* 2010). Also, enzymes harbouring both, a catalase and a peroxidase activity, such as the *Mycobacterium tuberculosis* KatG, are known (Heym *et al*., 1993). SODs are metalloenzymes, extensively studied in *E. coli*, which can harbour zinc, manganese, or iron as cofactor and catalyses the dismutation of $O_2^{\bullet-}$. The H_2O_2 released by this reaction can be subsequently detoxified by catalases and/or peroxidases. Enzymatic factors involved

in repair of ROS damage to the DNA comprise exo- and endonucleases as well as systems for nucleotide excision and recombination (reviewed in Demple and Harrison, 1994). Whereas protein damage can be encountered by chaperons and proteolytic enzymes, the former protecting and refolding, the latter degrading the damaged protein.

Some molecules (non-enzymatic antioxidants) are constitutively present and help to maintain the reducing environment of the cytoplasm and to keep protein thiols in their reduced state. Among these molecules are NADPH (Nicotinamide adenine dinucleotide phosphate) and NADH (Nicotinamide adenine dinucleotide), β-carotene, ascorbic acid, α-tocopherol and glutathione (GSH) (Cabiscol *et al*., 2000). Especially GSH, present at high concentrations, maintains a strong reducing environment in the cell, and its reduced form is maintained by glutathione reductase using NADPH as a source of reducing power (Masip *et al*., 2006). The maintenance of reduced conditions is further supported by thioredoxins and glutaredoxins (Cabiscol *et al*., 2000). Moreover, to prevent the formation of H_2O_2 and $O_2^{\bullet-}$ in the Fenton reaction (Fig. 6), excessive iron can be stored via the heme proteins ferritin and bacterioferritin (Imlay, 2008) (also see 1.8).

Photosynthetic organisms additionally carry carotenoids whose photoprotective function is already known since 1955 (Griffiths *et al*.). Carotenoids can prevent the harmful effect of $^1O_2$ by different approaches: they can directly quench the $^1O_2$ (Di Mascio *et al.,* 1989), plus they can quench the excited BChl sensitiser (Frank and Christensen, 1995). The first excited triplet state energy level of carotenoids lies below that of $^1O_2$ so that the excited carotenoid decays to the ground state harmlessly releasing the excess energy as heat (Frank *et al*., 1999). The quenching of excited BChl is supposed to occur on energy transfer between the BChl and carotenoids in close proximity (Cogdell *et al*., 2000).

All these defence factors are dependent on their expression level. While some factors are constitutively present (GSH, NADPH) others depend on induction via transcription factors such as OxyR (Green and Paget, 2004). Thus expression control by redox sensing factors (1.4) itself can also be seen as a defence mechanism, for example, in the presence of oxygen neither oxygen-sensitive proteins nor oxidative stress driving proteins from the photosynthetic apparatus are expressed (1.9.2).

1.8 Bacterial iron homoeostasis

With a few exceptions iron is essential for life in all forms since it acts in a variety of major biological processes such as photosynthesis, methanogenesis, N_2 fixation, respiration, gene regulation, oxygen transport, and DNA biosynthesis (reviewed in Andrews *et al*., 2003). But besides its beneficial role, iron also represents a threat to the cell as a source of ROS formation under aerobic conditions (1.2). In addition to its potential toxicity iron is poorly available for cells due to its occurrence in its

oxidised, insoluble, ferric form (Fe^{3+}). Thus, to achieve balanced iron homoeostasis organisms need to scavenge iron from their surrounding, possess efficient iron storage mechanisms, and reduce iron-containing proteins under iron-limiting conditions as well as to express the iron homeostatic machinery according to the iron availability. Bacteria can conduct the iron-uptake via siderophores, chelating and thereby solubilizing the iron prior to transport, metal-type ABC transporters (Köster, 2001), and the ferrous iron transporting Feo system first discovered in *E. coli* (Kammler *et al*., 1993). Iron storage serves as an alternative source of iron when external sources are restricted, and is known to be facilitated by three protein types in bacteria: the typical ferritins (FTN), the heme-binding bacterioferritins, and the more recently identified DNA-binding protein from starved cells (DPS). The former ferritins are found in all three domains of life whereas the latter two protein types are solely found in bacteria and archaea (Bai *et al*., 2015). In an overarching manner, the regulation of the iron metabolism genes controls the iron homoeostasis assured by iron uptake, storage, and consumption. This regulation is typically dependent on the iron availability, as represented by the well-characterized ferric uptake regulator (Fur) protein acting as a positive repressor via interaction with its co-repressor Fe^{2+} (Bagg and Neilands, 1987). A similar mode of action is known for the iron-sulphur cluster biogenesis transcriptional regulator IscR acting as repressor upon Fe-S cluster binding (Remes *et al*., 2015). Also, an sRNA was found to be involved in iron-dependent gene regulation. The *E. coli* sRNA RhyB directly represses 18 transcripts encoding iron-using proteins (Massé *et al*., 2005) while its expression is repressed by iron-interacting Fur (Massé and Gottesman, 2002).

1.9 *Rhodobacter sphaeroides*

1.9.1 Profile

Rhodobacter sphaeroides, along with *Rhodobacter capsulatus*, represents an extensively studied model organism regarding bacterial photosynthesis. *R. sphaeroides* is a rod-shaped, gram-negative α-proteobacterium with a length of 0.2 - 0.5 µm that carries one lateral flagellum (Imhof, 2001). Its genomic information is contained on two chromosomes and five circular plasmids with an overall size of ~4.6 Mbp (Choudhary *et al*., 2004), exhibiting a rather high GC-content of 65 - 69% (Imhof, 2001). By virtue of its vast metabolic versatility, *R. sphaeroides* can act as a model for various questions concerning the adaption to changing environmental conditions and the involved regulatory circuits. The metabolic pathways present in *R. sphaeroides* comprise the ability to perform fermentation when carbon sources, light and oxygen are missing and to respire anaerobically as soon as a suitable electron acceptor is present (Imhof, 2001). When low oxygen tensions and light availability characterise the surrounding, *R. sphaeroides* can perform anoxygenic photosynthesis and to fix atmospheric CO_2 and nitrogen. Aerobic respiration represents the most favoured pathway to

generate energy and will be performed whenever the oxygen tension is high enough (Tabita, 1995). In the habitats in which *R. sphaeroides* can be found, such as running and standing water, the metabolism determining factors can change; hence *R. sphaeroides* exhibits a wide variety of adaptation mechanisms and corresponding regulatory factors. Especially the presence of oxygen and light, as well as their harmful potential, shape the temporary physiology of *R. sphaeroides*. This also holds true for the availability of detrimental ions, such as iron, with great importance in enzyme activity. Besides the more general overview of these topics (1.4, 1.6, 1.8), the next chapters will give some additional information on *R. sphaeroides* in particular.

1.9.2 Photosynthesis gene regulation

As described in 1.2 photosynthetic complexes can harbour oxidative stress promoting factors, such as BChl. So besides induction of defence mechanisms when ROS occur, avoidance of those ROS formation promoting components plays a key role in cell protection for facultative photosynthetic microorganisms. The second reason for tight regulation of photosynthesis components is the optimisation of energy production: when oxygen is present the favoured metabolic pathway to gain ATP is aerobic respiration, which means the cost-intensive photosynthetic apparatus is not needed. Moreover, BChl and heme, which are both physiologically active tetrapyrroles and share common intermediates in the biosynthetic pathway from δ-aminolevulinic acid to protoporphyrin IX, are toxic when unbound (Yin *et al*., 2012). This explains the need to regulate the genes encoding the tetrapyrrole synthesis as well, which will be additionally discussed in further detail at the end of the chapter. The formation of photosynthesis complexes in the model organism of this work, *R. sphaeroides,* is regulated in an oxygen- and light-dependent manner. The most important proteins involved in regulation of photosynthesis genes (Fig. 10) are the aerobic repressor PpsR with its anti-repressor AppA, the PrrB/PrrA two-component system and the regulators FnrL and PpaA (summarised in Fig. 13).

PpsR, the *R. sphaeroides* homolog of CrtJ (1.4), inhibits transcription of photosynthesis genes, such as BChl (*bch*) and other tetrapyrrole synthesis genes, genes for carotenoid synthesis (*crt*) as well as the *puf* and *puc* operon, under aerobic conditions. A TGT-N12-ACA palindrome in the target genes upstream regions is believed to enable PpsR binding (Moskvin *et al*., 2005). PpsR/CrtJ homologs are known to be linked to gene clusters encoding proteins involved in tetrapyrrole synthesis in almost all purple phototrophic bacteria (Vermeulen and Bauer, 2015). In some species, PpsR occurs in two functional copies, as seen with the redox-responsive PpsR1 and the light-regulated PpsR2 in *Bradyrhizobium* ORS278 (Jaubert *et al*., 2004). Under aerobic conditions, the binding of PpsR to the DNA binding motif is stimulated by oxidation of a pair of redox active cysteine residues in the protein (Masuda and Bauer, 2002). Also heme binding via the PAS domain (PAS: Per – period circadian protein, Arnt – aryl hydrocarbon receptor nuclear translocator protein, Sim – single-minded protein) of PpsR has been reported to affect the DNA-binding activity (Yin *et al*., 2012).

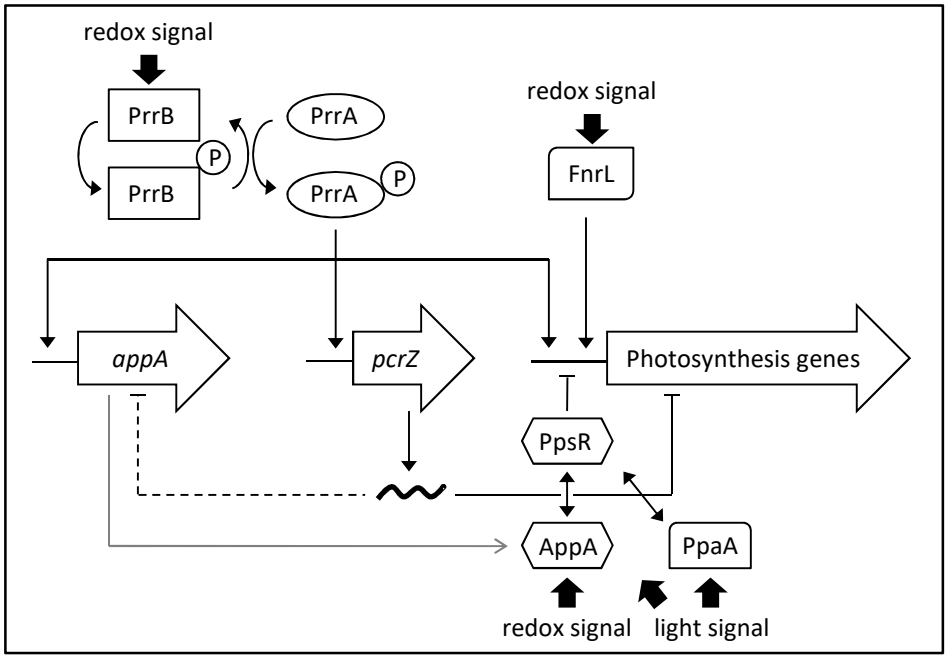

Figure 13: Overview of the regulatory network controlling the expression of the photosynthesis genes. Genes are depicted as white arrows, while proteins are shown as symbols containing the respective protein name. Upon a drop of oxygen tension the transcriptional regulators FnrL and PrrA, as well as the anti-repression of PpsR via AppA and PpaA activate the expression of the photosynthesis genes. At the same time PcrZ expression is triggered PrrA- and FnrL-dependent, leading to repression of photosynthesis genes and seemingly also AppA expression. Modified from Mank *et al*., 2012.

Several anti-repressor proteins are known to interact with PpsR to disrupt its DNA-binding. For example, binding of the anti-repressor AppA to PpsR, which is mediated by the heme-binding C-terminus of AppA (Han *et al*., 2004), antagonises PpsR's DNA-binding. Both, the redox state and light availability are responsible for AppA interaction with PpsR as described by Metz *et al*. (2012). During high O_2 tension, AppA is unable to bind PpsR due to its oxidised heme. With decreasing O_2 tension the heme can be reduced, and AppA can bind PpsR. When the oxygen tension is at intermediate levels and also light is present, the photoreceptor activity of AppA facilitated by its BLUF domain interferes with binding of PpsR (Han *et al*., 2004). A second light-regulated PpsR anti-repressor is represented by PpaA (AerR in some species), which as PpsR has a homolog in almost all purple phototrophic bacteria typically located upstream of the PpsR/CrtJ loci (Cheng *et al*., 2014). Even tough *R. sphaeroides* PpaA harbours a sequence with similarity to an SCHIC domain it was recently shown that instead of a heme PpaA binds cobalamin as a cofactor. The hydroxocobalamin (OH-Cbl) utilised as co-factor is known to be generated as a photohydrolysis product of light excitation of Ado-Cbl, which means the OH-Cbl selectivity could allow PpaA to indirectly sense the presence of light (Vermeulen and Bauer, 2015). Overall the effect of PpaA deletion in *R. sphaeroides* on the photopigment synthesis seems to be minimal (Vermeulen and Bauer, 2015), whereas the deletion of the PpaA homolog AerR in *R. capsulatus* exhibits a more severe phenotype regarding pigmentation (Cheng *et al*., 2014). Still, the capability of a PpaA over-expression restoring the AppA deletion phenotype in *R. sphaeroides* leads to the assumption that PpaA could act as an important PpsR anti-

repressor under some growth conditions (Vermeulen and Bauer, 2015).

A major role in gene regulation can be assigned to the PrrB/PrrA two-component system. Combined transcriptome and proteome analyses in 2008 revealed 1058 genes to be differentially regulated in the PrrA deletion mutant (PrrA2) in *R. sphaeroides* (Eraso *et al*.). This study has shown that genes encoding proteins involved in photosynthesis, but also N_2- and CO_2- fixation and H_2-oxidation are affected by PrrA. In addition to genes from metabolic pathways, genes whose encoded proteins have functions in translation, general transcription, energy production and conversion, repair to DNA and protein damage were indicated to be PrrA-dependently regulated. Since a large percentage of these genes encoded proteins related to protein synthesis and cell growth, the investigating laboratory created a new PrrA deletion strain (PrrA3) to rule out the possibility that these effects are reflecting a growth difference compared to the wild-type caused by unlinked mutations in the PrrA2 strain. When repeating the experiments using the new PrrA3 deletion mutant to compare to the wild-type only 255 genes from 182 operons remained to be differentially regulated (Imam *et al*., 2014). Consistent with previous, independent knowledge the differentially expressed genes that were identified in 2014 were enriched for genes known or predicted to be involved in photosynthetic processes. In addition to the photosynthesis-related functions, functions in TCA cycle, electron transport chain, and iron binding were found to be affected. Of the differentially expressed genes mRNA levels of 148 genes were shown to be increased while 107 were decreased in the presence of PrrA, which supports the hypothesis that PrrA acts as both a transcriptional activator and repressor (Eraso *et al*., 2008). Interestingly, in addition to protein encoding genes, also the oxygen-dependent expression of an sRNA, namely PcrZ, was found to be positively affected by PrrA (Mank *et al*., 2012). The activation of PrrA upon phosphorylation by its kinase partner PrrB under low oxygen conditions leads to formation of a PrrA dimer (Laguri *et al*., 2003) and binding to the variable consensus sequence [C/T][G/C]CGG[C/G]-gap-G[T/A]C[G/A][C/A] on the DNA (Mao *et al*., 2005). The activity of the PrrB sensor kinase was indicated to be regulated in a redox-dependent manner. The sensing of the redox state and the subsequent activation of PrrB relies on redox-reactive cysteine that is capable of undergoing metal-dependent formation of a disulphide bond (Swem *et al*., 2003). The *R. sphaeroides* FNR homolog FnrL was early identified as a transcriptional regulator under anaerobic conditions and was since found to enhance the expression of a variety of photosynthesis genes such as *puc*, *hemA*, *hemN*, *hemZ,* and *bchE* as well as the ccoNOQP operon encoding the *cbb3* oxidase (Zeilstra-Ryalls *et al*., 1998; Dangel and Tabita, 2009; Dufour *et al.*, 2010). Also, the already mentioned oxygen-dependent expression of sRNA PcrZ was shown to be affected by FnrL (Mank *et al*., 2012). A study in 2014 (Imam *et al*., 2014) even further enlarged the FnrL regulon using Chromatin immunoprecipitation followed by high-throughput sequencing (ChIP-seq) that identified 52 operons under the control of FnrL. This study expanded the functions of genes in the FnrL regulon to include nitrogen regulatory proteins, iron sulphur assembly proteins, ABC transporters, and additional transcription factors. Moreover, the two photo-oxidative

stress induced sRNAs RSs0019 and RSs2461 (1.9.5) were assumed to be FnrL dependent. Besides these well-studied regulatory proteins, there were more candidates predicted to be involved in photosynthesis gene regulation in *R. sphaeroides*. In the above-mentioned study by Imam *et al*. (2014) CrpK, a Cpr/FNR-type transcriptional regulator (Bateman *et al*., 2004), and MppG (modulator of photopigment genes, RSP_2888) were indicated to regulate a similar set of genes as FnrL (Fig. 14).

In addition to the listed proteins, at least one sRNA is involved in the photosynthesis gene regulation of *R. sphaeroides* (described in Mank *et al.,* 2012) (Fig. 13). The sRNA PcrZ is known to be expressed in an oxygen-dependent manner; its expression is induced upon a drop of oxygen tension with similar kinetics as genes encoding functions in photosynthesis. High expression of PcrZ is dependent on PrrA and FnrL as transcriptional activators. When expressed during microaerobic conditions, direct mRNA targets of PcrZ are *bchN* and *puc2A*, while also *appA* transcript levels are negatively affected which seems to be an indirect effect. The negative effect on *appA* consequently leads to stronger repression of the photosynthesis genes by PpsR. So overall the regulation entailed by PcrZ represents an incoherent feed-forward loop, reducing the expression of the photosynthesis genes whereby it is induced by activators of the photosynthesis genes itself.

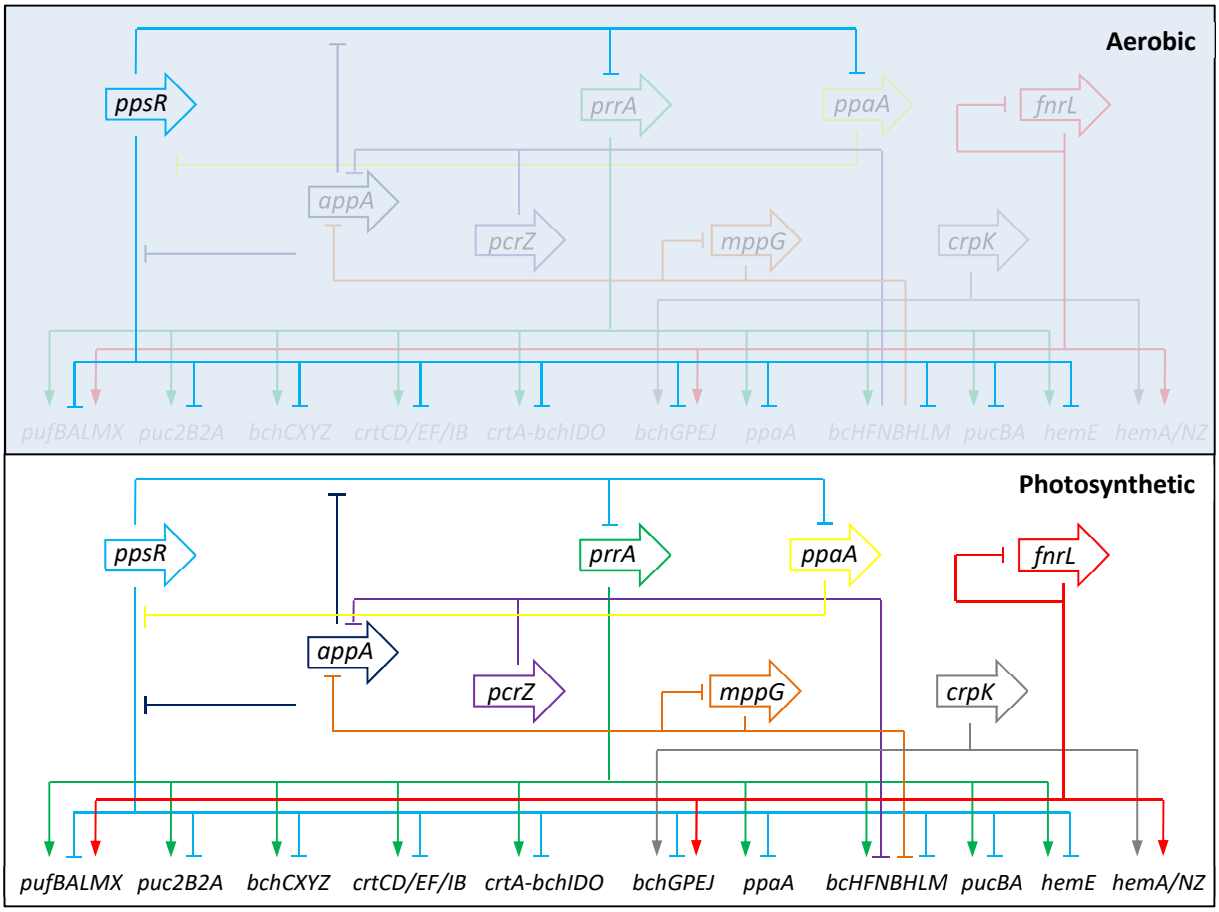

Figure 14: Activation and repression of photosynthesis genes under aerobic (upper panel) and photosynthetic conditions (lower panel). Photosynthetic conditions are characterised by low oxygen tension and light availability.The (assumed) regulatory factors, and the repression or activation they entail are marked as follows: PpsR – light blue, AppA – dark blue, PcrZ – purple, PrrA – green, MppG – orange, CrpK – grey, FnrL – red, PpaA - yellow.

Noteworthy, as implied above, the described regulatory factors are not only known to affect the mentioned target genes but also one another. The *ppaA* gene, for example, shows a PpsR binding site in its promoter region (Mao e*t al*., 2005) while *appA* was shown to be controlled by PrrA (Gomelsky *et al*., 2008; Eraso *et al.,* 2008). An overview of the so far predicted regulatory network is depicted in figure 14. As already implied, the synthesis of the tetrapyrroles (BChl, heme, and cobalamin) is complexly regulated. In general, tetrapyrroles are compounds consisting of four pyrrole rings, and especially the cyclic tetrapyrroles and their synthesis will be discussed here. The cyclic tetrapyrroles are synthesised in the so-called 'modern' tetrapyrrole pathway which branches starting from 5-aminolevulinic acid (ALA) as a precursor to the three end-products BChl, heme and cobalamin (Fig. 15).

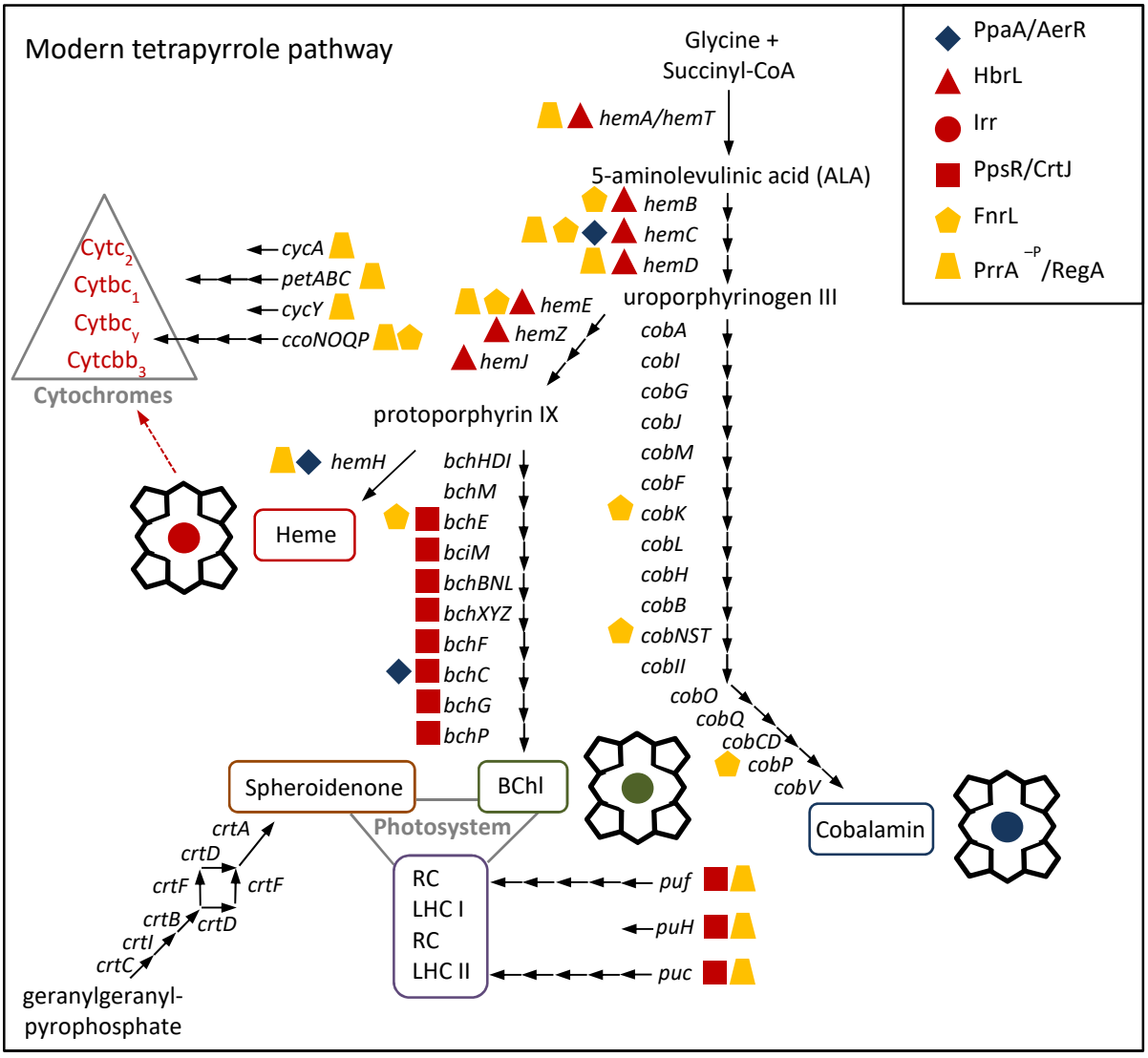

Figure 15: Overview of the modern tetrapyrrole pathway and its regulation, with BChl, heme, and cobalamin as end-products. The enzymes involved in the pathway are depicted with their gene names, while the regulators involved are depicted as coloured symbols (legend in the upper right; blue: cobalamin as co-factor, red: heme as co-factor, yellow: non-tetrapyrrole co-factor). The scheme also indicates the connection of heme to the cells cytochromes and the affiliation of BChl to the photosystem. The regulation of the carotenoids (Spheroidenone) synthesis and further photosystem components, and the regulation of genes involved in the cytochrome formation are depicted as well. Modified from Yin and Bauer, 2013.

After the three-step generation of the last common intermediate uroporphyrinogen III from eight ALA molecules the three specific pathways towards the end-products start. BChl and heme share three more steps towards the formation of protoporphyrin IX (Zappa *et al*., 2010). Finally, cobalamin is defined by the insertion of cobalt to the tetrapyrrole ring, while heme synthesis is completed by insertion of iron (Yin and Bauer, 2013), the synthesis of BChl ends with the insertion of magnesium and further enzymatic modifications (Hunter *et al*., 2009). Besides the above-described factors commonly involved in regulation of the photosynthesis genes (AppA, PpsR, PpaA, and PrrA) there are additional transcription factors seemingly involved in the tetrapyrrole regulatory circuit. For example, the heme biosynthesis was shown to be affected by the LuxR-type heme-binding transcriptional regulator HbrL (Heme binding regulator LyrsR-type) in *R. capsulatus* (Smart and Bauer, 2006). Most interestingly the tetrapyrrole synthesis shows feedback regulation in which the product of one branch influences the activity of the two other branches. A classic example for this feed back inhibition is the first enzyme of the tetrapyrrole pathway, the 5-aminolevulinic acid synthase (ALAS), whose enzymatic activity is inhibited by heme (Lascelles and Hatch, 1969). Besides heme, cobalamin is known for its role as an enzyme co-factor and in the control of bacterial gene expression. This is also true in the tetrapyrrole synthesis were the activity of the cyclase enzyme BchE from the BChl branch was shown to be cobalamin-dependent in many purple bacteria (Gough *et al*., 2000). Also, enzymes from the cobalamin synthesis itself, encoded by the *cob* genes, are directly affected by cobalamin which binds as adenosine-cobalamin to riboswitches in the 5'UTR of many *cob* mRNAs (1.1.3). The binding of the riboswitch results in a structural change of the mRNA masking the RBS (Vitreschak *et al*., 2003). The involvement of BChl in the regulation of the tetrapyrrole pathway was not shown so far but cannot be excluded.

1.9.3 Processing of the *puf* mRNA in *Rhodobacter*

As described above (1.5) the components of the photosynthetic apparatus in *Rhodoabacter* are needed in a given ratio such as 14 LH I α and β subunits per reaction centre. This stoichiometry is achieved by expressing the needed components from different operons (Fig. 10) with different expression levels, a regulated BChl synthesis (1.9.2), and additionally via posttranscriptional processing of the polycistronic *puf* mRNA. This processing results in segmental differences in stability of the *puf*-mRNA fragments (Fig. 16). The *puf* mRNA processing was studied in great detail in *R. capsulatus*, a close relative to *R. sphaeroides*. In RNA samples from both species, two RNA segments can be clearly detected via Northern blot analysis. The less abundant, larger *pufBALMX* fragment (2.7 kb) and the smaller *pufBA* fragment (0.5 kb), both originating from the *pufQBALMX* precursor mRNA (3.2 kb) which is not reliably detectable on a Northern blot due to its very short half-life. Determining the half-life period of the *pufBALMX* and the *pufBA* fragments revealed a half-life period of around 8 min and 22 - 33 min in *R. capsulatus* (Klug *et al*., 1987; Belasco *et al*., 1985) and 8 - 10 min and around 40 min in *R. sphaeroides* (Berghoff *et al*., 2011), respectively. Moreover, the stability of the

pufBALMX fragment in *R. capsulatus* was found to be changed upon the oxygen tension which is not true for the *pufBA* fragment. Upon high oxygen tension, the half-life period of *pufBALMX* is reduced to about three minutes (Klug, 1991).

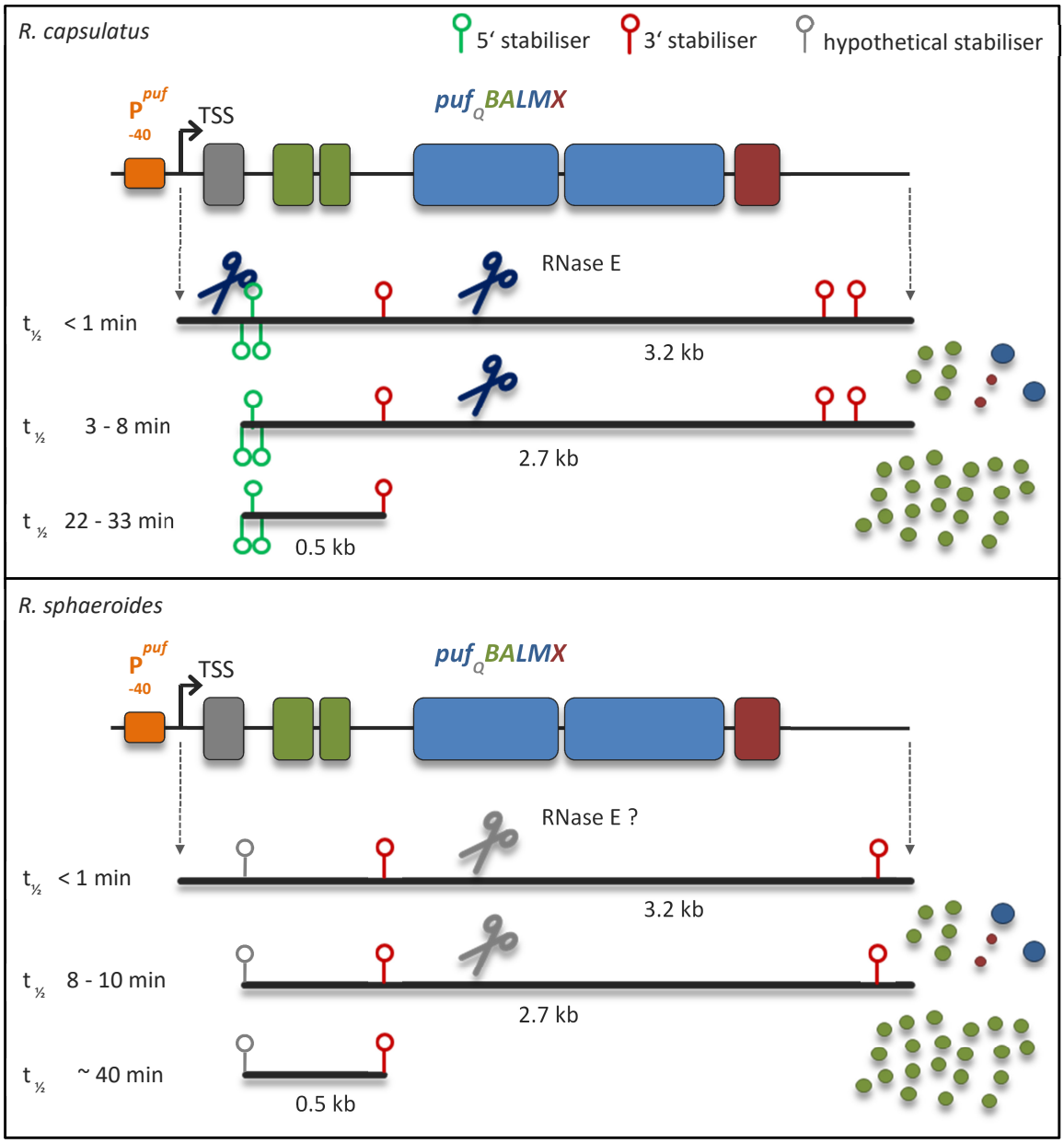

Figure 16: Schematic overview of the *puf* mRNA processing in *Rhodobacter* and the resulting stoichiometry of the photosynthesis core complex proteins. The upper panel shows the *R. capsulatus* situation, while the lower panel depicts the *puf* mRNA processing in *R. sphaeroides*. Known and hypothesised stabilisers (stem-loops) are indicated, as well as known (blue) and predicted (grey) RNase E cleavage sites (scissors). Coloured boxes indicate the *puf* genes whose transcription results in the polycistronic *puf* mRNA (grey line). Segmental differences in stability (half-life shown as $t_{½}$ in min) of the *puf* mRNA fragments leads to the needed stoichiometric amount of the encoded proteins (coloured circles: green – LH I αβ, *pufBA*; blue – reaction centre, *pufLM*; red – PufX scaffolding protein, *pufX*). Modified from Heck *et al*., 2000 and Rauhut and Klug, 1999.

For *R. capsulatus* it was shown that a secondary structure (stem-loop) in the intercistronic region between *pufA* and *pufL* stabilises the *pufBA* fragment since it protects the RNA fragment against 3' – 5' exonucleolytic degradation after processing from the *pufBALMX* fragment (Belasco *et al.*, 1985). When removing this stem-loop, the small *pufBA* fragment is dramatically less abundant and the RC-LH I stoichiometry is impaired (Chen *et al.*, 1988; Klug *et al.*, 1987). Also, two stem-loops were found to protect and stabilise the 3' end of the *pufBALMX* fragment (Klug and Cohen, 1990), whereas three stabilising stem-loops were found at the 5' end of the *pufBALMX* and *pufBA* fragment (Heck et al., 1996) (Fig. 16). The segmental differences found in both *Rhodobacter* strains indicate the existence of similar stabilising structures in *R. sphaeroides*. At least in the in the intercistronic region of *pufA* and *pufL* and downstream of *pufX* stem-loop structures could be identified (Lee *et al*., 1989). Those two stem loops, as well as a hypothesised stabilising structure at the *puf* mRNAs 5' end, are indicated in figure 16.

Furthermore the processing of the *puf* mRNA in *R. capsulatus* is known to be dependent on the initial endonucleolytic cleavage by RNase E. RNase E cleavage sites were identified in the coding region of *pufL* (Fritsch *et al*., 1995) as well as upstream of *pufB* in the *pufQ* coding region (Heck *et al*., 2000) (Fig. 16). Very recently an RNAseq study in our group comparing the wild-type with a mutant carrying a thermosensitive *E. coli* RNase E variant (unpublished) revealed a potential RNase E cleavage site in the *R. sphaeroides pufL* coding region as well. More intriguing, anti-sense to the *pufL* 5' region and thereby the potential RNase E cleavage site an asRNA (aspufL) can be found.

1.9.4 Alternative sigma factor-dependent stress response

General strategies of defence against oxidative stress are described in chapter 1.7. For the model organism *R. sphaeroides*, a microorganism performing photosynthesis, it is of particular importance to cope with the formation of the highly reactive $^1O_2$ in the presence of O_2 (1.2). Part of the response triggered under these harmful conditions comprises of a cascade of alternative sigma factors (Fig. 17). A major player involved is represented by the alternative sigma factor RpoE, which is released from its anti-sigma factor ChrR upon $^1O_2$ stress (Anthony *et al*., 2005). The activation of RpoE leads to the induction of a rather small set of genes encoding proteins involved in DNA repair upon UV damage (photolyase, *phrA*), energy metabolism (cytochrome A, *cycA*; the cyclopropane/cyclopropene fatty acid synthesis RSP_1091 protein), gene regulation (the *tspO*-like RSP_1409 protein), transformation of thiols (RSP_3184 and *dsbG*), hypothetical functions (RSP_1465 and RSP_1852) (Glaeser *et al*., 2011; Dufour *et al*., 2008; Anthony *et al*., 2004) as well as the coding sRNA Pos19 (Müller *et al*., 2016). But interestingly RpoE also activates its own expression and the expression of a second alternative sigma factor, RpoHII (following information on the RpoHII regulon from Nuss *et al*., 2009). RpoHII, in turn, controls the expression of several genes encoding proteins involved in the GSH-dependent and –independent detoxification of $^1O_2$ reaction products. The genes controlled by RpoHII can be roughly divided into three groups. The first group containing genes that

function in the GSH-dependent detoxification of $^1O_2$, the second comprising genes encoding functions in the degradation of peroxides, and the third group including gene products involved in methylglyoxal removal. Moreover, iron storage proteins such as Bfr (bacterioferritin) and the ferredoxin-like protein (RSP_3164) acting beneficially under oxidative stress by restraining free iron from the Fenton reaction (1.2 and 1.8), are under the control of RpoHII. While the gene activation by RpoE alone does not exhibit a sufficient protection against $^1O_2$, together with the gene products triggered by the RpoE-dependent RpoHII, the removal of organic peroxides generated by the reaction of $^1O_2$ with macromolecules is provided, and accumulation of toxic by-products such as methylglyoxal is prevented. RpoHII above all shares a 46% amino acid identity with the alternative sigma factor RpoHI and both sigma factors were shown to complement a heat-sensitive *E. coli rpoH* mutant strain (Green and Donohue, 2006). Heat stress and photo-oxidative stress in natural habitats are both caused by high solar radiation; it is therefore not surprising, that these two stresses and the response they trigger are tightly linked in photosynthetic bacteria. The investigation of RpoHI and RpoHII in *R. sphaeroides* revealed that the two sigma factors share an overlapping regulon, including several genes encoding proteins and several sRNAs. Nevertheless, it is proposed that RpoHI is the major player in the heat stress response while RpoHII is more important in response to $^1O_2$ stress (Nuss *et al*., 2010).

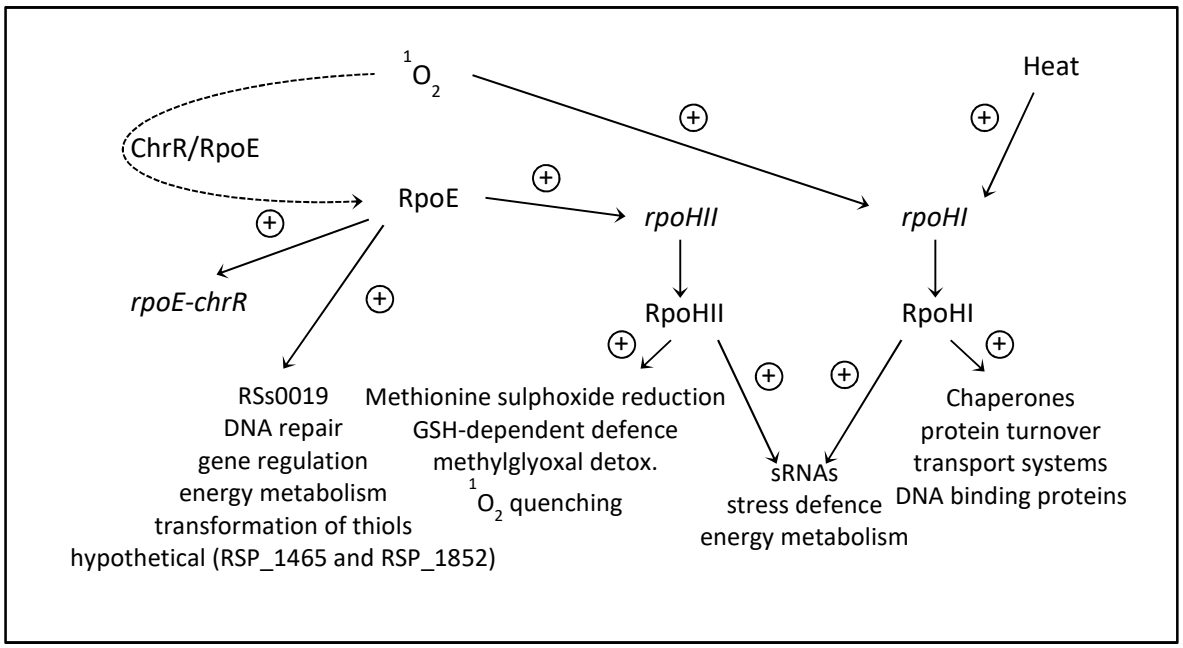

Figure 17: Sigma factor cascade in the stress response of *R. sphaeroides*. The scheme shows the three alternative sigma factors and their regulons described in 1.9.4. The release of RpoE from its anti-sigma factor ChrR upon $^1O_2$ stress is indicated by a dotted line. Activation of gene expression is depicted as +. Modified from Nuss *et al*., 2010.

1.9.5 Small regulatory RNAs in *Rhodobacter sphaeroides*

In chapter 1.1 the importance and variety of sRNAs as regulators was already described, in general. Thus the following chapter will additionally give only a brief insight into the state of knowledge about sRNA regulation in *R. sphaeroides*. Most of the sRNAs studied in *R. sphaeroides* were identified by an RNA-Seq study in 2009, (Berghoff *et al.*). Of the 20 sRNAs (18 in IGRs, 2 asRNAs) found to be upregulated upon $^1O_2$ stress up to now four were studied in more detail. The sRNA SorY (singlet oxygen resistance RNA Y, former RSs1543) which is induced in a RpoHII-dependent manner upon several additional stresses, including oxidative stress, heat stress, salt stress, and more. The over-expression of SorY confers an increased $^1O_2$ stress resistance by reducing the metabolite flux into the tricarboxylic acid cycle (TCA cycle) by decreasing malate import. This is achieved by direct interaction with the *takP* mRNA encoding a TRAP-T transporter (Adnan *et al*., 2015). A decrease of the TCA cycle activity is known to enhance the production of the protective NADPH over the prooxidant NADH (Bignucolo *et al*., 2013; Rui *et al*., 2010).

The sRNA SorX (singlet oxygen resistance RNA X, former RSs2461) was described increasing the resistance towards $^1O_2$ and H_2O_2 stress by reducing the spermidine import, which is achieved by targeting *potA* from the PotABCD spermidine transporter system. The RpoHI/II-induced sRNA SorX is derived from the 3' UTR of the mRNA of an OmpR-like regulator by RNase E cleavage (Peng *et al*., 2016).

Also, the sRNAs CcsR1-4 (conserved CCUCCUCCC motif stress-induced RNAs 1 to 4, former RSs0680a-d) are known to balance metabolic fluxes. The over-expression of CcsR1-4 leads to a decrease in expression of genes involved in the C1 metabolism, encoding components of the pyruvate dehydrogenase, as well as *flhR* encoding an activator of the glutathione-dependent methanol/formaldehyde metabolism. The FlhR-dependent downregulation of the pyruvate dehydrogenase complex reduces a primary target of ROS and additional reduces aerobic electron transport, a major source of ROS (Billenkamp *et al*., 2015).

As a fourth member of the studied sRNA regulators, PcrZ (Photosynthesis control RNA Z, former RSs2430) is found as homolog in all so far sequenced *R. sphaeroides* genomes while not in other species. PcrZ was shown to be induced PrrA and FnrL dependently upon a drop of oxygen tension and to be involved in the balanced formation of the photosynthetic apparatus (Mank *et al*., 2012). PcrZ counteracts the redox-dependent induction of the photosynthesis genes while being activated by PrrA, a positive regulator of the photosynthesis genes (incoherent feed-forward loop, 1.9.2).

1.10 Objective

In *R. sphaeroides* a variety of regulatory factors involved in the adaption to environmental changes and the follow-up alteration of the gene expression are known and studied (1.9.2 – 1.9.5). Hitherto, most of the characterised players, especially in the photosynthesis gene regulation, are so far represented by proteins. In the last years, regulatory sRNAs were identified as a versatile and potent group of bacterial regulators. Due to this growing interest in sRNA regulators as well as the availability of a sound basis of RNA-Seq data and established RNA-protocols in our group, the presented work was aimed towards a more detailed understanding of the role and function of sRNAs in *R. sphaeroides*. As described above (1.9.5) sRNAs in *R. sphaeroides* were found to be involved in the alteration of metabolic fluxes during stress conditions and the oxygen-dependent regulation of the photosynthesis genes. To characterise three additional sRNAs (Fig. 18), with potentially similar functions, they were investigated regarding their expression profiles, candidate target mRNAs, and biological function. The first investigated sRNA RSs0019 was known to be induced by $^1O_2$ stress in a RpoE-dependent manner (Berghoff *et al*., 2009). The second candidate RSspufX was of interest since it is found right downstream of *pufX*, the last gene of the *puf* operon, and apparently, shares a transcription terminator with the operon. The third sRNA in focus, RSs0827, was shown to be induced under iron-limiting conditions (Peuser *et al*., 2012).

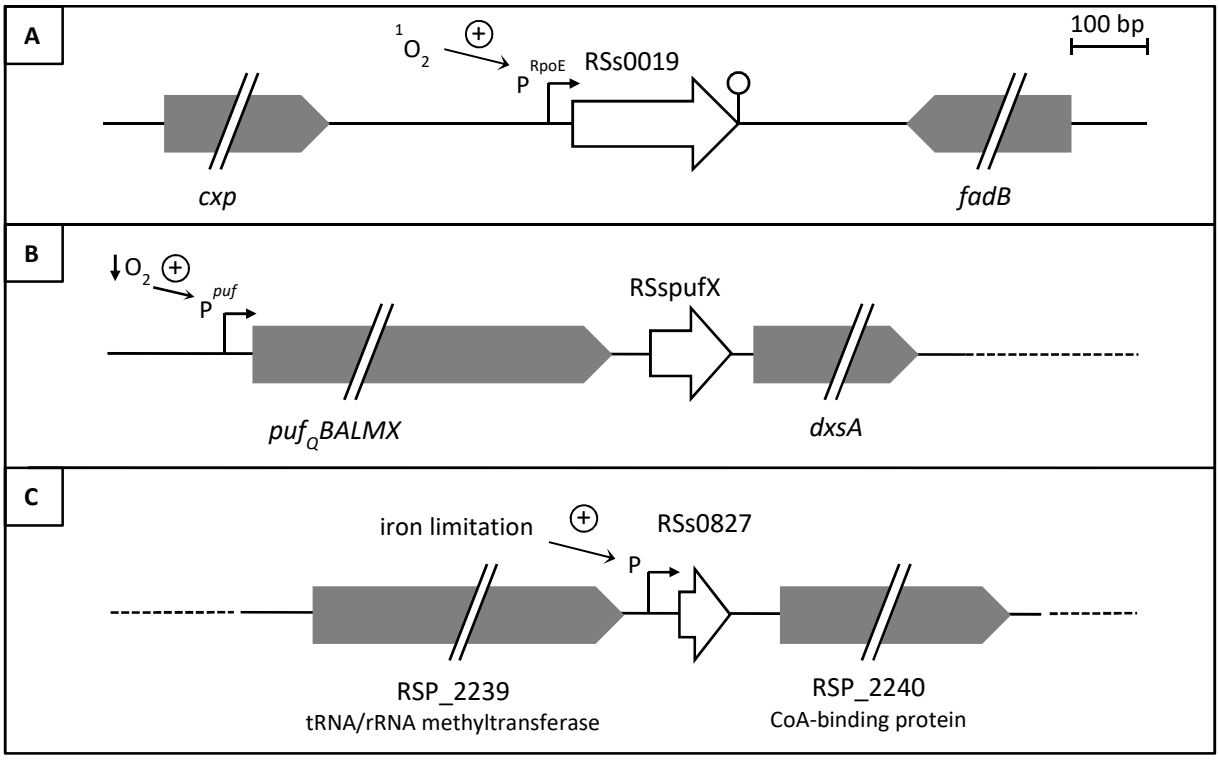

Figure 18: Illustration of the three *R. sphaeroides* sRNAs investigated in the presented work. (A) RSs0019 (219 nt) is encoded between the *cxp* and *fadB* gene on chromosome 2. Its expression upon $^1O_2$ stress is known to be RpoE-dependent. (B) The sRNA RSspufX (107 nt) is located 46 nt downstream of the *puf* operon and 20 nt upstream of the *dxsA* gene encoding a 1-deoxy-D-xylulose-5-phosphate synthase. A promotor structure could not be identified; the expression of the *puf* operon is known to be oxygen dependent. (C) RSs0827 (67 nt) is induced during iron-limiting conditions and is encoded between RSP_2239 and RSP_2240 on chromosome 1.

2. Material and Methods

2.1 Material

The material and methods chapter starts with a listing of the used strains, plasmids, oligonucleotides, laboratory material, equipment, and chemicals. Some compositions of standard buffers are listed below (2.1.10), while additional, specific buffers are described within the particular method chapters.

2.1.1 Strains

The strains used in this work are listed below in the order of their appearance in the text.

Table 1: Strains used in this work.

R. sphaeroides

Strain	**Description**	**Reference**
2.4.1	Wild-type	van Niel, 1944
TF18	*rpoE-chrR* mutation in 2.4.1, Tp^r	Schilke and Donohue, 1995
2.4.1 *rpoHI*:: ΩSp	*rpoHI* mutation in 2.4.1, Sp^r	Nuss *et al.,* 2009
2.4.1 *rpoHII*::Km	*rpoHII* mutation in 2.4.1, Km^r	Nuss *et al.,* 2009
2.4.1 *rpoHI*:: ΩSp, *rpoHII*::Km	*rpoHI* and *rpoHII* mutation in 2.4.1, Km^r, Sp^r	Nuss *et al.,* 2010
2.4.1 *pos19*::Km	*pos19* mutation in 2.4.1 (ΔPos19), Km^r	3.1.3
2.4.1 0557::Km	RSP_0557 mutation in 2.4.1 (Δ0557), Km^r	3.1.11
2.4.1 hfq::ΩSp	*hfq* mutation in 2.4.1 (Δhfq), Sp^r	Glaeser *et al.,* 2007
2.4.1 hfq+	2.4.1Δhfq harbouring pRK2.4.1*hfq*, Spr, Tc^r	Glaeser *et al.,* 2007
2.4.1 3xFLAGhfq+	2.4.1Δhfq harbouring pRK2.4.1-3xFLAG*hfq*, Sp^r, Tc^r	Berghoff *et al.*, 2011
2.4.1*prrA*:: Sp	*prrA* mutation in 2.4.1 (PRRA2), Sp^r	Eraso and Kaplan, 1995
2.4.1 *fnrL*:: ΩKm	*fnrL* mutation in 2.4.1 (JZ1678), Km^r	Zeilstra-Ryalls and Kaplan, 1995
2.4.1 Δrnj	RNase J (RSP_2534) mutation in 2.4.1, Km^r	T. Rische (3.2.5)
2.4.1 Δrnr	RNase R (RSP_1126) mutation in 2.4.1, Km^r	T. Rische (3.2.5)
2.4.1 Δrnc	RNase III (RSP_1675) mutation in 2.4.1, Km^r	L. Weber (3.2.5)
2.4.1 Δrnc/Δrnj	RNase III and RNase J mutation in 2.4.1, Km^r, Gm^r	T. Rische, K. Haberzettl (3.2.5)
2.4.1 ΔrppH	Mutation of putative RNA pyrophosphohydrolase (RSP_0931, *ialA*), Km^r	T. Rische, K. Haberzettl (3.2.5)

Table 1 continuing:

Strain	Description	Reference
2.4.1 ΔybeY	*YbeY* (RSP_3598) mutation in 2.4.1, Gm^r	T. Rische, K. Haberzettl (3.2.5)
2.4.1 RNE^{therm}	E. coli RNase E gene instead of	L. Weber
2.4.1 ΔspufX	RSspufX deletion, bp 3 – 39 were deleted	4.2.4
2.4.1 (pBBR_RSs0827)	Over-expression strain of RSs0827 with own promoter on pBBR1-MCS-2, Km^r	J. Kiebel, 2013
2.4.1 ΔRSs0827	RSs0827 mutation, Sp^r	J. Kiebel, 2013

E. coli

Strain	Description	Reference
JM109	*endA1, glnV44, thi*$^-$1, *relA1, gyrA96, mcrB*$^+$, Δ(*lac-proAB*), *e14*$^-$, [F', *traD36, proAB*$^+$, *laclq, lacZΔM15*], *hdsR*17, ($r_K^-m_K^+$)	Yanisch-Perron *et al*., 1985
S17-1	*recA, pro, hsdR, RP4*$^{-2}$-(Tc::Mu)(Km::Tn7); Tp^r, Sp^r, Str^r	Simon *et al*., 1983

2.1.2 Plasmids

Table 2: Plasmids used in this work. Listed as used in general and according to the respective project.

General

Plasmid	Description	Source/Reference
pDrive	cloning vector, Ap^r, Km^r	Qiagen
pJET	cloning vector, Ap^r	Qiagen
pUC4K	source of Km^r cassette, Km^r	Vieira and Messing, 1982
pPHU281	Suicide vector for *R. sphaeroides*, Tc^r	Hübner *et al*., 1991
pBBR1MCS-2	Broad-host-range cloning vector, pBBR1MCS derivative, Km^r	Kovach *et al*., 1995
pBBR1MCS-3	Broad-host-range cloning vector, pBBR1MCS derivative, Tc^r	Kovach *et al*., 1995
pBBR4352	pBBR1MCS-2 containing RSP_4352 promoter pBBR16S, Km^r	Y. Hermanns (3.1.11)
pBBR1MCS-3-*lacZ*	Broad-host-range *lacZ* fusion vector, Tc^r	Fried *et al*., 2012
pPHU235	Broad-host-range transl. *lacZ* fusion vector, Tc^r	Hübner *et al*., 1991
pPHU236	Broad-host-range transkrip. *lacZ* fusion vector, Tc^r	Hübner *et al*., 1991
pRK4352	pRK415 containing RSP_4352 promoter, Tc^r	Mank *et al.,* 2102

Table 2 continuing:

Plasmid	Description	Reference
pPHU4352	pPHU235 containing RSP_4352 promoter, Tc^r	Mank *et al.,* 2012
pLO1	Suicide vector; *sacB*, RP4 *oriT*, ColE1 *ori*	Lenz *et al*., 1994

RSs0019 project

Plasmid	Description	Reference
pD_Pos19	pDrive cloning vector containing Pos19 with own promoter, Ap^r, Km^r	3.1.2
pPos19	pBBR1 containing Pos19 with own promoter, Km^r or Tc^r	3.1.2
pRK16S::Pos19	pRK4352 containing the *pos19* gene, Tcr	3.1.3
pPHU0019::Km	pPHU281 derivative for pos19 deletion, Tc^r	3.1.3
pD_0019ORF	pDrive containing the Pos19 ORF, Ap^r, Km^r	3.1.4.1
pPHU-wtORF	pPHU236 containing Pos19-ORF fused to *lacZ*, Tc^r	3.1.4.1
pPHU-Stop16	pPHU-wtORF with codon 16 GGA to TGA exchange, Tc^r	3.1.4.1
pPHU-Stop1	pPHU-wtORF with ATG1 to TGA exchange, Tcr	3.1.4.1
pPHU-Thr1	pPHU-wtORF with ATG1 to ACG exchange, Tc^r	3.1.4.1
pPHU-Stop2	pPHU-wtORF with ATG2 to TGA exchange, Tc^r	3.1.4.1
pPHU-Thr2	pPHU-wtORF with ATG2 to ACG exchange, Tc^r	3.1.4.1
pPHU-M4	pPHU-wtORF with SD AGGA to TCCT exchange, Tc^r	3.1.4.1
pPHU-M8	pPHU-wtORF with SD AGAAAGGA to TCTTTCCT exchange, Tc^r	3.1.4.1
pRK_Pos19strep	pRK415 with Pos19-sORF fusion to a *Strep*-tag with own promoter, Km^r	3.1.4.2
pBE4352::eCFP::eCFP	ecfp fusion vector, Km^r	Remes *et al*., 2015
pBE::Pos19up+ORF::eCFP	Pos19-sORF fusion to ecfp with own promoter, Km^r	3.1.4.2
pPos19-Stop16	pPos19 with codon 16 GGA to TGA exchange, Km^r or Tc^r	3.1.5
pPos19-Stop1	pPos19 with start codon 1 ATG to TGA exchange, Km^r or Tc^r	3.1.5
pPos19-Thr1	pPos19 with start codon 1 ATG to ACG exchange, Km^r or Tc^r	3.1.5

Table 2 continuing:

Plasmid	Description	Reference
pPHU*puc2A*	pPHU4352 containing *puc2A* fragment for *lacZ* fusion, Tc^r	Mank *et al*., 2012
pPHU*bchN*	pPHU4352 containing *bchN* fragment for *lacZ* fusion, Tc^r	Mank *et al*., 2012
pD_0557	pDrive containing RSP_0557 fragment, Ap^r, Km^r	3.1.6
pPHU0557	pPHU4352 containing RSP_0557 fragment for *lacZ* fusion, Tc^r	3.1.6
pPHU*cysH*	pPHU4352 containing *cysH* fragment for *lacZ* fusion, Tc^r	3.1.6
pPHU*takP*	pPHU4352 containing *takP* fragment for *lacZ* fusion, Tc^r	Adnan *et al*., 2015
pPHU0557M1	pPHU4352 containing mutated RSP_0557 fragment M1 for *lacZ* fusion, Tc^r	3.1.8
pPHU0557M3	pPHU4352 containing mutated RSP_0557 fragment M3 for *lacZ* fusion, Tc^r	3.1.8
pPos19M1	pBBR1 containing mutated Pos19M1 with own promoter, Km^r	3.1.8
pPos19M3	pBBR1 containing mutated Pos19M3 with own promoter, Km^r	3.1.8
pPHU0557-1	pPHU4352 containing mutated RSP_0557 fragment 1 for *lacZ* fusion, Tc^r	3.1.8
pPHU0557-2	pPHU4352 containing mutated RSP_0557 fragment 2 for *lacZ* fusion, Tc^r	3.1.8
pPHU0557-3	pPHU4352 containing mutated RSP_0557 fragment 3 for *lacZ* fusion, Tc^r	3.1.8
pPHU0557-4	pPHU4352 containing mutated RSP_0557 fragment 4 for *lacZ* fusion, Tc^r	3.1.8
pBBR 0557up-*lacZ*	pBBR1-*lacZ* containing RSP_0557 fragment for transcriptional *lacZ* fusion, Tc^r	3.1.8
p16S::0557	pBBR4352 containing the RSP_0557 gene, Km^r	3.1.11
pPHU0557::Km	pPHU281 derivative for RSP_0557 deletion, Tc^r	3.1.11

Table 2 continuing:

RSspufX project		
Plasmid	**Description**	**Reference**
p16S_*lacZ*	pBBR1-*lacZ* containing the 16S rRNA promoter for transcriptional *lacZ* fusion, Tc^r	A. Laux (3.2.3)
pPX_*lacZ*	pBBR1-*lacZ* containing 326 nt upstream of *spufX* for transcriptional *lacZ* fusion, Tc^r	3.2.3
pP470_*lacZ*	pBBR1-*lacZ* containing 470 nt upstream of *spufX* for transcriptional *lacZ* fusion, Tc^r	3.2.3
pP1200_*lacZ*	pBBR1-*lacZ* containing 1276 nt upstream of *pufB* for transcriptional *lacZ* fusion, Tc^r	3.2.3
pD_PcrX	pDrive containing the RSspufX gene, Ap^r, Km^r	3.2.6
pPcrX	pBBR4352 containing the RSspufX gene under the control of the 16S rRNA promoter, Km^r	3.2.6
pD_pufX	pDrive containing *pufX* fragment, Ap^r, Km^r	3.2.8.1
pPHU_pufX	pPHU4352 containing *pufX* fragment for *lacZ* fusion, Tc^r	3.2.8.1
pPHU_pufXM3	pPHU4352 containing mutatetd *pufX* fragment M3 for *lacZ* fusion, Tc^r	3.2.8.1
pPHU_pufXM4	pPHU4352 containing mutatetd *pufX* fragment M4 for *lacZ* fusion, Tc^r	3.2.8.1
pPcrXM4	pBBR4352 containing the mutated PcrXM4 fragment, Km^r	3.2.8.1
pDT7_spufX	pDrive containing RSspufX with t7 promoter, Ap^r, Km^r	3.2.8.2
pdT7_pufX	pDrive containing *pufX* with t7 promoter, Ap^r, Km^r	3.2.8.2
RSs0827project		
Plasmid	**Description**	**Reference**
pBBR_RSs0827	pBBR1 containing the RSs0827 gene with own promoter, Km^r	J. Kiebel, 2013
pDrpoE	pDrive containing *rpoE* fragment, Ap^r, Km^r	3.3.1
pPHU_1092	pPHU4352 containing *rpoE* (RSP_1092) fragment for *lacZ* fusion, Tc^r	3.3.1
pPHU_1092M3	pPHU4352 containing mutatetd *rpoE* fragment M3 for *lacZ* fusion, Tc^r	3.3.2
pPHU_1092M4	pPHU4352 containing mutatetd *rpoE* fragment M4 for *lacZ* fusion, Tc^r	3.3.2

2.1.3 Oligonucleotides

The used oligonucleotides are listed separatley according to the three presented projects, in the order of their appearance in the text.

Table 3: Oligonucleotides used in this work, listed according to the respective project.

RSs0019 project

Name	Sequence 5' – 3'	Purpose
0019	GAGATAGCTCATCGGTCAGGTCC	Northern probe
5S	CTTGAGACGCAGTACCATTG	Northern probe
RSs0019_up	CGTGGTGGTCGGCTGAAC	Cloning – over-expression
RSs0019_down	GGCGGCAGGAAGGATGTC	Cloning – over-expression
1669-A (*rpoZ*)	ATCGCGGAAGAGACCCAGAG	RT-PCR
1669-B	CATCAGCTGGTAGCTCTC	RT-PCR
0557-A	CCATCTCCACCTTCCACTTC	RT-PCR
0557-B	CAGAGACCGATGTCGTCGAG	RT-PCR / Northern probe
0130-A (*metI*)	CACGCTTCAGACGCTCTACA	RT-PCR
0130-B	GAATAGCCGATGAGGCTGAC	RT-PCR
1351-A (*serC*)	CCTATTCGCTGGACCTTCTG	RT-PCR
1351-B	GTCGCAGATGGTGAGACCTT	RT-PCR
1941-A (*cysH*)	TGCATCTCGTCTCGGTCATC	RT-PCR
1941-B	TCGGTGTTGTAGCGGTTCAG	RT-PCR
1942-A (*cysI*)	AGTTCAAGATCGCCATGACC	RT-PCR
1942-B	GCCCGGTAGAAATCGTCATA	RT-PCR
3697-A (*cysP*)	AATGCGCGCTACACCTATCT	RT-PCR
3697-B	GTCATGCACCCGGTAGAAAT	RT-PCR
0799-A (*gloB*)	GAACAATTACGCCTTCTC	RT-PCR
0799-B	CATCAGCTGGTAGCTCTC	RT-PCR
1586-A (*cheW*)	CCTCCGGTTGTGACTTTCAT	RT-PCR
1568-B	AGAGCGGTGACCTGAATCAC	RT-PCR
0043-A (*cheY6*)	AGATCTGCATGCTGTCCTC	RT-PCR
0043-B	CTTCGAGATCATGCGAGAC	RT-PCR
0069-A (*fliC*)	TCGAACGACACCAACACC	RT-PCR
0069-B	CACCTTCATGCCGTTGAA	RT-PCR
0440-A (*sufB*)	ACATCGTGCGGCTGATCT	RT-PCR
0440-B	CGGCTTCACATCCATGCT	RT-PCR
0437-A (*sufC*)	GAGAAGAAGCGCAACGCG	RT-PCR
0437-B	GCGGATATGATCGACCAG	RT-PCR
0434-A (*sufD*)	CGCGGTTCTGCACCATTG	RT-PCR
0434-B	TTGGCCGTCAGCGTGAAG	RT-PCR
0443-A (*iscR*)	GGTGGAAGAGACGCTCAA	RT-PCR
0443-B	ATAGACATGCGCCGAGAC	RT-PCR
0442-A (*iscS*)	TAGAATCGGCGTTGTGCG	RT-PCR
0442-B	CGCCAGATCCATCTGCAT	RT-PCR
RSs0019_for_Bam	GGATCCCGATCAACCCAAGCAGAA	Cloning - over-expression
RSs0019_rev_Eco	GAATTCGGATGTCCCGCTCAGG	Cloning - over-expression
0019-up-Eco	GAATTCGCTCTACCGGCCGCACGAG	Cloning - knockout
0019-up-Pst	CTGCAGCCTGATCACGCCTCGGCCG	Cloning - knockout
0019-down-Sph	CTGCAGGAGCTTCCGACGACGCGAG	Cloning - knockout
0019-down-Pst	GCATGCGCGTGGCGGCCTTCCTCG	Cloning - knockout
0019-ORF-Hind	AAGCTTTCGGCCACGGCCGCCTCG	Cloning - *lacZ* fusion
0019_Stop16_fw	CACCCTCTGATTCGTGCTCGCGCTGGCC	Cloning
0019_Stop16_rev	CACGAATCAGAGGGTGCCGAAGGTCAG	Cloning
0019_Stop1_fw	CTGACCGTGAAGCTATCTCTTCATGGAATC	Cloning
0019_Stop1_rev	ATAGCTTCACGGTCAGGTCCTTTCTGCTTG	Cloning

Table 3 continuing:

Name	Sequence 5' – 3'	Purpose
0019_Thr1_fw	CTGACCGACGAGCTATCTCTTCATGGAATC	Cloning
0019_Thr1_rev	ATAGCTCGTCGGTCAGGTCCTTTCTGCTTG	Cloning
0019_Stop2_fw	CTCTTCTGAGAATCCGTTCTGACCTTCG	Cloning
0019_Stop2_rev	CGGATTCTCAGAAGAGATAGCTCATCGG	Cloning
0019_Thr2_fw	CTCTTCACGGAATCCGTTCTGACCTTCG	Cloning
0019_Thr2_rev	CGGATTCCGTGAAGAGATAGCTCATCGG	Cloning
0019_SD-M4_fw	CAAGCAGAATCCTCCTGACCGATGAGCTATC	Cloning
0019_SD-M4_rev	AGGAGGATTCTGCTTGGGTTGATCGTGCAC	Cloning
0019_SD-M8_fw	CAAGCTCTTTCCTCCTGACCGATGAGCTATC	Cloning
0019_SD-M8_rev	AGGAGGAAAGAGCTTGGGTTGATCGTGCAC	Cloning
0019ORFupHind	AAGCTTCGTGGTGGTCGGCTGAAC	*Strep*-tag cloning
0019ORFstrepPst	CTGCAG TCATTTTTCGAACTGCGGGTGGCTCCAAG CGCT TTCGGCCACGGCCGCCTC	*Strep*-tag cloning
0019_ORF_fw	TGGTCTAGACGTGGTGGTCGGCTGAACCACCCG	Cloning – *eCFP* fusion
0019_ORF_rev	TGGCATATGTTCGGCCACGGCCGCCTCGAGGCCCTG	Cloning – *eCFP* fusion
up-0557-for-Xho	CTCGAGGCTAGCACGAAGCGGGAACACCTG	Cloning – *lacZ* fusion
up-0557-rev-Hind	AAGCTTCGCCGGGCGGGTCGTCTCGAAG	Cloning – *lacZ* fusion
up-cysH-for-Bam	GGATCCGCGACGGCACCGAGACGGCG	Cloning – *lacZ* fusion
up-cysH-rev-Hind	AAGCTTGTGCTTGTAGCGACCGTTGAGC	Cloning – *lacZ* fusion
0019-M1-fw	CTCGAGCCGGCCGTGGCCGAATGATGC	Cloning
0019-M1-rev	CCACGGCCGGCTCGAGGCCCTGGCGGC	Cloning
0019-M3-fw	CTCGACCGGGCCGTGGCCGAATGATGC	Cloning
0019-M3-rev	CCACGGCCCGGTCGAGGCCCTGGCGGC	Cloning
0557-M1-fw	CATGGCCGGCTTCGAGACGACCCGCC	Cloning
0557-M1-rev	CTCGAAGCCGGCCATGGCGTCTGTCC	Cloning
0557-M3-fw	CATGGCCCGGTTCGAGACGACCCGCC	Cloning
0557-M3-rev	CTCGAACCGGGCCATGGCGTCTGTCC	Cloning
0557-mut1-fw	CGCCTTCCTGACGACCCGCCCGGCGCCC	Cloning
0557-mut1-rev	GGTCGTCAGGAAGGCGGCCATGGCGTCT	Cloning
0557-mut2-fw	GGCCGCGTACGAGACGACCCGCCCGGCGC	Cloning
0557-mut2-rev	GTCTCGTACGCGGCCATGGCGTCTGTCC	Cloning
0557-mut3-fw	GCCATGGGGGCCTTCGAGACGACCCGCC	Cloning
0557-mut3-rev	CGAAGGCCCCCATGGCGTCTGTCCTTTT	Cloning
0557-mut4-fw	ACAGACGGGATGGCCGCCTTCGAGACG	Cloning
0557-mut4-rev	CGGCCATCCCGTCTGTCCTTTTTTCAA	Cloning
GA_P0557_fw	GGTAGTCAATAAACCGGTCTTCTTCCGCGTGATAC	Cloning
GA_P0557_rev	GGGATCCACTAGTTCTAGAAACAGGCAAATAAGCC	Cloning
T7_0019_fwd	TAATACGACTCACTATAGGCACGATCAACCCAAG CAGAAAGG	Template ivT
T7_0019_rev	ACACCGGCCGGGCAATCG	Template ivT
T7_0557_fwd	TAATACGACTCACTATAGGCAGACGCAGCGATG CTGT	Template ivT
T7_0557_rev	CTGAGCTTCGACAGCGCC	Template ivT
0557-UTR-Bam	GGATCCAGACGCAGCGATGCTGTG	Cloning – over-expression
0557-down-Xba	TCTAGACTCGTGGCGCGGCTG	Cloning – over-expression
0557-up-EcoRI	CGCGAATTCATATTCGCCGACCGCCAG	Cloning - knockout
0557-up-PstI	CGCCTGCAGGAAGTGGAAGGTGGAGATGG	Cloning - knockout
0557-down-SphI	CGCGCATGCCCTATCTCGCCCAAGGATTC	Cloning - knockout
0557-down-Pst-2	CGCCTGCAGGGCGATATCGATGACATCTGC	Cloning - knockout

Table 3 continuing:

RSspufX project

Name	Sequence 5' – 3'	Purpose
NB_spufX.2	AAGGGAACCGGGCTGTGGTGTC	Northern probe
PX_fw_Age	ACCGGTCTGGCGGCGTGTTCT	Cloning – promoter fusion
P470_fw_Age	TGGACCGGTCGCCACGATGGAAGG	Cloning – promoter fusion
PX/P470_rev_Xba	TCTAGACGGCGATATGGCCC	Cloning – promoter fusion
P1200_fw_Age	TGGACCGGTCGCCAACATCGTCATG	Cloning – promoter fusion
P1200_rev_Xba	TGGTCTAGACGCCACATGCTGGTG	Cloning – promoter fusion
RT-pufX-fw	AAGACCAACCTTCGCCTCTG	RT-PCR / Co-transcription PCR
RT-pufX-rev	TTGATCAGCTCGATCCCGGT	RT-PCR
RT-spufX_rev	CACCAGGTCCCTGTCGCC	Co-transcription PCR
p-pufBA_fw	ACATCTGGCGTCCGTGGTTC	Template for Northern probe
p-pufBA_rev	ATCACCGCGAGGAGGAACAG	Template for Northern probe
p-14S	CTTAGATGTTTCAGTTCCC	Northern probe
Pas1-for-Bam	GGATCCTCCGGGCCATATCGCCG	Cloning – over-expression
Pas1-rev-Xba	TCTAGACGTGAATGTCAAAAGGGTGCCG	Cloning – over-expression
1669-A (*rpoZ*)	ATCGCGGAAGAGACCCAGAG	RT-PCR
1669-B	CATCAGCTGGTAGCTCTC	RT-PCR
6108-A *(pufB)*	CAGGCGCAGGAATTGCACTC	RT-PCR
6108-B	GAACCACGGACGCCAGATGT	RT-PCR
pufBA-A	CGAAGCCGAAGAAGTTCA	RT-PCR
pufBA-B	TTCACCACGAGCCAGATT	RT-PCR
0290-A	CTGCTCTATGTCATGTTCC	RT-PCR
0290-B	CGTCCTGCATGTTGAAGG	RT-PCR
1945-A	AGCGGAAGTTTCTCAAGG	RT-PCR
1945-B	CTTGATCTCCTCCATCGAG	RT-PCR
2376-A (*kbl*)	TCAACCATGCGAGCATCAT	RT-PCR
2376-B	GCAATCGTCCACCATGACA	RT-PCR
0285-A (*bchN*)	TCGAGGAGAAGGATCTCG	RT-PCR
0285-B	GAGCCGGAGAAGTTGTAGAC	RT-PCR
0261-A (*bchY*)	CAATTCGGAATCGCTCGT	RT-PCR
0261-B	ACGCAGAGGTTCGTCACC	RT-PCR
pufX_fw_Xho	TTGCTCGAGGGAGCGATCACAATGGCTGA	Cloning – *lacZ* fusion
pufX_rev_Hind	TGGAAGCTTGACGAGATGCTTGATCAGCTC	Cloning – *lacZ* fusion
pufX_fw_M3	GATGATCCGTGCGGGCTGGG	Cloning
pufX_rev_M3	CGCACGGATCATCATCTGGAA	Cloning
spufX_fw_M4	CGACACCACAGTAGAGTTCCCTTC	Cloning
spufX_rev_M4	AGGGAACTCTACTGTGGTGTCGC	Cloning
T7spufX_fw	TAATACGACTCACTATAGGGTCCGGGCCAT ATCGCCG	Template ivT
T7spufX-rev	TGTCAAAAGGGTGCCGTGCG	Template ivT
T7pufX_fw	TAATACGACTCACTATAGGGAAGACCAAC CTTCGCCT	Template ivT
T7pufX_rev	TCTCCTGGATCGGAAGCAT	Template ivT
T7sM4_fw	GCGACACCACGATTCGGTTC	Cloning
T7sM4_rev	GGAAGGGAACCGAATCGTGG	Cloning
T7XM4_fw	TGAAGGGTGCGAATCGGGC	Cloning
T7XM4_rev	CGCCAGCCCGATTCGCA	Cloning

Table 3 continuing:

RSsp0827 project		
Name	**Sequence 5' – 3'**	**Purpose**
1092_fwd_16S	TCTAGAAGGACGTTAAGATCACGGC	Cloning – *lacZ* fusion
1092_rev	AAGCTTCACCTTCGGCGCAAAG	Cloning – *lacZ* fusion
rpoE_M3_fw	CATGCGTGGCTTCCGGGA	Cloning
rpoE_M3_rev	CGGAAGCCACGCATGAGC	Cloning
rpoE_M4_fw	CTGGGTCGCGTCATGCGT	Cloning
rpoE_M4_rev	CATGACGCGACCCAGTCCG	Cloning
T7_0827_fw	TAATACGACTCACTATAGCCGTTCTACCTT CACTGTC	Template ivT
T7_0827_rev	AAAAAAAAGCGCCCTGAC	Template ivT
T7_rpoE_fw	TAATACGACTCACTATAGGGCAAGGGGA AGGCCT	Template ivT
T7_rpoE_rev	CTGCCGGATTTCATCAGGAAG	Template ivT

2.1.4 Laboratory Material and Equipment

Table 4: Particular material and equipment used in this work, listed alphabetically with manufacturers.

Material	**Manufacturer**
Electroblotter, *Perfect-Blue 'Semi-dry'-Blotter*	VWR PeqLab
Glaswool, silanized	Serva
Imaging Screen	Fuji / Bio-Rad
Membrane Filter, *Cellulose Nitrate*	GE Healthcare
Nylonmembrane, *Roti®-Nylon plus*, 0.45 µm	Roth
Oxygen electrode, *GMH 3610*	Greisinger
PCR RT cyler, *Rotor-Gene 300*	Qiagen
PCR cyler, *Thermal cyler S1000* and *T100*	Bio-Rad
Phosphoimager (*Molecular Imager FX*)	Bio-Rad
Scintillation counter	Beckmann Coulter
Spectrophotometer, *Specord 50*	Analytik Jena
Ultrasound sonicator, *Sonoplus GM70*	Bandlin
Vacuum blotter	Appligene
Vacuum dryer, *concentrator plus*	Eppendorf

2.1.5 Size standards for gel electrophoresis

Size standard	Manufacturer
GeneRuler 1 kb Plus	Thermo Scientific
GeneRuler 100 bp Plus	Thermo Scientific
PageRuler™	Thermo Scientific

2.1.6 Radioactive nucleotides

Nucleotide	Manufacturer
[γ32P]ATP; 3000 Ci/mmol	Hartmann Analytik
[γ32P]CTP; 3000 Ci/mmol	Hartmann Analytik
[γ32P]UTP; 3000 Ci/mmol	Hartmann Analytik

2.1.7 Molecular biological kits

Table 5: Molecular biological used in this work, listed alphabetically with manufacturers.

Kit	Purpose	Manufacturer
Brilliant III Ultra-Fast SYBR® Green QPCR	RT-PCR	Agilent
innuPREP DOUBLEpure	DNA gel extraction and PCR purification	Analytik Jena
Lumi-LightPLUS Western Blotting	Western blot development	Roche
Prime-a-Gene® Labeling System	Random priming for probe labelling	Promega
QIAex Gel Extraction	DNA gelextraction	Qiagen

2.1.8 Enzymes

Table 6: Enzymes used in this work, listed alphabetically with manufacturers. All restriction endonucleases used (not listed) were manufactured by Thermo Scientific.

Enyzme	Manufacturer
DNase I (50-375 U/µl)	Invitrogen
Glutathione Reductase (1 U /µl)	Sigma-Aldrich
Lysozym	Boehringer Ingelheim
Proteinase K	Sigma Aldrich
RNase A (7 U/µl)	Qiagen
RNasin® (20-40 U/µl)	Promega
T4 DNA ligase (5 U/µl)	NEB
T4 Polynucleotide kinase (10 U/µl)	NEB
T7 RNA polymerase (50 U/µl)	NEB

2.1.9 Chemicals and Antibiotics

Table 7: Crucial chemicals used in this work, listed alphabetically with manufacturers. Standard chemicals were obtained from Roth and Sigma-Aldrich, unless specified otherwise.

Material	**Manufacturer**
Bovine serum albumin, Fraction V	Roth
ß-mercaptoethanol	Roth
Bradford reagent, *Rotiquant*	Roth
Dimethyl sulfoxide	Roth
DTT, 1,4-Dithiothreitol	Sigma Aldrich
Fe-(II)-citrate	Sigma Aldrich
Formaldehyde	Applichem
Formamide	Applichem
L-Glutathione reduced (≥98.0%)	Sigma Aldrich
Hydrogen peroxide	Roth
Magnesium sulphate	Merk
Methylene blue	Sigma Aldrich
NADPH	Roth
Ortho-Nitrophenyl-β-galactoside	Serva
Paraquat dichloride hydrate	Sigma Aldrich
peqGOLD TriFast reagent	Peqlab
Sodium chloride, NaCl (> 99.8%)	Roth
Sodium dodecyl sulphate, SDS	Serva
Sodium hydroxide, NaOH (> 99%), Pearls	Roth
5-Sulfosalicylic acid dihydrate	Sigma Aldrich
Tert-butyl hydroperoxide	Sigma

Table 8: Antibiotics used in this work, listed alphabetically with manufacturers.

Material	**Manufacturer**
Ampicillin	Roth
Gentamycin	Roth
Kanamycin	Roth
Rifampicin	Serva
Spectinomycin	Sigma Aldrich
Streptomycin	Serva
Tertracyclin	Serva
Trimethoprim	Roth

2.1.10 Standard buffers and solutions

Table 9: Composition of common solutions and buffers in alphabetical order.

10% CTAB w/V in 0.7 M NaCl		
Component	**Amount**	
Sodium chloride	4.1g	[0.7 M]
ddH_2O	80 ml	
Cetrimonium bromide	10 g	[10%]
	stir and heat (65°C) until dissolved	
ddH_2O	*ad* 100 ml	
DNase I buffer (for Invitogen DNase I; 10 ml)		
Component	**Amount**	
1M Tris HCl pH 8.4	2 ml	[200 mM]
1M $MgCl_2$	0.2 ml	[20 mM]
1M KCl	5 ml	[500 mM]
ddH_2O	*ad* 10 ml	
10x Laemmli buffer (1 l)		
Component	**Amount**	
Tris HCl	30 g	[0.19 M]
Glycin	144 g	[1.9 M]
SDS	10 g	[1 %]
ddH2O	*ad* 1000 ml	
10x MOPS (1 l)		
Component	**Amount**	
3-(N-morpholino) propanesulfonic acid (MOPS)	41.9 g	[200 mM]
Sodium acetate tetrahydrate	8.2 g	[50 mM]
EDTA (disodium salt)	3.72 g	[10 mM]
ddH_2O	800 ml	
	adjust the pH to 7.0	
ddH_2O	*ad* 1000 ml	
5M NaCl (100 ml)		
Component	**Amount**	
Sodium chloride	29.2 g	[5 M]
ddH_2O	80 ml	
	stir until dissolved	
ddH_2O	*ad* 100 ml	
5N NaOH (100 ml)		
Component	**Amount**	
Sodium hydroxide	20 g	
ddH_2O	80 ml	
	stir and cool until dissolved	
ddH_2O	*ad* 100 ml	

Table 9 continuing:

1x Phosphate-buffered saline, PBS (1 l)		
Component	**Amount**	
KH_2PO_4	0.24 g	[1.47 mM]
Na_2HPO_4	1.44 g	[4.3 mM]
Potassium chloride	0.2 g	[2.7 mM]
Sodium chloride	8.0 g	[137 mM]
ddH_2O	800 ml	
adjust the pH to 7.4 with concentrated HCl		
ddH_2O	*ad* 1 l	
20% SDS w/v (100 ml)		
Component	**Amount**	
Sodium dodecyl sulfate	20 g	[20%]
ddH_2O	*ad* 100 ml	
20x SSC (1 l)		
Component	**Amount**	
Sodium chloride	175.32 g	[3 M]
Sodium citrate dihydrate	77.42 g	[0.3 M]
ddH_2O	*ad* 1 l	
20x SSPE (1 l)		
Component	**Amount**	
NaH_2PO_4	24 g	[0.2 M]
Sodium chloride	175.32 g	[3 M]
EDTA (disodium salt)	5.84 g	[0.02 M]
ddH_2O	800 ml	
adjust the pH to 7 with concentrated HCl		
ddH_2O	*ad* 1 l	
STE buffer (100 ml)		
Component	**Amount**	
5M NaCl	2 ml	[100 mM]
1M Tris HCl pH 7.5	2 ml	[20 mM]
EDTA (disodium salt)	0.37 g	[0.01 M]
ddH_2O	*ad* 100 ml	
10x TAE (Tris, acetic acid, and EDTA; 1l)		
Component	**Amount**	
Tris base [tris(hydroxymethyl)aminomethane]	48.4 g	[0.4 M]
Glacial acetic acid	11.4 ml	[0.2 M]
EDTA (disodium salt)	3.7 g	[0.01 M]
ddH_2O	*ad* 1 l	
10x TBE (Tris, borate, and EDTA; 1l)		
Component	**Amount**	
Tris base [tris(hydroxymethyl)aminomethane]	121.1 g	[1 M]
Boric acid	61.8 g	[1 M]
EDTA (disodium salt)	7.4 g	[0.02 M]
ddH_2O	*ad* 1 l	

Table 9 continuing:

TE buffer (100 ml)		
Component	**Amount**	
1M Tris HCl pH 8.0	1 ml	[10 mM]
EDTA (disodium salt)	0.04 g	[1 mM]
ddH_2O	*ad* 100 ml	
1x Tris-buffered saline, TBS (1 l)		
Component	**Amount**	
Tris	6.05 g	[50 mM]
Sodium chloride	8.76 g	[150 mM]
ddH_2O	800 ml	
adjust the pH to 7.5 with concentrated HCl		
ddH_2O	*ad* 1 l	
1M Tris HCl, various pH (100 ml)		
Component	**Amount**	
Tris base [tris(hydroxymethyl)aminomethane]	12.1 g	[1 M]
ddH_2O	80 ml	
adjust the pH with concentrated HCl		
ddH_2O	*ad* 100 ml	

Table 10: Potassium phosphate buffer. Composition for 100 ml 1M potassium phosphate buffer from 1M potassium phosphate dibasic (K_2HPO_4) and 1M potassium phosphate monobasic (KH_2PO_4) buffers.

pH	**1M K_2HPO_4 [ml]**	**1M KH_2PO_4 [ml]**
5.8	8.5	91.5
6.0	13.2	86.8
6.2	19.2	80.8
6.4	27.8	72.2
6.6	38.1	61.9
6.8	49.7	50.3
7.0	61.5	38.5
7.2	71.7	28.3
7.4	80.2	19.8
7.6	86.6	13.4
7.8	90.8	9.2
8.0	94.0	6.0

Table 11: Composition of loading-dyes for DNA and RNA.

DNA loading-dye	
Component	**Concentration**
Glycerin	60%
Bromphenol blue	0.1%
Xylene cyanol	0.1%
RNA loading-dye for PAA-urea gel (FU mix)	
Component	**Concentration**
Urea	6 M
Formaide, deionized	80%
10x TBE	10%
Bromphenol blue	0.1%
Xylene cyanol	0.1%
RNA loading-dye for Foramide-agarose gel	
Component	**Concentration**
Glycerine	60%
Bromphenol blue	0.1%
EDTA	0.01M
adjust the pH to 7.0 with concentrated HCl	
EMSA loading dye	
Component	**Concentration**
TBE	0.05x
Glycerine	50%
Bromphenol blue	0.1 %
5x SDS loading dye for proteins	
Component	**Concentration**
Tris HCl	0.225 M
Glycerine	50%
SDS	50%
Bromphenol blue	0.05%
DTT	0.25 M

2.2 Microbiological Methods

2.2.1 *Rhodobacter sphaeroides* liquid culture

R. sphaeroides liquid cultures are incubated shaking (140 rpm) at 32°C in Rhodobacter malate medium (*Rhodobacter Äpfelsäure*, RÄ; Tab. 12). The medium has to be supplemented with 8 ml vitamins (Tab. 14) and 20 ml phosphate per litre (Tab. 15). Antibiotics needed for selection are added according to table 18. For inoculation, cell material is taken with a sterile inoculating loop from glycerine stock (2.2.7) or plate culture (2.2.4) and is added to the media. Particular growth conditions are described in the following chapters. To ensure the cells have completely adapted to the desired conditions before starting an experiment, it is necessary to incubate the cells at least for one doubling time.

Table 12: Composition of 1 litre Rhodobacter malate medium (RÄ).

Component	**Amount**	**Action**
Malic acid	3.0 g	[20 mM]
Ammonium sulphate	1.2 g	[9 mM]
Magnesium sulphate-7-dihydrate	0.2 g	[0.8 mM]
Calciumchloride dihydrate	0.07 g	[0.4 mM]
Trace elements solution (Tab. 13)	1.5 ml	
ddH_2O	*ad* 1 l	
		Autoclave
Vitamins (Tab. 14)	8 ml	
Phosphate (Tab. 15)	20 ml	

Table 13: Composition of 1 litre trace elements solution for Rhodobacter malate medium.

Component	**Amount**	**Action**
Fe-(II)-citrate	500 mg	[2 mM]
MgCl2 x 4 H2O	20 mg	[0.05 mM]
ZnCl2	5 mg	[0.03 mM]
LiCl	5 mg	[0.1 mM]
KI	2.5 mg	[0.02 mM]
KBr	2.5 mg	[0.02 mM]
CuSO4	0.15 mg	[0.9 µM]
Na2MoO4 x 2 H2O	1 mg	[0.002 mM]
CoC12 x 6 H2O	5 mg	[0.02 mM]
SnCl2 x 2 H2O	0.5 mg	[0.002 mM]
BaCl2	0.5 mg	[0.002 mM]
AlCl3	1 mg	[0.007 mM]
H3BO4	10 mg	[0.1 mM]
EDTA	20 mg	[0.06 mM]
ddH2O	ad 1 l	
		Autoclave

Table 14: Composition of 1 litre Vitamins for Rhodobacter malate medium.

Component	Amount	Action
Niacin	3.0 g	[24 mM]
Thiamine hydrochloride	1.2 g	[3.5 mM]
Nicotinamide	0.2 g	[1.6 mM]
Biotin	0.07 g	[0.3 mM]
ddH_2O	*ad* 1 l	
		Autoclave

Table 15: Composition of 1 litre phosphate solution for Rhodobacter malate medium.

Component	Amount	Action
Potassium phosphate dibasic	45 g	[260 mM]
Potassium phosphate monobasic	35g	[250 mM]
ddH_2O	*ad* 1 l	
		Autoclave

2.2.1.1 Aerobic cultivation of *Rhodobacter sphaeroides*

For aerobic growth, *R. sphaeroides* cultures are incubated in baffled flasks, filled to 40 percent of their capacity. The cultures are incubated shaking at 140 rpm at 32°C. These conditions result in an oxygen content of 5 - 6 mg/l O_2 in the culture.

A second method to incubate cultures aerobically is used for the singlet oxygen stress experiment. Here the cultures are grown in *Meplat* bottles and are aerated trough *Pasteur* pipettes via an aquarium pump, which also leads to an oxygen content of 5 - 6 mg/l O_2. The optimal growth temperature of 32°C is here ensured via a water bath.

2.2.1.2 Microaerobic cultivation of *Rhodobacter sphaeroides*

To achieve microaerobic conditions, resulting in an oxygen content of about 0.5 mg/l, *Erlenmeyer* flasks are filled to 75 percent of their capacity. Cultures are incubated shaking at 140 rpm and 32°C as well.

2.2.1.3 Phototrophic cultivation of *Rhodobacter sphaeroides*

Phototrophic cultivation is carried out in completely filled, airtight sealed *Meplat* bottles. The cultures are incubated at 32°C and are illuminated permanently with white light (60 W/m^2, fluorescent tube, TLD 58W/25). Under these conditions, the cells will perform anoxygenic photosynthesis.

2.2.1.4 Anaerobic cultivation of *Rhodobacter sphaeroides*

In favour of anaerobic growth in the dark, the cultures are complemented with 0.5% v/v of dimethyl sulfoxide (DMSO) as a terminal electron acceptor. In addition, 0.1% yeast extract (10% w/v stock, autoclaved) is added. Incubation of anaerobic cultures is carried out shaking at 32°C in completely filled 50 ml *Sarstedt* falcons which are sealed light- and airtight.

2.2.1.5 Aerobic cultivation with subsequent photo-oxidative stress

For the so-called stress experiment, the *R. sphaeroides* cultures are grown under aerobic conditions to the exponential growth phase and are illuminated with high light starting from a defined time point to obtain photo-oxidative stress conditions. The addition of the photosensitiser methylene blue leads to increased formation of singlet oxygen.

The cultures are prepared in *Meplat* bottles (60 ml in a 100 ml bottle; 2.2.1.1) and methylene blue is added to a final concentration of 0.2 µM. The bottles are packed light-tight in tinfoil and are placed in a heated water bath at 32°C. There the cultures are aerated with air via an aquarium pump trough *Pasteur* pipettes resulting in approx. 5 - 6 mg/l dissolved oxygen in the cultures. When the cultures reached the desired $OD_{660,}$ the tinfoil is removed, and the cultures are illuminated with high light intensities (800 W/m^2 white light, 500 W halogen heater).

2.2.1.6 Microaerobic cultivation of *Rhodobacter sphaeroides* under iron limitation

To achieve iron-limiting conditions, *R. sphaeroides* is cultivated without adding external iron to the RÄ medium and transferring 1 ml of preculture into fresh iron-free medium (composition of medium Tab. 12; prepared with Fe-(II)-citrate **free** trace elements) three times. Also, the iron chelator 2,2'-dipyridil (Merck) is added to the third culture step in a final concentration of 30 µM.

2.2.1.7 Microaerobic cultivation of *Rhodobacter sphaeroides* under sulphur reduction

The growth of *R. sphaeroides* under sulphur-reduced conditions was achieved by reducing the sulphur concentration in the RÄ medium (Tab. 12) to a fourth of the standard concentration and preparing two pre-cultures steps in the sulphur-reduced medium before the experiments. The ammonium sulphate was reduced to 0.3 g per litre, while 0.72 g ammonium chloride were added to compensate the thus lacking ammonium (Tab. 16).

Table 16: Composition of 1 litre sulphur-reduced Rhodobacter malate medium (RÄ).

Component	Amount	Action
Malic acid	3.0 g	[20 mM]
Ammonium sulphate	0.3 g	[2.3 mM]
Ammonium chloride	0.72 g	[13.5 mM]
Magnesium sulphate-7-dihydrate	0.2 g	[0.8 mM]
Calciumchloride dihydrate	0.07 g	[0.4 mM]
Trace elements solution (Tab. 13)	1.5 ml	
ddH_2O	*ad* 1 l	
		Autoclave
Vitamins (Tab. 14)	8 ml	
Phosphate (Tab. 15)	20 ml	

2.2.1.8 Cultivation of *Rhodobacter sphaeroides* while shifting the growth conditions

Some RNAs investigated in this work are found to be induced by a drop of the oxygen tension. To provide for this drop of oxygen tension the liquid cultures are prepared for aerobic growth in baffled flasks (2.2.1.1), cultivated to the desired OD_{660} and after sampling a sufficient amount of culture is transferred to an *Erlenmeyer* flask for microaerobic growth (2.2.1.2). To shift a culture to phototrophic growth conditions, it has to be transferred to *Meplat* bottles and illuminated as described in 2.2.1.3.

2.2.2 *Rhodobacter sphaeroides* growth analysis

To compare the growth of two or more *R. sphaeroides* strains, pre-cultures of biological triplicates of each strain are prepared under the growth conditions investigated, with respective antibiotics added to the medium. The next day the pre-cultures should be in the exponential growth phase (OD_{660} 0.4 – 0.8) and are diluted to an OD_{660} of 0.1 or 0.2 (the latter for iron-limiting conditions) without the addition of antibiotics. The growth under the desired conditions is monitored by measuring the OD_{660} every 1.5 h or 3 h, the latter for phototrophic growth. At each timer point, the sample volume is replaced by fresh medium under sterile conditions.

2.2.3 *Rhodobacter sphaeroides* cultivation for determination of RNA half-life

To determine the half-life (t ½) of an RNA first of all the transcription in the cells has to be arrested. This arrest is achieved by the addition of the antibiotic rifampicin to the growing culture. Rifampicin specifically inhibits the DNA-dependent RNA-polymerase (Hartmann *et al*., 1967) which prevents further transcription of RNA and subsequently only allows degradation of RNA. Samples for RNA

isolation are taken directly before addition of rifampicin (t 0) and at pre-defined time points after the addition. With this set-up the decay of RNA over time can be determined afterwards, using RNA quantification methods such as Northern blot (2.4.6) or qRT-PCR (2.2.4.3.3). The time in which half of the amount of the analysed RNA was degraded is defined as its half-life.

The *R. sphaeroides* culture of interest is incubated under the desired growth condition (2.2.1.1-7) to the desired growth phase. After taking sample t 0, rifampicin (dissolved in water and 3.2% 5N NaOH) is added to a final concentration of 0.2 mg/ml. Cells are harvested (10.000 rpm, 10 min, 4°C) at the defined time points and the pellets are frozen at -20°C until RNA isolation (2.4.7.3).

2.2.4 *Rhodobacter sphaeroides* plate culture

Agar plates for *R. sphaeroides* cultivation are prepared from molten RÄ agar (8 g bacto agar per 0.5 l RÄ Tab. 12) which is supplemented with 20 ml phosphate (Tab. 15) and 8 ml vitamins (Tab. 14) per litre. Antibiotics needed for selection are added according to table 18 before pouring the lukewarm agar into Petri dishes. The plates are then allowed to cool until the agar is solidified. *R. sphaeroides* cell material from a glycerine stock (2.2.7), or a liquid culture (2.2.1) is spread on the agar plate with a sterile inoculation loop or *Drigalski* spatula, respectively. By spreading small amounts of cell material or dilution series on plates, single colonies can be obtained. Plates are wrapped with cling film and incubated at 32°C. For incubation the plates are placed upside down, to prevent condensed water from the lid of the Petri dish to drop onto the agar.

2.2.5 *Escherichia coli* liquid culture

E. coli liquid cultures are incubated in test tubes (3 - 5 ml) or *Erlenmeyer* flasks filled to 60% of their capacity with Standard-I Medium (St-I, Tab. 17) at 37°C in the dark, shaking at 180 rpm for aerobic conditions. The here indicated shaking speed applies to all *E. coli* cultures described unless mentioned otherwise. Antibiotics for selection are added to the medium according to table 18. Inoculation is carried out as described for *R. sphaeroides*, see 2.2.1.

Table 17: Composition of 1 litre Standard I medium.

Component	**Amount**	**Action**
Standard I Nutrient agar	25 g	
ddH_2O	*ad* 1 l	
		Autoclave

2.2.6 *Escherichia coli* plate culture

For *E.coli* plate cultures, agar plates are prepared from molten St-I agar (8 g bacto agar (Gibco) per 0.5 l St-I medium Tab. 17) in Petri dishes. Antibiotics needed for selection are added according to table 18 before pouring the agar. Spreading of cell material from an *E. coli* glycerine stock (2.2.7) or a liquid culture (2.2.5) on the plate is done with a sterile inoculation loop or *Drigalski* spatula, respectively. By spreading small amounts of cell material or dilution series on plates, single colonies can be obtained. Plates are wrapped with cling film and incubated at 37°C. For incubation the plates are placed upside down, to prevent condensed water from the lid of the Petri dish to drop onto the agar

Table 18: Concentrations of antibiotics for *R. sphaeroides* and *E.coli* cultivation.

Antibiotic	**Stock [mg/ml]**	**dissolved in**	***R.spaheroides* [µg/ml]**	***E.coli* [µg/ml]**
Tetracycline	10	75% ethanol	15	200
Kanamycin	10	water	250	250
Ampicillin	100	water	-	200
Gentamycin	4	water	250	250
Streptomycin	1.5	water	250	660
Spectinomycin	10	water	100	100
Trimethoprim	25	DMF*	200	-

*DMF = Dimethylformamide

2.2.7 Glycerine stocks

The here described procedure for the preparation of glycerine stocks applies for both, *R. sphaeroides* and *E. coli*. Glycerine stocks are used to store bacterial strains at -80°C permanently.

The preparation should take place using filter tips, on ice and with precooled solutions. Cells from two times 2 ml of an exponential grown liquid culture (OD 0.4 – 0.6) are harvested at 8.000 rpm in a table top centrifuge (*biofuge pico 17*) at RT. To get rid of any remaining antibiotics in the medium the supernatant is discarded, and the cells are resuspended in 1 ml of the respective medium. After repeated centrifugation, the supernatant is discarded, and one cell pellet is resuspended in 750 µl of the respective medium and combined with the second cell pellet. The cell suspension is subsequently mixed with cold 80% glycerine in a 2 ml cryovial (Roth) and immediately frozen in liquid nitrogen. As a result, the cells can be stored at -80°C without taking any greater harm. For inoculation of liquid or plate cultures, the glycerine stocks can be transported and stored short-time in liquid nitrogen.

2.2.8 Optical density measurement of liquid cultures

Based on the spectrophotometrically measured optical density (OD) one can determine the total amount of cells in a culture and the cells growth phase. For the measurement 1 ml of the respective liquid culture is transferred into a polystyrene cuvette while 1 ml of medium serves as the reference ("blank"). The OD of *R. sphaeroides* is measured at 660 nm whereas the OD of *E. coli* is measured at 600 nm. An OD of 1 for *R. sphaeroides* is equivalent to $2*10^9$ cells/ml and for *E. coli* to $5*10^8$ cells/ml. Samples with an OD higher than 1 should be diluted and measured again.

2.2.9 Full-cell spectra of *Rhodobacter sphaeroides*

The pigment-protein complexes of *R. sphaeroides* absorb light with different wavelengths; therefore their composition and relative amount can be measured and illustrated as absorption values between 300 and 950 nm. To measure a full-cell spectrum, 1 ml of medium as reference and 1 ml liquid culture are given into polystyrene cuvettes each, and a pre-set program of the spectrophotometer measuring the absorbance in one nm steps is used, placing the cuvette in the rear tray. The spectra of different samples can be normalised to OD_{660}.

2.2.10 Measurement of the bacteriochlorophyll content of *Rhodobacter sphaeroides*

To measure the cells' bacteriochlorophyll content, the bacteriochlorophyll is extracted with a mixture of acetone and methanol (7:2). For this purpose, the OD_{660} of the respective *R. sphaeroides* culture is measured (2.2.8), and cells from 1 ml of the culture are harvested (13.000 rpm, 5 min, RT; *biofuge pico 17*). The cell pellet is resuspended in 50 µl Roth H_2O, and 500 µl of the acetone/methanol mixture is added. After vortexing the sample for 10 sec and centrifugation at 13.000 rpm for 5 minutes (RT, *biofuge pico 17*), the absorption of the supernatant can be measured in a quartz cuvette. Acetone/methanol is used as reference and the absorption is measured at 770 nm. The bacteriochlorophyll concentration is calculated using the extinction coefficient of 76 mM^{-1} cm^{-1} at 770 nm (Clayton, 1966) as follows:

Calculation 1: BChl µM / OD_{660} = $$\frac{Abs770 \; x \; 1000 \; x \; V \; acteone/methanol}{76 \; x \; 1 \; x \; V \; cells \; x \; OD660}$$

V: volume

2.2.10 a Quantification of the light harvesting complexes of *Rhodobacter sphaeroides*

For the quantification of the light harvesting complexes I and II (LHC I and II) as described by Oh and Kaplan (1998), *R. sphaeroides* is cultivated anaerobically as described in 2.2.1.4 (or under any other desired growth condition). When the cultures reach the exponential growth phase (OD_{660} 0.4 - 0.6), 30 ml are centrifuged at 8.000 rpm for 15 minutes at 4°C (*Sorvall RC 6 plus*/*RC 5C plus*). The harvested cells are resuspended in 500 µl 1x ICM buffer (Tab. 19) and transferred into 1.5 ml microcentrifuge tubes. Afterwards, the cells are broken by sonication with the *Sonoplus GM70* (parameters: Power MS 72/D, cycle 70%, 30 sec). Every cell sample is sonicated on ice five times pausing for 30 seconds to cool down between the sonication steps. Cell debris and insoluble proteins are pelleted by centrifugation (13.000 rpm, 20 min, 4°C; *biofuge fresco 17*). The supernatants are transferred into virgin 1.5 ml microcentrifuge tubes, and the protein concentration is determined with the help of a Bradford assay (2.5.1). On the basis of the total protein concentration the later measured values for the respective proteins can be normalised. For each measurement 300 µl of cell extract are mixed with 600 µl 1x ICM buffer in a cuvette and the absorption is measured at 820, 849, 878, and 900 nm using 900 µl of 1x ICM buffer as reference. The obtained values can be used to calculate the amount of the light harvesting complexes as follows:

Calculation 2:

LHC I: B_{875nm} $$(\text{nmoles / mg protein}) = [(73\ (\text{Abs}_{878\text{nm}} - \text{Abs}_{820\text{nm}}))/2] \text{ / mg protein}$$

LHC II: $B_{800\text{-}850nm}$ $$(\text{nmoles / mg protein}) = [(96\ (\text{Abs}_{849\text{nm}} - \text{Abs}_{900\text{nm}}))/3] \text{ / mg protein}$$

Table 19: Composition of 50 ml 10x ICM buffer for quantification of light harvesting complexes.

Component	**Amount**	
EDTA [250 mM]	2 ml	[10 mM]
Potassium phosphate buffer [1M] pH 7.2	5 ml	[100 mM]
ddH_2O	*ad* 50 ml	

2.2.10 b Cell-free spectra of *Rhodobacter sphaeroides*

A second method to measure the absorption spectra (2.2.9) is using cell-free extracts, more precise the cell debris-free supernatant after sonication and centrifugation (2.2.10 a). Especially the peaks for the carotenoids can be measured more distinct in such samples. Since for those samples, one cannot normalise to the OD, the protein concentration of the supernatant needs to be determined as described in 2.5.1, so that equal amounts of protein can be used for the measurement. In a total volume of 400 µl, filled up with 1x ICM buffer, an amount of 200 µg protein is used. The spectrum

from 300 to 950 nm is taken with a pre-set program as described for the full-cell spectra (2.2.9) in a polystyrene cuvette using 1x ICM buffer as reference.

2.2.11 Preparation of electrocompetent *Escherichia coli* cells

Electrocompetent *E. coli* cells are used for transformation (2.2.12) of plasmid DNA and ligation mixtures. During the applied electrotransformation any salt ions can lead to a fatal short circuit. Thus the cells are freed of remaining salt from the medium by several washing steps.

A fresh overnight culture (30 ml) of the *E. coli* strain of choice, for example JM109, is inoculated into 1 l of pre-warmed St-I medium and incubated shaking at 37°C until an OD_{600} of 0.6 – 0.8 is reached. Before starting the washing procedure, the cells are incubated on ice for 30 min. To harvest the cells, the culture is split into 500 ml centrifuge beakers and centrifuged at 6.000 rpm for 8 min (all centrifugation steps at 4°C, in F10-S rotor, *Sorvall RC 6 plus/RC 5C plus*). The supernatant is discarded, and all cell pellets are pooled in 350 ml cold Roth H_2O. After centrifugation for 5 min, the washing step is repeated once with 200 ml cold Roth H_2O. Now the cell pellet is resuspended in 20 ml cold 10% glycerine solution and is centrifuged for 10 min. To prepare the cells for storage they are resuspended in 3 ml cold 10% glycerine solution and aliquoted into 1.5 ml microcentrifuge tubes. The aliquots are immediately frozen in liquid nitrogen and can be stored at -80°C.

2.2.12 Electrotransformation of DNA to *Escherichia coli*

To transform plasmid DNA or a DNA ligation to *E. coli* cells that is making the uptake of DNA possible for the cells, a 2.5 kV electric shock is used (*Micro Pulser*, BioRad). During this short electric pulse, the cell wall integrity is disturbed in a reversible manner so that uptake of DNA is possible.

For the electrotransformation 50 µl of electrocompetent cells (2.2.11) are thawed on ice. The cells are given into an electroporation cuvette together with 50-100 ng of plasmid DNA or 5 µl of purified ligation mixture (2.4.4.2). The cuvette is placed in the *Micro Pulser,* and the voltage of 2.5 kV is created for 5 ms. Speedy after the electro pulse 500 µl of St-I medium are added to the cells, the mixture is transferred to a virgin 1.5 ml microcentrifuge tube, and the tube is incubated shaking at 37°C for 30-50 min. After the incubation, portions of the cells are spread on St-I agar plates containing the respective antibiotics which are incubated at 37°C overnight.

2.2.13 Plasmid conjugation to *Rhodobacter sphaeroides*

Since electrotransformation of DNA to *R. sphaeroides* is not possible, the di-parental conjugation (horizontal gene transfer) is used to transfer plasmid DNA. As the donor for the desired plasmid DNA, the *E. coli* strain S17-1 is used. This strain has to be transformed with the plasmid which is to be conjugated. On the plasmids used, the so-called mobilisation (*mob*) genes are encoded. The *mob* genes are needed for single strand breaks in the plasmid DNA. Plasmids with single strand breaks can be transferred to the recipient (here *R. sphaeroides*) via rolling circle replication. For this purpose, a cell-cell contact needs to be established which is achieved via the F-pilus that is chromosomally encoded by the *E. coli* transfer (*tra*) genes.

For the di-parental conjugation, 1 ml of *R. sphaeroides* liquid culture from exponential growth phase is mixed with *E. coli* S17-1 cells from plate culture (one inoculation loop of cells) carrying the plasmid of choice. The cells are centrifuged at 8.000 rpm for 5 min (*biofuge pico 17*), and the supernatant is discarded. The cells are resuspended gently in 100 µl RÄ medium, and the cell solution is dropped on a sterile membrane filter (*Cellulose nitrate*, GE Healthcare) which was placed on peptone yeast agar plates (PY plates; Tab. 20). Now the actual conjugation can take place during incubation at 32°C for 8 to 14 hours. Afterwards, the filter with the cells is transferred into a 1.5 ml microcentrifuge tube with 1 ml RÄ medium in which the cells are carefully rinsed from the filter. Taking this cell suspension a dilution series ($10^0 – 10^{-4}$) is prepared in RÄ medium, and 100 µl each are spread on RÄ agar plates containing the respective antibiotics. The plates are incubated at 32°C for around three days until single colonies have grown.

Table 20: Composition 1 l PY-agar.

Component	Amount	Action
Peptone	10 g	[1 % w/v]
Yeast extract	0.5 g	[0.05%]
$CaCl_2$ [1 M]	2 ml	[2 mM]
$MgCl_2$ [1 M]	2 ml	[2 mM]
$FeSO_4$ [0.5 %]	2.4 ml	[0.0012%]
ddH_2O	*ad* 800 ml	
	adjust to pH 7.0	
ddH_2O	*ad* 1000 ml	
Bacto Agar	8 g	[1.6% w/v]
		Autoclave

2.2.14 Determination of resistance towards oxidative stress - Zone of inhibition assay

With the help of the so-called zone of inhibition assay, the resistance or sensitivity of an *R. sphaeroides* strain towards different stresses can be tested. With increasing resistance the zone in which a tested reagent inhibits growth gets smaller. The here tested reagents are hydrogen peroxide (H_2O_2) and tertbutyl hydroperoxide (tBOOH) for inducing oxidative stress and methylene blue (MB)

together with light for photo-oxidative stress. When using MB the plates are incubated beneath a light source with illumination of 85 µmol m^{-2} s^{-1} white light (fluorescent tube, *TLD 58W/25*), while when using H_2O_2 and tBOOH the plates are incubated in the dark, both at 32°C. The zone of inhibition is measured and depicted as diameter in cm.

For the zone of inhibition assay the *R. sphaeroides* strains of interest are cultivated under microaerobic conditions (2.2.1.2) in biological triplicates. For the preparation of the plates, 800 µl culture with an OD_{660} 0.4 (when OD differs, volume has to be adjusted accordingly) are added to 20 ml lukewarm top-agar (1:2 RÄ agar / RÄ medium) and mixed on the vortexer. The mixture is spread in portions of 5 ml each on prepared plates containing 15 ml of solidified RÄ agar. Of each strain, technical duplicates are prepared for each tested chemical. When the top-agar is solidified, a filter disk (0.5 cm diameter; blotting paper, Albet LabScience) is soaked with 5 µl of the respective stress reagent (concentrations see results) and placed in the centre of the top-agar with a sterile tweezer. After incubating the plates for 48 h at 32°C, the cells have grown as a lawn in the top-agar, with the exception of the zone of inhibition which can be measured now. When the edges of the zones of inhibition are vague, storage at 4°C overnight can help to define them.

2.2.15 ß-galactosidase activity assay

The ß-galactosidase activity assay, by Miller (1972), is a fast method to measure the amount of translation of a gene section of interest (translational fusion) or the transcription following a promoter of interest (transcriptional fusion). Additionally, the potential effect of different factors such as sRNAs or growth conditions on the respective DNA part can be monitored. For this purpose reporter plasmids carrying the *lacZ* gene, which encodes ß-galactosidase, are used for gene fusions. ß-galactosidase is an enzyme which catalyses the hydrolysis of the spectrophotometric substrate *ortho*-nitrophenyl-β-galactoside (ONPG) to galactose and *ortho*-nitrophenol. The latter has a yellow colour which can be measured as the absorption at 420 nm, where the amount of yellow colour directly correlates with the amount of enzyme and thereby the rate of translation or transcription.

For the ß-galactosidase activity assay the *R. sphaeroides* strains of interest, such as wild-type and knockout, for example, have to be prepared as two variants each: one carrying the reporter plasmid while the other variant carries the respective empty vector control. All strains needed are cultivated in biological triplicates under the desired growth conditions (see 2.2.1.1 – 2.2.1.7). At each time point of cultivation that is to be monitored, samples are taken in technical duplicates, and the OD_{660} needs to be measured. The sample volume (200 – 2000 µl) depends on the amount of ß-galactosidase in the sample which should in total not be as high as the assay reaches its saturation (~A_{420} > 1.5). Therefore a test with different sample volumes should be performed in advance. The sample is transferred to a 2 ml microcentrifuge tube and centrifuged at 13.000 rpm and 4°C for 10

min (*biofuge fresco 17*). The supernatant is discarded, and the cell pellet is stored at -20°C until it is used in the assay (< 12 h). For the assay, each cell pellet is resuspended in 750 µl Z-buffer which is supplemented with 2.7 µl/ml ß-mercaptoethanol freshly before every assay (Tab. 21). As a reference 750 µl Z-buffer is treated as the other samples from this point on. In the next step, the cells are lysed by adding 10 µl 10% SDS and 20 µl chloroform and vortexing the samples for 30 sec. The assay is carried out at 28°C, after an incubation time of 5 min, the reaction can be started by adding 200 µl preheated ONPG (4 mg/ml, 28°C) to each sample and inverting. To stop the reaction, 500 µl sodium carbonate (1M, Na_2CO_3) is added, and the samples are mixed again by inverting. Since it is important to stop the reaction after an exact time point in every sample, one should add the ONPG in defined time intervals. When all reactions are stopped the samples are centrifuged at 13.000 rpm and RT for 3 min to spin down the cell debris. For the measurement, 800 µl of each sample, as well as the blank, are transferred into polystyrene cuvettes, and the absorption is measured at 420 and 550 nm. The former displays the yellow colour and the latter the remaining cell debris. From these data and the measured OD_{660} the following calculation can be carried out to receive values for the ß-galactosidase activity depicted in Miller Units (MUs).

Calculation 3: Miller Units = $$\frac{[1000*(A420-1{,}82*A550)]}{(\mathrm{V}*\mathrm{t}*\mathrm{OD660})}$$

V: Sample volume [ml]

t: Reaction time [min]

Table 21: Composition of 1 l Z-buffer for the ß-galactosidase activity assay.

Component	**Amount**	
Sodium phosphate dibasic	10.7 g	[60 mM]
Sodium dihydrogen phosphate	6.24 g	[40 mM]
Potassium chloride	0.75 g	[10 mM]
Magnesium sulfate heptahydrate	0.25 g	[1 mM]
	adjust to pH 7.2	
ddH_2O	*ad* 1 l	
Fresh before use: ß-mercaptoethanol	2.7 µl / ml	[50 mM]

2.2.16 Measurement of total cellular glutathione

To determine the cellular glutathione (GSH) amount in a sample, the Ellman's reagent (5,5'-dithiobis-(2-nitrobenzoic acid) or DTNB) is used. DTNB, first described by George Ellman 1959, is a chemical used to quantify the thiol groups in a sample. Thiols react with DTNB cleaving the disulphide bonds to give 2-nitro-5-thiobenzoate (TNB^-), which ionises to the yellow coloured dianion TNB^{2-} that can be measured spectrophotometrically.

For the GSH assay, the OD_{660} of each tested culture is determined, and 10 ml are harvested by centrifugation at 10.000 rpm, at 4°C for 10 min (*Sorvall RC 5C plus / RC 6 plus*; *SS-34* rotor). The cells are transferred into a virgin 1.5 ml microcentrifuge tube and are re-suspended in 100 µl ddH_2O. To lyse the cells, 300 µl of 5% sulfosalicylic acid (w/v; SSS; 5-Sulfosalicylic acid dihydrate, Sigma Aldrich) are added, and the samples are vortexed vigorously for 20 sec. After incubation at RT for 5 min, the samples are centrifuged at 10.000 rpm at 4°C for 10 min (*biofuge fresco*). For each reaction 50 µl of the supernatant is mixed with 845 µl sample buffer (with NADPH; Tab. 22) in a polystyrene cuvette. For the calibration curve 10 – 40 µl GSH solution (100 µM) is added instead of the sample and a cuvette without sample or GSH is prepared as the blank. To compensate the SSS from the sample, 50 µl of 3.75 % SSS are added to the calibration reactions and the blank. After 100 µl of DTNB (6 mM) was added, the reactions are incubated at RT for 10 min in the dark. To start the reaction, 5 µl of glutathione reductase (GR, from bakers yeast, Sigma-Aldrich; 100 U/ml in sample buffer) is added, and the sample is mixed by pipetting up and down. The GSH and glutathione disulphide (GSSG) that is reduced by the GR to GSH oxidises the DTNB to TNB^- which can be measured at 412 nm spectrophotometrically. Measurement takes place every 5 sec for 30 sec since depending on the amount of GSH the TNB^- increases over time. So this increase gives information on the amount of GSH in the sample. From the data of the reactions containing defined amounts of GSH (10 – 40 µM) a calibration curve can be drawn which is used to calculate the sample's GSH amount as shown below:

Calculation 4: Calibration curve (linear regression): $y = ax - b$

$$GSH\ [\mu M] = [(Abs_{sample} - Abs_{blind} - b)/a)]*D1*D2$$

D1: dilution factor (H_2O and SSS) D2: dilution factor (sample buffer)

Table 22: Composition of 1 l sample buffer for GSH assay.

Component	**Amount**
NaH_2PO_4 dihydrate	22.3 g [143 mM]
EDTA (disodium salt)	1.75 g [6 mM]
ddH_2O	800 ml
	adjust to pH 7.5 with 1N NaOH
ddH_2O	*ad* 1 l
Fresh before use: NADPH	3 mg / ml

2.2.17 Measurement of reactive oxygen species

To detect ROS in a biological sample the oxidant-sensitive probe 2',7'-dichlorodihydrofluorescein (DCFH) can be utilised. The reduced DCFH, which is non-fluorescent, is oxidised by ROS to its highly fluorescent parent dye molecule DCF. The reaction is not specific for a particular ROS species, but will

rather give a value for the total ROS level in the sample (Marchesi *et al*., 1999). To measure the ROS level in a cell sample, DCFH is added to the cells as diacetate (DCFH-DA; Molecular Probes) which can diffuse across the cell membrane.

For the measurements performed in this work, four 180 µl aliquots from each culture that is to be measured are given to wells on a black 96 well plate. To three of the samples 20 µl 100 µM DCFH-DA is added, the fourth is used as background fluorescence control (blank). The plate is incubated shaking at 32°C for 30 min. The fluorescence intensities (excitation 492 nm, emission 525 nm) are evaluated in the *Infiniti M200* microplate reader (Tecan). After subtraction of the autofluorescence (blank) from the samples, the fluorescence, which corresponds to the amount of ROS, can be normalised to the OD_{660} of the culture and depicted in arbitrary units or relative fluorescence (Calculation 3).

Calculation 5: Arbitrary Units = $[(\bar{x}\ \text{Emission}\ 525_{\text{sample 1-3}}) - \text{Emission}_{\text{blank}}]/\text{OD}_{660}$

2.3 Electrophoresis techniques

2.3.1 Agarose gel electrophoresis of DNA

Agarose gels are used to separate DNA fragments according to their size. For bigger fragments of a size between 2 and 25 kb one uses 1% TAE (Tris base, acetic acid, and EDTA; Tab. 9) gels, while fragments between 0.4 and 2 kb are better separated on 1.5 – 2% TBE (Tris base, borate, EDTA; Tab. 9) gels. As running buffer 1x TAE or 1x TBE is used, respectively.

To prepare an agarose gel, the needed amount of agarose is weighed in, the according amount of buffer is added, and the gel mixture is boiled until the agarose has melted completely. The gel is poured into a gel tray, and a comb is inserted to form the pockets. The solidified gel can be placed into a running chamber containing the respective running buffer. As size standard, the 1 kb plus ladder (Qiagen; 2.5.1) is used of which 4 µl are loaded. To the samples, one volume of 10x DNA loading dye (Tab. 10) is added, containing glycerine that ensures that the samples sink into the pockets. The gel run is carried out at 100-120 V for 30 to 60 min. On the basis of the two dyes contained in the loading dye, xylene cyanol and bromphenol blue, one can estimate how far the DNA fragment of interest has already run (compare Tab. 23). After finishing the gel run the DNA in the gel can be stained in an ethidium bromide bath. Ethidium bromide intercalates double stranded DNA and is fluorescent under UV light so that the stained DNA can be detected and photographed on a UV-transilluminator (*UVT-20 M/W*, HeroLab).

Table 23: Running behaviour of xylene cyanol and bromphenol blue according to agarose concentration.

Agarose (w/v)	Xylene cyanol	Bromphenol blue	Recommended for fragment sizes
0.5%	10 kb	1 kb	1 to 30 kb
1.0%	3 kb	300 bp	0.5 to 7 kb
1.5%	1 kb	120 bp	0.2 to 3 kb
2.0%	0.8 kb	< 100 bp	0.1 to 2 kb

2.3.1.1 DNA extraction from an agarose gel (Kit)

To extract DNA, for example, a PCR product or a plasmid after restriction, from an agarose gel the *InnuPREP DOUBLEpure* kit (Analytik Jena) can be used. The kit, according to the manual, applies best for DNA fragments of a size between 0.5 and 10 kb.

Since the DNA fragment that is to be extracted should be protected against potential mutations caused by the ethidium bromide and UV light, all here described gel extraction methods are based on the following procedure. The sample is loaded in an enlarged pocket next to the DNA ladder. After the gel run, the ladder plus a part of the large pocket containing the sample can be cut off and stained. On the stained gel piece, one can mark, via cutting with a scalpel, the location of the desired DNA fragment. When now laying the stained and the unstained gel pieces together corresponding to the mark on the stained piece the DNA fragment can be cut out of the unstained piece (Fig. 19).

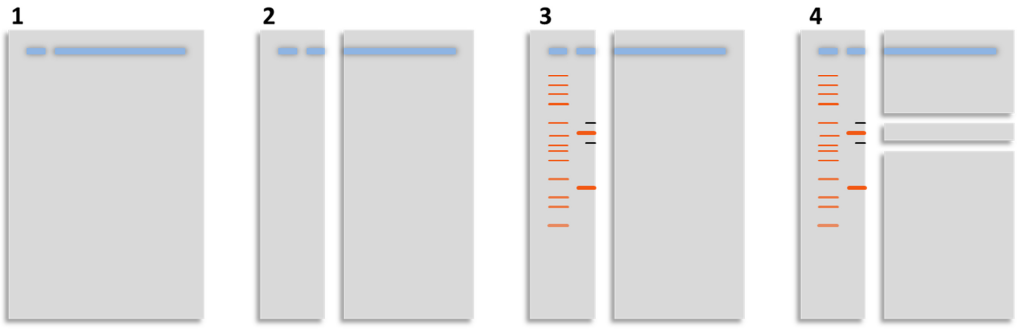

Figure 19: Gel extraction – Scheme for cutting the gel pieces. Before staining the lane containing the marker and a piece of the enlarged lane containing the sample is cut off (1+2). The cut off piece is stained (3), and according to marks made on the stained piece, the gel fraction containing the fragment of interest is cut out (4) for gel extraction.

The cut out gel slice is transferred into a virgin 2 ml microcentrifuge tube and weighed. The extraction succeeds according to the manual for the *InnuPREP DOUBLEpure* kit (Analytik Jena). Merely the incubation time in the last extraction step is changed from 2 to 5 min to increase the yield of DNA.

2.3.1.2 DNA extraction from an agarose gel (Glass wool)

When the DNA fragment which is to be extracted from the agarose gel is larger than 10 kb the yield of the extraction kit described in 2.3.1.1 is quite low. In this case, the alternative is the extraction via self-made glass wool columns.

For this purpose, the gel slice containing the DNA fragment of interest is prepared as described in 2.3.1.1. The self-made column is built out of a 1.5 ml microcentrifuge tube, a 0.5 ml microcentrifuge tube and silanised glass wool (Serva) as depicted in figure 20. The 0.5 ml microcentrifuge tube is placed in the 1.5 ml microcentrifuge tube. A hole is made in the bottom of the 0.5 ml microcentrifuge tube using a hollow needle that is heated and pierced trough. Two-thirds of the upper tube is filled tight with glass wool using sterile tweezers. The cut gel slice is placed on top of the glass wool, and the column is centrifuged at 8.000 rpm for 3 min at RT (*biofuge pico 17*). The flow-through contains the DNA which can be purified via phenol purification as described in 2.4.5. The purified DNA is dissolved in Roth H_2O and stored at -20°C.

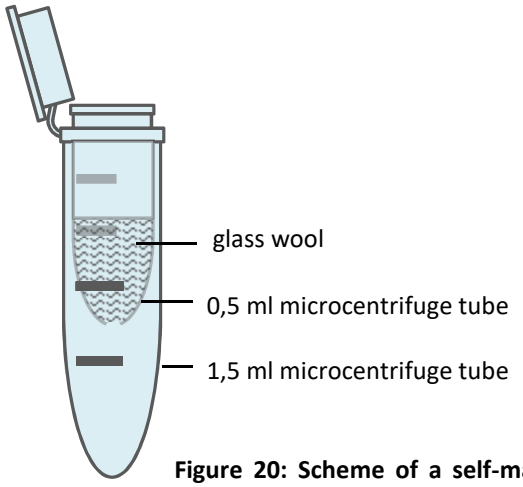

Figure 20: Scheme of a self-made glass wool column for gel extraction of DNA. A 0.5 ml microcentrifuge tube with a hole pierced trough the bottom and filled to two-thirds with glass wool, is placed into a 1.5 ml microcentrifuge tube.

2.3.2 Polyacrylamide gel electrophoresis of DNA

To separate small DNA fragments (< 0.12 kb) 12% polyacrylamide (PAA) gels can be used (Tab. 24). But the use of PAA gels has the disadvantage that extraction from those gels is quiet complex and the yield is rather low (for description see 2.3.2.1). So for evaluating aspects such as separation of test restrictions polyacrylamide gels are useful, while for extraction of DNA they should only be used for really small fragments below 0.4 kb which can not be extracted nicely with the kit (2.3.1.1).

For PAA gels, all components are pipetted into a beaker according to the order in table 24 and are mixed by swivelling. The gel mixture is pipetted between a glass and a ceramic plate, which are placed in the gel pouring device (*Multiple Gel Caster*, Serva). A comb for the needed number of pockets is placed into the gel, and the gel is left until it has polymerised. The gel run is carried out in a

mini-gel system (Serva) with 1x TBE as running buffer at 100 - 120 V. The DNA in the gel is stained in an ethidium bromide bath and documented as described for agarose gels (2.3.1).

Table 24: Composition of a 12% polyacrylamide gel for DNA separation.

Component	Amount	
Acrylamide [40%]	1.5 ml	[12% v/v]
10x TBE	0.6 ml	[1x]
ddH_2O	3.9 ml	
Ammonium persulfate [10% w/v]	24 µl	
TEMED*	6 µl	

*Tetramethylethylenediamine

2.3.2.1 DNA-Extraction from a polyacrylamide gel

To extract DNA from a PAA gel, the principle of diffusion is used. The gel slice containing the DNA of interest is incubated in diffusion buffer consisting of 0.5 M ammonium acetate and 1 mM EDTA (Tab. 25). The gel slice is prepared as described for the extractions from agarose gels (2.3.1.1). It is placed in a virgin 1.5 ml microcentrifuge tube where it is frozen and then milled with a pipette tip before adding 300 µl diffusion buffer. The incubation takes place at 37°C for >12 h. After the incubation, the supernatant is transferred into a virgin 1.5 ml microcentrifuge tube, and the gel slice is rinsed with 200 µl diffusion buffer once. Both supernatants are joined, and the DNA is precipitated by adding 1 volume isopropanol, incubating for > 30 min at -20°C and subsequent centrifugation with 13.000 rpm for 30 min at 4°C (*biofuge Fresco17*). The DNA pellet is washed once by adding 200 µl cold 70% ethanol and centrifugation for 10 min. After the ethanol is discarded, the DNA pellet is dried for 10 min in the *SpeedVac* (vacuum dryer, Eppendorf). The dried DNA pellet is dissolved in 10 -20 µl Roth H_2O and stored at -20°C.

Table 25: Composition of 80 ml diffusion buffer for DNA extraction from a polyacrylamide gel.

Component	Amount	
EDTA [250 mM]	0.32 ml	[1 mM]
Magnesium acetate	0.11 g	[10 mM]
Ammonium acetate	3.1 g	[500 mM]
ddH_2O	*ad* 80 m l	

2.3.3 Gel electrophoresis of RNA

The separation of RNA in a polyacrylamide (PAA) urea or formaldehyde agarose gel is described in detail in the chapters 2.4.6.1 and 2.6.4.2 on the Northern blot techniques. Especially the PAA urea gel can be used to check the quality of the RNA, meaning its intactness. For this purpose a PAA urea gel can be cast in the gel system described for PAA DNA gels (2.3.2). Moreover, RNA can be also loaded

and separated on a non-denaturing polyacrylamide gel which is described in detail in chapter 2.4.13 on the EMSA technique. After separation in these gels, the RNA can be stained with ethidium bromide and documented as described for DNA 2.3.1.

2.4 Molecular biological methods

2.4.1 Extraction and Usage of nucleic acids

The initial step for the extraction of nucleic acids is the cell lysis, for which different approaches can be used: detergents such as sodium dodecyl sulphate (SDS) and ethylene diamine tetra-acetic acid (EDTA), an enzymatic cell lysis using lysozyme, or the alkaline lysis trough addition of sodium hydroxide (NaOH). These approaches can also be used in combination. To separate the nucleic acids from the cell lysate ethanol, phenol, or a combination of both can be applied. The protocols used to prepare nucleic acids needed for different applications are listed below.

2.4.1.1 Extraction of chromosomal DNA from *Rhodobacter sphaeroides*

The chromosomal DNA of *R. sphaeroides* is mainly used for the amplification of gene parts via PCR (2.4.3.1) for following cloning steps and is therefore extracted from wild-type cells.

For the extraction, cells from 10 ml of *R. sphaeroides* liquid culture with an OD_{660} of approx. 0.6 are harvested by centrifugation at 8.000 rpm for 10 min at 4°C (*RC 5C plus*/ *RC 6 plus*; *SS-34* rotor). The cells are resuspended in 700 µl TE buffer (Tab. 9), which is prepared fresh with 1 mg/ml of lysozyme (Boehringer Ingelheim) and are transferred into a virgin 1.5 ml microcentrifuge tube. The lysis of the cells takes place via incubation at RT for 10 min. To lyse the cellular proteins 30 µl 10% SDS and 16 µl proteinase K (20 mg/ml) are added. The samples are mixed trough inverting and are incubated for 1 h at 37°C. After the incubation, 100 µl of 5M sodium chloride (NaCl) and 80 µl Cetrimonium bromide (CTAB; detergent) in NaCl are added. The sample is heated at 65°C for 10 min in a heating block. To precipitate the cell debris and proteins, 750 µl of a chloroform/isoamyl alcohol mixture (24:1) are added, and the sample is mixed by inverting the tube. To gain the needed phase separation, the sample is centrifuged at 13.000 rpm for 5 min at RT (*biofuge pico 17*) and 650 µl of the upper, aqueous phase is transferred into a virgin 1.5 ml microcentrifuge tube. One volume of a phenol/chloroform/isoamyl alcohol mixture (25:24:1; AppliChem) is added, the sample is mixed by inverting, and centrifuged at 13.000 rpm for 5 min at RT (*biofuge pico 17*). After transferring 550 µl of the upper, aqueous phase into a virgin 1.5 ml microcentrifuge tube, 0.6 volume of isopropanol is added. The DNA is precipitated by incubation at RT for 5 min and subsequent centrifugation with 3.000 rpm for 3 min at RT (*biofuge pico 17*). The supernatant is discarded carefully, and the DNA is

washed by adding 200 µl of cold 70% ethanol and repeated centrifugation. The supernatant is discarded again; the DNA is dried in the *SpeedVac* (vacuum dryer, Eppendorf) for 10 min and dissolved in TE buffer to be stored at 4°C.

2.4.1.2 Extraction of plasmid DNA

The extraction of plasmid DNA from bacterial cells also called plasmid prep, is based on the alkaline lysis first described in 1979 by Birnboim and Doly. The DNA gained from the lysed cells is precipitated using ethanol.

For the here applied mini prep, small volumes of cell culture (1 – 4 ml) are centrifuged at 8.000 rpm for 5 min at RT (*biofuge pico 17*) and the supernatant is discarded. The cells are resuspended in 100 µl mini prep solution I (Tab. 26) and 200 µl mini prep solution II (Tab. 26) is added. The samples are mixed by inverting six times and are incubated at RT for 5 min. After adding 150 µl mini prep solution III (Tab. 26) the samples are again mixed by inverting and incubated on ice for 10 min. The cell debris is precipitated from the sample by centrifugation with 13.000 rpm at 4°c for 10 min (*biofuge fresco*), and 95% of the supernatant is transferred into a virgin 1.5 ml microcentrifuge tube. This step is repeated once, and the gained supernatant is mixed with 1 ml cold 96% ethanol. To precipitate the plasmid DNA, the samples are centrifuged at 13.000 rpm at RT for 30 min (*biofuge pico 17*). The DNA pellet is washed with 200 µl cold 75% ethanol by centrifugation (10 min) before drying it in the *SpeedVac* (Eppendorf). The dried plasmid DNA is diluted in H_2O and stored at -20°C until further use.

Table 26: Composition of Mini Prep solutions I, II and III.

Solution I			
Component		**Amount**	
Glucose		0.9 g	[50 mM]
1 M Tris HCl	pH 8.0	2.5 ml	[25 mM]
0.5 M EDTA		2 ml	[10 mM]
ddH_2O		*ad* 100 ml	
			Autoclave and store at 4°C
			Add fresh 4 µl/ml RNase A (100 mg/ml)
Solution II			
Component		**Amount**	
1N NaOH		4 ml	[0.2 N]
10% SDS		2 ml	[1 %]
ddH_2O		*ad* 20 ml	
			Store at RT; refresh every 3 weeks
Solution III			
Component		**Amount**	
Potassium acetate		29. 4 g	[3 M]
Glacial acetic acid		adjust to	pH 5.6
ddH_2O		*ad* 100 ml	
			Autoclave and store at 4°C

2.4.1.3a Extraction of total RNA from *Rhodobacter sphaeroides* – hot phenol

To extract total RNA from *R. sphaeroides* cells, two methods can be used. The first, in the following described, method is the so-called hot phenol extraction based on Scherrer and Darnell (1962) and is used to extract high quantities of RNA. This RNA can be used for Northern blot analysis (2.4.6) but has the disadvantage that it is prone to DNA contamination and can leave residual phenol in the sample. Hence there is a second method to extract RNA, the TRIzol extraction, which shall be used to prepare RNA for RT-PCR and is described below (2.4.1.3b). In addition to the described advantages of the two different extraction methods, it was shown that hot phenol enriches RNAs with a size between tRNAs and large rRNAs, while the TRIzol extraction enriches RNAs smaller than tRNAs (Damm *et al.*, 2015). Thus not only depending on the later usage but also depending on the experimental question one can choose between the two methods.

As needed, cells from 10 - 30 ml *R. sphaeroides* liquid culture are harvested in centrifuge beakers prefilled to one-third with ice by centrifugation with 10.000 rpm for 10 min at 4°C (*RC 5C plus* / *RC 6plus*; *SS-34* rotor). The cell pellet is transferred into a 1.5 ml safe-lock microcentrifuge tube and resuspended in 125 µl of cold RNA solution I (Tab. 27). After addition of 125 µl cold RNA solution II (Tab. 27) which contains SDS to lyse the cells, the sample is firmly vortexed until it is homogenous and incubated in a water bath at 65°C for 90 sec. In the next step, 250 µl of prewarmed (65°C) phenol-water (AppliChem) is added, the sample is vortexed again and incubated for 3 min at 65°C. The sample is frozen for at least 30 sec in liquid nitrogen and centrifuged at 13.000 rpm for 10 min at RT (*biofuge pico 17*) to separate the phases. The two phases occur since water and phenol are immiscible, and the denser phenol sits at the bottom of the tube. Through vortexing, the phenol is forced into the aqueous phase where it forms droplets in which the proteins partition so they can be centrifuged into the phenol phase. Approximately 90% of the upper, aqueous phase is transferred into a virgin 1.5 ml safe-lock microcentrifuge tube and the phenol addition, 65°C incubation, freezing and centrifugation is repeated two times. The third portion of the aqueous phase is transferred into a virgin 1.5 ml microcentrifuge tube where it is mixed with 250 µl chloroform/isoamyl alcohol to get rid of the remaining phenol, which will be dissolved in the chloroform/isoamyl alcohol to be precipitated into the lower phase. After centrifugation for 3 min again 90% of the aqueous phase is transferred into a virgin 1.5 ml microcentrifuge tube and mixed with 2.5 volume of cold 96% ethanol and 1/10 volume of 3M sodium acetate (NaOAc, pH 4.5). The mixture is incubated at -20°c for at least 4 h before the RNA is precipitated by centrifugation with 13.000 rpm, at 4°C for 20 min (*biofuge fresco*). The supernatant is discarded, and the RNA washed by addition of 200 µl cold 75% ethanol and centrifugation. When the ethanol is discarded the pellet can by dried in the *SpeedVac* (Eppendorf). The dried RNA is dissolved in 20-40 µl of Roth H_2O and stored at -20°C.

Table 27: Composition of 100 ml RNA solution I and II.

RNA Solution I			
Component		**Amount**	
Saccharose		10.27 g	[300 mM]
3M NaOAc	pH 4.5	0.33 ml	[10 mM]
ddH_2O		*ad* 100 ml	
			Autoclave and store at 4°C
RNA Solution II			
Component		**Amount**	
20% SDS		10 ml	[2%]
3M NaOAc	pH 4.5	0.33 ml	[10 mM]
ddH_2O		*ad* 100 ml	
			Autoclave and store at 4°C

2.4.1.3b Extraction of total RNA from *Rhodobacter sphaeroides* - TRIzol

As already mentioned, there is a second method to extract total RNA from *R. sphaeroides* cells. This method is based on the *peqGOLD TriFast* reagent manufactured by PeqLab, correctly called guanidinium thiocyanate-phenol-chloroform extraction. Using this method, the sample can be separated into three phases: a lower, organic phase mostly containing proteins, a DNA-containing interphase and an upper phase containing the RNA (PeqLab *TriFast* data sheet). Via this separation the residual DNA amount in the sample as well as remaining phenol contamination is minimised which is ideal for following DNase I digestion and RT-PCR (2.4.4.3 and 2.4.3.3).

For the TRIzol extraction cells from 10 ml *R. sphaeroides* liquid culture are harvested by centrifugation at 10.000 rpm for 10 min at 4°C (*RC 5C plus* / *RC 6plus*; *SS-34* rotor). The supernatant is discarded, and the cell pellet transferred into a virgin 1.5 ml microcentrifuge tube. The cells are resuspended in 500 µl *peqGOLD TriFast* reagent and incubated on ice for 5 min. When 200 µl of chloroform was added the sample is vortexed and incubated for further 15 min on ice. To separate the three phases, the sample is centrifuged at 13.000 rpm for 10 min at RT (*biofuge pico 17*), and the upper, aqueous phase is transferred into a virgin 1.5 ml tube. It is mixed with 1 volume of isopropanol and incubated on ice for at least 15 min. To precipitate the RNA, the sample is then centrifuged at 13.000 rpm for 15 min at 4°C (*biofuge fresco*). The supernatant is discarded again, and the RNA pellet is washed once with 200 µl cold 75% ethanol. After drying the RNA in the *SpeedVac* (Eppendorf) it can be dissolved in 20 - 40 µl Roth H_2O and stored at -20°C. To use the RNA for RT-PCR, the remaining DNA has to be removed by DNase I digestion (2.4.4.3).

2.4.2 Quantification of nucleic acids

To quantify the diluted nucleic acids (2.4.1.1 – 2.4.1.3), the absorption at 260 nm is measured spectrophotometrically. Absorption of 1 means 50 µg of DNA and 40 µg of RNA, respectively. Also, the absorption at 280 nm is measured, which provides information about potential protein contamination. The ratio between 260 and 280 nm speaks for the purity of the measured nucleic acid. For DNA a ratio of 1.8 while for RNA a ratio of 2.0 is desired.

2.4.3 Amplification of DNA

The amplification of DNA using a polymerase chain reaction (PCR) is the tool for cloning of genes and a method to determine the presence and amount of an investigated nucleotide sequence in a plasmid, DNA or RNA sample. The key elements for PCR are a thermostable polymerase, an adequate template, and two oligonucleotides called primers, which are complementary to the 5' and 3' ends of the particular DNA segment. The primers – with few exceptions (see 2.2.4.3.2) - face towards each other to amplify the desired DNA fragment from the template as well as the arising amplificates (Mühlhardt, 2009). Applications using the PCR principle are described in the following three chapters.

2.4.3.1 Amplification of DNA fragments via PCR

To amplify a DNA fragment of interest, the PCR method is used. The required enzyme is the DNA polymerase, which can synthesise DNA molecules from deoxyribonucleotide. The principle of PCR can be summed up as follows: the template DNA is melted to single strands, at 96° - 98°C depending on the polymerase used, the sense and antisense primer are allowed to anneal to the DNA strands, and the polymerase elongates the newly synthesised strand by adding deoxyribonucleotides to the 3' end. The PCR (composition in Tab. 28) is assembled on ice in PCR tubes, and the PCR protocol (Tab. 29) is carried out in a Thermal cycler (*S1000* or *T100*, BioRad).

Table 28: Composition of a 10 µl standard PCR (example, can be scaled up).

Component	***Taq*-based**	***Phusion*-based**
ddH_2O	6.4 µl	6.3 µl
dNTPs [2.5 mM each]	0.4 µl [0.1 mM]	0.2 µl [0.05 mM]
Primer forward [10 µM]	0.5 µl [0.5 µM]	0.2 µl [0.2 µM]
Primer reverese [10 µM]	0.5 µl [0.5 µM]	0.2 µl [0.2 µM]
10x *Taq* buffer	1 µl [1x]	-
5x GC-buffer	-	2 µl [1x]
Taq polymerase [5 U/µl]	0.2 µl [0.1 U/µl]	-
Phusion polymerase [2 U/µl]	-	0.1 µl [0.02 U/µl]
Template*	1 µl	1 µl

*DNA: chromosomal [100 ng/µl]; plasmid [30 ng/µl]; Negative control: ddH_2O

Tab. 29: Standard PCR program

1.	Initial Denaturation	95°C (*Taq*) / 98°C (*Phusion*)	5 min
2.	Denaturation	95°C (*Taq*) / 98°C (*Phusion*)	30 sec
3.	Annealing	Primer-specific temperatue	30 sec
4.	Extension	72°C	1 min/kb (*Taq*) / 30 sec/kb (*Phusion*)
Back to step 2 for 34 times			
5.	Final Extension	72°C	10 min
6.	Hold	8°C	∞

2.4.3.2 Site-directed mutagenesis using an inverse PCR

Site-directed mutagenesis is a technique used to insert specific and intentional changes to a DNA sequence of interest. To exchange the desired nucleotides, a primer pair containing the mutated sequence is designed. This primer pair is used for a so-called inverse PCR with a plasmid, carrying the DNA sequence that should be mutated, as template. Both primers face in different directions from the region that is mutated onwards to amplify the whole plasmid so that the PCR results in a linear plasmid carrying the mutated DNA sequence (Fig. 21). The unmutated plasmid template is digested using the enzyme DpnI which solely digests methylated GATC sites, which is cell-derived plasmid DNA.

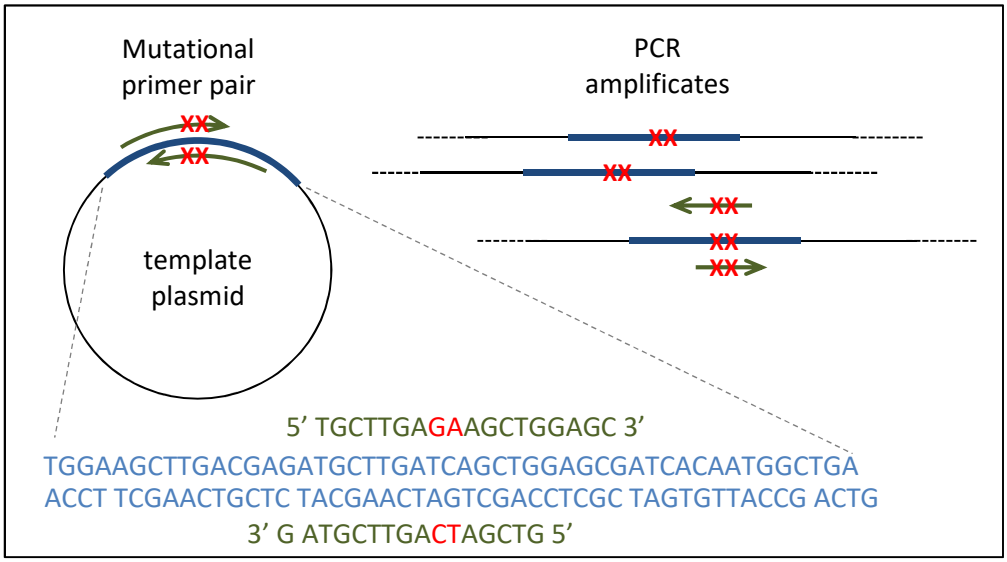

Figure 21: Scheme of site-directed mutagenesis by inverse PCR. Plasmid template (black circle) with the sequence of interest (blue) and primer pair (green) with mutations (red crosses). The binding site of the primer pair is depicted in more detail below and the PCR amplificates with by now perfect complementarity to the primer pair are shown on the right.

2.4.3.3 Quantitative real-time RT-PCR

The principle of the PCR can also be used to amplify DNA in a quantitative approach for gene expression analysis in a quantitative real-time RT-PCR (qRT-PCR; short RT-PCR). Here the amplification of DNA is monitored during the reaction and not at its end. Using this method, the amount of an mRNA of interest in an RNA sample can be determined. A complementary DNA (cDNA) of the mRNA of interest is synthesised and used as the template for the PCR reaction. To monitor the amplification from the cDNA in real time the reaction contains, besides dNTPs and polymerase buffer, the asymmetrical cyanine dye *SYBR Green I*. This fluorescent dye intercalates into the newly synthesised dsDNA and the resulting DNA-dye-complex absorbs blue light (λmax = 497 nm) and emits green light (λmax = 520 nm). The initial copy number of the mRNA of interest can be quantified according to the threshold cycle (Ct) that has been shown to be inversely proportional to the initial copy number. The Ct is defined as the cycle at which the fluorescence in the sample is determined to be above background (set to 0.002).

For the RT-PCR, total RNA isolated with the TRIzol method (2.4.1.3b) is used in technical duplicates. The composition of the RT-PCR reaction using the *Brilliant III Ultra - Fast SYBR® Green QRT-PCR master mix* kit (Agilent) is shown in table 30. Besides an RT-PCR run for the mRNA of interest (target), a run with a primer pair for the house-keeping gene *rpoZ* (reference) is needed for normalisation. The calculation of the relative expression ratio (R) of a target gene in comparison to the reference gene (ref) is carried out using the efficiency corrected quantification model by Pfaffl (2001):

Calculation 6:
$$R = \frac{(E_{target})\Delta Ct_{target}(control-sample)}{(E_{Ref})\Delta Ct_{Ref}(control-sample)}$$

In this calculation, E is the primer efficiency for the used primer pairs, while the value ΔCt gives the difference of the cycles of the control and the sample in which the fluorescence exceeds the set threshold. The control, in this case, is mostly an earlier time point (when comparing stressed samples of one strain) or the wild-type or control strain (when comparing two strains). By using RNA isolated from samples of a half-life experiment (2.2.3) for an RT-PCR, the resulting values can be applied to calculate the half-life of the tested RNA as described in 2.4.12 b.

Table 30: Composition of a 10 µl RT-PCR reaction.

Component	Amount
Enzyme Mix[1]	5 µl
Primer forward [10 µM]	1 µl [1 µM]
Primer reverese [10 µM]	1 µl [1 µM]
DTT[1]	0.1 µl
RT block[1]	0.4 µl
Roth H_2O	0.5 µl
Template*	2 µl [40 ng]

[1] contained in the *QRT-PCR master mix* kit (Agilent); *RNA [20 ng/µl]; Negative control: Roth H_2O

2.4.4 Enzymatic modification of nucleic acids

2.4.4.1 Restriction analysis of DNA

The restriction of palindromic DNA sequences using restriction enzymes is carried out to either test for the existence of restriction sites in a cloned DNA fragment, to check the size of a fragment ligated into a cloning vector (2.4.4.2), or to cut a cloned DNA fragment out of a plasmid for further use. The restriction is carried out according to the manufactures manual based on the definition that 1 unit restriction enzyme cuts 1 µg of DNA in 1 h in a 50 µl reaction. A test restriction is carried out in a small volume (10 µl) for around 1 h while preparative restrictions are incubated for 2 – 3 h in larger volumes (40 – 50 µl).

2.4.4.2 Ligation of DNA

Using the T4 DNA ligase, an enzyme that catalyses the ATP-dependent formation of a phosphodiester bond, ends of DNA strands can be rejoined. The ends of the DNA strands used can show different characteristics: cohesive and complementary ends created by restriction enzymes (2.4.4.1), a deoxyadenosine triphosphate (dATP) overhang synthesized by the *Taq* polymerase, or blunt ends resulting from amplification with the *Phusion* polymerase. The former can be ligated into a vector prepared with the corresponding restriction enzymes, while the latter two can be ligated into the pDrive cloning vector with deoxythymidine triphosphate overhangs (TA–cloning; Qiagen) or the pJET cloning vector with blunt ends (Qiagen), respectively.

For ligation of a DNA fragment (insert) into a vector, both prepared by restriction, a molar ratio of 3:1 insert to vector is used. The total amount of DNA in the reaction should hereby not exceed 100 ng. The ligation reaction contains insert, vector, 10x ligase buffer (contains ATP; NEB) and T4 DNA ligase ([5 U/µl], NEB) filled to a volume of 20 µl with ddH_2O. The ligation reaction is incubated for 2 – 16 h at 16°C in a water bath before it gets heat-inactivated at 70°C for 10 min. Alternatively, for pDrive and pJET cloning the manufacturers manual is followed. To use the ligated DNA for transformation to *E. coli* cells, it can be precipitated using n-butanol to clear the reaction of salts

from the buffer. The ligation mix is filled to 50 µl with ddH_2O and 500 µl n-butanol is added. When precipitated via centrifugation with 13.000 rpm for 30 min at 4°C (*biofuge fresco*), the DNA can be washed with 70% ethanol and dried in the *SpeedVac* (Eppendorf), before resolving in 10 – 15 µl Roth H_2O. After the n-butanol precipitation, the ligated DNA can be used for transformation (2.2.12).

2.4.4.3 Digestion of remaining DNA from RNA samples

The RNA which is used for RT-PCR (2.4.3.3) has to be free of DNA, which otherwise could be amplified in the PCR step and falsify the result. All potential remaining DNA is digested using DNase I which is an endonuclease that non-specifically cleaves DNA.

For DNase I digestion, each RNA sample is measured and made up to 100 µl with ddH_2O. If digesting several samples, a master mix is prepared containing DNase I ([50-375 U/µl], Invitrogen) and the respective buffer (Tab. 9). It is valid to use 3-4 U DNase I to digest DNA in a 10 µg RNA sample. The RNA solution is mixed with 20 µl master mix and incubated at 37°C for 45 min. After the incubation, the reaction is made up to 200 µl with ddH_2O and the RNA is purified via phenol purification. One volume of phenol/chloroform/isoamyl alcohol (25:24:1; AppliChem) is added to each sample and mixed in by vortexing. When centrifuged at 13.000 rpm for 10 min at RT (*biofuge pico 17*) 180 µl of the aqueous, upper phase is transferred into a virgin 1.5 ml microcentrifuge tube and 200 µl of chloroform/isoamyl alcohol (24:1) is added. After vortexing, the sample is again centrifuged for 3 min and 160 µl of the aqueous, upper phase is transferred into a virgin 1.5 ml microcentrifuge tube. Prior to the precipitation 1 volume of isopropanol and 1/10 volume of 3M sodium acetate (NaOAc, pH 4.5) are added and the sample is incubated on ice for at least 1 h. To precipitate the RNA the sample is centrifuged at 13.000 rpm for 30 min at 4°C (*biofuge fresco*) and the supernatant is discarded. The pellet is washed twice with 200 µl cold 75% ethanol and dried in the *SpeedVac* (Eppendorf). To test whether the RNA is DNA-free after this treatment a PCR using primers for the gene *gloB* (RSP_0799) is carried out. For this purpose the RNA is diluted to a concentration of 20 ng/µl, which is also used later on for RT-PCR (2.4.3.3). Chromosomal DNA (2.4.1.1) is used as a positive control while ddH_2O is used as negative control. The PCR is carried out as described in 2.4.3.1 (*Taq*-based).

2.4.5 *In vitro* transcription

In vitro transcription is used to synthesise RNA from a linear DNA template of choice. Therefor a suitable phage polymerase promoter has to be added to the 5' end of the template sequence. The addition of a promoter can either be achieved by adding the promoter sequence to the primer used for template amplification or by fusing the template sequence to a promoter on a plasmid – the T7 promotor on the pDrive (Qiagen) for example. By addition of rNTPs, the corresponding phage RNA

polymerase and an adequate buffer, RNA can be synthesised from such a promotor-containing template.

Templates were produced via PCR (2.4.3.1) using primer pairs carrying the T7 promoter (TAATACGACTCACTATA) fused to each forward primer (Tab. 3). The PCR products are purified using the *doublePURE INNUprep* kit (Jena Analytik) and measured using the NanoDrop (2.4.2). For a 25 µl *in vitro* transcription reaction, 2 - 5 pmol of a template are required. The reaction composition is listed below (Tab. 31). When the *in vitro* transcript is to be radio-labelled, [γ32P]dUTP is added to the reaction (2.4.7.3 for details). After incubation of the reaction for 7 h at 37°C, 1 µl TURBO DNase (2 U/µl; Ambion) is added to the reaction and incubated for 20 min at 37°C to digest the DNA template. To precipitate the *in vitro* transcript, the reaction is filled to 100 µl with Roth H_2O and 100 µl phenol-water (AppliChem) is added. The reaction is mixed, and phase separation is achieved by centrifugation at 13.000 rpm for 10 min at RT (*biofuge pico 17*). When 85 µl of the upper, aqueous phase is transferred to a virgin 1.5 ml microcentrifuge tube, 100 µl of chloroform/isoamyl alcohol (24:1) is added and mixed in. After a second centrifugation step (10 min, RT) 70 µl of the upper, aqueous phase are transferred to a virgin 1.5 ml microcentrifuge tube and 1 volume of isopropanol and 1/10 volume of 3M NaOAc are added before incubation at 4°C overnight. Precipitation is carried out by centrifugation at 13.000 rpm for 30 min at 4°C (*biofuge fresco*). After washing and drying the RNA pellet, it can be dissolved in 20 µl of Roth H_2O and stored at -20°C. The success and quality of the *in vitro* transcription can be monitored on a PAA urea mini gel (Tab. 32).

Table 31: Composition of an *in vitro* transcription reaction.

Component	**Amount**	
Template	set 2-5 pmol	
Magnesium chloride [40 mM]	2 µl	[3.2 mM]
DTT*[100 mM]	2 µl	[8 mM]
rRNasin [40 U/µl]	0.8 µl	[1.3 U/µl]
rRNTPs [25 mM each]	2 µl	[2 mM each]
10x RNA polymerase buffer	2.5 µl	[1x]
T7 RNA polymerase [50 U/µl]	1.5 µl	[5 U/µl]
ddH_2O	*ad* 25 µl	

Table 32: Composition of a PAA urea mini gel.

Component	**Amount**	
Urea	4.2 g	[7 M]
Acrylamide [40%]	2 m	[8%]
10x TBE	1 ml	[1x]
ddH_2O	*ad* 9 ml	
Dissolve urea by stirring on magnetic stirrer		
ddH_2O	*ad* 10 ml	
Ammonium persulfate [10% w/v]	40 µl	
TEMED*	10 µl	

*Tetramethylethylenediamine

2.4.6 Northern blot for detection and analysis of RNA

Northern blot originally designates the transfer of RNA to a membrane (blotting), which was first described in 1977 by Alwine, Kemp, and Stark. Here, Northern blot is used as an umbrella term for one method used to study the expression of genes on RNA level. For the Northern blot experiment total RNA (2.4.1.3) is separated on a gel, blotted onto a nylon membrane, and the RNA of interest is detected using a radioactively labelled hybridisation probe (2.4.7). Since equal amounts of total RNA are loaded on the gel, the strength of the hybridisation signal provides information on the expression level of the tested RNA. To study sRNAs and small mRNAs below 600 nt the total RNA is separated on a PAA urea gel, for studying larger RNAs, a formaldehyde agarose gel is used. Depending on the gel also the blotting method differs. Both methods are described below.

2.4.6.1 Northern blot of RNA with polyacrylamide urea gel

For the PAA urea gel-based Northern blot, a 8% PAA urea gel (Tab. 33) is poured between two glass plates (square and ear plate) which are assembled with three 1 mm thick spacers and clamps (two on each side and three at the bottom). A comb to form the pockets is placed into the gel. To allow the gel to polymerise standing vertically, one can seal the glass plate spacer sandwich with melted agarose from outside. This will lead to far better gel pockets since the gel will not run behind the comb as it would when laying down the gel to polymerise. The gel run is carried out in a vertical perspex gel chamber (Werkstatt JLU Gießen) with 1x TBE as running buffer. Equal amounts of total RNA (6-8 µg; quantification 2.4.2) are aliquoted into virgin 1.5 ml microcentrifuge tubes, and 0.7 volume formamide urea mix (FU mix; Tab. 10) is added. To denature secondary RNA structures, which would alter the migration in the gel, the samples are incubated at 65°C for 10 min. The comb is withdrawn from the polymerised gel, the gel is placed in the buffer-filled gel chamber, and the samples are loaded with the help of an *Exmire Microsyringe* (Roth/Ito Corporation) into the gel pockets. Each pocket is rinsed with running buffer before loading a sample. First, the gel is run for 10 min at 100 V which is increased to 300 – 400 V to separate the RNA according to size. The gel run takes around 3 h; the separation of the RNA has shown to be best when the bromophenol blue dye which is contained in the FU mix has run out of the gel. To blot the RNA from the gel to a nylon membrane (*Roti®-Nylon plus*, pore size 0.45 µm; Roth) a semi-dry electro-blot is carried out. Therefor a stack of blotting paper (Albet LabScience), the membrane and the gel is placed on the anode plate of an electroblotter (PeqLab). The size of the blotting paper and the membrane is hereby equivalent to the size of the gel that is to be blotted. The stack is arranged in the following order: three blotting papers soaked in 1x TBE, nylon membrane, gel and three blotting papers soaked in 1x TBE. It is essential to avoid air bubbles between the layers and that the gel overlaps the membrane and blotting papers underneath and touches the anode plate since this would lead to current flow through the gel only instead of through the blotting stack. The electro-blot runs at 250 mA for 2.5 h.

After the blotting, the RNA is cross-linked to the membrane with UV light (2 times, 1200 kjoule UV light) using the *UV Stratalinker 1800* (Stratgene). The membrane can be stored between two dry blotting papers at RT before being used for hybridisation (2.4.9). The gel can be stained with ethidium bromide after blotting to check whether the RNA was blotted completely, which shows when only large rRNAs remained in the gel. Detection of an RNA with a hybridisation probe is described in 2.4.10.

Table 33: Composition of an 8% polyacrylamide-urea gel for RNA separation.

Component	**Amount**	
Urea	16.8 g	[7 M]
Acrylamide [40%]	8 ml	[8%]
10x TBE	4 ml	[1x]
ddH_2O	*ad* 38 ml	
Dissolve urea by stirring on magnetic stirrer		
ddH_2O	*ad* 40 ml	
Ammonium persulfate [10% w/v]	120 µl	
TEMED*	20 µl	

*Tetramethylethylenediamine

2.4.6.2 Northern blot of RNA with formaldehyde agarose gel

For Northern blot using a formaldehyde agarose gel, the gel tray and running chamber have to be cleaned by rinsing once with 1 N NaOH and twice with DEPC-H_2O. The preparation of the gel, as well as the gel run, is carried out on a plate which can be evened with an integrated level. The gel (Tab. 34) is poured into the cleaned gel tray which is closed with tape, and one or two combs are placed into the gel. Equal amounts of total RNA (10 - 12 µg; quantification 2.4.2) are aliquoted into virgin 1.5 ml microcentrifuge tubes and are evaporated almost completely (1 - 2 µl left) in the *SpeedVac* (Eppendorf). The concentrated RNA is dissolved in 9 µl freshly prepared RNA sample buffer (Tab. 35) and heated at 65°C for 10 min. After heating, 1 µl loading dye (Tab. 10) is added, and the samples are loaded onto the gel placed in 1x MOPS/DEPC-H_2O running buffer (10x MOPS see Tab. 9) in the running chamber. The first and last pocket of each row must be left empty. It is important to dip the yellow tip to the bottom of the pocket to load the sample because due to the high surface tension of the 1x MOPS the sample would flow out of the pocket otherwise. The gel run is started at 100 V for 10 min to let the samples run from the pockets to the gel. The current transmitter is turned up to 120 V and the tube-pump (NeoLab) connected to the running chamber is turned on. This will pump the running buffer constantly to the upper buffer chamber avoiding a change of pH in the 1x MOPS by ion flow to the lower chamber part. The gel is run until the bromophenol blue band has migrated 6.5 cm (two combs) or 10.5 cm (one comb) from the pockets through the gel. Before blotting the RNA from the gel to the membrane, the gel is incubated shaking in two buffers one after the other. First, it is incubated for 45 - 60 min in denaturing buffer (Tab. 36) and afterwards is

transferred into a neutralising buffer (Tab. 36) for 45 - 60 min. The blot itself is carried out with a vacuum blotter (Appligene). The blot is assembled in the following order: a blotting paper bigger than the mask is placed on the frit of the blotter. The mask is placed on top overlapping the blotting paper which is soaked with DEPC-H_2O. The blotter is closed by placing the blotter frame on the mask and closing the hinges. A nylon membrane (*Roti®-Nylon plus*, pore size 0.45 µm; Roth) as long as the cut-out of the mask and as wide as the gel section loaded with samples is placed on the blotting paper and soaked in 10x SSC (in DEPC-H_2O). Now the gel can be transferred carefully onto the membrane where it has to overlap the edges of the mask on each side; this is also why the first and last pocket of each row is left empty. The vacuum blotter is turned on and run at 50 - 65 mbar for 1 h. During the blotting, the upper side of the gel has to be kept in 10x SSC (in DEPC H_2O) to avoid drying and cracking of the gel. When the blot was disassembled, the RNA is cross-linked to the membrane as described for the semi-dry electro-blot (2.4.6.1). Detection of RNA with a hybridisation probe is described in 2.4.9-10.

Table 34: Composition of agarose formaldehyde gel for Northern blot.

Component	**Amount**
DEPC-H_2O	80 ml
Agarose	1.1 g [1%]
Boil until agarose has melted completely	
Let cool down for 10 min	
10x MOPS	11 ml [1x]
Formaldehyde [37%]	20 ml [6.7%]

Table 35: Composition of 1 ml RNA sample buffer for agarose formaldehyde Northern blot.

Component	**Amount**
10x MOPS	100 µl [1x]
Formamide	500 µl [50% v/v]
Formaldehyde [37%]	180 µl [8.5%]

Table 36: Composition of 250 ml denaturing and neutralising buffer for agarose formaldehyde Northern blot.

Denaturing buffer

Component	**Amount**
1 N NaOH	12.5 ml [0.05 N]
5 M NaCl	7.5 ml [0.15 M]
DEPC-H_2O	*ad* 250 ml

Neutralizing buffer

Component		**Amount**
1 M Tris HCl	pH 7.5	25 ml [0.05 N]
5 M NaCl		7.5 ml [0.15 M]
DEPC-H_2O		*ad* 250 ml

2.4.7 Radioactive labelling of nucleic acids

To detect an RNA of interest on a membrane from the Northern blot technique described above 2.4.6, one needs a hybridisation probe complementary to that RNA. The here used probes are

labelled with radioactively labelled nucleotides. Besides for the use as hybridization probes, nucleic acids can be labelled for detection in a gel when needed, for example, in interaction studies (2.4.13). To incorporate the labelled nucleotides in the needed nucleic acid the below-described techniques can be used.

2.4.7.1 End-labelling with polynucleotide kinase

One opportunity to prepare a hybridisation probe is to end-label a single stranded oligonucleotide by using the enzyme polynucleotide kinase (PNK). The PNK catalyses the transfer and exchange of P_i from the γ position of an ATP (here [γ^{32}P]dATP) to the 5'-hydroxyl terminus of polynucleotides (here single-stranded DNA oligo).

For the labelling reaction, the DNA oligo [10 µM] is mixed with PNK [10 U/µl] plus its corresponding buffer A (Thermo Scientific) and 30 µCi [γ^{32}P]dATP (Hartmann Analytic). The reaction (Tab. 37) is incubated at 37°C in a heating block for 1 h. Afterwards, the reaction is stopped by adding 40 µl STE buffer (Tab. 9) which results in a volume of 50 µl. To get rid of the remaining enzyme, buffer and free dATPs, the reaction is purified using a *MicroSpin G25 illustra* column (GE Healthcare; see 2.4.8).

Table 37: Reaction for oligonucleotide end labelling with polynucleotide kinase (PNK).

Component	Amount	
Oligonucleotide [10 µM]	2 µl	[2 µM]
PNK buffer A	1 µl	[1x]
T4 PNK [10 U/µl]	1 µl	[1 U/µl]
ddH_2O	3 µl	
[γ^{32}P]dATP [10 µCi/µl]	3 µl	[3 Ci/µl]

2.4.7.2 Random priming

A second method to prepare a radioactively labelled hybridisation probe is the so-called random priming. Here the *Prime-a-Gene®* Labeling System manufactured by Promega is used. The reaction is set up and carried out as described in the manufacturer's manual. Additionally, the labelled DNA template (here PCR product) is purified with a *MicroSpin G50 illustra* column manufactured by GE Healthcare as described in 2.4.8.

2.4.7.3 Hot *in vitro* transcription

There is a third method to label nucleic acids with labelled nucleotides, which is based on the *in vitro* transcription using T7 RNA polymerase. The RNA polymerase can incorporate radioactively labelled nucleotides added to the reaction during the transcription. For details on *in vitro* transcription see 2.4.5 and for the composition of hot *in vitro* transcription see table 38 below.

Besides using the hot *in vitro* transcript for interaction studies (EMSA 2.4.13), the labelled nucleic acid can be used as riboprobe for hybridisation of e.g. Northern blot membranes (2.4.6).

Table 38: Composition of a hot *in vitro* transcription reaction.

Component	**Amount**	
Template	set 2-5 pmol	
Magnesium chloride [40 mM]	2 µl	[3.2 mM]
DTT*[100 mM]	2 µl	[8 mM]
rRNasin [40 U/µl]	0.8 µl	[1.3 U/µl]
rRNTPs (low UTP)**[25:25:25:5 mM]	2 µl	[1:1:1:0.2 mM]
10x RNA polymerase buffer	2.5 µl	[1x]
T7 RNA polymerase [50 U/µl]	1.5 µl	[5 U/µl]
ddH_2O	*ad* 22 µl	
[γ^{32}P]dUTP [10 µCi/µl]	3 µl	[3 µCi/µl]

* Dithiothreitol

** 25 mM ATP/CTP/TTP each plus 5 mM UTP

2.4.8 Purification of radioactively labelled nucleic acids

To get rid of free nucleotides and salt from the buffer, labelling reactions (2.4.7.1 – 2.4.7.3) can be purified using *MicroSpin illustra* columns manufactured by GE Healthcare. The *G25* columns are used for labelled oligonucleotides since they are suited best for nucleic acids greater than 10 bases in length. The *G50* columns are used for nucleic acids larger than 30 bases in length.

The resin contained in the columns is resuspended by vortexing, and the columns are opened by removing the bottom closure. The storage buffer is removed from the resin by centrifugation of the column in a collector tube at 2.600 rpm for 1 min at RT (*biofuge pico17*). Now the columns can be placed into virgin 1.5 ml microcentrifuge tubes, and the reaction which is to be purified is pipetted carefully on top of the resin without disturbing the resin bed. The columns are centrifuged again for 2 min, and the purified sample is collected in the microcentrifuge tube. The radioactively labelled nucleic acids can be stored at -20°C until further use. For hybridisation of a Northern blot membrane (2.4.9) 500.000 – 2.000.000 cpm of a probe are added. To determine the cpm of a purified reaction, 2 µl of a purified probe or *in vitro* transcript can be measured with the help of a scintillation counter (Beckman Coulter).

2.4.9 Hybridisation with radioactively labelled nucleic acids

To detect a specific RNA on a Northern blot membrane (2.4.6), the membrane is prehybridised and hybridised using the Church and Gilbert buffer system (short Church buffer; Tab. 39). Either hybridisation step is carried out in the same buffer. The stringency of the buffer used (high, moderate or low) depends on the length of the hybridisation probe – here short probes (end-labelled

oligos) are hybridised in low stringency Church buffer while longer probes (random primed PCR products) are hybridised in moderate stringency Church buffer.

The membrane is prehybridised in 30 ml Church buffer rotating at 42°C for > 1 hour in the hybridisation oven (Agilent). After prehybridisation, the radioactively labelled probe (2.4.7) complementary to the RNA of interest is added (500.000 cpm for loading controls, 2 mio cpm for every else). The probe should be pipetted carefully into the hybridisation tube so that it does not touch the membrane before being diluted in the buffer. Hybridisation takes place overnight at 42°C, rotating in the hybridisation oven. To wash away unbound probe the membrane is slewed in Church wash buffer (0.01% SDS; 5x SSC in ddH_2O). Washing is repeated in 30 sec steps until the corners of the membrane do not show background signal when checking with the Geiger-Müller counter (*Mini 900 Ratemeter*, Thermo Scientific). Now the membrane can be shrink-wrapped into a polypropylene disposal bag (Roth) and exposed on an imaging screen (Fuji/BioRad; 2.4.10).

Table 39: Composition of Church hybridisation buffers (100 ml) for Northern blot.

Component	low stringency	moderate stringency	high stringency
Potassium phosphate buffer [1 M]	50 ml	50 ml	20 ml
Bovine serum albumin	1 g	1 g	1 g
SDS [20% w/v]	35 ml	35 ml	35 ml
EDTA [250 mM]	0.4 ml	0.4 ml	0.4 ml
Formamide	-	15 ml	15 ml
ddH_2O	15 ml	-	30 ml

2.4.10 Exposure of a membrane on an imaging screen and phospho-imaging

The washed and shrink-wrapped membrane is exposed on an imaging screen (Fuji/BioRad) for, depending on the signal intensity, 0.5 to 72 h. Through the radiation of the probe the BaFBr crystals in the grid of the imaging screen are transferred to their excited state, which can be imaged using the HeNe laser (600 nm) of the phosphor-imager (*Personal Molecular Imager FX*, BioRad). Before exposing again on the imaging screen, the excited state is reversed by exposure to yellow light (*Screen Eraser-K*, BioRad) for 30 min.

2.4.11 Stripping of Northern blot membranes

To hybridise a Northern blot membrane with further probes, the previously used probe has to be stripped of the membrane, since it would otherwise interfere with the signal of the next probe. For stripping, the membrane is unpacked from the polypropylene bag und transferred into a glass bowl. The membrane is covered with stripping buffer (0.1% SDS; 5x SSC in ddH_2O) and incubated shaking

at 96°C in water bath for 20 min. Afterwards, the membrane is rinsed with water and stored at RT or used for hybridisation (2.4.9) again.

2.4.12a Quantification of phosphor-imaging signals using the Quantity-One analysis software

To determine the intensities of phosphor-imaging signals from exposed Northern blot membranes the Quantity-One 1-D analysis software (BioRad) is used. The determined signal intensities can be used for calculation of the ratio between two sample signals.

To quantify the signals the phosphor-imaging scan (2.4.10) is opened with the Quantity-One software, the function "volume rectangle tool" from the volume tab is chosen, and a first rectangle is drawn around the largest signal on the scan. The rectangle size is kept throughout the whole quantification step. The first rectangle (U1) is placed around the first signal and is then copied by holding the Strg key and pulling the copied rectangle (U2) to the next signal. Like that, rectangles are placed around all signals, in doing so the rectangles should not overlap. The last rectangle is placed at a position with an even background, and its function is changed to "background" by double-click and selection of the "background" option. The values from the placed rectangles (example in Fig. 22) can be shown and exported by choosing the "Volume Analysis Report" button in the tab report. The values are given in volume as counts/mm^2 (CNT*mm2), adjusted volume as CNT*mm2 (displaying the signals minus the background) and as adjusted volume percent (%). To calculate the ratio between two signals from one probe each signal value has to be divided by its loading control signal value (5S or 14S rRNA) to adjust for loading inaccuracy. The signal values corrected to the loading control can be divided to gain the ratio sample A/ sample B.

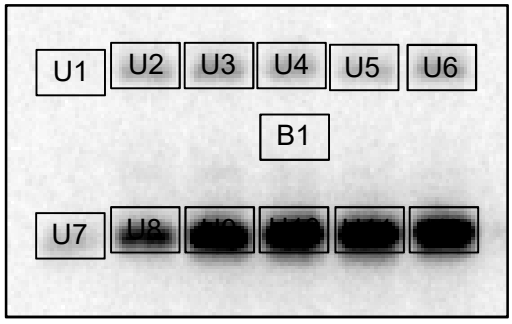

Figure 22: Exemplary Northern blot quantification. The rectangles are placed around each signal (UX) according to the size of the strongest signal (U12) and do not overlap. Even background is chosen (B1).

2.4.12b Use of quantified phosphor-imaging signals for half-life calculation

The description of RNA half-life calculation is adapted from Yannick N. Hermanns' PhD thesis ("Die Auswirkung von Umwelteinflüssen auf die mRNA Stabilitäten in *Rhodobacter sphaeroides"*; 2014).

For the calculation of the RNA half-life, one expects that the RNA decay rate is constant over the time investigated. First, ratios of the amount of RNA at the tested time points in comparison to time point 0 (t 0, before addition of rifampicin) are calculated on the basis of the Northern blot signals (2.4.12a).

When the decay rate is constant, the logarithmic ratios should decrease linearly over time (decay profile). According to the decay profile the slope (m) of the regression line can be calculated as m = Δy / Δx, with Δy and Δx standing for the changes in the Y and X coordinates respectively. From the slope the half-life (t ½) is calculated as follows:

Calculation 7: $$t\ ^1/_2 = \frac{-1}{m}$$

2.4.13 Electrophoretic mobility shift assay (EMSA)

To investigate the direct interaction between two molecules, an electrophoretic mobility shift assay (EMSA) can be carried out. Here the interaction of two RNA molecules was to be investigated. For this purpose, the radiolabelled RNA of interest is incubated with a binding-candidate RNA under variable experimental conditions. When binding occurs the RNA:RNA complex shows a retarded migration in a non-denaturing polyacrylamide gel compared to the radiolabelled RNA alone. In each lane, equal amounts of radiolabelled RNA (here always sRNA of interest) is loaded. Depending on the sample, varying amounts of non-labelled RNA (here always potential mRNA target or mRNA control) are added. In the samples in which the interaction should be investigated the sRNA and the mRNA are de- and renatured separately. To achieve a quite likely interaction, which can act as the positive control to monitor the electrophoretic mobility of the RNA:RNA complex, one can de- and renature both RNAs together. Further controls are the radiolabelled sRNA alone and the sRNA together with an excess of non-target mRNAs, which should show no interaction.

A non-denaturing PAA gel (Tab. 40) is poured between two glass plates assembled with three 0.2 mm thick spacers as described for the PAA urea gel (2.4.6.1). After polymerisation, the gel is pre-run for one hour at 100 V at 4°C (cold room). Microcentrifuge tubes with needed amounts (indicated in the respective results part) of non-labelled mRNA are prepared on ice, and the sample volume is increased to 7.5 µl with Roth H_2O. The same is done for the radiolabelled sRNA; only for the positive control mRNA and sRNA are prepared in one tube. Now the samples are incubated for 1 min at 96°C in a water bath and then put back on ice. When the samples cooled down for 2 min, they are incubated at 32°C for 5 min. After these de- and renaturing steps the hot sRNA and cold mRNA can be joined in one tube and structure buffer (Tab. 41) is added (final concentration indicated in the respective results part). To allow the interaction of the RNAs, the samples are incubated at 32°C for 20 min. Now 0.15x volume of loading dye (Tab. 10) is added, and the samples are loaded onto the non-denaturing polyacrylamide gel (Tab. 40). Since the loading buffer is only slightly dyed the sample is not clearly visible during loading. Therefore one needs to carefully watch the glycerine of the buffer sinking into the pocket making sure the sample is correctly loaded. The gel run is carried out with 100 - 200 V at 4°C for 2 - 3 h. When the gel run is finished, one glass plate is removed, and the

gel is transferred to a blotting paper (Albet LabScience) with a size of 20x20 cm. A second blotting paper is placed under the first paper, and the gel plus blotting papers are wrapped in cling film, leaving an open space at the back. The gel can be dried wrapped like this on a gel dryer (*SLab Gel Dryer GD5040*, Scie-Plas) at 80°C for 45 min. The dried gel is kept wrapped and is exposed on an imaging screen (Fuji / BioRad) as described for Northern blot membranes (2.4.10) overnight. The gel is documented using the phosphorimager.

Table 40: Composition of non-denaturing PAA gel for EMSAs.

Component	Amount	
40% acrylamide	3 ml	[6%]
10x TB	0.5 ml	[0.25 x]
1M $MgCl_2$	0.2 ml	[10 mM]
DEPC-H_2O	16.3 ml	
10% APS	120 µl	
TEMED	12 µl	

Table 41: Composition 10 ml 10x structure buffer for EMSA samples.

Component	Amount	
1M Tris HCl pH 7.0	1 ml	[100 mM]
1M $MgCl_2$	1 ml	[100 mM]
KCl	0.75 g	[1 M]
DEPC-H_2O	*ad* 10 ml	

2.5 Protein biochemical methods

2.5.1 Bradford-assay for the determination of the protein concentration

The Bradford assay, described by Bradford in 1976, is a spectroscopic method to measure the total protein concentration in a solution, in the range of µg/ml. The assay is based on the absorbance shift of the triphenylmethane dye *Coomassie-Brilliant blue G-250*. The dye is red in its cationic state showing an absorption maximum at 470 nm. While forming complexes with cationic and covalent side chains of proteins the dye is stabilised in its anionic, blue form which has an absorption maximum at 595 nm. The increase in absorption at 595 nm in the tested sample can be quantified on the basis of a calibration curve.

To prepare the calibration curve a dilution series of a protein standard, here bovine serum albumin (BSA), ranging from 1 to 10 mg/ml is used. The reference consists of 595 µl ddH_2O and 250 µl Bradford reagent (*RotiQuant*, Roth), whereas the samples additionally contain 5 µl of the solution

of interest, usually cell extract (e.g. see 2.2.10b). Each sample is prepared in technical duplicates. After mixing the reference, samples for calibration curve, and samples of interest in polystyrene cuvettes, the reaction is incubated in the dark at RT. The absorption is measured at 470 and 595 nm in the photometer. According to the calibration curve the protein amount in the sample can be calculated using the following calculation:

Calculation 8: Calibration curve (linear regression): $y = ax - b$

Protein [µg/µl] = $[(\bar{x}\ Abs_{595\ 1\text{-}2} + b)/a)]/D$

D: dilution factor

2.5.2 Western blot

The Western blot analysis is used to detect proteins in biological samples. As for the Northern blot analysis, the samples are separated on a gel before blotting them onto a membrane for detection. The separation takes place according to the proteins molecular weight and the detection is enabled by antibodies, either directed specifically against the investigated protein or against a tag added to the protein (fusion protein). An example of the latter is a poly-His tag that can be detected with a corresponding His antibody. Depending on the used primary antibody, often a secondary antibody directed against the primary one is needed, e.g. Horseradish peroxidase coupled, to enable a detectable reaction at the primary antibody binding site. According to the size of the investigated protein, two different gel electrophoresis types can be utilised as described in the following chapters.

2.5.2.1 Western blot – Laemmli-SDS-PAGE

A Western blot can be based on a so-called Laemmli-SDS-polyacrylamide gel electrophoresis (PAGE), first described in 1970 by Laemmli. An SDS-PAA gel is used to separate proteins in a mass range of 100 - 250 kDa. Here, the SDS contained in gel and sample loading buffer leads to denaturation of the proteins. SDS disrupts non-covalent bonds and thereby denatures the proteins and in addition imparts a negative charge on the proteins.

To prepare protein samples for a Western blot analysis, the needed strains are cultivated under the desired conditions (2.2.2.1.1 - 2.2.1.8). For each sample, cells from 20 ml culture are harvested by centrifugation at 9.000 rpm, at 4°C for 10 min (*RC 5C plus* / *RC 6 plus*, *SS-34* rotor). The cells are transferred to virgin 1.5 ml microcentrifuge tubes and are re-suspended in 500 µl resuspension buffer (1x PBS; 10% Glycerin; 1 mM phenylmethanesulphonyl fluoride, PMSF) each. The cells are broken by sonication, eight times 30 sec with the *Sonoplus GM70* (parameters: Power MS 72/D, cycle 70%) with 30 sec pause on ice. The cell debris is removed by centrifugation at 13.000 rpm

for 10 min at 4°C (*biofuge fresco*) and transferring 450 µl of the supernatant into a virgin 1.5 ml microcentrifuge tube. The samples can be stored at -20°C. To load equal amounts of protein for the Western blot, the protein concentration of each sample is determined via a Bradford assay (2.5.1). The protein samples are mixed with 5x SDS sample loading buffer (Tab. 10) in a 1:5 ratio and heated at 100°C for 5 min. Until loading of the gel, the denatured samples can be stored on ice. For gel preparation a 6 - 12% separation gel (Tab. 42) is poured between two glass plates assembled as described for the Northern blot technique (2.4.6.1) and 70% ethanol is added on top. The covering with ethanol limits the contact of the gel with the surrounding oxygen and thereby speeds up the polymerization. As soon as the gel has solidified, the ethanol can be removed, a 5 - 10% stacking gel (Tab. 42) is poured on top of the separation gel and a comb is inserted. Using separation and stacking gel (disc electrophoresis) allows concentrating the proteins to a joint starting point before separation. The pH within the stacking gel helps to stack the proteins so that they reach the separation gel in one thin starting zone. Next the higher pH within the separation gel increases the net charge of the proteins and thereby their effective mobility, the proteins now resolve according to their molecular mass (for additional information on disc electrophoresis see e.g. Reisfeld *et al*., 1962). Loading of a prestained protein marker (here *PageRuler*^{TM}, Thermo Scientific) allows subsequent size determination. The gel run is carried out for 3 h with 150 – 200 V using 1x Laemmli (Tab. 9) as running buffer. Afterwards the gel, as well as six blotting papers and a nitrocellulose membrane (size of the gel), are placed in transfer buffer (prepare fresh; Tab. 43). The electroblot is prepared as follows: three blotting papers placed on the anode of an electroblotter (PeqLab), ontop of the blotting papers the nitrocellulose membrane (GE Healthcare), the gel, and three more blotting papers are piled up free of air bubbles. To transfer the proteins to the membrane 0.8 mA cm^{-2} are applied for 1 h. The success of the blotting can be examined by staining with Ponceau S solution (Sigma Aldrich), which will additionally fix the proteins onto the membrane. The Ponceau-stained membrane can be documented by scanning and the Ponceau is removed using ddH_2O and 1N NaOH. The membrane is incubated in blocking solution (Tab. 44) for 2 h at RT or overnight at 4°C. The SDS-PAGE based Western blots described in 3.1.4.2 were then incubated with the purified primary antibody α-GFP, diluted 1:4000 in blocking buffer, for 1 h at RT. To incubate the membrane with the secondary antibody (anti-mouse IgG conjugated with horse-radish peroxidases, produced in goat, Sigma-Aldrich) the membrane is washed in 1x TBS 3 times for 5 min. The secondary antibody is added diluted 1:5000 in blocking buffer for 1 h. When washed for 3 times again, the Western blot is developed using the *Lumi-Light Western Blotting Substrate* 1 and 2 (Roche) according to the manufacturer's manual, and analysed and documented on a Chemiluminescence-Imaging System (*Fusion-SL4*; Peqlab).

Table 42: Composition of 30 ml stacking and separation gel.

Stacking gel			
Component		**Amount**	
1.5 M Tris HCl	pH 6.8	7.5 ml	[0.375 M]
40% Acrylamide		4.5 - 9 ml	[6 – 12%]
10% SDS		0.3 ml	[0.1%]
10% APS		0.3 ml	
TEMED		0.015 ml	
ddH_2O		*ad* 30 ml	

Separation gel			
Component		**Amount**	
1.5 M Tris HCl	pH 8.8	7.5 ml	[0.375 M]
40% Acrylamide		4.5 - 9 ml	[6 – 12%]
10% SDS		0.3 ml	[0.1%]
10% APS		0.3 ml	
TEMED		0.015 ml	
ddH_2O		*ad* 30 ml	

Table 43: Composition of 1 l transfer buffer.

Component	**Amount**	
Tris	3.02 g	[25 mM]
Glycin	14.26 g	[190 mM]
Methanol	200 ml	[20%]
ddH_2O	*ad* 1000 ml	

Table 44: Composition of 100 ml Western blot blocking solutions.

For eGFP-antibody		
Component	**Amount**	
10x TBS	10 ml	[1x]
Milk powder	5 g	[5% w/v]
ddH_2O	*ad* 100 ml	
For *Strep*-Tactin conjugate		
Component	**Amount**	
10x PBS	10 ml	[1x]
BSA	3 g	[3% w/v]
Tween 20	0.5 ml	[0.5% v/v]
ddH_2O	*ad* 100 ml	

2.5.2.2 Western blot - Tricine-SDS-PAGE

A Tricine-SDS-PAGE gel electrophoresis, as first described by Schägger *et al*. (1986 and 1987), is used to separate proteins in the mass range of 1 - 100 kDa (Schägger, 2006). The gel containing SDS, AB-3 solution (acrylamide/bis-acrylamide) and gel buffer is run with a Tris-HCl anode buffer and a Tricine containing Tris-HCl cathode buffer (AB-3 solution, buffers, and gel compositions in Tab. 45 - 47). The gel preparation, run, blotting and blocking are carried out as described in 2.5.2.1. The Tricine-SDS-PAGE-based Western blots described in 3.1.4.2 were used to detect a *Strep*-tag protein in cell extracts. Therefor the *Strep*-Tactin® horseradish peroxidase conjugate (IBA) was used for detection according to the manufactures manual. Washing was performed using PBS-Tween buffer (1x PBS, 0.1% Tween 20 w/v). The development was again carried out using the *Lumi-Light Western Blotting Substrate* 1 and 2 (Roche) as described above (2.5.2.1).

Table 45: Buffers used for Tricine-SDS-PAGE Western blot, compositions for 1 l each.

3x Gel buffer		
Component	**Amount**	
Tris	363.42 g	[3 M]
HCl	36.64 g	[1 M]
20% SDS	15 ml	[0.3%]
	adjust to pH 8.45	
ddH_2O	*ad* 1000 ml	
10x Anode buffer		
Component	**Amount**	
Tris	121.14 g	[1 M]
HCl	8.2 g	[0.225 M]
	adjust to pH 8.9	
ddH_2O	*ad* 1000 ml	
10x Cathode buffer		
Component	**Amount**	
Tris	121.14 g	[1 M]
Tricine	179.17 g	[1 M]
20% SDS	50 ml	[1%]
	adjust to pH ~8.25	
ddH_2O	*ad* 1000 ml	

Table 46: Composition of 100 ml AB-3 stock solution for Tricine-SDS-PAGE Western blot.

Component	**Amount**
Acrylamide	48 g
Bisacrylamide	1.5 g
ddH_2O	*ad* 100 ml

Table 47: Composition of Tricine-SDS-PAGE stacking and separation gel.

4% Stacking gel		
Component	**Amount**	
AB-3	1 ml	[4%]
3x gel buffer	3 ml	[0.75x]
ddH_2O	8 ml	
10% APS	90 µl	
TEMED	9 µl	

16% Separation gel		
Component	**Amount**	
AB-3	10 ml	[16%]
3x gel buffer	10 ml	[1x]
ddH_2O	10 ml	
10% APS	100 µl	
TEMED	10 µl	

3. Results

Small RNAs (sRNAs) function as cellular regulators in all kingdoms of life (Wagner & Romby, 2015) and their role in the response to environmental factors in prokaryotes has been studied intensively in recent years (Wassarman *et al*., 2016; Lalaouna *et al*., 2013). In this work three sRNAs (1.10) were investigated in the facultatively photosynthetic model organism *R. sphaeroides*: the oxidative stress induced, coding sRNA Pos19 (3.1), the photosynthesis regulating, 3'UTR derived sRNA PcrX (3.2), and the RpoHI/ RpoHII dependent sRNA RSs0827, which directly interacts with the *rpoE* mRNA (3.3).

3.1 Characterisation of the sRNA Pos19

The sRNA Pos19 (Photo-oxidative stress induced sRNA 19, former RSs0019) was initially identified in an RNA-seq study comparing RNA levels in the *R. sphaeroides* wild-type before and after photo-oxidative stress ($^1O_2$ stress; Berghoff, 2009).

3.1.1 Expression pattern

Pos19 was first shown to be strongly up-regulated upon $^1O_2$ stress (Berghoff *et al*., 2009). Later peroxide stress and iron limitation were found to induce the Pos19 expression, while superoxide radicals (O_2^-) did not lead to Pos19 induction (Fig. 23). Furthermore, the induction of Pos19 was found to be dependent on the alternative sigma factor RpoE, but independent of the alternative sigma factors $RpoH_I$ and $RpoH_{II}$ (Fig. 23). When the *rpoE-chrR* locus is deleted (TF18 strain), there is no expression of Pos19 upon $^1O_2$, H_2O_2 or tBOOH stress (Fig. 23). Whereas in the *rpoHI* and the *rpoHII* deletion mutants, Pos19 is induced upon $^1O_2$ stress, as in the wildtype, and induction upon $^1O_2$ stress is also found in the *rpoHI*/*rpoHII* double mutant (Fig. 23). In line with these observations, a RpoE promoter motif (TGATCC(N_{15})GCGTA) (Newman *et al*., 1999) can be found upstream of Pos19 (Fig. 24). The expression pattern (Fig. 23) was tested by Northern blot analysis (2.4.6). Therefor total RNA was isolated from samples harvested at the designated time points from the indicated strains (Fig. 23), grown under microaerobic (2.2.1.2) or stress conditions. $^1O_2$ stress was generated as described in 2.2.1.5, while the remaining stress conditions were created by adding the following chemicals [final concentration] after taking the 0 min samples: H_2O_2 [1 mM], paraquat causing superoxide stress [250 µM], and tBOOH [300 µM]. Iron-limiting conditions were achieved as described in 2.2.2.1.6. The probes for detection of Pos19 and the 5S rRNA loading control are listed in table 3. Radiolabelling and membrane hybridisation, as well as phospho-imaging, was carried out as described in 2.4.7 – 2.4.10.

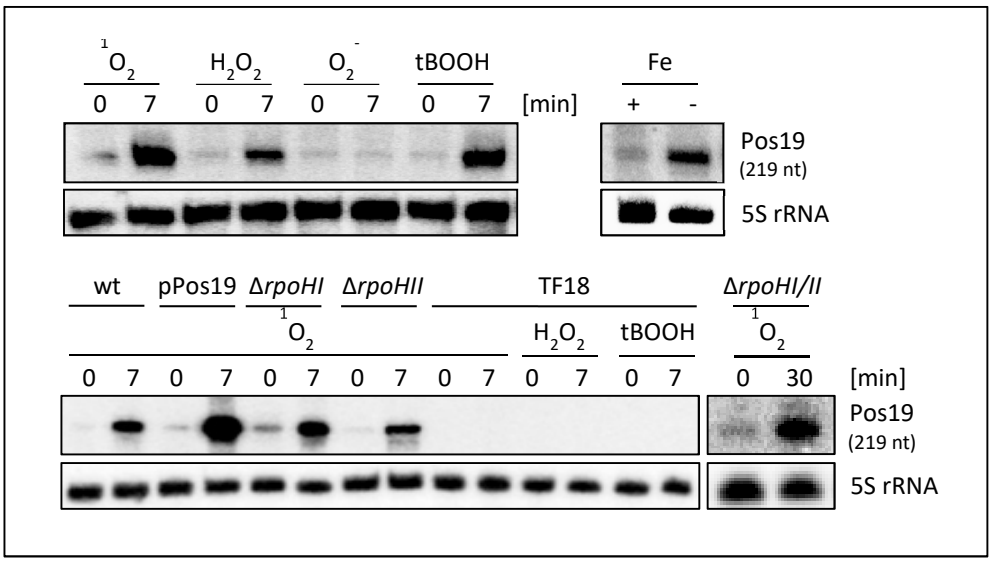

Figure 23: Expression profile of Pos19 in the *R. sphaeroides* wild-type (upper panel), and a Pos19 over-expression strain (3.1.3) as well as knockout mutants of alternative sigma factors: Δ*rpoHI*, Δ*rpoHII*, *ΔrpoHI/II* and TF18, which lacks the *rpoE-chrR* locus (lower panel). The Northern blots were carried out using 8% PAA-urea gels and 8 µg RNA per lane. The 5S rRNA was probed as loading control. Northern blots for iron limitation (+/- Fe, upper right) and the Δ*rpoHI/II* strain (lower right) were performed by Bernhard Remes and Sabine Martini, respectively.

RpoE-dependent promoter

GCCGAGGCG**TGATCC**GGGGTGCGCGACCCT**GCGTA**AGCTGTGCACGATCAACCCAAGCAGAAAGGACCTGACC

+1 10 20 30

GATGAGCTATCTCTTCATGGAATCCGTTCTGACCTTCGGCACCCTCGGATTCGTGCTCGCGCTGGCCTACGTCAA

40 50 60 70 80 90 100

CATCCGCCAGACCGAGAAGCAGCTCGAAGAGAGCCGCAAGCGCCGCCAGGGCCTCGAGGCGGCCGTGGCCGA

110 120 130 140 150 160 170

A**TGA**TGCTGT***CGGGCCGGGCGAGCGATTGCCCGGCCGG***TGTTGCCCCGGAGAAGGCCCGCG

180 190 200 210 220 230

Figure 24: Detailed illustration of the *pos19* gene. The -35 and -10 motifs of the RpoE promoter are marked. The 219 nt long sRNA is shaded in grey and the Rho-independent terminator predicted by TransTermHP (Kingsford *et al*., 2007) is shown in italic letters.

3.1.2 Effects of the Pos19 over-expression

Oxidative and photo-oxidative stress are known sources of great damage to macromolecules in the cell (discussed in 1.3). Moreover, iron limitation is known to increase intracellular ROS levels (1.2 and 1.8). By virtue of the Pos19 expression pattern under these conditions (Fig. 23), a role of Pos19 in the oxidative stress defence was hypothesised. To learn more about this predicted function, a Pos19 over-expression strain was constructed. The *pos19* gene together with its native RpoE-dependent promoter (Fig. 24) was amplified with the primer pair RSs0019_up / RSs0019_down using

chromosomal *R. sphaeroides* DNA as template. The PCR product was subcloned into the pDrive cloning vector (Qiagen) and ligated into the pBBR1 broad-host-range cloning vector (Kovach *et al*., 1995) after digestion with BamHI and HindIII. The over-expression strain displays a $^1O_2$ stress-induced Pos19 level 15 fold higher (after 7 min of stress) than the wild-type (Fig. 25).

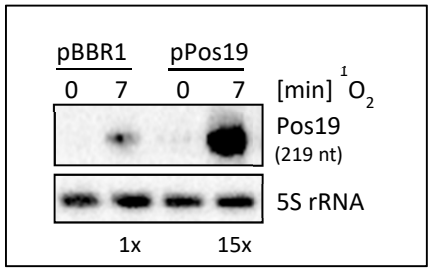

Figure 25: Validation of the Pos19 over-expression. Northern blot with 8 µg of total RNA samples from the EVC (pBBR1) and the Pos19 over-expression strain (pPos19). Hybridisation was carried out using a Pos19 and a 5S rRNA-specific probe. After 7 min of $^1O_2$ stress, a 15-fold higher expression of Pos19 was found in the over-expression strain compared to the EVC (fold changes represent mean values of three independent replicates).

The total RNA levels in the Pos19 over-expression strain and the corresponding empty vector control strain (EVC; pBBR1) were compared after 7 min of $^1O_2$ stress in a microarray analysis carried out by B. Berghoff (for full data set see Supp. 1) (Müller *et al*., 2016). Sixteen genes were found to be differentially expressed with a $\log_2$ ratio ≥ 1.0 or ≤ - 1.0 upon stress in the Pos19 over-expression strain compared to the EVC strain (Tab. 48). Among the down-regulated mRNAs, RSP_0557 (encoding a hypothetical protein) was most strongly affected ($\log_2$ ratio -2.3) by Pos19 over-expression. A second mRNA from a hypothetical protein (RSP_6037) was down-regulated with a $\log_2$ ratio of -1.0. In addition, mRNAs from genes and operons with a function in serine (*serC*, *serA*) and sulphur metabolism (*cysH*, *cysI*, RSP_1943, *cysG*/*cobA*) exhibited decreased mRNA levels. RSP_0557 and its potential interaction with Pos19 were studied in more detail (3.1.7 – 3.1.9). Also, the regulation of the genes involved in sulphur and serine metabolism was further elucidated (see below).

Table 48: Genes with differential mRNA levels upon Pos19 over-expression, $\log_2$ ratios ≥ 1 and ≤ -1.0

Gene Number	Gene Name	$\log_2$ ratio pPos19 vs. pBBR1	Function
Down-regulated			
RSP_0557		-2.3	Hypothetical protein
RSP_1351	*serC*	-1.0	Phosphoserine aminotransferase
RSP_1352	*serA*	-1.0	D-3-phosphoglycerate dehydrogenase
RSP_1941	*cysH*	-1.1	Phosphoadenosine phosphosulphate reductase
RSP_1942	*cysI*	-1.3	Sulphite/nitrite reductase hemoprotein subunit
RSP_1943		-1.4	Sulphite reductase (ferredoxin)
RSP_1944	*cysG/cobA*	-1.3	Uroporphyrin-IIIC-methyltransferase
RSP_6037		-1.0	Hypothetical protein

Tab. 48 continuing:

Up-regulated			
RSP_0069	*fliC*	1.6	Flagellar filament protein
RSP_2590		1.2	Hypothetical protein
RSP_2876	*coxM*	1.2	Carbon monoxide dehydrogenase medium chain
RSP_2877	*coxL*	1.5	Carbon monoxide dehydrogenase large chain
RSP_2878	*coxS*	1.9	Carbon monoxide dehydrogenase small chain
RSP_2879	*coxG*	1.6	Carbon monoxide dehydrogenase subunit G
RSP_3469		1.1	Hypothetical protein
RSP_6085		1.0	Hypothetical protein

Log_2 ratios were calculated from two individual microarray analyses; each containing pooled biological triplicates per strain. Reproducibility was high as reflected by a correlation coefficient (Pearson) of r = 0.92. Genes were considered to be differentially regulated when mRNA levels were changed with a log_2 ratio ≥ 1.0 or ≤ -1.0 Genes located in an operon are grouped together. Adopted from Müller *et al*., 2016.

The microarray results suggested particularly genes from the sulphur and serine metabolism to be down-regulated upon Pos19 over-expression. Thus the microarray data was re-inspected for genes down-regulated with a log_2 ratio ≤ -0.6 to see whether more genes from these metabolic pathways are negatively affected by Pos19 over-expression (Tab. 49).

Table 49: Genes with differential mRNA levels upon Pos19 over-expression, log_2 ratios ≤ -0.6.

Gene Number	**Gene Name**	**Log_2 ratio pPos19 vs. pBBR1**	**Function**
With function in sulphur metabolism and close pathways			
RSP_0129	*metN*	-0.8	ABC D-methionine uptake transporter, ATPase subunit
RSP_0130	*metI*	-0.8	inner membrane subunit
RSP_0132	*metQ*	-0.7	substrate-binding protein
RSP_0437	*sufC*	-0.6	ABC transporter, from *isc-suf* operon
RSP_1575	sopT	-0.8	Sulphate adenylyltransferase
RSP_2738	TST	-0.8	Probable Rhodanese-related sulphurtransferase

Tab 49 continuing:

RSP_1109	*cysK*	-0.7	Cysteine synthase
RSP_3697	*cysP*	-0.7	ABC sulfate/thiosulfate transporter
Without function in sulphur metabolism			
RSP_0147	*glnA*	-0.6	Glutamine synthetase class-I
RSP_1110		-0.7	Hypothetical protein
RSP_1547		-0.7	Probable bacterioferritin-associated ferredoxin
RSP_1987		-0.6	Hypothetical protein
RSP_2017		-0.7	Hypothetical protein
RSP_2115	*envA*	-0.7	Putative UDP-3-O-acyl N-acetylglucosamine deacetylase
RSP_2739		-0.6	Hypothetical protein
RSP_3095		-0.6	RNA polymerase sigma-70 factor
RSP_3715		-0.7	pH adaption potassium efflux system, PhaB subunit
RSP_4254	*rnk*	-0.9	putative regulator of nucleoside diphosphate kinase protein
RSP_4255		-0.9	Mechanosensitive (MS) ion channel protein
RSP_6029		-0.6	Hypothetical protein
RSP_6066		-0.6	Hypothetical protein
RSP_6180		-0.6	Hypothetical protein

Log_2 ratios were calculated from two individual microarray analyses, each containing pooled biological triplicates per strain. Reproducibility was high as reflected by a correlation coefficient (Pearson) of r = 0.92. Genes were considered to be differentially regulated when mRNA levels were changed with a log_2 ratio ≤ -0.6 Genes located in an operon are grouped together. Adopted from Müller *et al.*, 2016.

The examination revealed 22 more genes to be down-regulated (Tab. 49). Eight of which are also involved in sulphur metabolism or close pathways (upper part of Tab. 49), such as methionine uptake (RSP_0129, RSP_0130, and RSP_0132) and cysteine synthesis (RSP_1109), both sulphur-containing amino acids. The function of most of the regulated genes and the interconnection of the sulphur and cysteine pathways are depicted in figure 26.

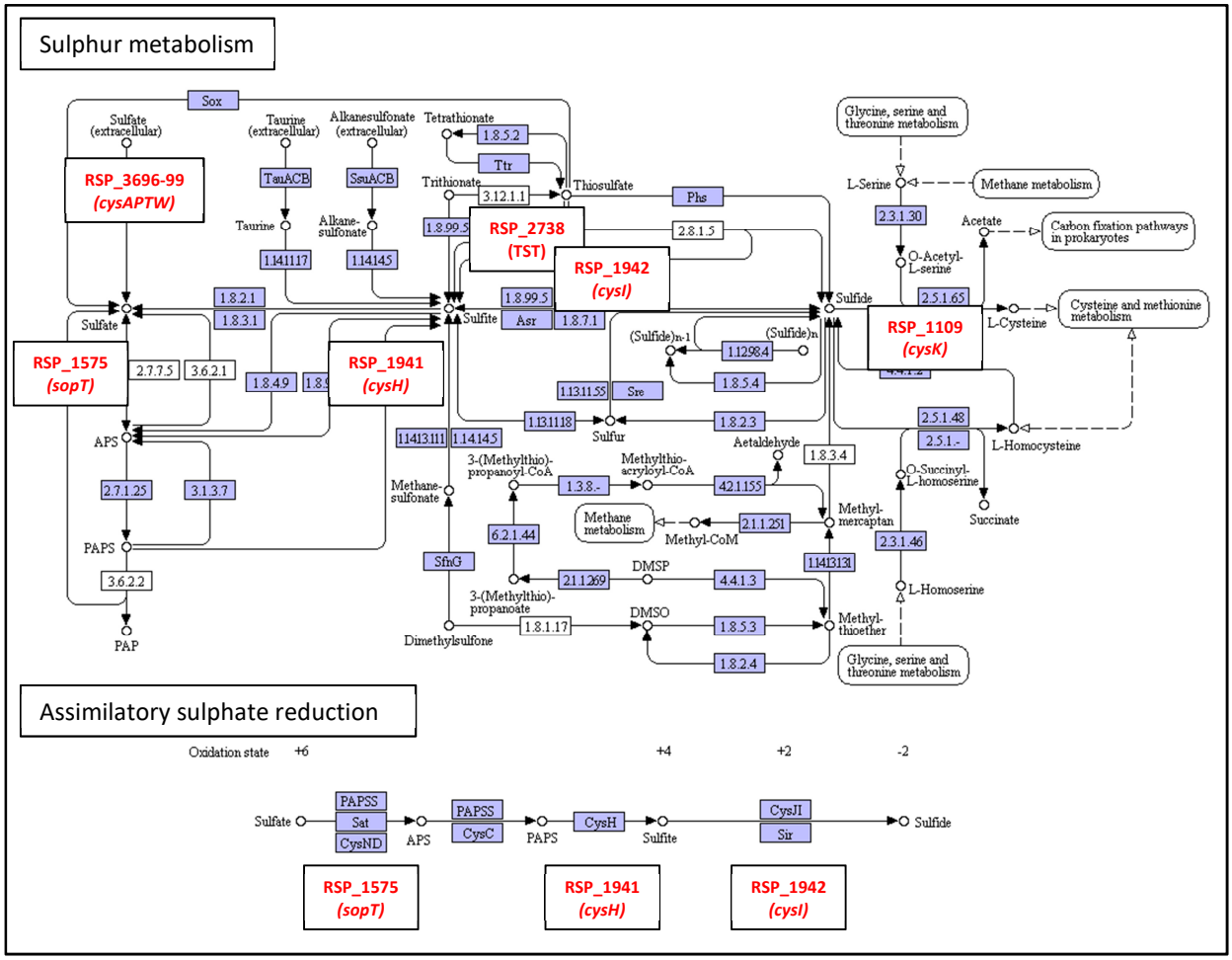

Figure 26: Sulphate metabolism and assimilatory sulphate reduction as illustrated in KEGG pathway maps (http://www.genome.jp/kegg/). *R. sphaeroides* genes (RSP) that have a function in these pathways and were shown to be affected by Pos19 in the microarray, are highlighted in red. Adapted from Müller *et al.*, 2016

To verify the altered mRNA expression levels in the Pos19 over-expression strain, an RT-PCR analysis (2.4.3.3) was carried out for selected genes. In the RT-PCR, mRNA levels before (0 min) and after 7 min of $^1O_2$ stress were compared in the empty vector control (EVC; pBBR), as well as in the Pos19 over-expression strain (pPos19). Cells were harvested from biological triplicates of each strain, before and after 7 min of stress, and the RNA was prepared as described in 2.4.1.3 b.

Besides RSP_0557 as the potential main target, *cysH*, *cysI*, and *serC* were tested as strongly regulated target candidates (log_2 ratio ≤ -1.0), while *metI* and *cysP* were tested as weaker regulated mRNAs (log_2 ratio -0.8 and -0.7). *RpoZ* was used as the reference gene, while *gloB* was used as a control. *GloB* is known to be up-regulated upon $^1O_2$ stress (Nuss *et al.*, 2009), but seemed not to be affected by Pos19 according to the microarray analysis (average log_2 ratio 0.12; Supp. 1). Primer pairs used for this RT-PCR analysis are listed in table 3. In the EVC strain, all tested genes were up-regulated upon stress as expected. Since the EVC strain reflects the wild-type situation, the RT-PCR verified the up-regulation that was found in the wild-type in a former RNAseq study (Berghoff *et al.*, 2009). When Pos19 was over-expressed from its own promoter, the induction of the tested genes

disappeared and mRNA levels remained unchanged (RSP_0557, *metI*, *cysH,* and *cysP*) or were even slightly reduced (*serC* and *cysI*) upon $^1O_2$ stress (Fig. 27). Taken together the RT-PCR analysis verified the findings from the microarray analysis.

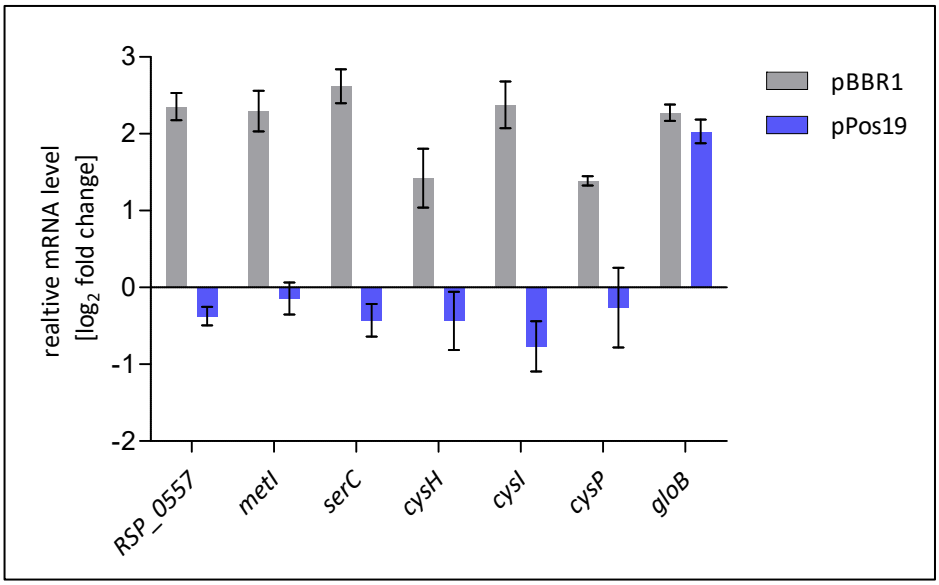

Figure 27: RT-PCR comparing mRNA levels before (0 min) and after (7 min) $^1O_2$ stress in the EVC (pBBR1; grey) and the Pos19 over-expression strain (pPos19; blue). Strains were grown as biological triplicates under aerobic conditions to the exponential phase and exposed to $^1O_2$ stress generating conditions for 7 min. The RNA for the RT-PCR analysis with the indicated primer pairs (listed in table 3) was isolated using the TRIzol method.

In addition to the RT-PCR analyses shown above (Fig. 27), further genes were tested regarding their expression in the Pos19 over-expression strain. On the one hand, the expression levels of genes known to encode proteins with functions in motility (*cheW*, *che6Y*, *fliC*) were investigated, due to the fact that the most strongly up-regulated gene found in the Pos19 microarray is *fliC*, encoding a flagellar filament protein (Tab. 48). On the other hand genes from the *isc-suf* operon, encoding proteins with central functions in the FeS-cluster assembly were tested. Since *sufC* was found among the mildly down-regulated genes (Tab. 49) and the potential connection of Pos19 and the iron homoeostasis (Fig. 23) was to be further investigated. The primer pairs used are listed in table 3. Both RT-PCR analyses showed only minor differences in expression of the tested motility and *isc-suf* operon genes (*sufB*, *sufC*, *sufD*, *iscR*, *iscS*; Fig. 28), even though, the tested motility genes show a trend towards up-regulation in the Pos19 over-expression strain.

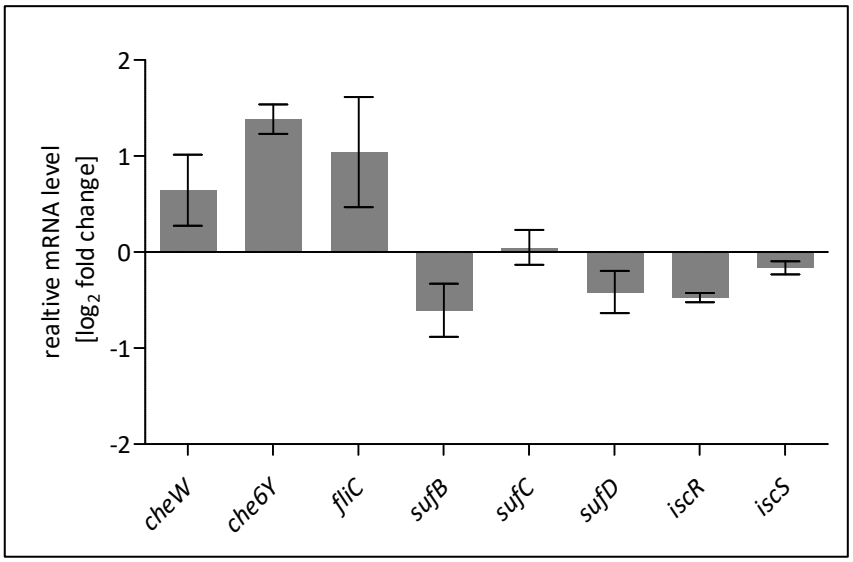

Figure 28: RT-PCR comparing mRNA levels after 7 min of $^1O_2$ stress in the Pos19 over-expression strain (pPos19) to the EVC strain (pBBR1). Expression level determined for motility genes (*cheW*, *che6Y*, *fliC*) and genes from the *isc-suf* operon (*sufB, sufC, sufD, iscR, iscS*). Strains were grown as biological triplicates under aerobic conditions to the exponential growth phase and exposed to $^1O_2$ stress generating conditions for 7 min. RNA was isolated using the TRIzol method for the RT-PCR that was carried out with the indicated primer pairs listed in table 3.

3.1.3 Phenotypic characterisation

For a more detailed investigation of the Pos19 function in *R. sphaeroides* a second, this time constitutive, over-expression (Yannick Hermanns) and a chromosomal deletion mutant (knockout mutant; Bork Berghoff) of Pos19 were constructed. The former was constructed amplifying the Pos19 sequence using the primers RSs0019_for_Bam and RSs0019_rev_Eco (Tab. 3) and subcloning it into the pDrive cloning vector (Qiagen). After restriction (2.4.4.1) with BamHI and EcoRI, the fragment was ligated (2.4.4.2) into the pRK4352 (pRK16S; based on pRK415) (Mank *et al*., 2012.) under the control of the 16S rRNA promoter (16S, RSP_4352). The plasmid was conjugated (2.2.13) to the *R. sphaeroides* wild-type, resulting in a constitutive over-expression of Pos19 (p16S::Pos19). The latter was achieved by homologous recombination. For this purpose, a 464 bp upstream and a 315 bp downstream fragment of the Pos19 locus were amplified using primer pairs 0019-up-Eco/0019-up-Pst and 0019-down-Sph/0019-down-Pst, respectively. The corresponding fragments were cloned into the EcoRI and SphI sites of the suicide plasmid pPHU281 (Hübner *et al*., 1991) after restriction with EcoRI and PstI (upstream fragment) or SphI and PstI (downstream fragment). The kanamycin resistance cassette from plasmid pUC4K (Vieira and Messing, 1982) was cloned into the newly generated PstI site between the upstream and downstream fragment. The resulting plasmid pPHU0019::Km was transferred to *R. sphaeroides* by conjugation. The recombinants were selected on RÄ medium agar plates containing kanamycin and subsequently screened for tetracycline sensitivity to exclude single crossover events (2.2.2.4). The absence of Pos19 in the knockout mutant (ΔPos19) and the constitutive over-expression of Pos19 (p16S::0019) were confirmed via Northern

blot analysis (Fig. 29). Hybridisation was carried out with the Pos19 and the 5S rRNA probes (Tab. 3) as described in 2.4.9.

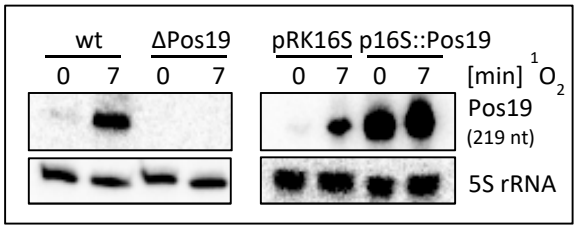

Figure 29: Verification of the Pos19 knockout and constitutive over-expression. *R. sphaeroides* wild-type (wt) and the Pos19 knockout mutant (ΔPos19) were grown for sampling before (0 min) and after 7 min of $^1O_2$ stress (left). Same was done for the pRK16S EVC strain and the strain constitutively over-expressing Pos19 from the 16S rRNA promoter (p16S::Pos19; right). 8 µg of total RNA from each sample, isolated via the hot phenol method were used for Northern blot with an 8% PAA urea gel. The Pos19 and 5S rRNA were probed, the latter served as loading control.

3.1.3.1 Physiological assays

Both described Pos19 strains, the constitutive over-expression (p16S::Pos19) and the knockout mutant (ΔPos19), were applied for different physiological assays. As a control, an *R. sphaeroides* strain carrying the insert-less pRK4352 vector (pRK16S) (Mank *et al.*, 2012) was used.

The first assay was conducted to measure the intracellular GSH level. GSH is a sulphur-containing antioxidant which could be affected by changes in sulphur metabolism and as well plays a role in oxidative stress response. Measurement of GSH (2.2.16) was carried out using the so-called Ellman's reagent (DTNB), with cell samples from three biological replicates and technical duplicates of the strains p16S:Pos19, ΔPos19 and pRK16S. The strains were grown under microaerobic conditions (2.2.1.2) to an OD_{660} of 0.4-0.5 and cells were harvested on ice. The assay was carried out using this set-up two times, and the relative mean values in percent with relative standard errors of the mean are presented in figure 30. Statistical analysis was performed using the directed, unpaired students T-test in Microsoft Excel († $0.05 < p < 0.1$ and * $p < 0.05$). In summary, the GSH assay revealed that compared to the control strain (pRK16S), the constitutive Pos19 over-expression harbours a significantly lower GSH level (76 %), while the knockout (ΔPos19) shows an increased GSH level (119 %; Fig. 30). Regarding the increased intracellular GSH levels in the Pos19 over-expression strain and assuming a role of Pos19 in oxidative stress defence, an improved resistance towards oxidative stress was hypothesised for the Pos19 over-expression strain (p16S::Pos19). This hypothesis was tested using a zone of inhibition assay (2.2.14). Again the Pos19 knockout (ΔPos19) was tested in addition, and the pRK16S strain was used as a control. All three strains were cultivated under microaerobic conditions to an OD_{660} of 0.4 to prepare the top-agar. The stress-inducing chemicals applied to the filter disks were [final concentration]: methylene blue [10 mM], tBOOH [500 mM],

H_2O_2 [1M; 2 M], and diamide [500 mM]. For all tested chemicals there were only slight differences for all three tested strains in the diameter of the zones of inhibition (Fig. 30).

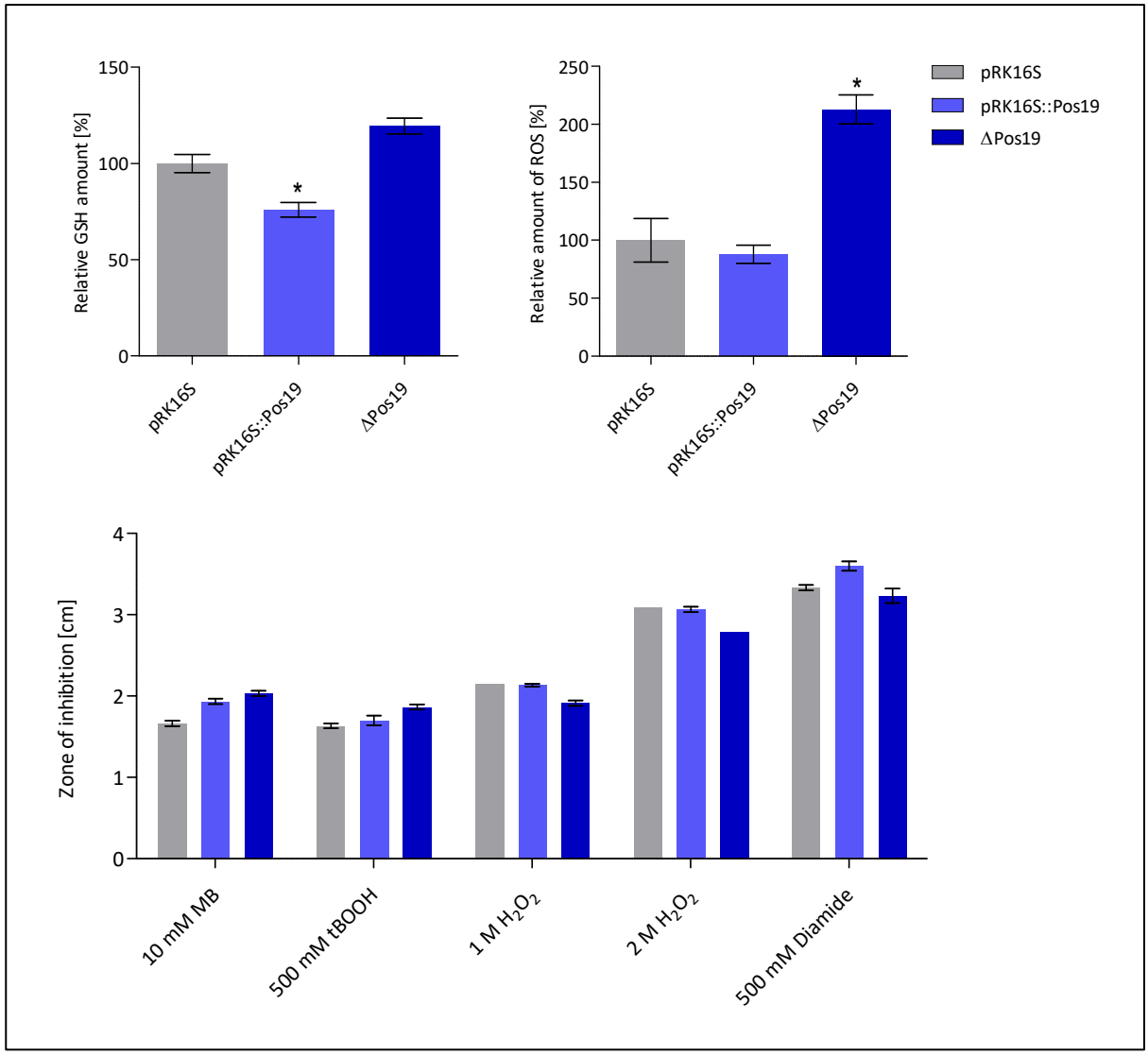

Figure 30: Physiological assays comparing the EVC strain (pRK16S, grey), the constitutive Pos19 over-expression (pRK16S::Pos19; light blue), and the Pos19 knockout (ΔPos19; dark blue). The measurement of total intracellular glutathione (GSH; upper left) was carried out using Ellmann's reagent (DTNB). The relative GSH amount is depicted in percent; the GSH amount of the empty vector control (pRK16S) was set to 100 percent. The cellular ROS levels (upper right) were analysed after the reaction with 10 mmol/L 2,7-dihydrodichlorofluorescein diacetate. The fluorescence intensity was normalised to the optical density of the samples. The resulting arbitrary units are depicted in percent. The results of the inhibition zone assay (lower panel) using 10 mM methylene blue (MB) in the light, 500 mM tBOOH, 1 M and 2 M hydrogen peroxide (H_2O_2), and 500 mM diamide are depicted as diameter in cm. The results represent the mean of three (ROS and inhibition zone) or six (GSH) independent biological replicates with technical duplicates. Error bars reflect the standard error of the mean. For the GSH and ROS measurement the level of significance compared to the control (pRK16S) is indicated († $0.05 < p < 0.1$ and * $p < 0.05$).

The third assay carried out comparing the three strains (pRK16S, p16S::Pos19, ΔPos19), was a measurement of the intracellular ROS levels (2.2.17). Again biological triplicates of each strain were grown microaerobically to an OD_{660} of 0.4, and the assay was carried out as described in 2.2.17. Statistical analysis was performed using the directed, unpaired students T-test in Microsoft Excel († $0.05 < p < 0.1$ and * $p < 0.05$). While the ROS level of the Pos19 over-expression strain (p16S::Pos19; 88 %) did not differ significantly from the control strain (pRK16S), the ROS level in the knockout strain (ΔPos19) was significantly higher (213 %) than in the control and over-expression strain (Fig. 30). In addition to the physiological assays described above, growth analyses (2.2.2) were performed using the p16S::Pos19, ΔPos19, and the pRK16S strains.

Of the genes affected by the Pos19 over-expression, many are involved in sulphur metabolism and related pathways (3.1.2). When regulation of the sulphur metabolism and/or uptake is one of Pos19's functions, a growth phenotype upon alteration of sulphur availability could be possible. To test this assumption, a growth analysis of the strains constitutively over-expressing (p16S::Pos19) or lacking Pos19 (ΔPos19) in comparison to the EVC (pRK16S) was carried out in sulphur-reduced medium (¼ of standard sulphur concentration; 2.2.1.7). The analysis revealed an altered growth for the Pos19 knockout mutant compared to both, constitutive Pos19 over-expression and EVC strain (Fig. 31).

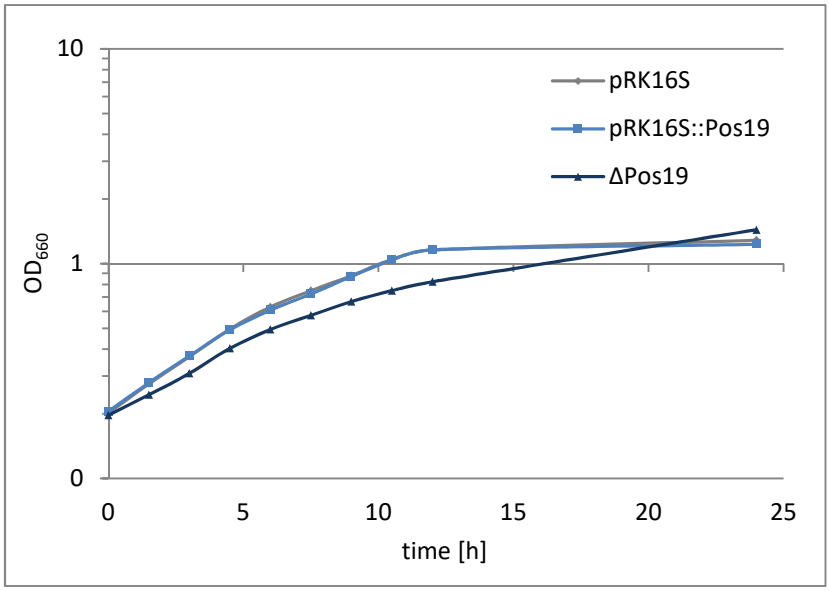

Figure 31: Growth analysis under sulphur-reduced conditions. The strains (pRK16S - grey, pRK16S::Pos19 – light blue, and ΔPos19 – dark blue) were grown in sulphur-reduced medium and utilised for the growth analysis after two pre-culture steps in the sulphur-reduced medium. The OD_{660} was plotted semi-logarithmically against the time.

In the following growth analyses, the Pos19 knockout mutant was compared to the *R. sphaeroides* wild-type. Since Pos19 is induced under iron-limiting conditions (Fig. 23), the growth of the strain lacking Pos19 (ΔPos19) was compared to the growth of the *R. sphaeroides* wild-type under these

conditions (2.2.1.6). The growth analysis exhibited that both strains, knockout mutant and wild-type, are impaired in growth under iron limitation in comparison to standard medium. The growth impairment of the Pos19 knockout was somewhat more pronounced (Fig. 32).

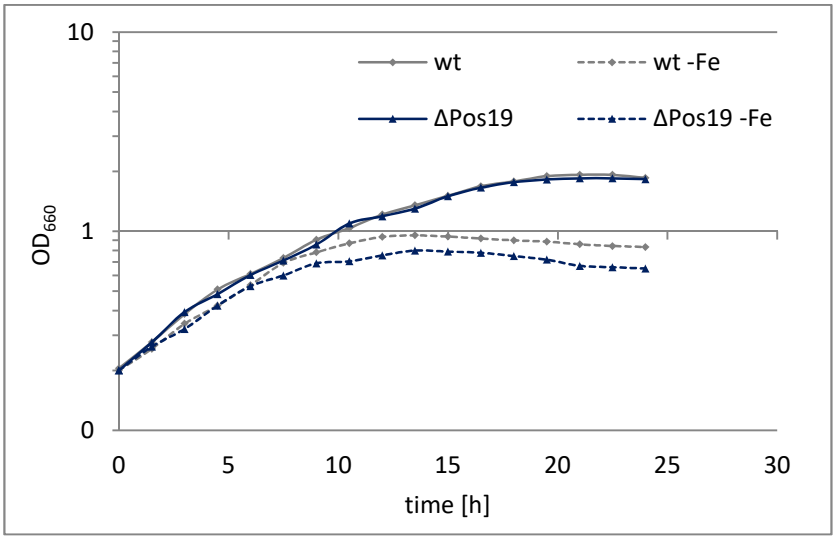

Figure 32: Growth analysis under microaerobic and iron-limiting conditions. The growth of the *R. sphaeroides* wild-type (wt, grey) and the Pos19 knockout mutant (ΔPos19, dark blue) was monitored in normal RÄ medium (solid lines) and iron-free medium (dotted lines). The OD_{660} was plotted semi-logarithmically against the time.

As described in 1.2, parts of the photosynthetic complexes display a potential source for $^1O_2$ stress. Due to this involvement of the photosynthetic apparatus in $^1O_2$ stress, a potential connection of the $^1O_2$ stress induced Pos19 and the photosynthesis in *R. sphaeroides* was to be tested. The growth of the Pos19 knockout mutant (ΔPos19) and the *R. sphaeroides* wild-type was compared under phototrophic conditions (2.2.1.3). This growth analysis showed that the Pos19 knockout mutant was slightly impaired in growth compared to the wild-type (Fig. 33).

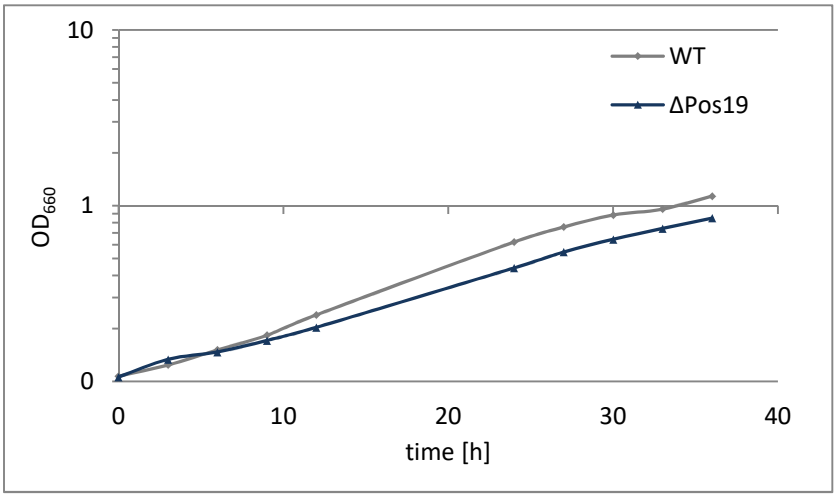

Figure 33: Growth analysis under phototrophic conditions. The *R. sphaeroides* wild-type (wt, grey) and the Pos19 knockout mutant (ΔPos19, dark blue) were grown under phototrophic conditions to monitor their growth. The OD_{660} was plotted semi-logarithmically against the time.

All in all, the physiological assays revealed mainly minor differences when comparing the constitutive over-expression and knockout of Pos19 to a control strain (pRK16S or wt). Only the GSH and ROS measurements exhibited a significant difference each, showing an increase for the over-expression and a decrease for the knockout, respectively (Fig. 30).

3.1.3.2 Target mRNA levels in the knockout and constitutive over-expression of Pos19

Besides the physiological examination of the constitutive over-expression and the knockout of Pos19 (3.1.3.1), RNA from both strains was applied for an RT-PCR analysis.

Before cells were harvested biological triplicates of the Pos19 knockout mutant and the *R. sphaeroides* wild-type were exposed to $^1O_2$ stress for 7 min (2.2.1.5. The RNA was extracted using the TRIzol method (2.4.1.3 b), and the mRNA levels of RSP_0557, *cysH*, *cysI*, *cysP*, *serC* and *metI* (primer pairs in Tab. 3) were investigated using RT-PCR (2.4.3.3). *RpoZ* was used as reference gene while *gloB* was used as control. Against the expectations, the mRNA levels were not increased to obvious higher levels in the Pos19 knockout mutant compared to the wild-type upon 7 min of $^1O_2$ stress (Fig. 34).

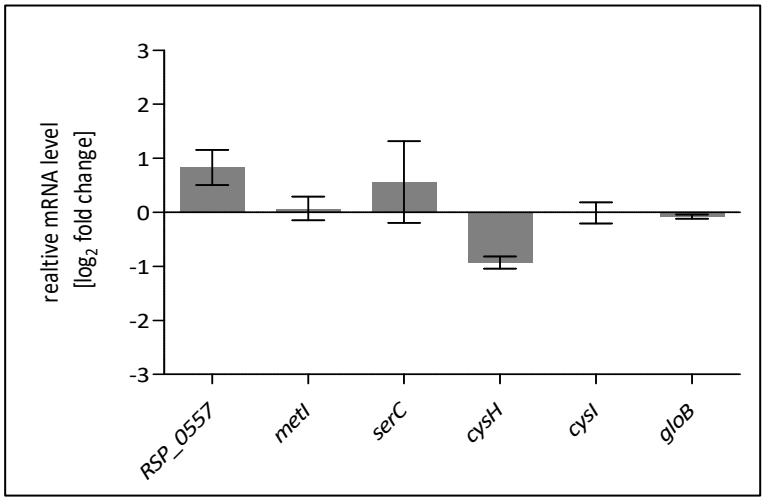

Figure 34: RT-PCR comparing mRNA levels after 7 min of $^1O_2$ stress in the Pos19 knockout mutant (ΔPos19) to the *R. sphaeroides* wild-type. Strains were grown as biological triplicates under aerobic conditions to the exponential phase and exposed to $^1O_2$ stress generating conditions for 7 min. RNA was isolated using the TRIzol method, and an RT-PCR was carried out with the indicated primer pairs (Tab. 3).

In addition, RNA from samples of the strain constitutively over-expressing Pos19 (pRK16S::Pos19) and the corresponding EVC (pRK16S) grown as biological triplicates under microaerobic conditions was used for RT-PCR. This was to test whether an excess of Pos19 affects the tested target genes already under non-stress conditions. According to this RT-PCR analysis the mRNA levels of *RSP_0557*, *metI*, *serC*, *cysH*, *cysI*, and *gloB* were not shown to be significantly different between the strains pRK16S::Pos19 and pRK16S (Fig. 35).

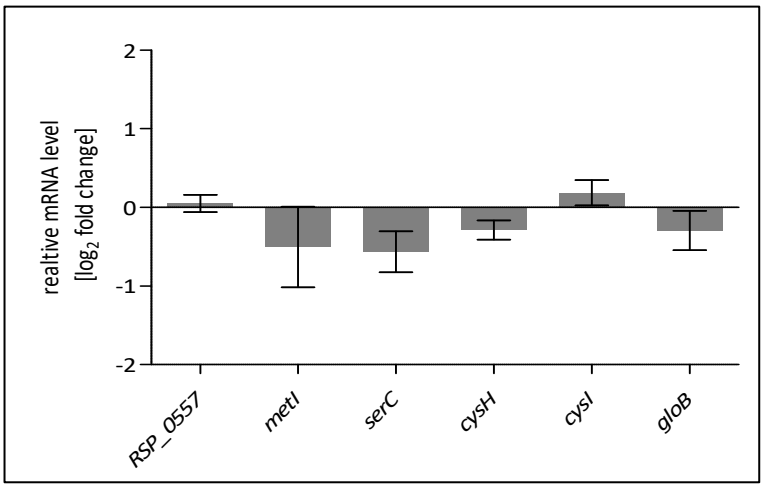

Figure 35: RT-PCR comparing mRNA levels in the constitutive Pos19 over-expression (pRK16S::Pos19) to the EVC (pRK16S). Strains were grown as biological triplicates under microaerobic conditions. RNA was isolated using the TRIzol method, and RT-PCR was carried out with the indicated primer pairs (Tab. 3).

3.1.4 A small ORF contained in the Pos19 sequence

Besides the effect on potential target genes, the analysis of Pos19 revealed two putative small open reading frames (sORFs) within its sequence (Fig. 24). Both sORFs share the same stop codon while depending on the start codon (ATG1 or ATG2) they exhibit a length of 150 or 135 nt respectively. Moreover, a Shine-Dalgarno-like sequence (SD; AGAAAGGA) can be found just upstream of the two start codons. There are different aspects of studying concerning the sORFs: first of all, it has to be elucidated whether the sORFs are translated *in vivo* at all. If *in vivo* translation can be found, it is curious to check whether both or just one start codon is used for translation.

3.1.4.1 *LacZ*-based *in vivo* reporter assay

To answer these questions, the Pos19-sORF together with its own promoter was translationally fused to a promoterless *lacZ* gene. Therefor the Pos19-sORF was amplified using primers RSs0019_up and 0019-ORF-Hind and subcloned into the cloning vector pDrive (Qiagen; pDrive_0019ORF). After restriction with BamHI and HindIII, the sORF could be ligated into the reporter plasmid pPHU236 (Hübner *et al*., 1991) resulting in the reporter pPHU_0019ORF. Moreover, a second reporter plasmid pPHU_Stop16, carrying an internal stop codon at position 16 of the Pos19 sequence (Fig. 38), was constructed using a similar strategy. The nucleotide exchange was achieved using the primers 0019-Stop16-fw and 0019-Stop16-rev (Tab. 3) in a site-directed mutagenesis PCR approach (2.4.3.2) with the pDrive_0019ORF as template.

To test for *in vivo* translation of the Pos19-*lacZ* fusions, the reporter plasmids were transferred to the Pos19 knockout mutant via conjugation (2.2.13). Cells from the resulting reporter strains (pPHU_0019ORF and pPHU_Stop16) were harvested for a ß-galactosidase activity assay

(2.2.15) from six biological replicates in technical duplicates before (0 min) and 60 min after $^1O_2$ stress (2.2.1.5). The wild-type fusion (pPHU_0019ORF) gave a β-galactosidase activity of 116 Miller Units (MUs) before stress, which was increased to 408 MUs after 60 min of $^1O_2$ stress. Whereas for the pPHU_Stop16 variant, 2.3 MU before and 5.0 MUs after stress were measured. A strain carrying the empty vector (pPHU_236) was used as negative control and gave 0.77 MU before and 0.88 MU after stress (Fig. 36). These results verified *in vivo* translation of the Pos19-sORFs, which could be almost completely abolished by inserting an internal stop codon. In the next step, the pPHU_0019ORF reporter plasmid was transferred to the *R. sphaeroides* TF18 mutant strain, which lacks the *rpoE-chrR* gene locus. In this strain the reporter activity was negligible (Fig. 36), confirming the dependency of Pos19 transcription on the alternative sigma factor RpoE.

Additional questions concerning the characteristics of the sORFS were approached by mutating further sites of the Pos19-*lacZ* fusion (pHU_0019ORF; mutations in Fig. 36). This was done using primers for site-directed mutagenesis listed in table 3, with the pD_0019ORF as the template, followed by BamHI and HindIII cloning to the pPHU_236, as described above. The two potential start codons (ATG1 and ATG2) were changed to either a stop codon (TGA; Stop1 and Stop2) or a threonine codon (ACG; Thr1 and Thr2) each. To test for the need of the SD-like sequence for translation, four and eight base pairs in this sequence were mutated (M4 and M8), respectively. For the ß-galactosidase activity assay, the reporter plasmids were conjugated to the Pos19 knockout mutant and cells were harvested before and after 60 min of $^1O_2$ stress (six biological replicates and technical duplicates).

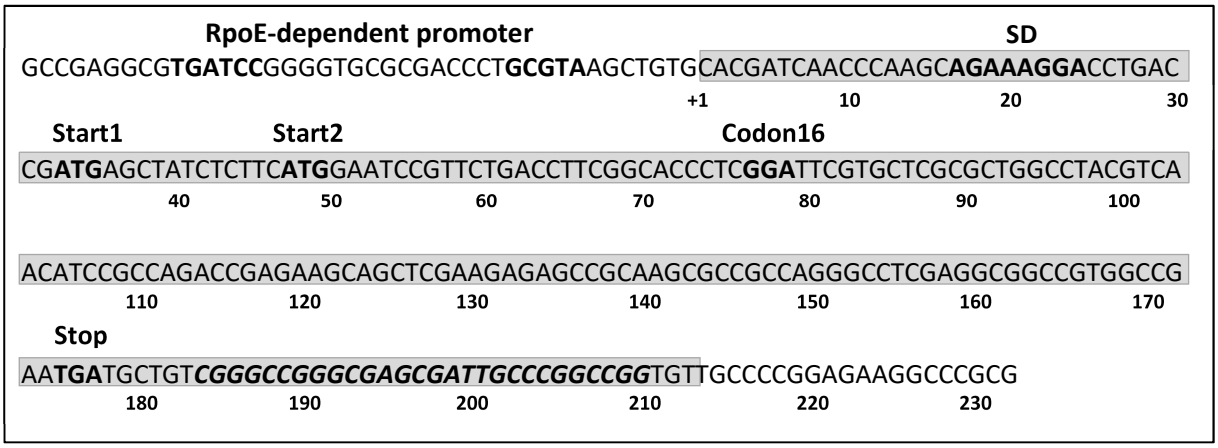

SD	AGAAAGGA	Start 1	ATG	Start 2	ATG	Codon 16	GGA
M4	TCCT	Stop 1	TGA	Stop 2	TGA	Stop 16	TGA
M8	TCTTTCCT	Thr 1	ACG	Thr 2	ACG		

Figure 36: Detailed illustration of the *pos19* gene. Relevant features are shown in bold. The -35 and -10 motifs of the RpoE promoter are marked. The 219 nt long sRNA (shaded in grey) contains two potential ORFs with lengths of 150 (Start1) and 135 nt (Start2). The Rho-independent terminator (italic letters) was predicted by TransTermHP (Kingsford *et al*., 2007). The Shine-Dalgarno (SD) sequence, the two start codons as well as one internal codon (Codon 16) were mutated according to the chart below the sequence.

Mutations in the first start codon (Stop1 and Thr1) as well as the mutation that introduces an internal stop codon at the ATG2 position (Stop2) nearly abolished β-galactosidase activity. In contrast, mutating the second start codon to ACG (Thr2) did not affect the reporter activity. These findings rather argue for the first start codon to be essential for translation initiation. The SD mutations M4 and M8 did not completely impede the translation, and reporter activities remained at fairly high levels, especially under stress conditions (Fig. 37). In summary, translation initiation of the Pos19-sORF occurs at the first start codon and only partly relies on an intact SD sequence (Fig. 37). The sRNA Pos19 including the sORF was uniquely found in *R. sphaeroides* strains were it is quite conserved (Fig. 38), but could not be identified in other even closely related bacteria such as *R. capsulatus*.

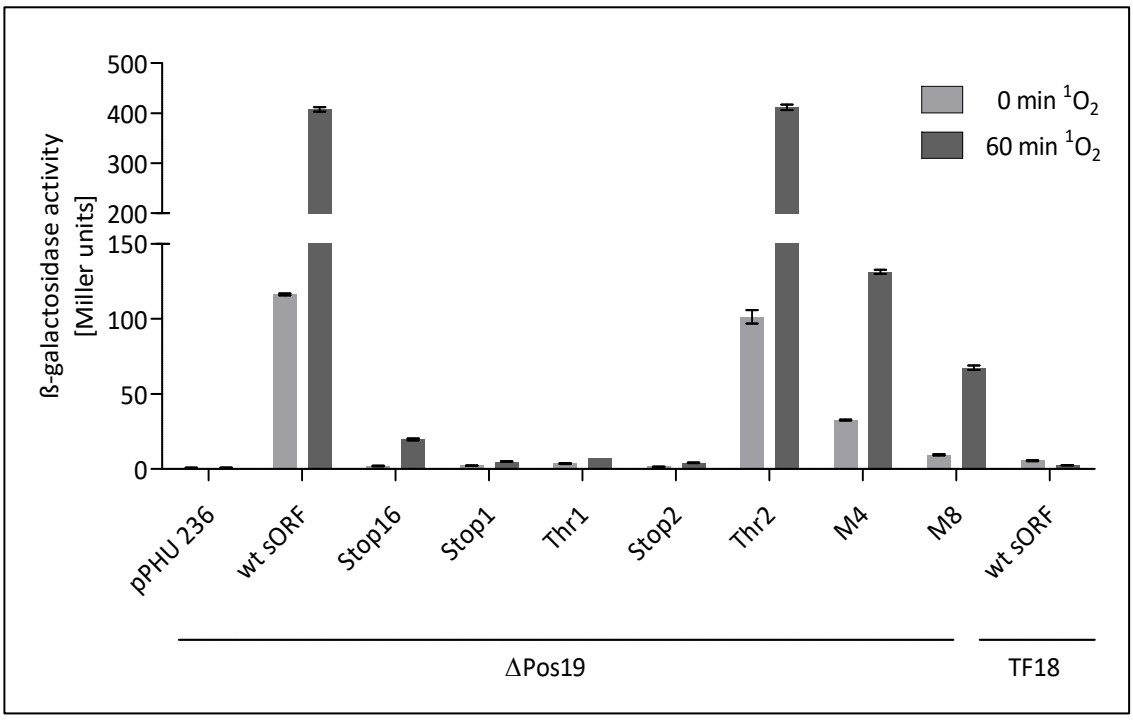

Figure 37: *In vivo* translation of the native and mutated Pos19-sORFs was monitored by translational *lacZ* fusions. A 300 bp fragment containing the RpoE-dependent promoter and the first 178 bp of the *pos19* gene (including codons 1-48) was fused to the promoterless *lacZ* gene on reporter plasmid pPHU236. The wild-type (wt) sORF was subsequently mutated as shown in figure 38. The fusion plasmids and empty vector pPHU236 were transferred to *R. sphaeroides* ΔPos19 or strain TF18, which lacks the *rpoE-chrR* locus. The corresponding strains were subjected to $^1O_2$ stress for 60 min with samples collected at the indicated time points. β-galactosidase activities were measured from six (ΔPos19) or three (TF18) biological replicates in technical duplicates. Error bars represent the standard error of the mean.

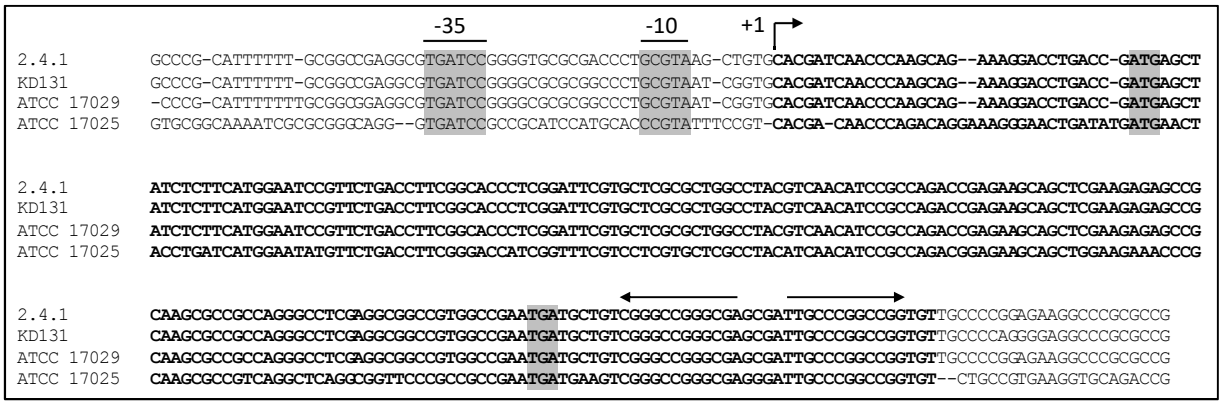

Figure 38: Alignment of the *pos19* locus from four different *R. sphaeroides* strains. Strain 2.4.1 represents the wild-type strain used in this work. The promoter motif is indicated by -35 and -10, while +1 indicates the transcriptional start site. Start (ATG) and stop (TGA) codons of the sORF are marked in grey. Adopted from Müller *et al*., 2016.

3.1.4.2 Pos19 peptide detection

To confirm the expression of the Pos19 peptide, a *Strep*-tagged Pos19 over-expression variant was constructed (designed by Bork Berghoff). The Pos19 sORF together with its own promoter was amplified from chromosomal DNA (2.4.3.1) using the primer pair 0019ORFupHind and 0019ORFstrepPst. The reverse primer 0019ORFstrepPst contains the sequence for a *Strep*-tag (AGCGCTTGGAGCCACCCGCAGTTCGAAAAATGA). During amplification, this primer will bind the sequence right upstream of the sORF stop codon adding the *Strep*-tag sequence and an artificial stop codon to the amplificate (Fig. 39). After sub-cloning to the pJET 1.2 cloning vector (Qiagen) and restriction with HindIII and PstI (2.4.4.1), the Pos19-ORF_*strep* fragment was ligated (2.4.4.2) to the pRK415 vector (Keen *et al*., 1988), resulting in a plasmid over-expressing the Pos19 sORF with a *Strep*-tag from its own RpoE-dependent promoter (pRK_Pos19*strep*). The plasmid pRK_Pos19*strep* was transferred to *R. sphaeroides* wild-type via conjugation (2.2.13).

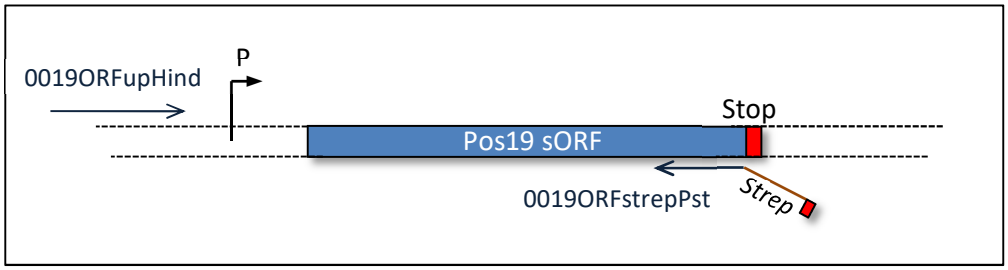

Figure 39: Schematic overview of cloning design for the *Strep*-tagged Pos19 variant. The Pos19 sORF is shown in light blue, with the indicated promoter. The original stop codon is shown as a red box at the end of the sORF and the artificial stop codon at the 5' end of the reverse primer 0019ORFstrepPst. Primer binding of 0019ORFupHind and 0019ORFstrepPst on the chromosome is indicated by dark blue arrows while the attached *Strep*-tag sequence is indicated in brown.

Cell extracts from the pRK_Pos19*strep* strain were applied for a Tricine-SDS-PAGE Western blot as described in 2.5.2.2. As a negative control cell extract from the Pos19 knockout mutant was prepared. While as a positive control a purified *Strep*-tagged protein was used (kindly provided by Kathrin Baumgardt), which could be already detected using the *Strep*-Tactin® horseradish peroxidase conjugate (IBA). Besides unspecific signals in samples from both strains and the signal for the positive control, there was no specific signal for the *Strep*-tagged Pos19 peptide (predicted size: 5 kDa) detectable on the Western blot membrane (Fig. 40). The experiment was repeated two times, with different amounts of protein per sample, showing the same negative result.

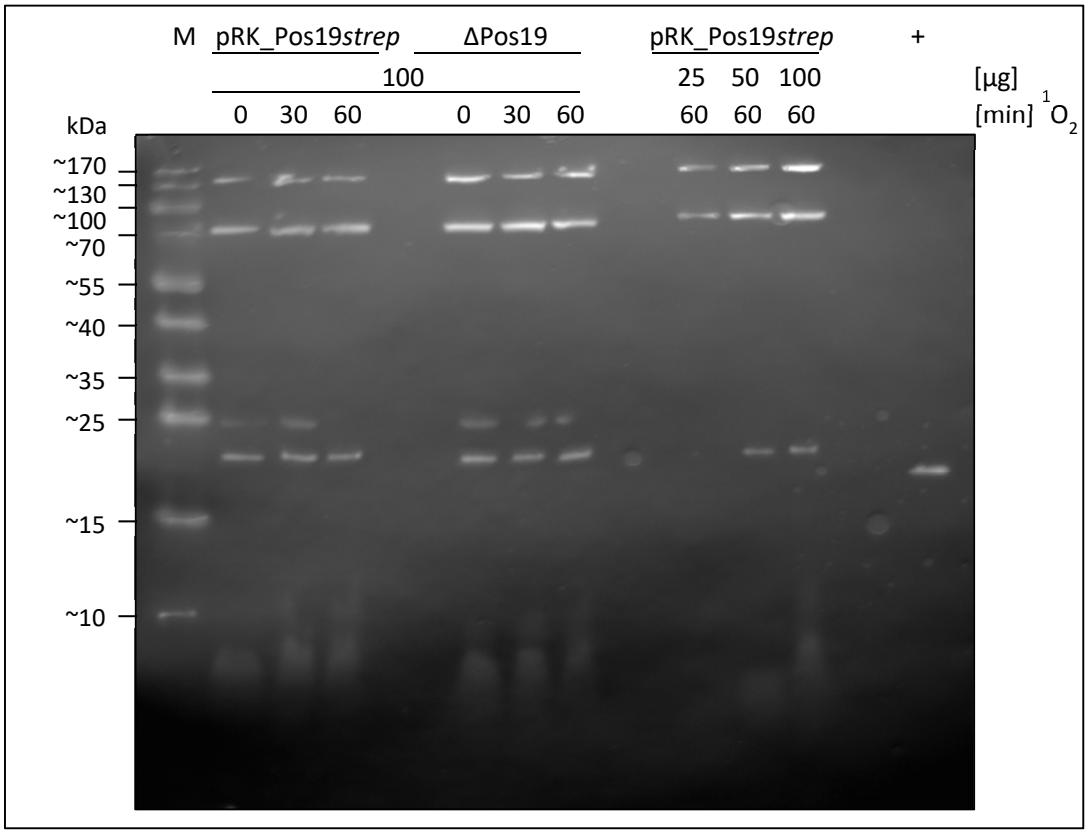

Figure 40: Tricine-SDS-PAGE based Western blot to monitor *in vivo* translation of the *Strep*-tagged Pos19 peptide. Cultures were exposed to $^1O_2$ stress and samples were collected at the indicated time points. The amount of total protein extract used is shown above. An already verified *strep*-tagged protein (K. Baumgardt) was used as positive control (+). M = *PageRuler*™ Prestained 10 - 180 kDa (Thermo Scientific).

Additional to the *Strep*-tagged Pos19 and the Pos19-*lacZ* reporter fusions a second reporter gene, *eCFP*, was used for investigation of *in vivo* translation (designed by Benjamin Eisenhardt). Again the Pos19-sORF with its own promoter and without stop codon was amplified (primer pair 0019_ORF_fw and 0019_ORF_rev) from chromosomal *R. sphaeroides* DNA and subcloned into the pDrive vector (Qiagen). After digestion with XbaI and EcoRI, the fragment was inserted into the corresponding sites of the pBE4352::eCFP::eCFP vector (as described in Remes *et al.*, 2015). The resulting plasmid expresses the Pos19 peptide; C-terminally tagged with eCFP, from its own promoter. In total protein

extracts from *R. sphaeroides* cells carrying the reporter plasmid, the eCFP tagged Pos19 peptide could be detected on a Western blot (2.5.2.1) using an anti-eGFP antibody. Following the results from the ß-galactosidase *in vivo* reporter assays, $^1O_2$ stress induced Pos19 *in vivo* translation could be verified (Fig. 41).

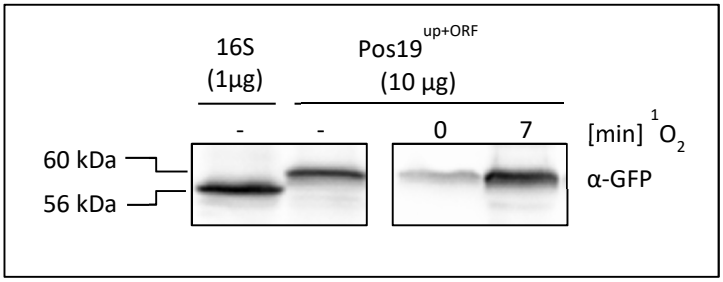

Figure 41: *In vivo* translation of the Pos19-sORF was monitored by translational eCFP fusion. The Pos19 peptide, C-terminally fused to eCFP (Pos19up+ORF), was detected with an anti-GFP antibody. The amount of total protein extract used is shown in brackets. Protein from a strain carrying the pBE_eCFP::eCFP with 16S rRNA promoter (16S) was used as control. The size difference between control and Pos19 fusion of around 4 kDa corresponds to the predicted molecular weight of the Pos19 peptide. The western blot was carried out by Benjamin Eisenhardt.

3.1.5 Regulation - sRNA versus sORF

In line with the sORF mutations used for the *in vivo* reporter system (3.1.4.1), Pos19 over-expression plasmids were constructed harbouring either a stop (TGA, Stop1) or a threonine codon (ACG, Thr1) instead of the first start codon or an internal stop codon at position 16 (Stop16; compare Fig. 36). Since the *in vivo* reporter assay showed that these mutations abrogate the translation of the Pos19 peptide (Fig. 37), the strains carrying the mutated Pos19 over-expression plasmids can be used to study the effect of the Pos19 sRNA alone. To construct the mutated over-expression variants the primers for the native over-expression (RSs0019_up and RSs0019_down) were used to amplify (2.4.3.1) the Pos19 sequence which could be sub-cloned into the pDrive cloning vector (pDrive_0019). Using this pDrive_0019 as the template, the mutations could be inserted using site-directed mutagenesis PCR (2.4.3.2; primer pairs listed in Tab. 3). The mutated fragments can be ligated (2.4.4.2) into the pBBR1 broad host range vector after restriction (2.4.4.1) with BamHI and HindIII. All three mutated Pos19 variants could be over-expressed in *R. sphaeroides* to comparable levels as the native Pos19 (Fig. 42). The sRNA levels were investigated using the Northern blot technique (2.4.6.1) with RNA isolated using the hot phenol method (2.4.1.3 a).

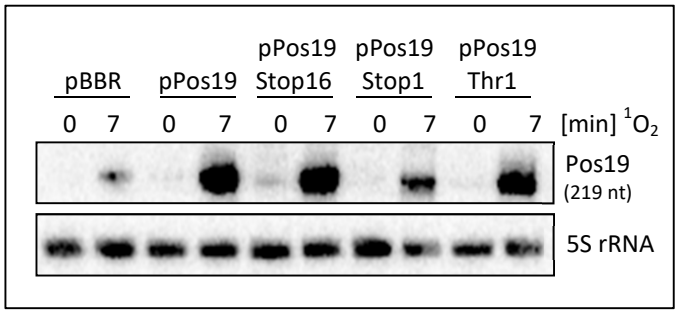

Figure 42: Verification of over-expression of the mutated Pos19 variants (Pos19Stop16, Pos19Stop1, Pos19Thr1). The strains indicated were exposed to $^1O_2$ stress for 0 and 7 min. The total RNA was separated on a 8% PAA-urea gel for Northern blot analysis and Pos19 and the 5S rRNA were detected using radio-labelled hybridisation probes.

To further study the expression of the potential target genes without a possible side-effect from the Pos19 peptide, RNA was isolated from the mutated Pos19 over-expression strains (pStop16, pStop1, pThr1) via the TRIzol method described in 2.2.1.3 b. Samples for this purpose were taken before (0 min) and after 7 min of $^1O_2$ stress (2.2.1.5). The mRNA level of RSP_0557, *cysH*, *cysI*, *cysP*, *serC*, and *metI* were tested again via RT-PCR (2.4.3.3), as already described for the EVC and over-expression pPos19 (3.1.2). The levels of *rpoZ* and *gloB* were tested as reference and control, respectively. As for the unmutated over-expression pPos19, all three mutated over-expression variants negatively affect the mRNA levels of the tested target genes upon $^1O_2$ stress. The induction of the target genes upon stress seen in the EVC is diminished in the Pos19 over-expression strains, whereas *gloB* is induced in all tested strains as expected (Fig. 43). Taken together these results show that the effect of Pos19 on the selected genes is independent of the small peptide and displays a regulatory sRNA function.

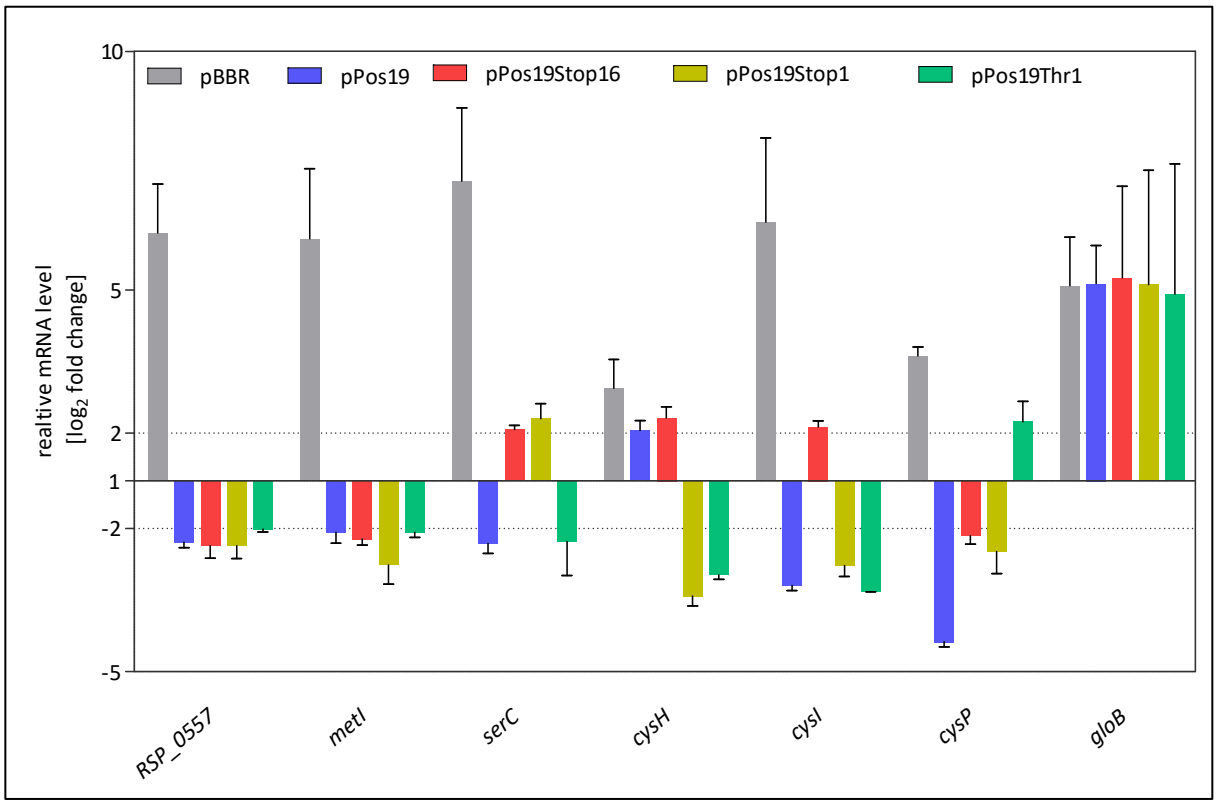

Figure 43: mRNA levels for selected genes in the original and mutated Pos19 over-expression strains. The indicated strains were subjected to $^1O_2$ stress and samples were collected at time points 0 and 7 min of stress. Selected mRNA levels in stress samples (7 min) were calculated relative to unstressed samples (0 min) as $\log_2$ ratios, using *rpoZ* as the reference gene. Results were obtained from three independent biological experiments. Error bars represent the standard error of the mean.

3.1.6 Target *in vivo* reporter system

The regulatory potential of Pos19 described in 3.1.2 and 3.1.5 was further investigated using a second *lacZ* based *in vivo* reporter system. On the reporter plasmid pPHU4352 (Mank *et al*., 2012) the sequences of potential target mRNAs, always containing the encoded proteins start codon, were translationally fused in frame to the *lacZ* gene under the control of the 16S rRNA promoter. For this purpose, the sequence parts of interest were amplified using the primer pairs up-0557-for-Xho / up-0557-rev-Hind and up-cysH-for Bam / up-cysH-rev-Xho (Tab. 3) and subcloned into the pDrive cloning vector (Qiagen). After restriction with XhoI or BamHI and HindIII (2.4.4.1), the fragments were ligated (2.4.4.2) into the corresponding sites of the pPHU4352. Using that approach, reporter plasmids for the potential targets RSP_0557 and *cysH* were constructed. As controls, reporter fusion constructs of *puc2A* and *bchN*, encoding a ß-subunit of LHC II and a subunit of the light-independent protochlorophyllide reductase, respectively (Mank *et al.,* 2012), were chosen. The reporter plasmids, as well as the insert-less pPHU4352, are transferred to selected *R. sphaeroides* strains via conjugation (2.2.13). Samples from these reporter strains are used for a ß-galactosidase activity assay (2.2.15) in which the resulting Miller Units correlate to the amount of translation of the target-*lacZ* fusion.

First of all, the reporter plasmids were transferred to the Pos19 over-expression strain (pPos19) and the corresponding EVC strain (pBBR). The RSP_0557 reporter was additionally conjugated to the strains carrying the mutated Pos19 over-expression plasmids pStop16, pStop1, and pThr1. Assuming that Pos19 negatively affects the tested targets one expects lower ß-galactosidase activity, meaning reduced translation, in the Pos19 over-expression strains. The strains carrying the reporter plasmids were cultivated in biological triplicates and samples were taken as technical duplicates after 60 min of $^1O_2$ stress (2.2.1.5). The ß-galactosidase activity measured from each reporter in the pBBR EVC strain samples was set to 100%. The reporter-fusions from the Pos19 over-expression strain gave around 75% activity for the *cysH*, *puc2A* and *bchN* fusion (Tab. 50). While the ß-galactosidase activity of the RSP_0557 reporter was reduced to ~35% in the Pos19 over-expression strain (Fig. 44 A). The activity of the RSP_0557 reporter was additionally measured in the mutated Pos19 over-expression strains pStop16, pStop1, and pThr1. As in the original over-expression pPos19, the reporter activity was reduced to ~35% in all three strains compared to the EVC (Fig. 44 A). The negative effect of the Pos19 over-expression on the control fusions (*puc2A* and b*chN*) was rather surprising since both genes were not found to be regulated (log_2 ratio -0.3 and -0.01) in the microarray analysis (3.1.2).

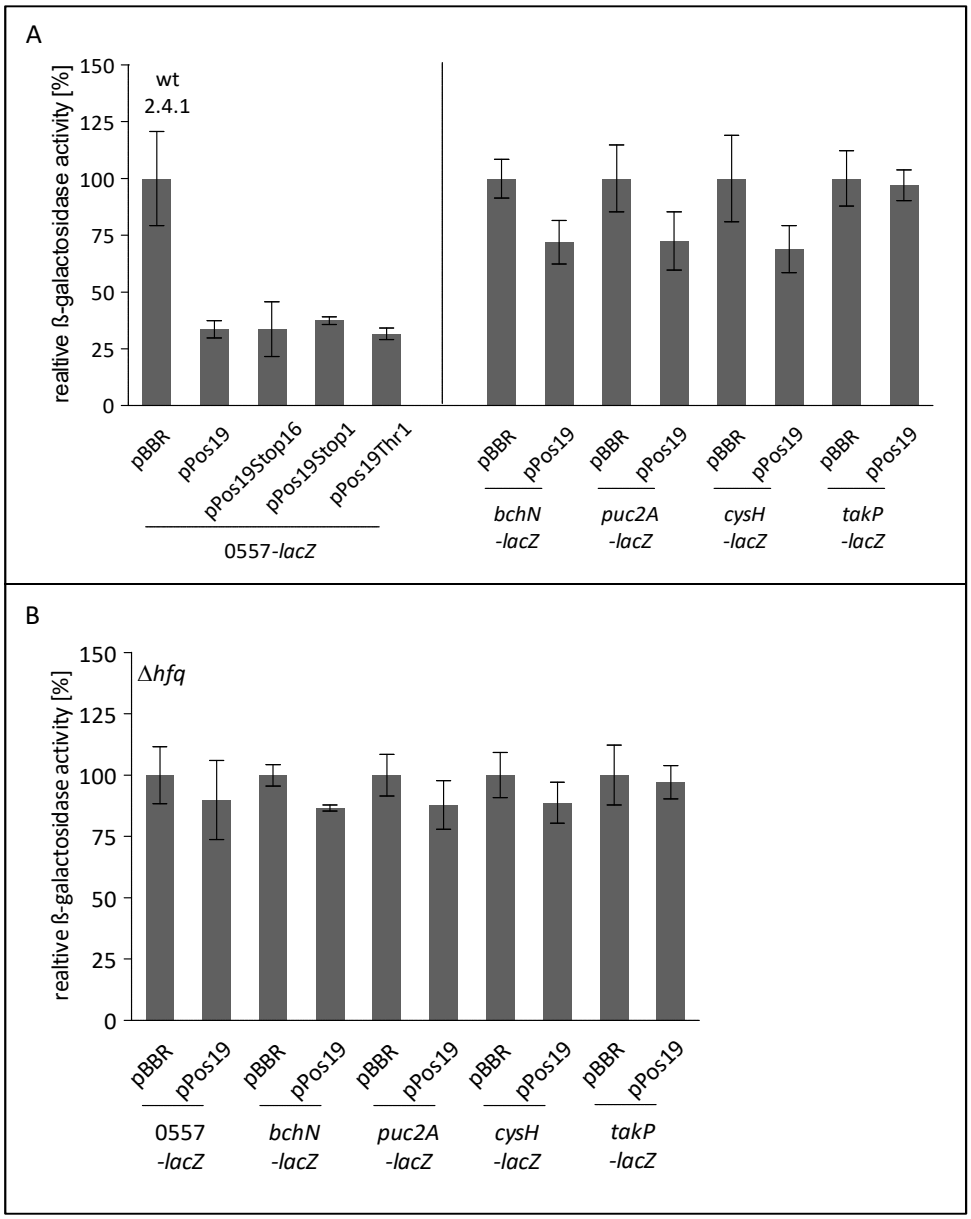

Figure 44: *LacZ*-based target *in vivo* reporter studies. Gene fragments of potential Pos19 targets (RSP_0557 and *cysH*) and control genes (*bchN*, *puc2A*, and *takP*) containing the first codons and part of the upstream region were translationally fused to the *lacZ* gene on plasmid pPHU235. The corresponding reporter plasmids were transferred to the control (pBBR) and over-expression strains of Pos19 (pPos19, pPos19Stop16, pPos19Stop1, pPos19Thr1) in A: the wild-type (wt 2.4.1) and B: the *hfq* deletion mutant (Δ*hfq*, B) background. Cultures were exposed to $^1O_2$ stress for 60 min before samples were subjected to β-galactosidase assays. Bars indicate the relative β-galactosidase activity in percent as calculated from the resulting Miller Units (with the pBBR1 control set to 100% for each construct). The results represent the mean from three independent experiments with technical duplicates and the error bars reflect the relative error of the mean.

To further characterise the effect on RSP_0557 and the potential effect on *cysH*, *bchN*, and *puc2A* entailed by the Pos19 over-expression, the described ß-galactosidase activity assay was repeated in the Δ*hfq* background. For this purpose, the Pos19 over-expression plasmid (pPos19) and the corresponding EVC (pBBR1) were transferred to the Δ*hfq* strain (Glaeser et al., 2007) via conjugation. Then the reporter plasmids (pPHU4352, pPHU_0557-*lacZ*, pPHU_*cysH-lacZ*, pPHU_*bchN-lacZ*, and

pPHU_*puc2A-lacZ*) were transferred to the resulting strains (Δ*hfq*_pPos19 and Δ*hfq*_pBBR1), again via conjugation. The reporter strains were exposed to $^1O_2$ stress for 60 min and cells were harvested for a ß-galactosidase activity assay (2.2.15). The assay revealed that the negative effect of Pos19 and the reporter fusions (RSP_0557, *cysH*, *bchN*, and *puc2A*) was abolished in the Δ*hfq* strain (Fig. 44 B), indicating that the regulation by Pos19 is Hfq-dependent. To exclude that the Pos19 over-expression affects the expression of translational fusions from the pPHU235 in general, via an effect on the *lacZ* gene for example, an additional reporter plasmid was tested. The pPHU_*takP-lacZ* reporter plasmid (takP encodes a TRAP-T transporter) (Adnan *et al*., 2015) was transferred to the Pos19 over-expression strain (pPos19) and the corresponding EVC (pBBR1) via conjugation. The strains were cultivated, and samples were harvested and applied for a ß-galactosidase activity assay as described above. The translation of the *takP-lacZ* fusion was shown to be unaffected by the Pos19 over-expression in the wild-type as well as the Δ*hfq* background (Fig. 44).

3.1.7 Interaction of Pos19 with Hfq

The dependency of Pos19 on Hfq to regulate the tested targets shown in 3.1.6 was rather surprising. In the first attempt investigating which RNAs are interacting with Hfq in *R. sphaeroides* (Berghoff *et al*., 2011) the sRNA Pos19 was not found amongst the identified Hfq-bound sRNAs. When repeating the coimmunoprecipitation (coIP) with 3xFLAG-tagged Hfq, with RNA from a strain over-expressing Pos19 (3.1.2), it could be demonstrated that Pos19 clearly binds Hfq when present in elevated amounts (Fig. 45).

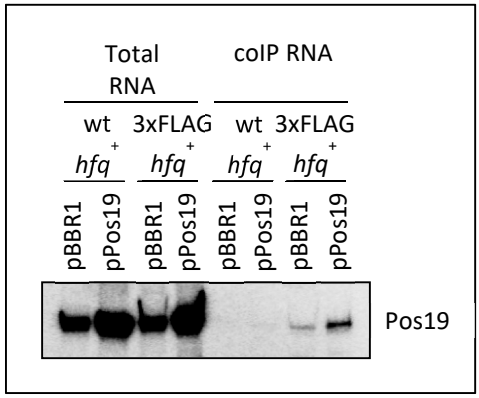

Fig. 45: Northern blot result from Hfq coIP experiments. Control plasmid pBBR1 and over-expression plasmid pPos19 were transferred to strains either expressing wild-type Hfq (wt hfq$^+$) or 3xFLAG-tagged Hfq (3xFLAG hfq$^+$). Resulting strains were exposed to $^1O_2$ for 30 min at an OD_{660} of 0.4. Cell extracts were applied to total RNA (input) and coIP RNA (output) extraction. 6 µg of total RNA and 350 ng of coIP RNA were loaded on polyacrylamide gels for detection of Pos19. Adopted from Müller *et al*., 2016.

3.1.8 RSP_0557 *in vivo* reporter – mutational analysis

RSP_0557, according to the microarray analysis, displays the most strongly regulated mRNA in the Pos19 over-expression strain upon stress (Tab. 48). Both, RT-PCR (Fig. 27) and *in vivo* reporter studies (Fig. 45) validated this regulation. To study the direct interaction between Pos19 and the RSP_0557

mRNA, the predicted seed region (Fig. 46) was mutated on the plasmids used for the *in vivo* reporter study (3.1.7). Assuming that the predicted seed region is responsible for direct binding of the RNAs, mutations in this sequence in one of the RNAs should abolish the regulation of RSP_0557 by Pos19. Analogously, the insertion of compensatory mutations in the opposite sequence should make regulation possible again.

Figure 46: Predicted interaction (seed region) of Pos19 and the RSP_0557 mRNA. Numbers for RSP_0557 mRNA indicate the position relative to the start codon (grey), while numbers for Pos19 refer to the 5' end. The interaction and free hybridisation energy (lower right) is depicted as predicted with IntaRNA (Wright *et al.*, 2014; Busch *et al.*, 2008) and RNAPredator (Eggenhofer *et al.*, 2011) webtools.

To test this theory, six different mutations (Fig. 47) were tested. As a first attempt, one (M1) and three (M3) nucleotides were exchanged in the seed regions of Pos19 and RSP_0557 by Bork Berghoff (Fig. 47). Therefor site-directed mutagenesis PCR (2.4.3.2) was carried out using the primers listed in table 3 (M1 and M3). As template the pDrive_Pos19 and pDrive_0557 constructed for the over-expression and reporter cloning (3.1.2 and 3.1.6) were used. The mutated Pos19 and RSP_0557 fragments can be ligated into the pBBR1 broad-host-range cloning vector (pPos19 mutated over-expressions) and the pPHU4352 (mutated RSP_0557 reporter plasmids) after restriction with BamHI and HindIII or XhoI and HindIII, respectively.

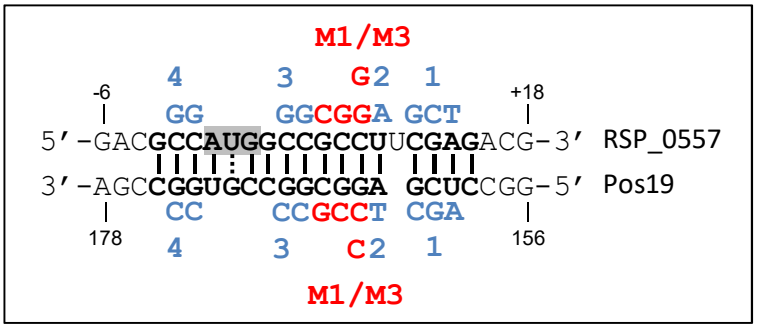

Figure 47: Overview of mutations and compensatory mutations in the Pos19 and RSP_0557 sequence. Mutations M1 (C to G) and M3 (GCC to CGG) are depicted in red; mutations 1 - 4 (GA to CT, TC to AG, CC to GG) are shown in blue.

The regulatory potential of the mutated Pos19 over-expression strains (pPos19 M1 and pPos19 M3) was investigated by measuring the ß-galactosidase activity of the RSP_0557 reporter plasmid (pPHU_0557) in those strains. This first combination of plasmids revealed that the mutated Pos19 variants M1 and M3 could not reduce the ß-galactosidase activity of the RSP_0557 reporter to the same extent as the unmutated variant (pPos19) and the one carrying the internal stop codon abolishing Pos19 peptide transcription (pStop16). While in the pPos19 M1 strain 65% of ß-galactosidase activity remained in comparison to the EVC strain (pBBR), in the pPos19 M3 strain

110% of activity could be measured (Fig. 48). To verify that the reduced regulation is due to the mutations in the seed region, the *vice versa* set-up was tested: the mutated RSP_0557 variants (pPHU_0557 M3 and pPHU_0557 M1) were transferred to the EVC and strains over-expressing the Pos19 sRNA (pPos19), the Stop16 (pStop16) and the corresponding mutated Pos19 variants (pPos19 M1 and M3) via conjugation. Different than expected, the original pPos19 and the pStop16 over-expression were able to reduce the ß-galactosidase activity of the RSP_0557 M1 reporter to 52% and 48% respectively and of the M3 reporter to 42% and 35% (Fig. 48). Moreover, the Pos19 M3, which in theory should bind to the RSP_0557 M3 best, did not change the reporter activity compared to the EVC (Fig. 48). This is also true for the Pos19 M1/RSP_0557 M1 combination. It was found in addition, that both mutated RSP_0557 reporter plasmids (M1 and M3) gave less ß-galactosidase activity than the unmutated RSP_0557 reporter overall, already in the EVC background (Tab. 51). These latter findings suggest that mutations in the RSP_0557-*lacZ* fusion result in a lower translation rate or reduced stability of the fusion product.

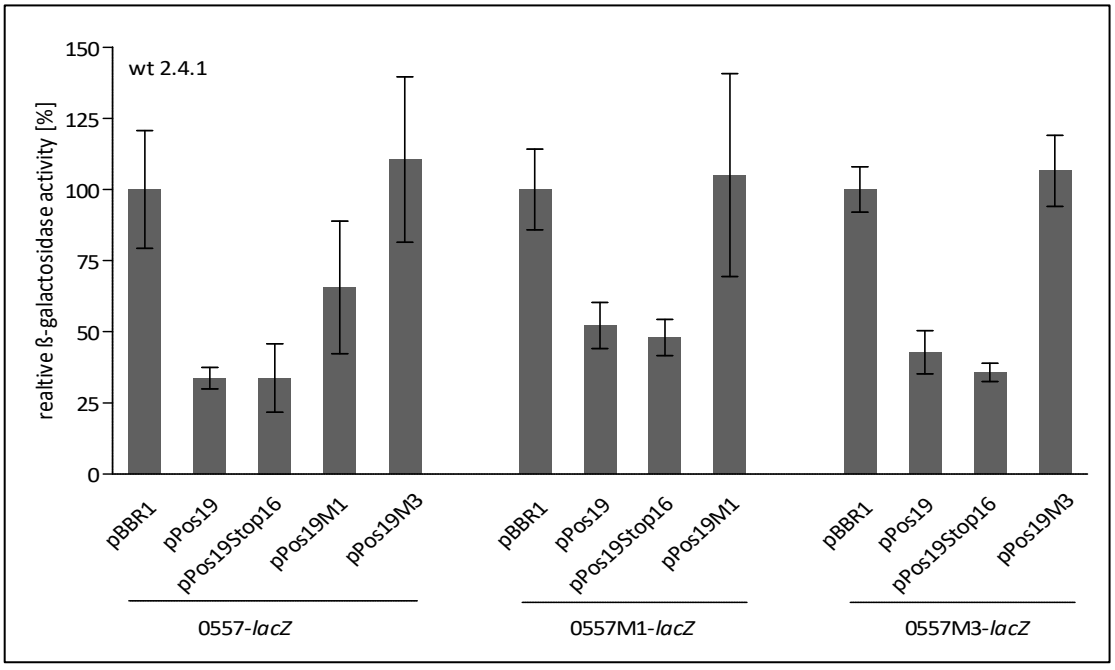

Figure 48: *LacZ*-based *in vivo* reporter assay with mutated reporter plasmid (0557-*lacZ*M1 and M3) and mutated Pos19 over-expression variants (pPos19M1 and M3). The native RSP_0557 sequence, as well as the RSP_0557 sequence containing the described mutations (M1 and M3; Fig. 47), were translationally fused to the *lacZ* gene on plasmid pPHU235. The resulting reporter plasmids were transferred to control (pBBR1) and over-expression strains of Pos19 (pPos19, pPos19Stop16, pPos19M1, pPos19M3) in wild-type background (wt 2.4.1). Cultures were stressed with $^1O_2$ for 60 min and samples subjected to β-galactosidase assays. Bars indicate the relative β-galactosidase activity in percent as calculated from Miller Units (with the pBBR1 control set to 100% for each construct). Results represent the mean from three independent experiments with technical duplicates and error bars reflect the standard deviation. Experiments carried out by Bork Berghoff.

Table 51: Raw data of the *in vivo* reporter study with mutated Pos19 and RSP_0557 seed region (M1 and M3) in Miller Units and percent after 60 min of $^1O_2$ stress. The data show mean values of biological triplicates and technical duplicates, with standard error of the mean and relative error, respectively.

Plasmid combination (pPHU / pBBR)	Miller Units	SEM	Percent [%]	rel. error [%]
0557 / pBBR	491.4	101.8	100.0	20.7
0557 /pPos19	165.4	18.7	33.7	3.8
0557 / pStop16	166.0	59.2	33.8	12.0
0557 /pPos19 M1	322.4	114.3	65.6	23.3
0557 /pPos19 M3	543.5	142.9	110.6	29.1
0557 M1 / pBBR	96.9	13.7	100.0	14.2
0557 M1 / pPos19	50.5	7.8	52.2	8.1
0557 M1 /pStop16	46.5	6.2	48.0	6.4
0557 M1 / pPos19 M1	101.7	34.6	105.0	35.7
0557 M3 / pBBR	143.3	11.4	100.0	8.0
0557 M3 / pPos19	61.3	10.8	42.8	7.6
0557 M3 / pStop16	51.2	4.6	35.7	3.2
0557 M3 / pPos19 M3	152.6	17.9	106.5	12.5

To exclude that the less pronounced regulation of the RSP_0557-*lacZ* fusion entailed by the pPos19 M1 and M3 over-expression strains is due to changed Pos19 levels in comparison to the original pPos19 over-expression, a Northern blot analysis was carried out.

Samples from the three over-expression strains (pPos19, pPos19 M1, and pPos19 M3) were withdrawn before (0 min) and after 10, 30 and 60 min of $^1O_2$ stress and equal amounts of isolated RNA (2.4.1.3 a) were separated on an 8% PAA-urea gel (2.4.6.1). After blotting, the membrane was hybridised with the Pos19 probe and the 5S rRNA probe as loading control (2.4.9). The Northern blot analysis showed that the sRNA induction and expression level did not differ between the three tested strains (Fig. 49).

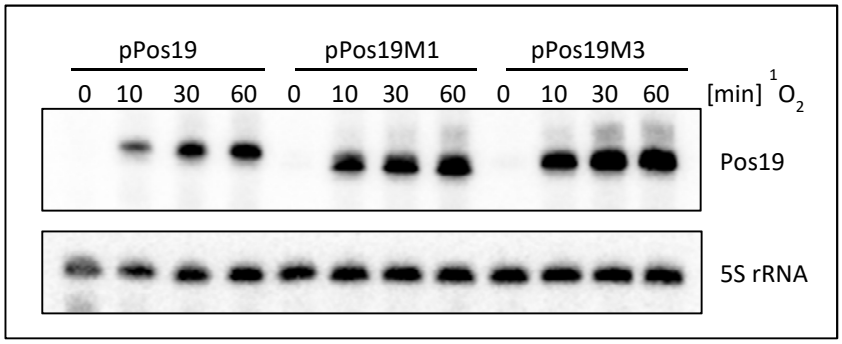

Figure 49: Verification of the over-expression level of Pos19M1 and Pos19M3. Strains were exposed to $^1O_2$ stress for 0, 30, and 60 min before harvesting the cells and isolating the RNA via the hot phenol method. 8 µg RNA each was separated on an 8% PAA urea gel, before blotting and hybridising the membrane with the Pos19 and the 5S rRNA probes.

Besides these first mutational variants (M1 and M3), four more variants (numbered 1-4) were constructed and tested. The nucleotides exchanged in these mutations are also depicted in figure 47.

Again the mutations were achieved by using the site-directed mutagenesis PCR with primers listed in table 3 (0557- 1-4). For the construction of the mutated Pos19 over-expression and RSP_0557 reporter plasmids, the same strategy as for M1 and M3 (described above) was intended. As a first attempt, all four mutated RSP_0557 reporter plasmids were constructed (primer pairs 0557-mut1 – 0557-mut4, Tab. 3) and conjugated to the EVC strain (pBBR) and the Pos19 over-expression strain (pPos19). Two of the four newly constructed reporter plasmids showed reduced ß-galactosidase activity in general, as it was found for the RSP_0557 M1 and M3 reporters. Compared to ~1400 Miller Units of the pPHU_0557 in the EVC background, pPHU_0557-3 gave only around 190 Miller Units and the activity of pPHU_0557-4 was even reduced to 49 Miller Units. When comparing the measured ß-galactosidase activity of all four mutated reporter plasmids after stress (60 min) in the Pos19 over-expression (pPos19) to the EVC (pBBR), they were all reduced to levels comparable to those of the unmutated RSP_0557 reporter (pPHU_0557). That means that despite the mutations in the predicted seed-region, Pos19 is able to repress the translation of the tested RSP_0557-*lacZ* fusions 1-4. Due to these results (Tab. 52) the *vice versa* set up, meaning testing the additional mutated pPos19 over-expression strains, was not attempted.

Table 52: Raw data of the *in vivo* reporter study with mutated RSP_0557 sequences (1-4) in Miller Units and percent after 60 min of $^1O_2$ stress. The data show mean values of biological triplicates and technical duplicates, with standard error of the mean and relative error, respectively.

Plasmid combination (pPHU / pBBR)	Miller Units	SEM	Percent [%]	rel. error [%]
0557 / pBBR	1424.5	363.5	100.0	25.5
0557 /pPos19	678.3	106.8	47.6	15.7
0557-1 / pBRR	1288.9	326.6	100.0	25.3
0557-1 / pPos19	461.8	75.8	35.8	16.4
0557-2 / pBRR	917.7	94.0	100.0	10.2
0557-2 / pPos19	392.4	50.7	42.8	12.9
0557-3 / pBBR	189.3	36.6	100.0	19.4
0557-3 / pPos19	80.5	7.3	42.5	9.0
0557-4 / pBRR	48.7	5.7	100.0	11.8
0557-4 / pPos19	26.6	2.3	54.6	8.5

The pPHU_0557 reporter cloned for the *in vivo* reporter system contains 290 bp upstream of the RSP_0557 start codon. In this sequence, a potential promoter (TTGCTCCGGAACCAATTGCCGACATCAA) can be found. To rule out that the regulation on the pPHU_0557 reporter by Pos19 is due to an effect on this promoter, and thereby rather on transcription than translation, a second reporter plasmid was constructed. For this second reporter plasmid only the upstream part of RSP_0557 fragment without the start codon was amplified and transcriptionally fused to the *lacZ* gene carrying its own RBS. For this purpose, a reporter plasmid namely pBBR1_MCS3_*lacZ* (Fried *et al*., 2012), based on the pBBR series (Kovach *et al*., 1995), was used. The 149 bp fragment upstream of the RSP_0557 start codon

was amplified using the primer pair GA_P0557_fw / GA_P0557_rev (Tab. 3), sub-cloned into the pDrive cloning vector (Qiagen), and ligated into the corresponding sites of the pBBR1_MCS3_*lacZ* after restriction with AgeI and XbaI. The transcriptional reporter fusion (pP0557-*lacZ*) was transferred to the Pos19 over-expression strain (pPos19) and the corresponding EVC (pBBR1). The resulting strains were cultivated in biological triplicates and exposed to $^1O_2$ stress for 60 min before harvesting cells for a ß-galactosidase activity assay (2.2.15). The assay revealed that the potential promoter gave active transcription of the *lacZ* gene (227 MUs in the pBBR1 strain), which was not affected by the over-expression of Pos19 (230 Miller Units; Fig. 50).

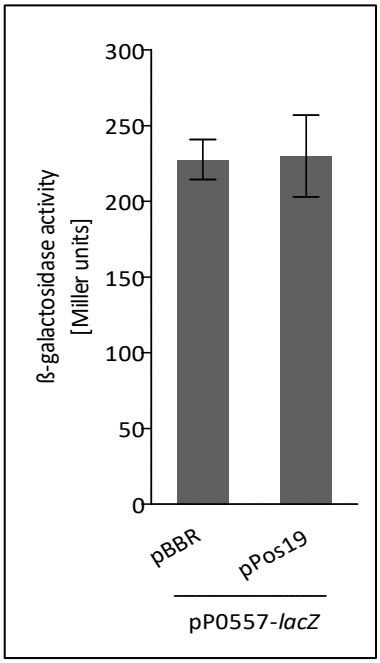

Figure 50: *LacZ*-based RSP_0557 promoter study. The reporter plasmid P0557-*lacZ* that carries the RSP_0557 upstream region (-149 bp from TSS) was transferred to the empty vector control strain (pBBR) and the Pos19 over-expression strain (pPos19). Samples were taken after 60 min of $^1O_2$ stress. The results represent the mean of technical duplicates from biological triplicates with the standard error of the mean.

3.1.9 Pos19-RSP_0557 interaction - EMSA

Since the compensatory mutations in the reporter system could not prove a direct interaction of Pos19 and the RSP_0557 mRNA and an effect on the RSP_0557 promoter could be ruled out (3.1.8), a second attempt to monitor the direct interaction of both RNAs was undertaken by EMSA experiments.

The complete Pos19 sequence and a 194 bp part of RSP_0557, containing the predicted binding site (Fig. 46) and the start codon, were amplified together with a T7 promoter (TAATACGACTCACTATA) for *in vitro* transcription (primer pairs in Tab. 3). The Pos19 *in vitro* transcript was radio-labelled (hot) by incorporation of [α^{32}P]UTP (Hartmann Analytic; 2.4.7.3) while the RSP_0557 transcript is prepared unlabelled (cold; 2.4.5). The T70557 transcript was controlled for purity on a PPA urea gel (2.4.6.1), while the purity of the hot T7Pos19 transcript (T7Pos19*) was checked later on the EMSA gel. For the EMSA, 150 fmol of T7Pos19* transcript was mixed with different amounts of cold T70557 transcript (Fig. 51). As a control, T7Pos19* is mixed with cold T71092 transcript (details in 3.2.7.2) in a 100-fold excess over T7Pos19*. EMSAs were carried out using *in vitro* transcripts from different batches and employing various gel and buffer variants. The gel and buffer conditions tested were: gel run at 4°C and RT, 0.5x TBE and 0.25x TBE, as well as 0.25x TB with 10 mM magnesium chloride ($MgCl_2$), and a final concentration of 0.5x, 0.75x and 1x structure

buffer in the samples. Also ratios of up to 1000:1 of T70557 over T7Pos19* were tested. With none of the experimental settings a direct binding of the T7Pos19* and RSP_0557 transcripts, resulting in a band shift of Pos19* in the gel, could be achieved; unless both RNAs were de- and renatured together. An exemplary EMSA scan can be seen in figure 51.

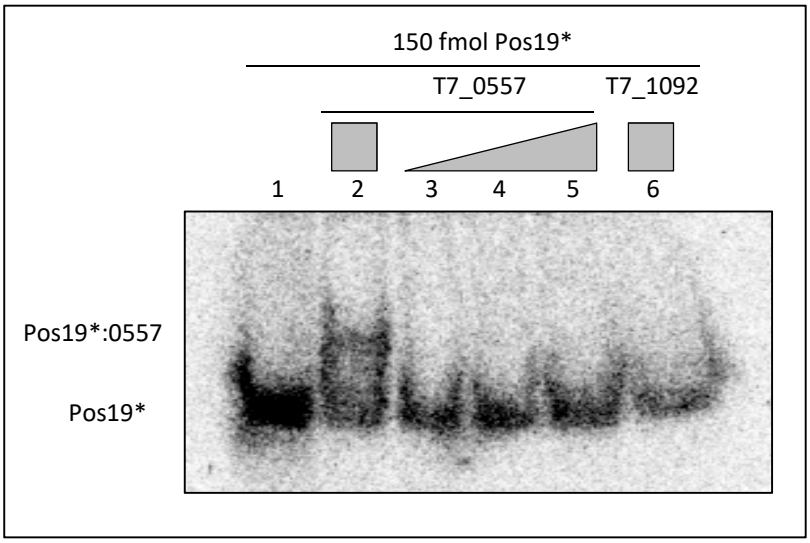

Figure 51: RSP_0557-Pos19 interaction study using EMSA. The figure exemplary shows the scan of one EMSA out of ten. The EMSA was carried out as described in 2.4.13 using a 0.25x TB gel and buffer with 10 mM $MgCl_2$, and 1x structure buffer in each sample. The samples were composed as follows: (1) 150 fmol Pos19*, (2) 150 fmol Pos19* and 15000 fmol T7_0557 (de- and renatured together), (3) 150 fmol Pos19* and 150 fmol T7_0557, (4) 1500 fmol Pos19* and 1500 fmol T7_0557, (5) 150 fmol Pos19* and 15000 fmol T7_0557, (6) 150 fmol Pos19* and 15000 fmol T7_1092.

3.1.10 Half-life determination of the RSP_0557 mRNA

In addition to the *in vivo* reporter system and EMSA experiments, the half-life of the RSP_0557 mRNA was determined in the Pos19 knockout mutant in comparison to the wild-type.

For this experiment both strains were grown under microaerobic conditions to the exponential phase (OD_{660} ~0.4) and the induction of Pos19 and RSP_0557 was achieved by adding H_2O_2 (final concentration [1 mM]) 10 min before adding the rifampicin. Cells were harvested before H_2O_2 addition, 10 min after the addition of H_2O_2 (0 min rifampicin) and after 2, 4, 7, and 10 min of rifampicin addition. The RNA was isolated using the hot phenol method (2.4.1.3 a) to apply it on a Northern blot (2.4.6.1). The oligos to detect Pos19, the RSP_0557 mRNA (RT-PCR revrese primer, Tab. 3), and the 5S rRNA as loading control were radio-labelled (2.4.7.1) and the membrane was hybridised as described in 2.4.9. The half-life (2.4.12 b) determined for RSP_0557 is 3.05 min in the wild-type but 9.24 min in the Pos19 knockout mutant (ΔPos19; Fig. 52), which would fit the assumption that Pos19 negatively affects the RSP_0557 mRNA. The half-life of Pos19 calculated from the wild-type signals is 13.9 min, which is inconsistent with previous findings (5 min; Berghoff *et al.*, 2009).

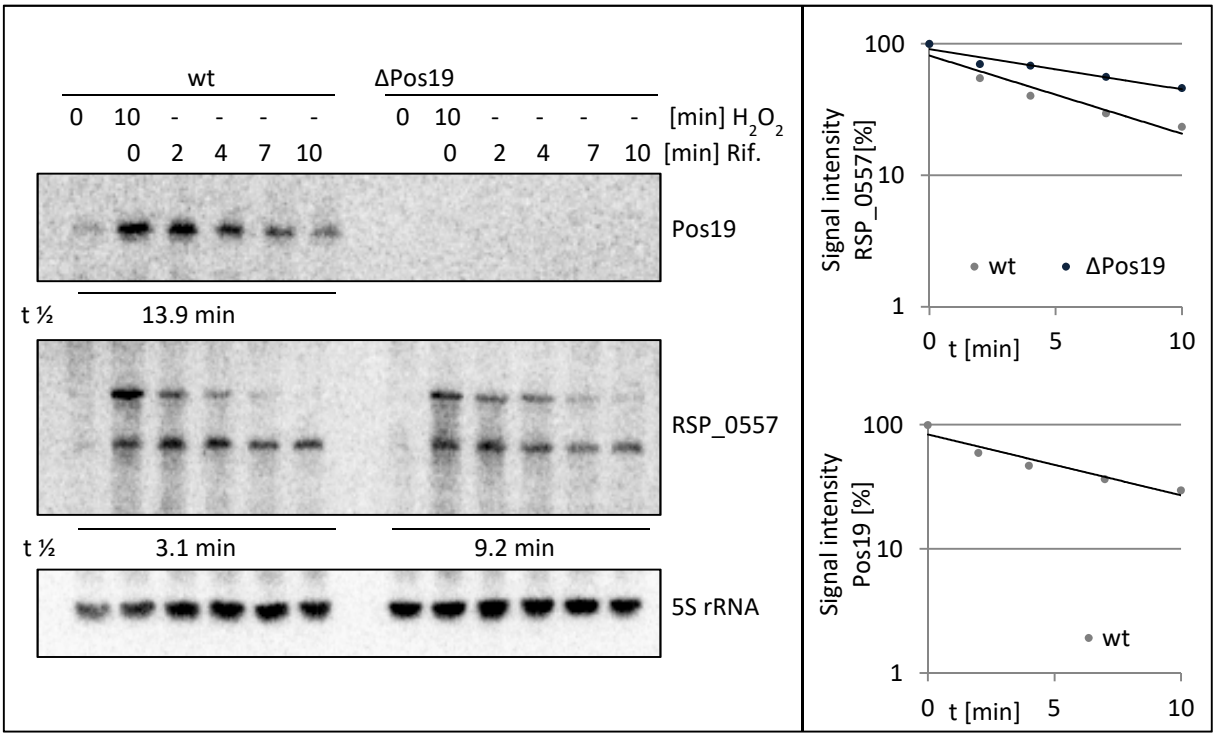

Figure 52: Half-life determination of the RSP_0557 mRNA. Left: The *R. sphaeroides* wild-type (wt) and the Pos19 mutant (ΔPos19) were grown microaerobically to the exponential phase (OD_{660} ~0.4). Cells were harvested at the indicated timepoints before and after addition of H_2O_2 (final concentration 1mM) and rifampicin (0.2 mg/ml). The RNA was isolated and subjected to Northern blot analysis. The half-life values calculated for Pos19 and the upper RSP_0557 signal are depicted in minutes below the blot. Right: The RNA signal intenisties were normalized by 5S rRNA signals and plotted semi-logarithmically in percent against the time in minutes.

3.1.11 Function of RSP_0557

While investigating the effect of Pos19 on RSP_0557, the function of this hypothetical protein got more and more intriguing. One hypothesis regarding RSP_0557 was that the function of Pos19 is sole to regulate RSP_0557 to contribute to the defence against oxidative stress. To elucidate the role of the RSP_0557 gene product, both an over-expression and a chromosomal deletion (knockout) of the gene were constructed. For the over-expression the RSP_0557 sequence together with a 396 bp upstream region from the start codon on was amplified using the primers 0557-UTR-Bam / 0557-down-Xba. This sequence was inserted via BamHI and XbaI into the pBBR4352 vector (constructed by Yannick Hermanns) under the control of the 16S rRNA promoter, resulting in the plasmid p16S::0557. The knockout mutant was constructed using the same strategy as for the Pos19 knockout (3.1.4). Upstream (700 bp) and downstream (485 bp) fragments of RSP_0557 were amplified using primer pairs 0557-up-EcoRI / 0557-up-PstI and 0557-down-SphI / 0557-down-Pst-2, respectively. The over-expression from the 16S rRNA promoter (p16S::0557), as well as the deletion (Δ0557) of RSP_0557, were verified using *R. sphaeroides* pRK16S (EVC) and wild-type (wt) RNA as the controls on a Northern blot (Fig. 53). For this purpose, the four strains were cultivated, and cells were harvested

before (0 min) and after (10 min) $^1O_2$ stress. The RNA was isolated using the hot phenol method (2.4.1.3 a). The blot, the radio-labelling of the probes (Tab. 3) and the membrane hybridisation were carried out as described in 2.4.6 – 2.4.11. Both membranes were additionally hybridised with the Pos19 specific probe, to check whether the over-expression or absence of RSP_0557 has an influence on the Pos19 expression level. There was no change observable due to the changed RSP_0557 expression when calculating the expression levels (fold change; two biological replicates each) of Pos19 (data not shown). The verification of the over-expression and deletion of RSP_0557 (Fig. 53) showed in addition that both signals already found on the membranes used for the half-life determination (Fig. 52) are true RSP_0557 signals.

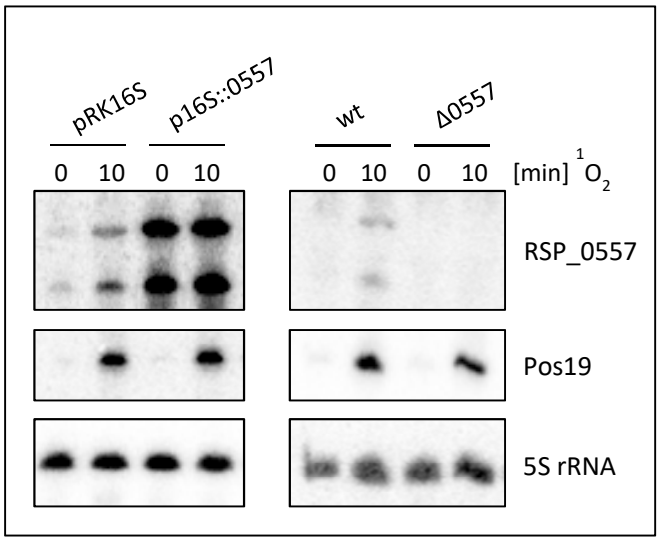

Figure 53: Northern blot verification of RSP_0557 knockout and over-expression. The indicated strains were exposed to $^1O_2$ stress for 0 and 10 min. The isolated RNA was subjected to Northern blot analysis using hybridisation probes for RSP_0557 (RT-Primer), Pos19 and the 5S rRNA, the latter is probed as loading control.

Before applying the newly constructed RSP_0557 strains in different assays, the expression pattern of RSP_0557 was further investigated. As the RT-PCR and microarray comparing 0 and 7 min of $^1O_2$ stress in the wild-type indicated, first Northern blots using the RSP_0557 probe confirmed that RSP_0557 is induced upon $^1O_2$ stress in the wild-type (Fig. 53). When taking a closer look on the RSP_0557 promoter motif (TTG(N^{19})TTATTT), it was found to resemble the RpoHI/II consensus sequence that was described for *R. sphaeroides* (Nuss *et al*., 2010). Therefore the expression of RSP_0557 was tested in the wild-type and the three *rpoH* knockout mutants - Δ*rpoHI,* Δ*rpoHII,* and Δ*rpoHI/II*. Due to its greater level of induction of RSP_0557 (preliminary experiments) heat stress (42°C) was chosen over $^1O_2$ stress in this experiment to induce the expression of RSP_0557. Both alternative sigma factors, RpoHI and RpoHII, are involved in the response to heat stress, but RpoHI is the major player under these conditions (Nuss *et al*., 2010). The *R. sphaeroides* wild-type and the three listed knockout mutants were shifted from 32°C to 42°C for 30 min during microaerobic cultivation (2.2.1.2) and cells were harvested before and after (30 min) the shift. After RNA isolation using the hot phenol method (2.4.1.3 a) a Northern blot (2.4.6.1) was performed. The Northern blot analysis confirmed the promoter of RSP_0557 to be RpoHI/RpoHII-dependent (Fig. 54). In the Δ*rpoHI* mutant the induction of RSP_0557 upon heat stress was clearly weaker than in the wild-type (wt) and

the Δ*rpoHII* mutant. When both alternative sigma factors are missing (Δ*rpoHI/II*) there was almost no induction of RSP_0557 when shifting the growth to 42°C.

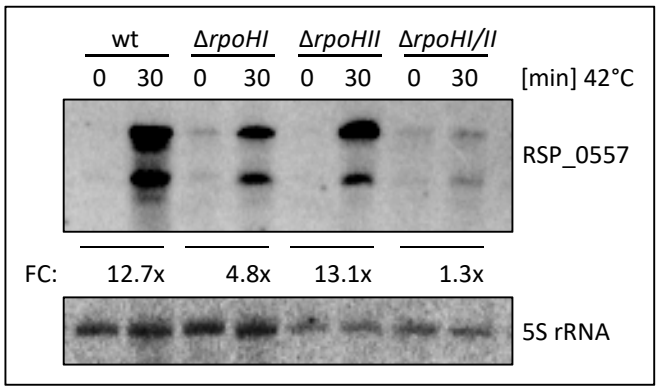

Figure 54: Sigma factor-dependency of RSP_0557 expression. The *R. sphaeroides* wild-type (wt) as well as the indicated sigma factor knockout mutants (Δ*rpoHI*, Δ*rpoHII*, and Δ*rpoHI/II*) were cultivated under microaerobic conditions (32°C) and cells were harvested before and 30 min after shifting the cultures to 42°C. The induction of RSP_0557 upon heat stress is depicted as fold change (FC; 30/0 min) for each strain. The experiment was carried out by S. Martini.

The two RSP_0557 strains (Δ0557 and p16S::0557) and adequate controls were used in physiological assays trying to further elucidate the function of RSP_0557 and its possible overlap with the Pos19 function. A growth analysis (2.2.2) comparing the RSP_0557 knockout (Δ0557) to the wild-type as well as the constitutive over-expression of RSP_0557 (16S::0557) to the corresponding EVC (pBBR16S), revealed a very slight growth impairment for both RSP_0557 strains (Fig. 55).

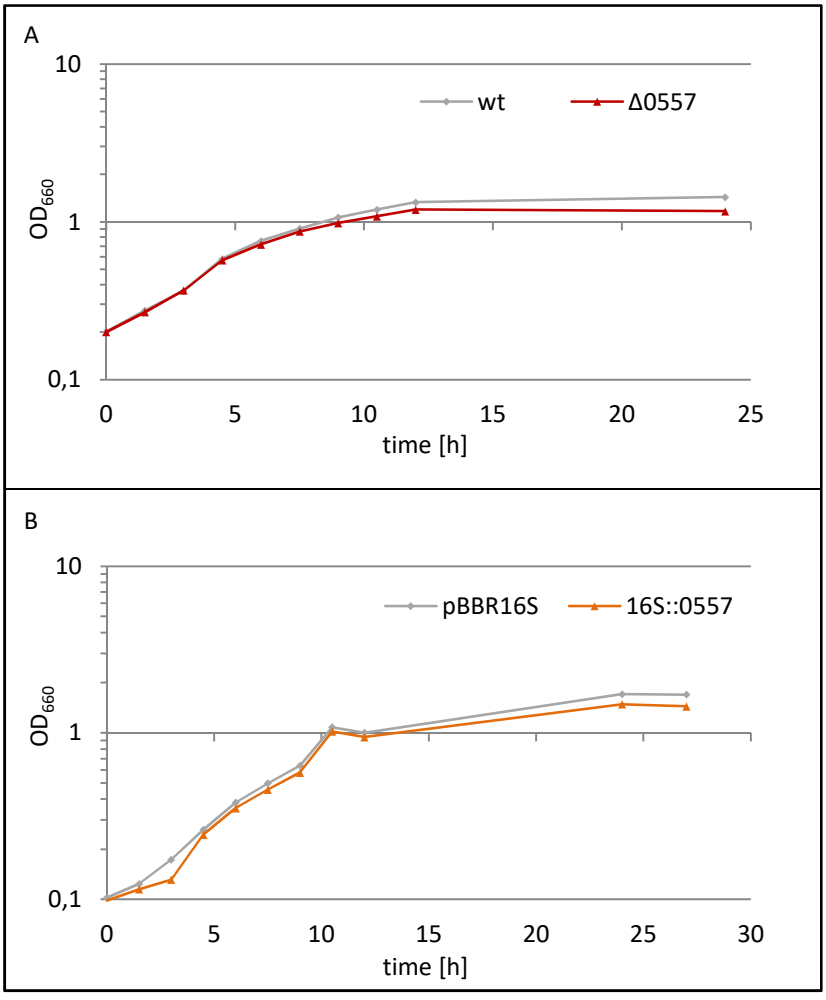

Figure 55: Growth analysis under microaerobic conditions. A: To analyse the growth behaviour the *R. sphaeroides* wild-type (wt, grey) and the RSP_0557 knock-out mutant (Δ0557, red) were grown microaerobically. B: The growth of the constitutive RSP_0557 over-expression strain (p16S::0557, yellow) and the corresponding EVC (pBBR16S, grey) were monitored under microaerobic conditions as well. The OD_{660} was plotted semi-logarithmically against the time.

In addition to the slight growth phenotype, the RSP_0557 knockout mutant (Δ0557) showed increased resistance towards H_2O_2 (1M) and $^1O_2$ (methylene blue, 50 mM) compared to the wild-type in a zone of inhibition assay (preliminary experiments). This displayed the first hint that the function of Pos19 in the stress defence is coupled to or is even fully dependent on RSP_0557, which is still assumed to be the main target of Pos19. Nevertheless, a repetition of the zone of inhibition assays also using the RSP_0557 over-expression strain (p16S::0557) and the corresponding EVC (pBBR16S) revealed a higher resistance of the RSP_0557 over-expression as well (Fig. 53).

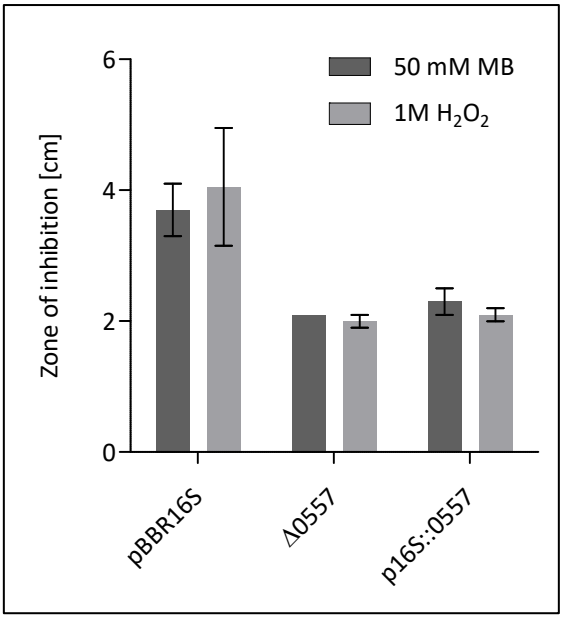

Figure 56: Zone of inhibition assay to test for resistance against $^1O_2$ and H_2O_2 stress. The diameter of the inhibition zones is depicted in cm for three *R. sphaeroides* strains: an empty vector control (pBBR16S), the RSP_0557 knockout mutant (Δ0557), and the RSP_0557 over-expression (p16S::0557). The results represent the mean of biological triplicates and technical duplicates with the standard error of the mean.

To investigate whether GSH plays a role in the increased resistance towards oxidative stress of the RSP_0557 strains (Δ0557 and p16S::0557), as it was supposed for the Pos19 over-expression (3.1.4.1), a GSH assay (2.2.16) was performed. Again, when comparing the RSP_0557 knockout (Δ0557) and constitutive over-expression (p16S::0557) to the EVC (pBBR16S) both RSP_0557 strains revealed slightly increased (128 and 127%) intracellular GSH levels (Fig. 57). The GSH assay was carried out using technical duplicates from biological triplicates of each strain grown under microaerobic conditions.

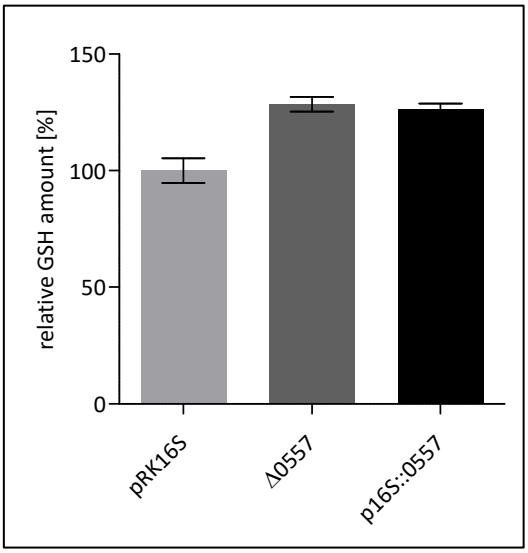

Figure 57: Measurement of total intracellular GSH levels. The GSH level was measured for three *R. sphaeroides* strains: an empty vector control (pBBR16S), the RSP_0557 knockout mutant (Δ0557), and the RSP_0557 over-expression strain (p16S::0557). The GSH amount is depicted in percent (mean of biological triplicates and technical duplicates) with standard deviation

Since the results of the physiological assays were rather inconsistent, the potential effect of RSP_0557 on the genes regulated by Pos19 was tested. Assuming that Pos19 acts via RSP_0557 indirectly on the sulphur genes, the regulation entailed by the Pos19 over-expression should vanish in the RSP_0557 knockout mutant. To test this hypothesis, the Pos19 over-expression plasmid pPos19 was transferred to the RSP_0557 knockout (Δ0557) via conjugation (2.2.13). The Pos19 over-expression strain pPos19 and the new strain Δ0557/pPos19 were cultivated in triplicates and cells were harvested before (0 min) and after 7 min of $^1O_2$ stress (2.2.1.5). The RNA was isolated for RT-PCR using the TRIzol method (2.4.1.3 b). Comparing the expression of selected mRNAs (compare Fig. 28) upon stress, showed no significant difference in the expression levels between the two strains wt/pPos19 and the Δ0557/pPos19 (Fig. 58).

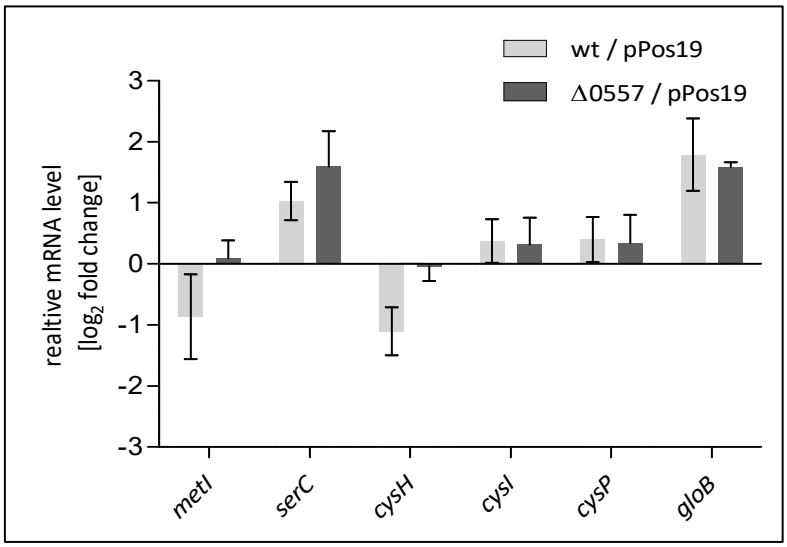

Figure 58: Effect of the RSP_0557 deletion on the Pos19-entailed gene regulation. The Pos19 over-expression plasmid (pPos19) was transferred to the *R. sphaeroides* wild-type (wt) and the RSP_0557 knockout mutant (Δ0557) via conjugation. The resulting strains (wt/pPos19, light grey and Δ0557/pPos19, dark grey) were exposed to $^1O_2$ stress for 0 and 7 min. The expression level of selected genes was determined comparing the stressed to the unstressed sample for each strain.

Overall the applied tests described above could not reveal a tangible function for RSP_0557 or substantiate the hypothesis that the effect entailed by the Pos19 over-expression solely depends on the expression or regulation of RSP_0557.

3.2 Characterisation of the sRNA PcrX (RSspufX)

The sRNA RSspufX, here named PcrX for photosynthesis control RNA X, was first identified in an RNA-seq study by Berghoff and colleagues in 2009. PcrX is encoded 46 nt downstream of *pufX*, the last gene of the *puf* operon, and shows a size of 107 nt (Fig. 18) according to the RNAseq data. Due to its close proximity to the *puf* operon, encoding reaction centre (RC) and light harvesting complex (LHC) I proteins, the idea arose that a potential role of the sRNA could be the regulation of the photosynthesis genes in *R. sphaeroides*.

3.2.1 Expression profile

PcrX is induced upon a drop from high to low oxygen tension, dependently on the two regulatory proteins PrrA and FnrL (Fig. 59 A). Overall, when comparing the PcrX level between different growth conditions, the expression was found to be highest during phototrophic growth, while lowest under aerobic conditions (Fig. 59 B). Taken together this expression profile resembles the one of the *puf* operon, with PrrA and FnrL being known regulators of the *puf* operon and other photosynthesis genes (1.9.2).

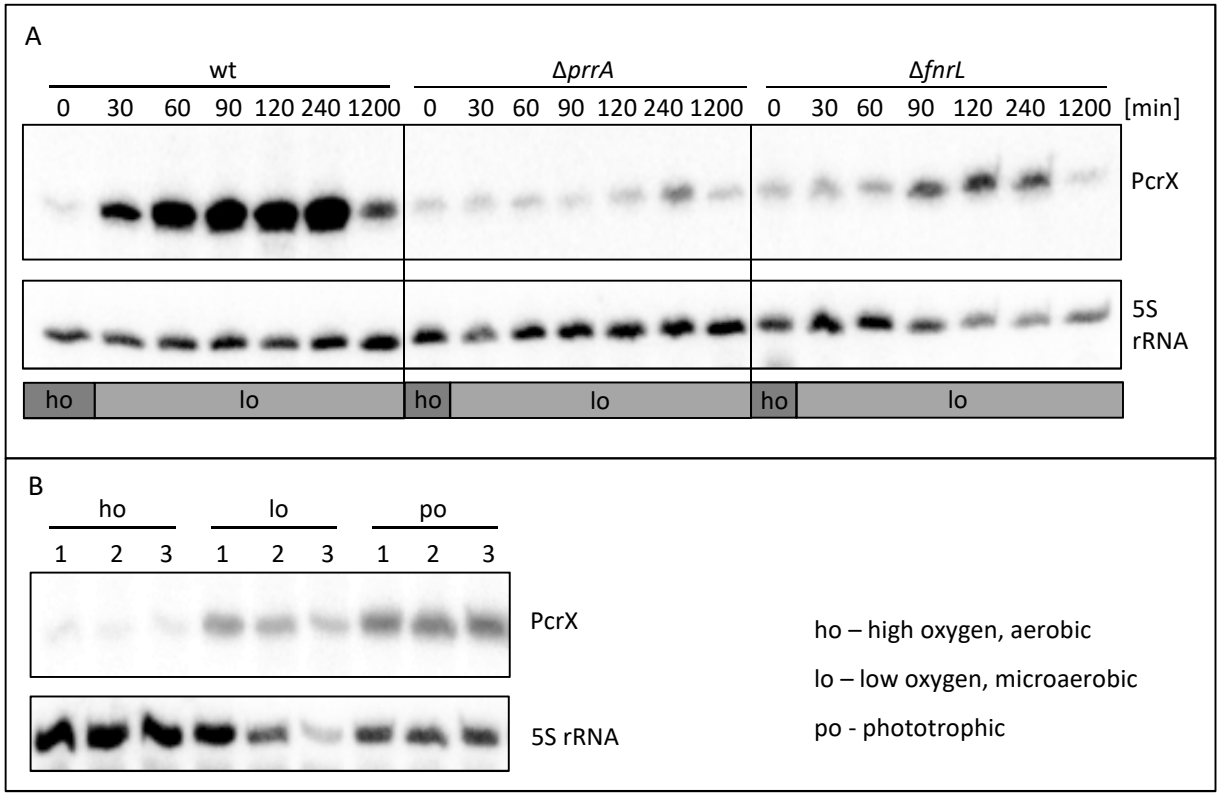

Figure 59: Oxygen-dependent expression pattern of PcrX. A: PcrX induction upon a shift from high (ho) to low (lo) oxygen conditions, in the *R. sphaeroides* wild-type (wt) and two regulator mutants, lacking either PrrA (Δ*prrA*) or FnrL (Δ*fnrL*). B: PcrX abundance during different growth conditions in the wild-type (exponential phase). Samples were taken from biological triplicates (1 - 3). The 5S rRNA was probed as loading control.

The expression was tested with the help of Northern blot analysis using RNA isolated from samples indicated in figure 59. The abbreviations indicating the cultivation conditions (2.2.1.1 – 2.2.1.3): **ho** – high oxygen, aerobic; **lo** – low oxygen, microaerobic; **po** – phototrophic, will be used throughout the text and figures in the following results part.

In addition to the expression profile shown above, a terminator prediction with the ARNold web tool (Gautheret and Lambert, 2001; Hofacker *et al*., 1994; Lesnik *et al*., 2001; Macke *et al*., 2001) was carried out. This prediction indicated that the sRNA PcrX and the *puf* operon share one Rho-independent terminator (Fig. 60). The predicted terminator shown in figure 60 is identical to the one previously suggested by Lee *et al*. in 1989.

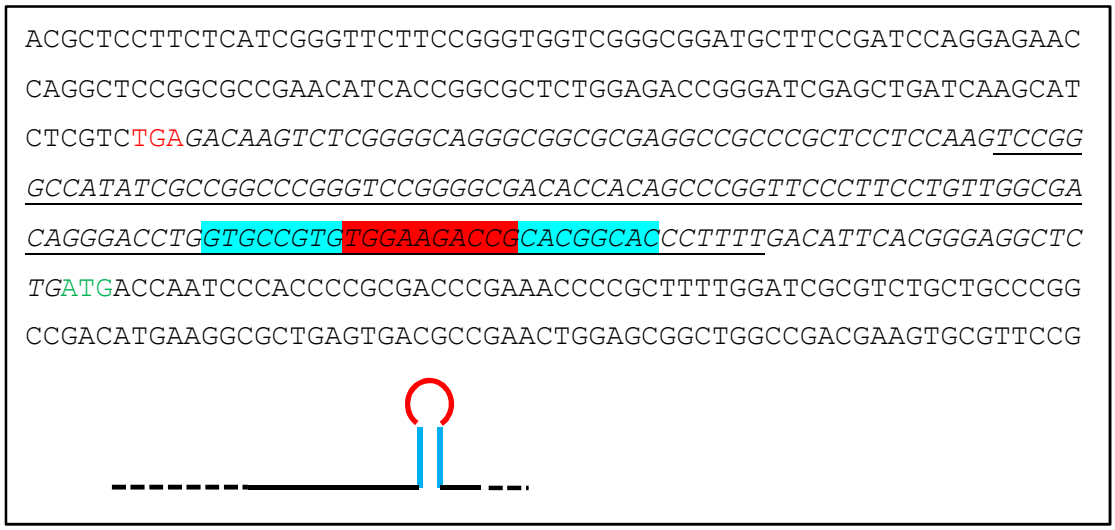

Figure 60: Sequence information – intergenic region (italics) between *pufX* (stop codon – red) and *dxsA* (start codon – green). The PcrX sequence is underlined, while the Rho-independent terminator is highlighted in blue (stem) and red (loop). The terminator is in addition depicted schematically below the sequence.

Taken together, these first findings supported the idea of a role of PcrX in photosynthesis gene regulation. They also led to the question whether PcrX possesses its own PrrA and FnrL dependent promoter or if it is co-transcribed together with the polycistronic *puf* mRNA. To enter into this question, transcriptional fusions of different promoters and potential promoter regions to a *lacZ* gene were constructed later on (3.2.3).

3.2.2 PcrX half-life determination

Besides the expression pattern (3.2.1) of the sRNA PcrX, its half-life was determined. For this purpose, the *R. sphaeroides* wild-type was cultivated under microaerobic conditions (2.2.1.2) to the exponential growth phase (OD_{660} ~0.4) and cells were harvested (t 0). After the addition of rifampicin, cells were harvested at the time points 30, 60, 120, and 180 min (the quite long time points result from preliminary results obtained by Benjamin Eisenhardt and Carina Reuscher). The RNA was isolated using the hot phenol method (2.4.1.3 a) and was applied on a PAA-urea gel-based

Northern blot (2.4.6). After hybridisation with the PcrX and 5S rRNA specific probes (2.4.9), the half-life of PcrX could be calculated as described in 2.4.12. To obtain reliable results, the experiment was carried out three times with independent biological replicates and the mean value and standard deviation of the three determined half-life values were calculated, resulting in a average half-life of 289 ± 58 min. Figure 61 shows one exemplary Northern blot from this experimental series.

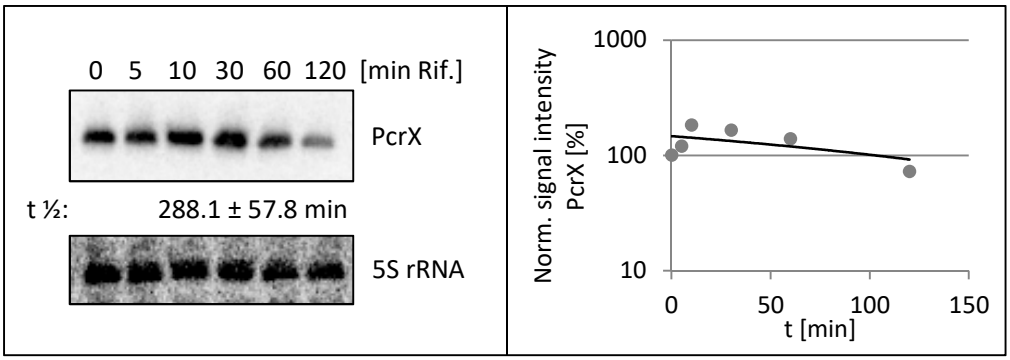

Figure 61: Half-life determination of PcrX via Northern blot. Left: RNA isolated from the *R. sphaeroides* wild-type before (0 min) and after rifampicin treatment (min rif.). The half-life ($t_{½}$) was calculated from three independent experiments and is shown as mean with standard error of the mean. The figure shows one exemplary Northen blot out of three. The 5S rRNA was probed as loading control. Northern blot carried out by Carina Reuscher. Right: sRNA signal intenisties were normalized by 5S rRNA signals and plotted semi-logarithmically in percent against the time in minutes.

3.2.3 PcrX promoter studies

For the promoter studies mentioned above (3.2.1), two sequence parts upstream of PcrX were chosen. Both start upstream of the transcriptional start site (TSS) of PcrX determined from the RNAseq data, one 326 nt upstream (named P326) and the other 470 nt upstream (named P470). The latter also contains the start codon and 160 nt upstream of *pufX*. These constructs were used to test for promoter activity upstream of PcrX. To gain overall insight into promotor strength in the *puf* operon context, a 1267 nt part upstream of *pufB* (named P1200) containing the *puf* Promotor (Vasilyeva *et al*., 1999) was used for transcriptional fusion. To exclude that the tested growth conditions affect transcription from the reporter plasmids in general, besides specific effects on the tested promoters, the reporter plasmid pBBR1_MCS3 carrying the *lacZ* gene under the control of the supposedly oxygen-independent 16S rRNA promoter (149 bp fragment, p16S_*lacZ*; constructed by Anke Laux) was used. The primer pairs to amplify the described sequences are listed in table 3, categorised as primer pairs for promoter fusions. The four sequences were sub-cloned into the pDrive cloning vector and ligated to the respective restriction sites of the pBBR1-MCS3_*lacZ* (Fried *et al*., 2012) after digestion with AgeI and XbaI, resulting in the reporter plasmids pP326_*lacZ*, pP470_*lacZ*, pP1200_*lacZ* and pP16S_*lacZ*. Those four reporter plasmids were conjugated to *R. sphaeroides* wild-type and the resulting strains were cultivated under aerobic conditions (2.2.1.1).

After taking samples from the aerobic cultures (exponential phase), the cultures were shifted to microaerobic conditions (2.2.1.2) and samples were taken after three different time-points: 30, 60 and 90 min after the shift. Finally, the cultures were shifted to phototrophic growth conditions (2.2.1.3) and samples were taken again after 30 min. The collected samples were applied for a ß-galactosidase activity assay (2.2.15), which revealed rather different activities for the tested (potential) promoters (Fig. 62). The strongest promoter activity was measured for the 16S rRNA promoter (pP16S) with 1500 – 1819 Miller Units (MUs), while the *puf* promoter fusion (pP1200) gave between 330 and 545 MUs. During the oxygen shift the 16S promoter activity differed only by 17 – 21% from the first sample taken (aerobic, exponential), whereas the activity of the *puf* promoter increases constantly from 100% to 165% during the shift (Fig. 62 and Tab. 53). Overall the activities of the P326 and P470 reporter fusions were very low (maximum 32 and 54 Miller Units), but a constant drop of the activity to 37% and 36%, respectively, was observed (Fig. 62 and Tab. 53). In comparison, the insertless reporter plasmid (pBBR_*lacZ*) gave around 5 MUs under all tested conditions (data not shown).

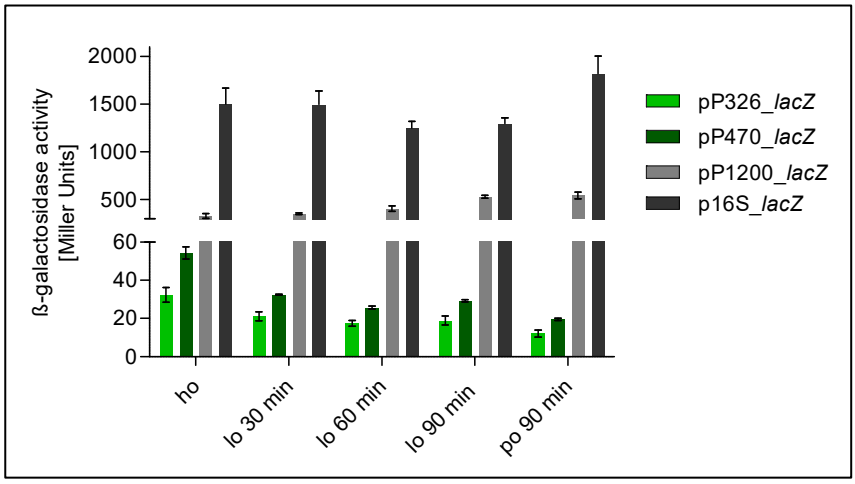

Figure 62: *LacZ*-based promoter studies. Potential promoter regions upstream of PcrX (P326 and P470) as well as known promoters (16S and P1200) were transcriptionally fused to the *lacZ* gene on the pBBR1MCS3_*lacZ*. Samples from biological triplicates were taken under the designated growth conditions at the indicated time points for a ß-galactosidase activity assay. The resulting Miller Units are depicted with standard error of the mean.

Table 53: Raw data of the promoter studies shown in figure 62. Mean values from biological triplicates and technical duplicates are shown as Miller Units and percent with standard error of the mean (SEM) and relative error, respectively. Cultures were shifted from aerobic (ho) to microaerobic (lo) and phototrophic (po) growth.

Promoter and sample time point	Miller Units	SEM	Percent [%]	rel. error [%]
P326 ho	32.4	3.9	100.0	12.0
P326 lo 30 min	21.2	2.3	65.3	7.2
P326 lo 60 min	17.5	1.5	54.2	4.5
P326 lo 90 min	18.9	2.4	58.4	7.5
P326 po 30 min	12.2	1.8	37.6	5.6

Table 53 continuing:

P470 ho	54.3	3.2	100.0	5.9
P470 lo 30 min	32.4	0.2	59.6	0.4
P470 lo 60 min	25.8	0.8	47.5	1.5
P470 lo 90 min	29.3	0.6	54.0	1.0
P470 po 30	19.6	0.6	36.2	1.0
P1200 ho	330.3	25.9	100.0	7.8
P1200 lo 30 min	352.6	9.2	106.8	2.8
P1200 lo 60 min	406.2	27.4	123.0	8.3
P1200 lo 90 min	531.3	16.4	160.9	5.0
P1200 po 30 min	545.1	35.4	165.0	10.7
P16S ho	1502.3	167.6	100.0	11.2
P16S lo 30 min	1496.8	143.2	99.6	9.5
P16S lo 60 min	1248.8	70.9	83.1	4.7
P16S lo 90 min	1296.3	63.1	86.3	4.2
P16S po 30 min	1818.8	185.3	121.1	12.3

3.2.4 Co-transcription

The promoter studies revealed no distinct promoter activity in a region up to 470 nt upstream of PcrX (3.2.3). Another source for PcrX expression could be co-transcription with the polycistronic *puf* mRNA and subsequent processing from this mRNA. To verify this hypothesis, cDNA was synthesised (cDNA step) from total RNA of *R. sphaeroides* wild-type grown under phototrophic conditions and tested for the presence of an mRNA carrying both sequences together (PCR step).

This was done in an RT-PCR reaction as described in 2.4.3.3 with the primer pair RT_pufX_fw / RT_spufX_rev (Tab. 3), the former complementary to the *pufX* sequence and the latter to the PcrX sequence. This primer pair is only able to amplify a product from the newly synthesised cDNA when an mRNA containing both *pufX* and PcrX is present as template for the cDNA synthesis (Fig. 63). The RT-PCR reaction gave a PCR product with the same size as a standard PCR (2.4.3.1) using the primer pair on chromosomal DNA from *R. sphaeroides* as the template (Fig. 63). As a control, H_2O was used as template in both PCR reactions and gave no PCR product (Fig. 63). Moreover, to exclude amplification from the input RNA instead of the newly synthesised cDNA, the input RNA was also used as a template. The input RNA control gave no product with the primer pair RT_pufX_fw / RT_spufX_rev when used in the standard PCR (Fig. 63). These results gave first evidence for co-transcription of PcrX with the *puf* mRNA.

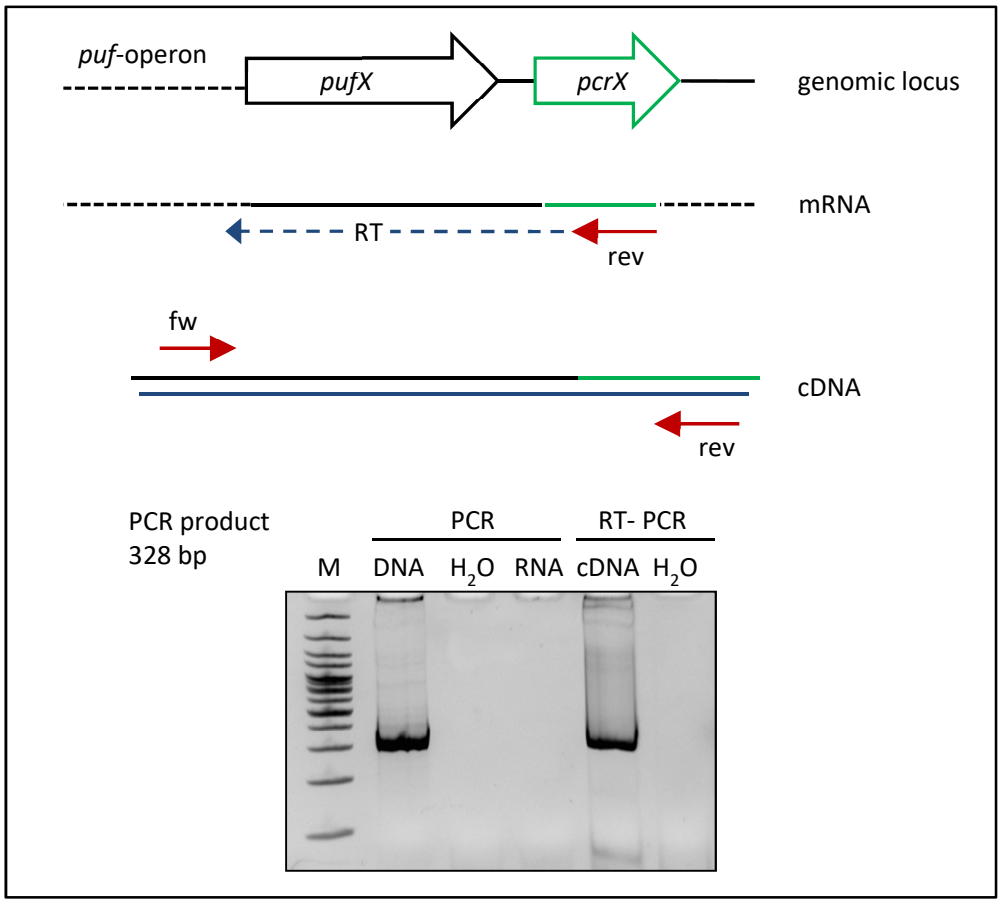

Figure 63: Testing for co-transcription of PcrX with the *pufX* mRNA. Schematic overview of the cDNA and PCR step: if an mRNA comprising *pufX* and PcrX exists, a PCR product can be generated from the respective cDNA. Gel below: In a standard PCR, the sequence containing *pufX* and PcrX plus the intergenic region was amplified with the primer pair RT_pufX_fw / RT_spufX_rev (fw / rev) using chromosomal DNA as template. As negative controls, H_2O and the input RNA used for the RT-PCR were chosen for the standard PCR. The RT-PCR reaction - with cDNA as the nascent template and H_2O as control – was loaded on the same 10% PAA gel as the standard PCR.

The above-presented findings were supported later when tentatively hybridising a Northern blot membrane, produced by blotting of an agarose gel (2.4.6.2) to detect the *puf* mRNA, with the PcrX specific probe (Tab. 3). On this Northern blot membrane, RNA samples from the PcrX over-expression (pPcrX) and the corresponding EVC (pBBR16S) cultivated under aerobic, microaerobic and phototrophic growth conditions (2.2.1.1 – 2.2.1.3) were investigated.

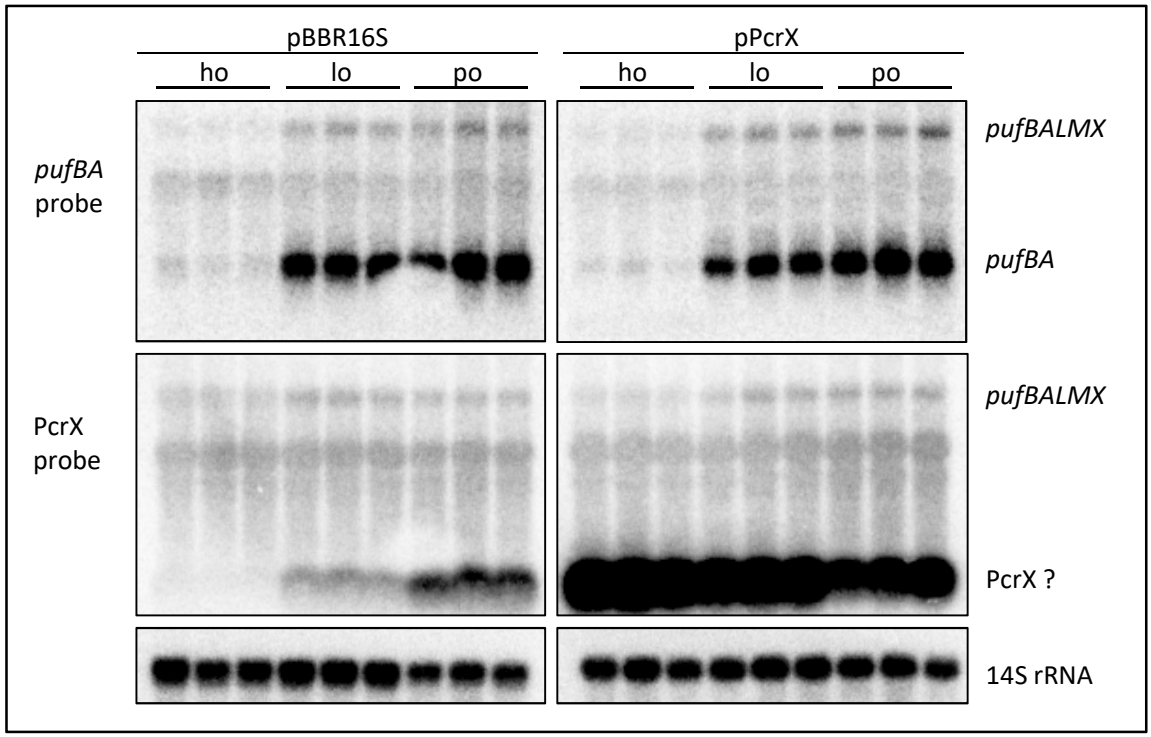

Figure 64: *Puf* mRNA detection with the PcrX probe on an agarose gel based Northern blot. Samples from the designated strains (biological triplicates) were withdrawn during the exponential growth phase from the indicated growth conditions. The pBBR16S samples were loaded on the upper gel part (left) and the pPcrX samples on the lower (right). Hybrdisation was carried out with the *pufBA* (upper panel), the PcrX (middle panel), and the 14S rRNA (lower panel) probes.

When comparing the signals obtained by hybridising the membrane subsequently with the *puf* and PcrX probes (Tab. 3) it became evident that the PcrX probe binds the *pufBALMX* mRNA fragment which is also detectable with the *puf* probe (Fig. 64), indicating that PcrX is present as a part of the polycistronic *puf* transcript. The described detection could be obtained again later on with various Northern blot membranes confirming that PcrX is co-transcribed together with the *puf* mRNA.

3.2.5 Processing from the parental *puf* mRNA

The hypothesis of PcrX being co-transcribed with the *pufX* mRNA could be supported by the results of the RT-PCR experiment and Northern blots as described in 3.2.4. Assuming co-transcription and with the distinct and stable PcrX signal on Northern blot (Fig. 59 and 61), the question arises which RNase might be responsible for the processing of PcrX from the polycistronic *puf* mRNA. To test potential candidates, several Northern blot experiments were carried out.

Therefor RNA was isolated using the hot phenol method (2.4.1.3a) from *R. sphaeroides* wild-type samples and samples that were taken from the knockout mutants indicated in figure 65 and described in more detail in table 1. The samples for the first tests were taken from cultures grown

under aerobic conditions to exponential phase and again after theses cultures were shifted to micro-aerobic conditions for 30 min (2.2.1.8). This shift is known to induce PcrX expression (Fig. 59), which was now compared between the tested mutants and the wild-type. Taken together the Northern blots performed did show an induction of PcrX upon the drop of oxygen tension in the tested mutants lacking RNaseR, RNaseJ, RNaseIII, RNaseJ and III in combination, RppH or YbeY (Fig. 65).

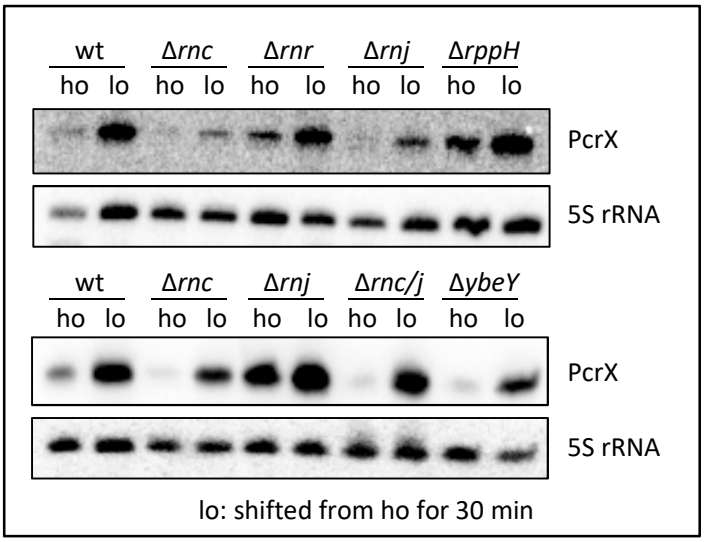

Figure 65: Northern blot analysis of PcrX induction in various RNase knockout mutants. PcrX induction was achieved by shifting the cultures from aerobic (ho) to microaerobic (lo) conditions for 30 min. RNA was isolated from samples taken at the indicated time points from the designated strains. Besides PcrX, the 5S rRNA was probed as loading control.

In addition to the described knockout mutants, an *R. sphaeroides* mutant strain harbouring a thermosensitive RNase E variant from *E. coli* (RNE^{therm}; obtained by Lennart Weber) instead of the endogenous RNase E was analysed regarding its PcrX RNA level. When shifting this strain to 42°C the mutated RNase E loses its activity. For the first attempt, samples from the wild-type and the RNase E mutant grown microaerobically were taken before and after 15 min of temperature shift (32°C to 42°C; performed by Carina Reuscher), RNA was isolated and used for Northern blot analysis (2.4.1.3a and 2.4.6.1). Hybridisation with the PcrX and 5S rRNA probe revealed unchanged levels of PcrX before and after the temperature shift in each of the two strains, while the RNase mutant (RNE^{therm}) exhibited an overall lower level of PcrX (Fig. 66).

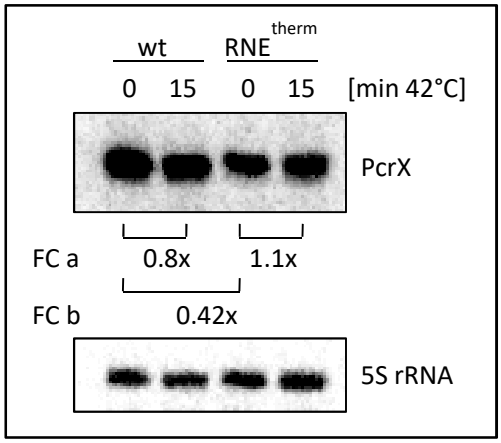

Figure 66: PcrX levels in microaerobically grown wild-type (wt) and RNase E mutant (RNE^{therm}). Both strains were shifted to 42°C for 15 min, which heat inactivates the RNase E in the mutant strain. RNA levels were analysed using the Northern blot technique (PAA-urea gel) and compared before and after the temperature shift in each strain (FC a). An additional comparison was drawn between the signals from the wild-type and mutant strain before the shift (FC b).

A half-life analysis of PcrX (3.2.2) has revealed a very long half-life of around 290 min for the PcrX under microaerobic conditions (Fig. 61). So the unchanged levels of PcrX in the first RNase E experiment (Fig. 66) might only imply that none of the already present PcrX was degraded after the shift and not that the further processing ("new synthesis") was abolished. To clarify this point, a second attempt was undertaken comparing the RNA levels in the wild-type and RNase E mutant. In this set-up both strains were cultivated under aerobic (ho) conditions to exponential phase, a sample was taken, and the cultures were shifted to microaerobic (lo) growth and 42°C at once. Samples from the shifted cultures were taken after 30, 60 and 90 min. RNA was isolated from all samples using the hot phenol method (2.4.3.1 a) and was applied for a Northern blot analysis (2.4.6.1). As a control, RNA samples isolated from cultures shifted from ho to lo conditions at 32°C were chosen. After hybridisation with the PcrX probe, signals could be detected in the 32°C samples only (upper panel Fig. 67). Since the phospho-imager will adjust all signals to the strongest signal, only the membrane part on which the 42°C RNA samples were blotted was exposed on the imaging screen again (Fig. 67). Now also for the 42°C samples a PcrX hybridisation signal could be detected. Contrary to the expectation, also in the samples from the heat sensitive RNase E mutant shifted to microaerobic and 42°C conditions a PcrX signal was detected (Fig. 67).

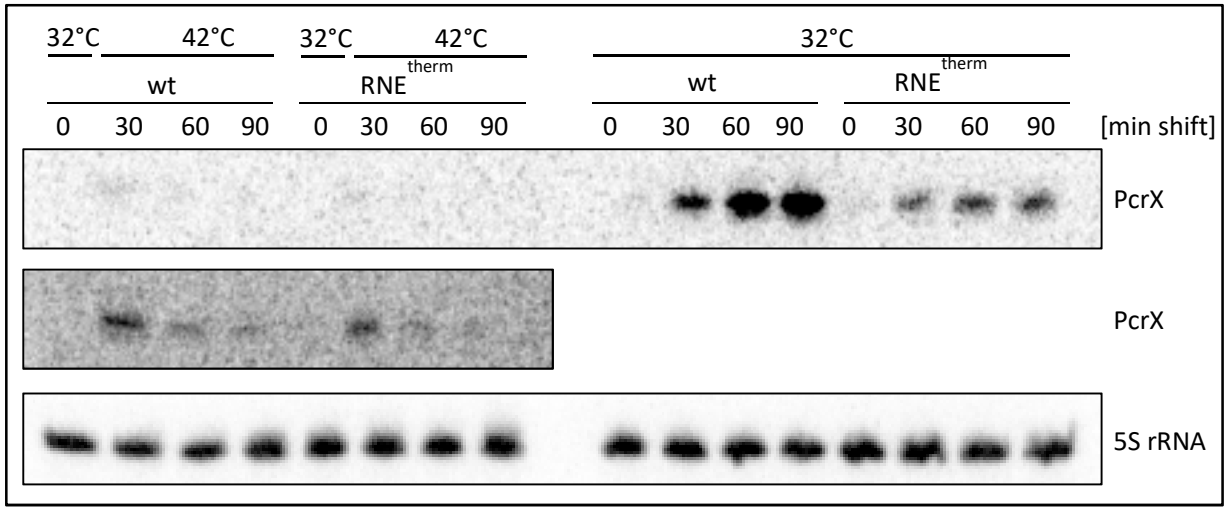

Figure 67: PcrX induction during simultaneous temperature and oxygen shift (left) in the *R. sphaeroides* wild-type (wt) and RNase E mutant strain (RNE^{therm}). Sample time points [min shift] after shifting to 42°C and microaerobic growth (left) or only to microaerobic growth (right) are indicated. The RNA was analysed on a PAA-urea gel based Northen blot. To improve the signal intensity of the samples from the temperature-shifted cultures, the membrane was only partially exposed on the imaging screen (middle panel).

Taken together these results so far indicate PcrX to be processed from the polycistronic *puf* mRNA independent of RNaseR, RNaseJ, RNaseIII, RppH, YbeY, and RNaseE.

3.2.6 Effects of PcrX over-expression

A full deletion of PcrX from the chromosome would also delete the terminator of the *puf* operon (Fig. 60) and thereby most likely influence the *puf* expression level. Hence, initially, a constitutive over-expression of PcrX was constructed to further analyse the sRNA's function. The PcrX sequence was amplified using the primer pair Pas1-for-Bam / Pas1-rev-Xba and sub-cloned into the pDrive cloning vector (Qiagen) resulting in pD_PcrX. After restriction with BamHI and XbaI, the PcrX fragment was ligated into the corresponding restriction sites of the pBBR1-MCS2_4352 under the control of the 16S rRNA promoter (promoter of RSP_4352, 16S). The resulting plasmid pPcrX expresses constitutive high levels of PcrX under all tested growth conditions (tested via Northern blot; Fig. 68). Intriguingly, while showing similar levels of over-expression upon aerobic (ho) and microaerobic growth (lo), the PcrX over-expression was found to be less pronounced during phototrophic growth (Fig. 68).

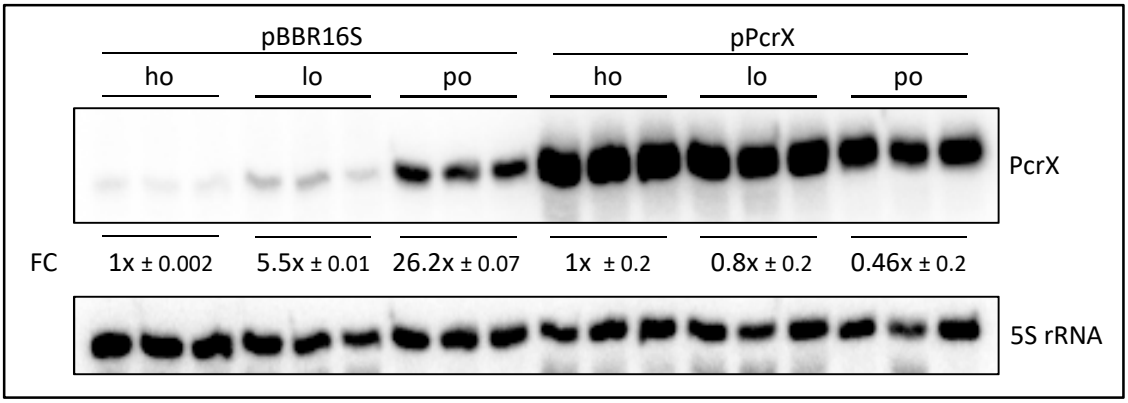

Figure 68: Verification of the plasmid-borne PcrX over-expression via Northern blot analysis. The PcrX over-expression strain (pPcrX), as well as the corresponding EVC (pBBR16S), were cultivated in biological triplicates under the three indicated growth conditions (ho, lo, and po). The relative expression levels in each strain (depicted as fold change – FC with SEM) were calculated as the mean of the biological triplicates relative to the level during aerobic growth (set to 1x). The 5S rRNA was probed as a loading control.

When cultivating the PcrX over-expression strain under microaerobic conditions its lighter pigmentation compared to the respective EVC strain (pBBR16S) became obvious (Fig. 69). To verify this observation, the bacteriochlorophyll (BChl) content was measured (2.2.10), the LHCs were quantified (2.2.10 a), and the full-cell spectra were recorded (2.2.9) comparing both strains (Fig. 70). The measurements were performed using biological triplicates of exponentially grown cultures from different growth conditions, which are described in more detail in 2.2.1.1 – 2.2.1.3 for the BChl measurement and full cell spectra and in 2.2.1.4 for the LHC quantification.

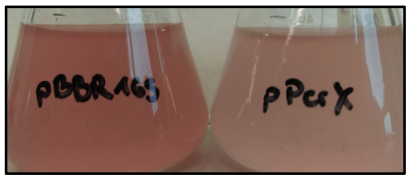

Figure 69: Photograph of the PcrX over-expression strain (pPcrX) and the corresponding EVC (pBBR16S). The strains were grown to an OD_{660} of 0.8 under microaerobic conditions.

The BChl measurement revealed reduced amounts in the PcrX over-expression strain (pPcrX) compared to the EVC (pBBR16S) under all three tested growth conditions (Fig. 70 A). Furthermore, LHC I and LHC II amount was found to be negatively affected by the PcrX over-expression (Fig. 70 B). Also, the full-cell spectra taken from the microaerobically grown cultures (exponential phase) were overall lower in the pPcrX strain (Fig. 70 C). All three results confirm the observed lighter pigmentation of the PcrX over-expression strain and further support the theory of PcrX's function in the photosynthesis gene regulation.

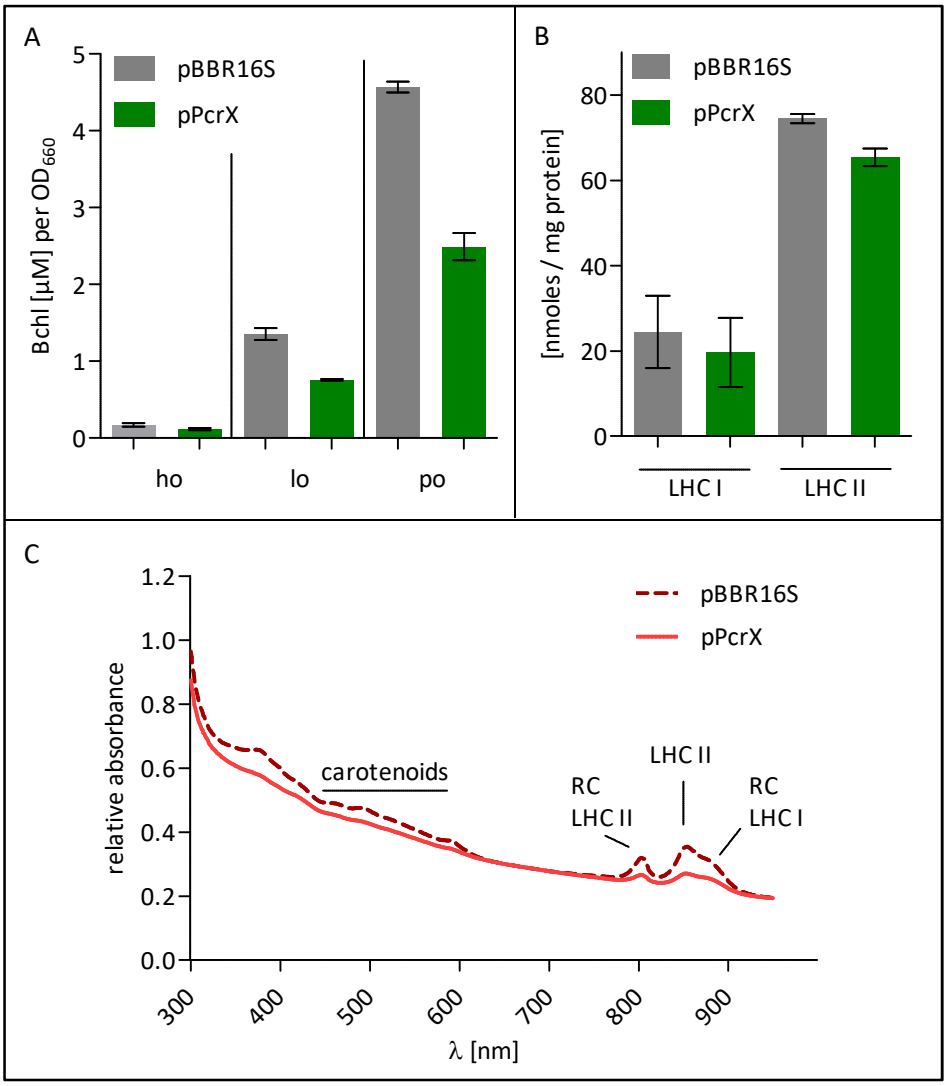

Figure 70: Bacteriochlorophyll (BChl) content, LHC I and II amount and full cell spectra of the PcrX over-expression strain (pPcrX) and the corresponding EVC (pBBR16S). A: The BChl content (µM/OD_{660}) is represented as mean from biological triplicates with the standard deviation. Samples were withdrawn during exponential growth under the indicated growth conditions. B: Triplicates of the PcrX over-expression (pPcrX) and the corresponding EVC (pBBR16S) were grown anaerobically to quantify the LHC I and II amount. The results are depicted as mean of three biological replicates in nmoles / mg protein with standard deviation.
C: The full cell spectra are shown as mean of three biological replicates per strain, grown to the exponential phase under microaerobic conditions. Region and peaks of photosynthetic components' absorbance maxima are labelled within the graph.

To test whether the overall lighter pigmentation of the PcrX over-expression affects the growth of the cells and their ability to adapt to photosynthetic conditions, a growth analysis (2.2.2) was carried out. Therefor biological triplicates of the PcrX over-expression (pPcrX) and the corresponding EVC (pBBR16S) were cultivated under microaerobic (lo) conditions to the late exponential phase (OD_{600} ~ 0.7) and diluted to an OD_{660} of 0.1 in bottles used for phototrophic growth (2.2.1.3). During the incubation under phototrophic conditions, the OD_{660} was measured every 3 h for 12 h and afterwards after 24, 27, 30, 33, 48, 51, and 54 h (Fig. 71 A).

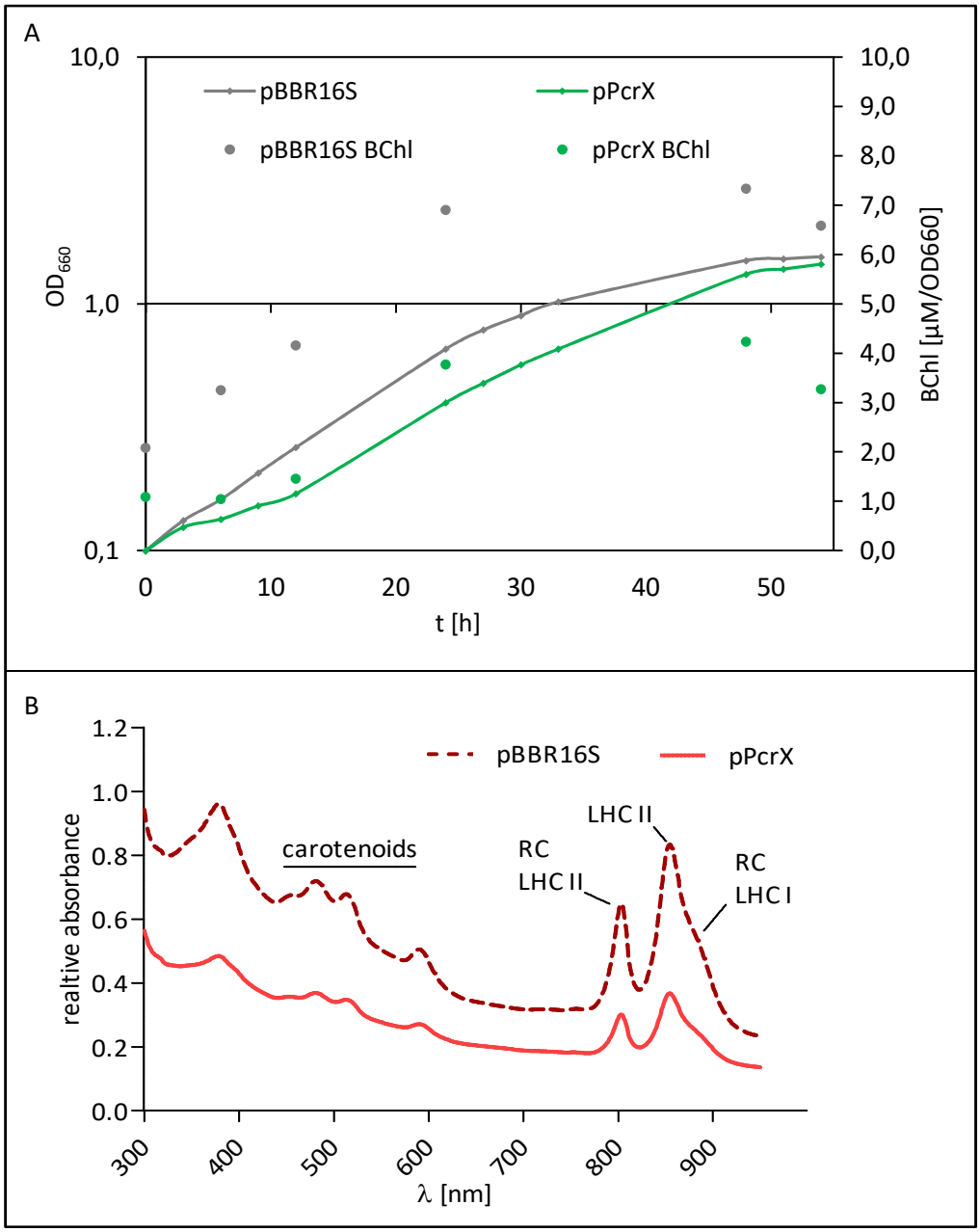

Figure 71: Growth, BChl content, and full cell spectrum of the PcrX over-expression strain (pPcrX) upon phototrophic conditions, compared to the corresponding EVC (pBBR16S). A: Biological triplicates of each strain were grown microaerobically to an OD_{660} of ~0.7 before diluting to 0.1, shifting to phototrophic growth and monitoring the growth. The OD_{660} was plotted semi-logarithmically against the time. B: Samples for the BChl measurement were taken at the indicated time points. Full cell spectra of both strains were measured 24 h after the shift to phototrophic growth.

Simultaneously, samples for a BChl measurement (2.2.10) were withdrawn at selected time points (indicated in Fig. 71 A). To complete the picture, after 24 h of phototrophic growth full cell spectra (2.2.9) of the cultures were measured (Fig. 71 B). At the 24 h time point, the EVC (pBBR16S) and over-expression strain pPcrX reached an average OD_{660} of 0.66 and 0.4, respectively. Thus the spectra do not match at the absorbance at 660 nm, as they usually should. Overall the analyses revealed an impaired growth of the PcrX over-expression strain compared to the EVC, even though both strains reach a similar OD_{660} (~ 1.45) after 52 h. The reduced growth is accompanied by lower BChl levels and full-cell spectra in the over-expression strain (Fig. 71).

3.2.7 Target search

Further analyses were undertaken to elucidate how the over-expression of PcrX leads to the reduction of the BChl content, LHC amount and full-cell spectra (3.2.6) – in particular, potential targets of the PcrX sRNA were investigated and verified. The effect on pigment and photosynthesis complex level (Fig. 70 and 71) gave the first allusion to potential target genes. So genes from the *puf* operon (*pufB*, *pufBA* in combination, and *pufX*), as well as genes encoding proteins from the LHC I assembly (RSP_0290), and chlorophyllide reductase subunits (*bchN* and *bchY*) were tested for their mRNA expression level in the PcrX over-expression strain (pPcrX) and the respective EVC (pBBR16S). Additionally, a target prediction using the web tool IntaRNA (Wright *et al*., 2014; Busch *et al*., 2008) was carried out. The prediction revealed RSP_2376, encoding the 2-amino-3-ketobutyrate coenzyme a ligase (*kbl*) and RSP_1945, encoding a transcriptional regulator (*AscN* family), as potential PcrX targets that were tested in addition.

The expression level of the described genes was analysed using RT-PCR (2.4.3.3) with primer pairs listed in table 3. The housekeeping gene *rpoZ* was used as reference gene. Again samples from cultures grown under three growth conditions (ho, lo and po) were chosen for RNA preparation and subsequent RT-PCR. The results showed no clear difference (threshold set $\log_2$ ratio > 1 and < -1) in mRNA expression levels under the tested conditions for the genes *pufB*, *pufBA*, RSP_0290, RSP_1945, and RSP_2376 between the EVC and PcrX over-expression strain (Fig. 72). Both chlorophyllide reductase subunit mRNAs, *bchN* and *bchY*, showed an increase in the PcrX over-expression under aerobic (ho) conditions, while only the level of *bchY* was decreased under microaerobic (lo) and phototrophic (po) growth conditions (Fig. 72). The most strongly affected mRNA found in the RT-PCR analysis is *pufX*. *PufX* appeared to be up-regulated upon aerobic (ho; $\log_2$ FC 3.3) and phototrophic growth (po; $\log_2$ FC 3.4), while being strongly down-regulated under microaerobic conditions (lo; $\log_2$ FC -4.3) in the PcrX over-expression (Fig. 72).

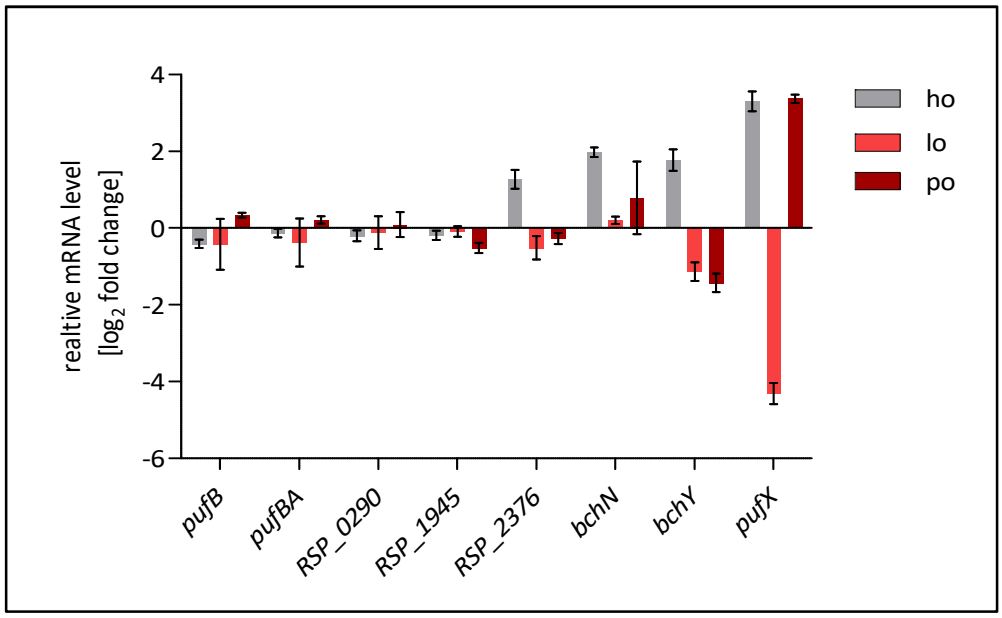

Figure 72: RT-PCR analysis comparing the mRNA levels in the PcrX over-expression strain (pPcrX) to the corresponding EVC (pBBR16S) under three different growth conditions. The genes *pufB*, *pufBA*, RSP_0290, RSP_1945, RSP_2376, *bchN*, *bchY*, and *pufX* were tested upon aerobic (ho, grey), microaerobic (lo, light red), and phototrophic (po, red) growth. The relative mRNA levels are depicted as log_2 fold change ratios (mean and SEM from biological triplicates and technical duplicates).

3.2.8 *PufX* as target

3.2.8.1 *LacZ*-based *in vivo* reporter

The RT-PCR carried out during the target search (3.2.7) identified *pufX* as potential PcrX target (Fig. 72). To elucidate whether PcrX and *pufX* directly interact, a *lacZ*-based *in vivo* reporter system was utilized. A similar strategy as described for the potential Pos19 targets (3.1.7) was pursued: a *pufX* fragment containing 12 bp upstream of the start codon and all subsequent codons (82), except the stop codon, was amplified using the primer pair pufX_fw_Xho / pufX_rev_Hind (Tab. 3). After sub-cloning into the pDrive cloning vector (pD_pufX; Qiagen) and digestion with XhoI and HindIII, the *pufX* fragment was ligated into the corresponding restriction sites of the reporter plasmid pPHU4352 (based on pPHU235) (Hübner *et al.*, 1991). The resulting reporter plasmid pPHU_pufX harbours a translational fusion of *pufX* to the *lacZ* gene under the control of the 16S rRNA promoter. Both, the pPHU_pufX and the insertless pPHU4352 (pPHU16S), were conjugated to the PcrX over-expression strain (pPcrX) and the corresponding EVC strain (pBBR16S). Samples for a ß-galactosidase activity assay (2.2.15) were withdrawn from biological triplicates of the four strains, grown under the three indicated growth conditions (2.2.1.1 – 2.2.1.3, Fig. 73). The resulting Miller Units revealed that the PcrX over-expression leads to repression of the *pufX-lacZ* translation under all three tested

conditions (Fig. 73). Testing the regulation of the *pufX-lacZ* fusion under phototrophic conditions in the hfq knockout mutant (Δ*hfq*) revealed that the regulation via PcrX is Hfq-independent (Fig. 73).

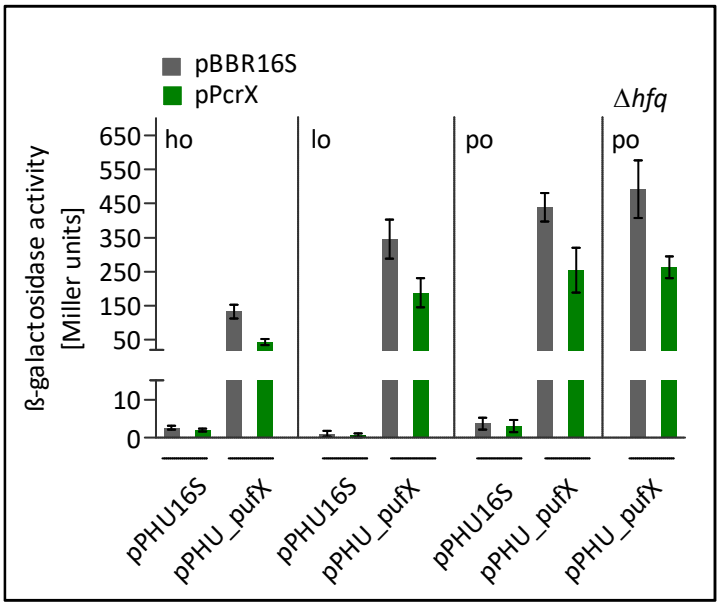

Figure 73: ß-galactosidase activity assay for the *pufX-lacZ* reporter. The *pufX-lacZ* reporter plasmid (pPHU_pufX) as well as the control plasmid (pPHU_16S) were transferred to the PcrX over-expression strain (pPcrX) and the EVC (pBBR16S) via conjugation. Samples from biological triplicates of each strain were taken from exponentially grown cultures upon the indicated growth conditions (ho, lo, and po). Additionally the *pufX-lacZ* reporter plasmid was transferred to the *hfq* knockout mutant (Δ*hfq*) together with either the EVC or the pPcrX over-expression plasmid to test for Hfq-dependency of the regulation entailed by PcrX. The ß-galactosidase activity is depicted in Miller Units with SEM.

To further prove the direct interaction of PcrX and the *pufX* mRNA, the *pufX* reporter plasmid as well as the PcrX over-expression plasmids were mutated. For these mutations, the potential binding site (seed region, Fig. 74) of the two RNAs was predicted using the IntaRNA webtool (Wright *et al.*, 2014; Busch *et al.*, 2008). According to this prediction three nucleotides in the *pufX* sequence were mutated (M3; Fig. 74).

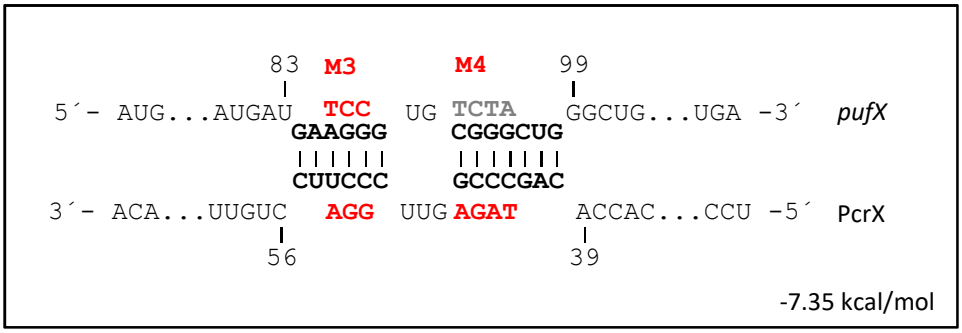

Figure 74: Predicted interaction site of PcrX and the *pufX* mRNA. Numbers refer to the start codon of *pufX* (AUG) and PcrX's 5' end. Mutations used for the *lacZ*-based *in vivo* reporter assays (M3 and M4) are indicated in red. The interaction and free hybridisation energy (Lower right) is depicted as predicted with IntaRNA webtool (Wright *et al.*, 2014; Busch *et al.*, 2008).

This was achieved by using the primer pair pufX_fw_M3 / pufX_rev_M3 (Tab. 3) with the pD_pufX as the template in a site-directed mutagenesis PCR (2.4.3.2). After confirming the mutations via sequencing, the mutated fragment was ligated to pPHU4352 after digestion with XhoI and HindIII. The mutated reporter plasmid pPHU_*pufX*M3 was conjugated to the PcrX over-expression strain as well as the corresponding EVC (pBBR16S). A ß-galactosidase activity assay was carried out with

samples from the resulting strains cultivated under microaerobic conditions (2.2.1.2). The assay revealed that the PcrX over-expression negatively affects the translation of *pufX*M3-*lacZ* fusion as strongly as translation from the un-mutated *pufX-lacZ* fusion (Fig. 75). Surprisingly, the mutated *pufX*M3-*lacZ* fusion exhibited a stronger activity than the *pufX-lacZ* fusion in general (Fig. 75).

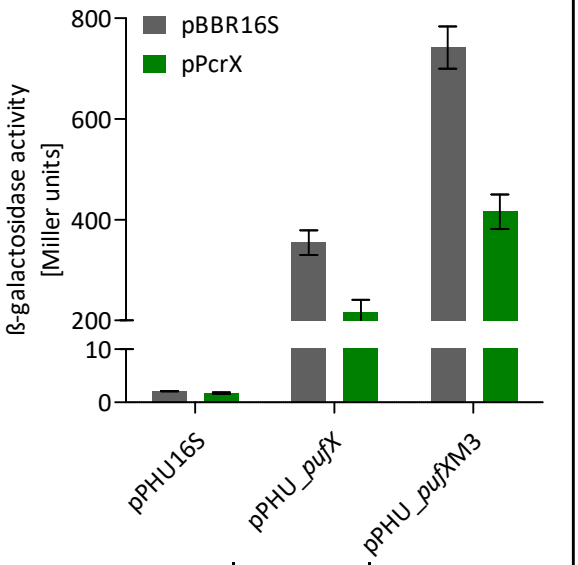

[%]	pBBR16S	pPcrX
pPHU_*pufX*	100 ± 7	60.7 ± 12
pPHU_*pufX*M3	100 ± 6	56.0 ± 8

Figure 75: ß-galactosidase activity assay additionally using the mutated *pufX*M3-*lacZ* reporter. The reporter plasmids (pPHU_pufX and pPHU_pufXM3), as well as the control plasmid (pPHU_16S), were transferred to the PcrX over-expression strain (pPcrX) and the EVC (pBBR16S) via conjugation. Samples from biological triplicates of each strain were taken from exponentially grown cultures during microaerobic conditions. The ß-galactosidase activity is depicted in Miller Units as mean with SEM, and additionally in percent with relative error (±) below the graph.

Since over-expressing the un-mutated PcrX was sufficient to regulate the *pufXM3-lacZ* fusion, the vice versa set-up using the PcrXM3 over-expression variant was not further tested. Instead, as a second attempt, four different nucleotides in the PcrX sequence were exchanged (M4; Fig. 74) and the mutated PcrX-M4 sequence was used for over-expression. The mutations were introduced with the primer pair spufX_fw_M4 / spufX_rev_M4 using the pD_spufX as the template in a site-directed mutagenesis PCR (2.4.3.2). After restriction with BamHI and XbaI, the PcrX fragment was ligated into the corresponding restriction sites of the pBBR1-MCS2_4352 under the control of the 16S rRNA promoter for over-expression. The PcrXM4 sRNA level was compared to the level in the EVC (pBBR16S) and the original over-expression (pPcrX) on a Northern blot (Fig. 76). It became obvious that the mutated PcrXM4 variant could not be over-expressed to a level comparable to the original over-expression (1.9-fold compared to 14.2-fold; Fig. 76). Therefore the mutated PcrXM4 variant was not used for further analyses.

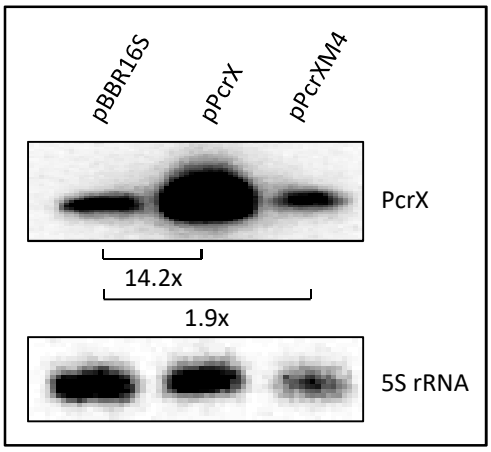

Figure 76: Northern blot analysis to test for the over-expression potential from the mutated pPcrXM4 plasmid. The three indicated strains were cultivated under microaerobic conditions to the exponential phase, before harvesting cells for RNA isolation. The expression level of PcrX in the over-expression strains (pPcrX and pPcrXM4) is depicted as fold change relative to the expression level in the EVC (pBBR16S).

3.2.8.2 *PufX* as a target - EMSA

Since mutations in the seed region of *pufX* and PcrX were so far not sufficient to verify direct interaction of the two RNAs using the *lacZ*-based reporter system (3.2.8.1), an electrophoretic mobility shift assay (EMSA; 2.4.13) was performed.

For the EMSA, a radio-labelled (hot) PcrX *in vitro* transcript (PcrX*) and a non-labelled (cold) *pufX in vitro* transcript were prepared. The PcrX sequence was amplified adding a T7 promoter by using the primer pair T7spufX_fw / T7spufX-rev (Tab. 3). The PCR product was applied as a template for hot *in vitro* transcription (2.4.7.3) resulting in PcrX*. A 134 nt fragment of the *pufX* sequence, containing the predicted PcrX binding site (Fig. 74), was amplified adding a T7 promoter using the primer pair T7pufX_fw / T7pufX_rev (Tab. 3). The T7pufX PCR product was used as the template for cold *in vitro* transcription (2.4.5). The resulting *pufX* transcript was controlled for purity on a PAA-urea gel (2.4.6.1). In each EMSA experiment, 150 fmol PcrX* was applied per sample, while the amount of cold *pufX* transcript was varied. For the first EMSA 150 fmol PcrX* was de- and re-natured together with 15000 fmol *pufX* transcript as a positive control, while 150 fmol PcrX* alone was used as negative control. For the investigation of the potential interaction, the *pufX* transcript was added to the re-natured PcrX* in increasing amounts (150 – 15000 fmol). The cold control transcript T70557 (3.1.9) was added in a 100-fold excess to the re-natured PcrX*. The first EMSA gel-run was carried out at 4°C, using 0.25x TB containing $MgCl_2$ in a final concentration of 10 mM, and a final concentration of 0.75x structure buffer in each sample (2.4.13). After drying the gel, it was exposed on an imaging screen overnight and imaged using the phospho-imager (2.4.10). The EMSA shows an increasing shift of PcrX* with increasing amounts of the *pufX* transcript (Fig. 77). The shifted PcrX*-*pufX* complex ran on the same height as the complex of the positive control. The addition of the unspecific T70557 transcript did not lead to a shift of PcrX* in the gel (Fig. 77).

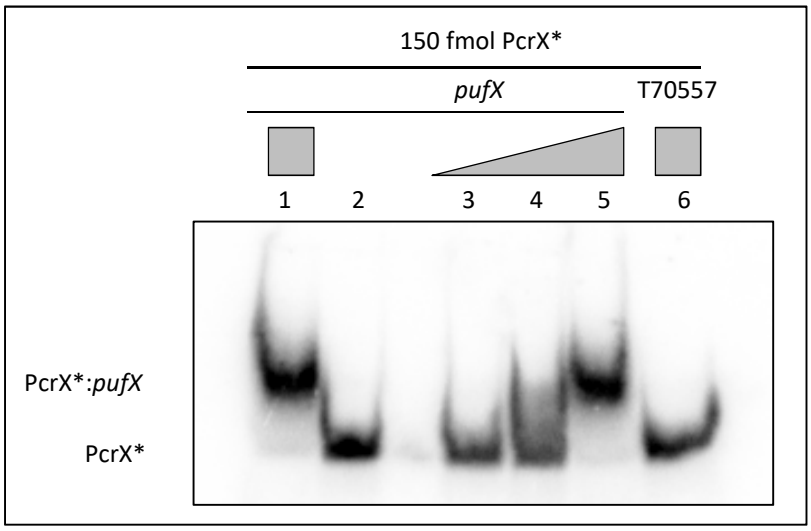

Figure 77: Testing the interaction between PcrX and *pufX* using an EMSA. The radio-labelled PcrX* *in vitro* transcript was de- and re-natured together with a 100-fold excess of cold *pufX* transcript (1), loaded alone (2), and was incubated with increasing amounts (150 – 15000 fmol) of cold *pufX* transcript (3-5) after the renaturing step. As a negative control, PcrX* was incubated with a 100-fold excess of cold T70557 transcript (6).

In a second EMSA, the interaction of PcrX* with *pufX* (150:15000 fmol) was competed by addition of un-labelled PcrX transcript (2.4.5) in a 10- and 100-fold excess over PcrX*. By adding cold PcrX transcript the interaction between the hot PcrX* and the *pufX* transcript was reduced (Fig. 78), since the cold PcrX can also bind to the *pufX* transcript. Again the T70557 transcript (3.1.9) was used as a negative control.

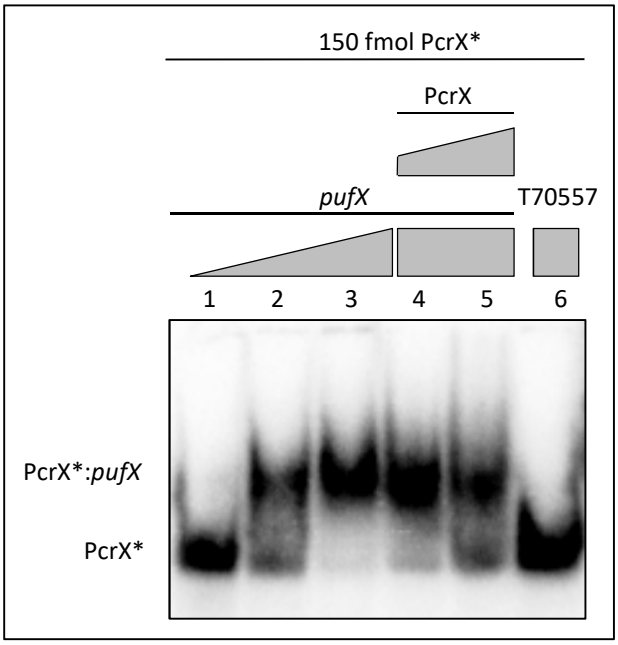

Figure 78: Competing the PcrX*:*pufX* interaction by adding cold PcrX *in vitro* transcript. Radio-labelled PcrX* transcript was incubated with increasing amounts (150 – 15000 fmol) of cold *pufX* transcript (1-3). 10- or 100-fold excess of cold PcrX transcript over radio-labelled PcrX* transcript were added to reactions containing PcrX*:*pufX* (150:15000 fmol) (4 and 5). 15000 fmol of T70557 transcript incubated with 150 fmol of PcrX* was used as the negative control (6).

As attempted for the *in vivo* reporter system (3.2.8.2), to validate the interaction of the RNAs at the predicted binding site (Fig. 79) four bases were exchanged (mut) in both RNAs. Since the mutations used for the *in vivo* reporter system did not give the desired results, new mutations shown in figure 79 were chosen. To produce the mutated *in vitro* transcripts, the T7spufX and T7pufX PCR products already used for the *in vitro* transcription (see above), were sub-cloned to the pDrive cloning vector

(TA-cloning; Qiagen) resulting in pD_T7spufX and pD_T7pufX. These plasmids could be used as templates in a site-directed mutagenesis PCR (2.4.3.2) with the primer pairs T7sM4_fw / T7sM4_rev and T7XM4_fw / T/XM4_rev, respectively. After confirming the mutations on the plasmids pD_T7spufXmut and pD_T7pufXmut by sequencing, they could be used to amplify the templates for hot and cold *in vitro* transcription using the primer pairs T7spufX_fw / T7spufX-rev and T7pufX_fw / T7pufX_rev described above.

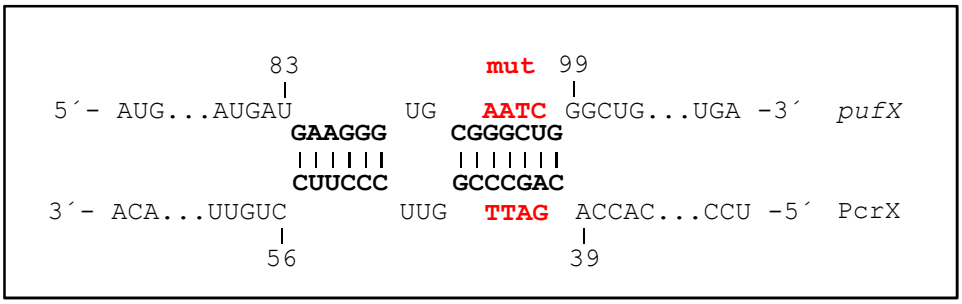

Figure 79: Predicted interaction site of PcrX and the *pufX* mRNA. Numbers refer to the start codon of *pufX* (AUG) and PcrX's 5' end. The mutations (mut) used for the *in vitro* transcripts for the EMSA are indicated in red. The interaction is depicted as predicted with IntaRNA webtool (Wright *et al*., 2014; Busch *et al*., 2008).

Using these amplificates for *in vitro* transcription resulted in the mutated *in vitro* transcripts PcrX-mut* and *pufX*-mut. Those were utilized for additional EMSA set-ups: first, the already shown competition of the PcrX*-*pufX* transcript interaction with cold PcrX was additionally performed with cold PcrX-mut. The PcrX-mut transcript was expected not to impede the interaction because of lowered complementarity to the *pufX* transcript. Unfortunately, also the mutated PcrX-mut transcript was sufficient to abolish the PcrX*:*pufX* interaction (Fig. 80).

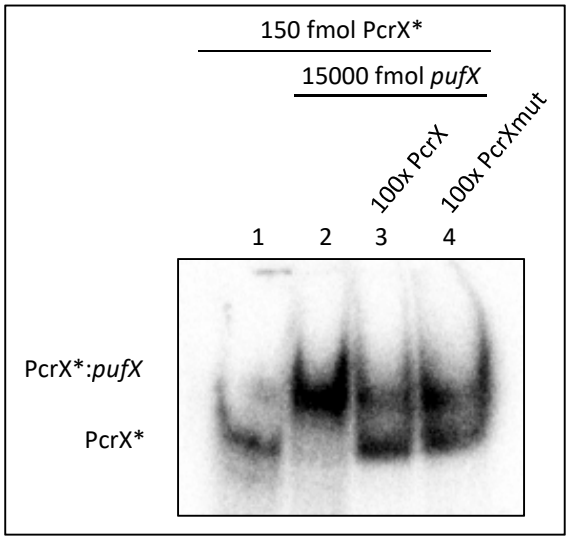

Figure 80: The cold *in vitro* transcript PcrXmut impairs the interaction between PcrX* and the *pufX* transcript. The radio-labelled PcrX* transcript was loaded alone (1) and after incubation with a 100-fold excess of cold *pufX* transcript (2 – 4). Additionally, a 100-fold excess of cold, un-mutated (3) or mutated (4) PcrX transcript was added to the reaction to compete with PcrX* for the interaction with *pufX*.

The additional set-up was used to compare the interaction of the PcrX* with the *pufX* transcript to the interaction of PcrX* with the *pufX*-mut transcript. This revealed that PcrX* interacts with the

mutated *pufX*-mut transcript as it does with the un-mutated *pufX* transcript. Meaning that the mutations in the seed region were not sufficient to abolish the interaction between PcrX* and the *pufX*-mut transcript.

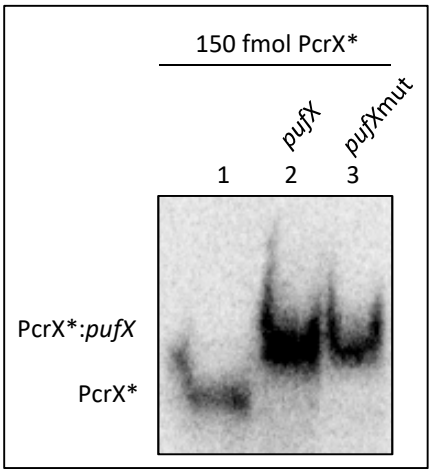

Figure 81: EMSA to test for interaction of the mutated *pufX* transcript with PcrX*. PcrX* (150 fmol) was loaded alone (1) and after incubation with a 100-fold excess of cold *pufX* transcript (2) and cold *pufX*-mut transcript (3).

3.2.9 Abundance of the *puf* mRNA

The *puf* mRNA, as well as other mRNAs encoding photosynthesis components, show their highest expression upon phototrophic growth while being less abundant and often not detectable under microaerobic and aerobic conditions, respectively. To test whether the interaction of PcrX with the *pufX* part of the *puf* mRNA (3.2.8) influences the expression level of the polycistronic *puf* mRNA, a Northern blot analysis was carried out.

To determine the *puf* mRNA levels, total RNA was isolated using the hot phenol method (2.4.1.3 a) and applied for agarose gel based Northern blot analysis (2.4.6.2). Samples for the RNA isolation were withdrawn from biological triplicates of the PcrX over-expression strain (pPcrX) and the corresponding EVC (pBBR16S) grown under two conditions, microaerobic (lo) and phototrophic (po) growth (2.2.1.1 – 2.2.1.2; performed by Daniel Scheller, Bachelorthesis). The *puf* mRNA was detected (2.4.9) using a hybridisation probe gained via random priming (2.4.7.2) that is directed against the *pufBA* part of the polycistronic mRNA, hence the *pufBALMX* as well as the *pufBA* fragment can be detected at the same time. As a loading control, the membrane is hybridised using a probe against the 14S rRNA (Tab. 3). The Northern blot analysis revealed that the over-expression of PcrX reduces the *puf* mRNA level compared to the EVC during both growth conditions (Fig. 82). This finding holds true for both detectable mRNA parts – *pufBALMX* and *pufBA*, being a little more pronounced for the longer *pufBALMX* fragment.

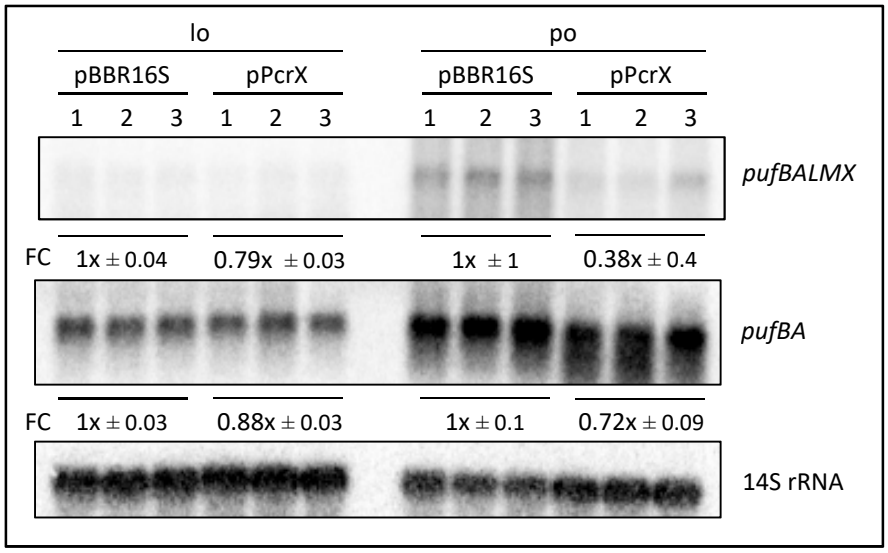

Figure 82: Abundance of the *puf* mRNA in the PcrX over-expression strain compared to the EVC strain. The *puf* mRNA level was tested using an agarose gel based Northern blot. Biological triplicates of the PcrX over-expression strain (pPcrX) and the corresponding EVC (pBBR16S) were grown under microaerobic (lo) and phototrophic (po) conditions to exponential phase before harvesting cells for the RNA isolation. The relative mRNA levels are depicted as average fold change of the triplicates with the standard error of the mean, comparing the level of the over-expression to the EVC seperatley for both conditions. Signals for *pufBALMX* and *pufBA* gained from the same scan are depicted in two separate panels since the *pufBALMX* signal intensity was too low and therefore adjusted digitally afterwards. The experiment was carried out by Daniel Scheller.

3.2.10 Half-life of the *puf* mRNA

Experiments to determine the half-life of the *puf* mRNA were carried out to further characterise the effect of PcrX on *pufX*, or potentially the whole *puf* mRNA.

The PcrX over-expression strain (pPcrX) and the corresponding EVC (pBBR16S) were cultivated under microaerobic conditions to the exponential phase (OD_{660} ~0.4) and rifampicin was added after taking a 0 min sample each. Continuing samples were taken 5, 10, 15, 20, and 30 min after the rifampicin addition. The RNA was isolated according to the hot phenol protocol (2.4.1.3 a) and an agarose gel based Northern blot (2.4.6.2) was conducted. After hybridisation (2.4.9) with the *pufBA* and the 14S rRNA specific probes (Tab. 3), the half-life of the *pufBALMX* and *pufBA* fragment was determined as described in 2.4.12 b. Altogether the half-life experiment was carried out three times (two times by Daniel Scheller, Bachelorthesis 2016). The average half-life of the *pufBALMX* mRNA was calculated as 21.5 min (± 2.9 min) in the EVC strain and 12.6 min (± 1.6 min) in the PcrX over-expression strain (Fig 83), which represents a significant difference in half-life between the two strains ($p = 0.027$; students T-test, one-tailed, unpaired). The half-life of the *pufBA* mRNA segment did not show a significant difference ($p = 0.26$) between the two strains, with calculated half-lives of 32.1 min (± 1 min) in the EVC and 30.4 min (± 2.1 min) in the PcrX over-expression strain (Fig. 83). One out of the three Northern blots is shown exemplary in figure 83.

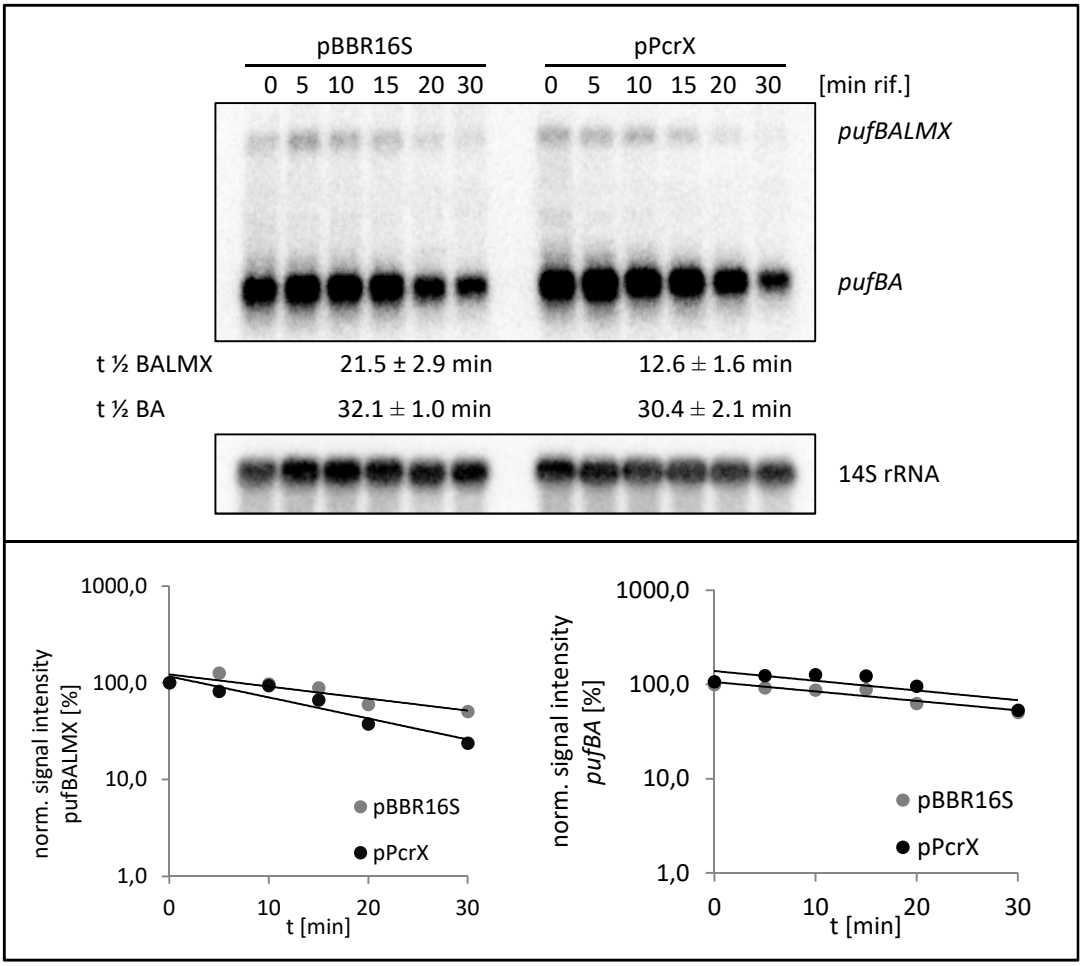

Figure 83: Half-life determination of the *puf* mRNA in the PcrX over-expression strain (pPcrX) and EVC (pBBR16S). Upper panel: The figure depicts an exemplary Northen blot (carried out by Daniel Scheller) from the *puf* half-life determination series. The two strains were grown under microaerobic conditions and cells for RNA isolation were harvested before (0 min) and at the indicated time points after rifampicin addition [min rif.]. The depicted half-lives (t ½) in min were calculated as the mean from three independent experiments and are shown with the the standard error of the mean, separate for the *pufBALMX* and *pufBA* fragments. Lower panel: The mRNA signal intenisties were normalized by 14S rRNA signals and plotted semi-logarithmically in percent against the time in minutes.

3.3 Additional characterisation of the sRNA RSs0827

3.3.1 Previous work on RSs0827

The sRNA RSs0827 had its first appearance when comparing RNA levels under microaerobic conditions and iron-limitation to those under microaerobic conditions (Peuser *et al*., 2012). In this study, RSs0827 was found to be strongly induced during iron starvation, a situation known to increase the intracellular ROS level (1.2). Therefore RSs0827 was predicted to act in the regulatory iron homeostasis and/or stress response network in *R. sphaeroides*. To test this hypothesis, the expression profile of RSs0827 was further characterised and potential mRNA target candidates were tested. Analysing the expression profile revealed that besides iron limitation, cadmium chloride, heat, and photo-oxidative stress induced the RSs0827 expression (Masterthesis J. Kiebel, 2013). Additionally, the potential connection between the transcriptional regulator IscR, by now described to function as a transcriptional repressor of genes involved in iron metabolism (Remes *et al*., 2015), and Rss0827 was tested in this work. It could be shown that RSs0827 is slightly (1.3-fold) induced in the IscR knockout mutant (Δ*iscR*) compared to the wild-type, while in IscR over-expression strain (pRK_*puf_iscR*) RSs0827 was reduced six-fold. Moreover, the plasmid-borne over-expression of RSs0827 expressed from its own promoter (pBBR_RSs0827) leads to a reduction of the *iscR* mRNA level with a log fold change of -1.5 (tested via RT-PCR). Physiological assays revealed that the RSs0827 over-expression (pBBR_RSs0827) results in a decreased intracellular ROS level accompanied by reduced pigmentation and increased growth under iron limitation, compared to the wild-type.

A second Masterthesis carried out regarding the RSs0827 project (M. Späth, 2014) could additionally show that the sRNA is induced during stationary phase, especially after 48 h. Moreover, an RSs0827 knockout mutant (ΔRSs0827) was now available (constructed by J. Kiebel) showing no difference in pigmentation and growth compared to the wild-type, but a slightly increased intracellular ROS level. A global transcriptome analysis (microarray) comparing the RNA levels in the RSs0827 mutant (ΔRSs0827) to the *R. sphaeroides* wild-type, revealed 76 genes to be down-regulated (log_2 ratio < -0.6) in the mutant strain. Besides 33 tRNA genes and 20 genes encoding hypothetical proteins, several IGRs (potential sRNAs) and fourteen already characterised genes were found amongst the down-regulated genes. Of those fourteen known genes, five were described with functions in iron metabolism (*feoA1*, *feoB*, a siderophore transporter, a probable ferredoxin, and a putative iron-regulated protein), two encode chaperones (*groEL* and *groES*), two code for ribosomal proteins (*rpl*R and *rplF*), and five belong to various metabolic systems (*ttuc*, *phbC*, *traI*, LysR protein, and enoyl-(acyl carrier protein) reductase) (Fig. 84 A). On the opposite, 17 genes were up-regulated (log_2 ratio > 0.6) in the RSs0827 mutant (ΔRSs0827), of which four are found in IGRs and three are hypothetical proteins. Moreover, of those up-regulated genes three belong to the fructose metabolism (*cfXA*, *cfxB*, and *fbpP*), two are included in the methionine metabolism (*cbbI* and

methionine synthase), and four are known from different metabolic pathways (*tklB*, a small heat shock protein, *fliC*, and acetolate-synthase III large subunit). Most interestingly, two genes encoding alternative sigma factors (*rpoE* and *rpoHII*) were found to be up-regulated in the RSs0827 knockout mutant (Fig. 84 B).

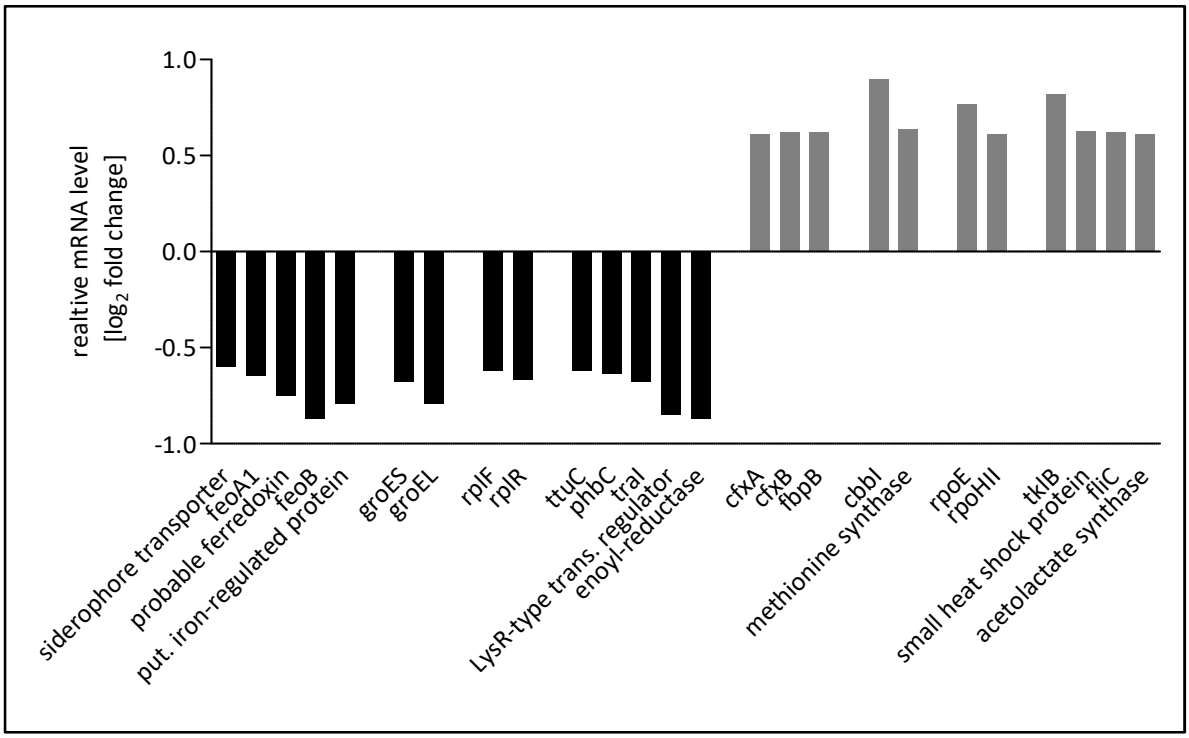

Figure 84: Selected genes down- or up-regulated in the RSs0827 knockout mutant (ΔRSs0827) compared to the *R. sphaeroides* wild-type. The relative expression levels calculated from the microarray experiment are depicted as $\log_2$ fold change. Black: Genes down-regulated in the RSs0827 knockout mutant. These genes encode proteins with functions in iron metabolism (*feoA1*, *feoB*, a siderophore transporter, a probable ferredoxin, and a putative iron-regulated protein), two encode chaperones (*groEL* and *groES*), two code for ribosomal proteins (*rpl*R and *rplF*), and five belong to various metabolic systems (*ttuc*, *phbC*, *traI*, LysR protein, and enoyl-(acyl carrier protein) reductase). Grey: Genes up-regulated in the RSs0827 knockout mutant. The genes encode proteins that belong to the fructose metabolism (*cfXA*, *cfxB*, and *fbpP*), two that are included in the methionine metabolism (*cbbI* and methionine synthase), two poteins that represent alternative sigma factors (*rpoE* and *rpoHII*), and four that are known from different metabolic pathways (*tklB*, a small heat shock protein, *fliC*, and acetolate-synthase III large subunit). Adapted from Markus Späth, 2014 (Masterthesis).

A binding prediction (M. Späth) using the IntaRNA webtool (Wright *et al*., 2014; Busch *et al*., 2008) narrowed the potential targets, gained from the transcriptome analysis, down to three interesting candidates (Tab. 54), regarding their predicted binding site (between -100 nt and +50 nt around the start codon) and free energy (> -12 kJ).

Table 54: Predicted interaction between RSs0827 and selected target mRNA candidates. The prediction was carried out using the IntaRNA webtool (Wright *et al*., 2014; Busch *et al*., 2008) with mRNA sequences including 100 nt upstream of the start codon.

Gene name / function (number)	interaction position mRNA	interaction position sRNA	energy
rpoE (RSP_1092)	1 – 25	26 – 49	-17.97 kJ
tklB (RSP_3268)	-15 – 7	26 – 47	-16.72 kJ
Eonyl-reductase (RSP_1256)	-44 – -12	35 – 79	-16.29 kJ

For those three candidates the *lacZ*-based *in vivo* reporter system, as described for the Pos19 (3.1.5.1) and PcrX (3.2.7.1) projects, was chosen to further analyse the regulatory potential of RSs0827 on the *rpoE*, *tklB*, and RSP_1256 mRNA. While for the *rpoE-lacZ* fusion the cloning was not successful, the *lacZ* fusions for *tklB* as well as RSP_1256 (together with the upstream RSP_1257 sequence and the shared promoter) were completed, but the reporter plasmids did not show exploitable ß-galactosidase activity (0.5 – 1 Miller Unit) after conjugation to the selected *R. sphaeroides* strains (Masterthesis M. Späth, 2014).

In 2015 another study, a Bachelorthesis under my supervision, was performed on the RSs0827 project (S. Martini). Already the expression pattern of RSs0827 – especially the induction upon oxidative and heat stress –hinted towards a dependency of the RSs0827 expression on the alternative sigma factors RpoHI and RpoHII (1.9.4). To verify this assumption, the RpoHI and RpoHII knockout mutants (Δ*rpoHI* and Δ*rpoHII*) as well as the double mutant (Δ*rpoHI*/*rpoHII*) were cultivated and exposed to photo-oxidative or heat stress for 30 min each. Cells were harvested before (t 0) and after stress, the RNA was isolated and applied for Northern blot analysis. The Northern blot revealed that the expression of RSs0827 is dependent on RpoHII during photo-oxidative stress and dependent on RpoHI during heat stress, while a double knockout (Δ*rpoHI*/*rpoHII*) prohibits the expression of RSs0827 under both tested conditions (Fig. 85). Overall these results confirm that RSs0827 is expressed from an RpoHI/RpoHII dependent promoter.

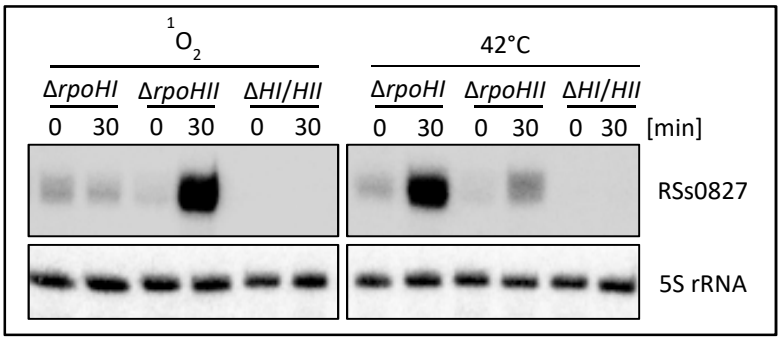

Figure 85: Expression pattern of the sRNA RSs0827 upon photo-oxidative ($^1O_2$) and heat (42°C) stress. The induction of RSs0827 after 30 min of stress was tested in the knockout mutants of the alternative sigma factors RpoHI and RpoHII (Δ*rpoHI* and Δ*rpoHII*) as well as in the double knockout (Δ*HI/HII*). The 5S rRNA was probed as loading control. The Northern blot was adapted from S. Martini, Bachelorthesis 2015.

Furthermore, the potential interaction between RSs0827 and the *rpoE* mRNA was investigated again. A 218 nt fragment (-101 – +111 from the start codon) of the *rpoE* sequence was amplified using the primer pair 1092_fwd_16S and 1092_rev. The fragment was subcloned into the pDrive cloning vector (Qiagen; pDrpoE), sequenced, and ligated into the corresponding sites of the pPHU4352 (Mank *et al*., 2012) after restriction with XbaI and HindIII. The resulting reporter plasmid pPHU_1092carrying the *rpoE-lacZ* fusion under the control of the 16S rRNA promoter (RSP_4352 promoter) was transferred to selected *R. sphaeroides* strains via conjugation. The subsequent ß-galactosidase activity assay showed that the over-expression of RSs0827 (pBBR_RSs0827) negatively affects the translation of the *rpoE-lacZ* fusion (~60%) compared to the wild-type, while increased translation of the fusion (~138%) could be measured in the RSs0827 knockout mutant (ΔRSs0827) (Fig. 86). The translation of the *rpoE-lacZ* fusion was significantly changed (directed, unpaired students T-test: † 0.05 < p < 0.1 and * p < 0.05) in the RSs0827 over-expression (p = 0.0005) as well as in the RSs0827 knockout mutant (p = 0.015), each compared to the wild-type.

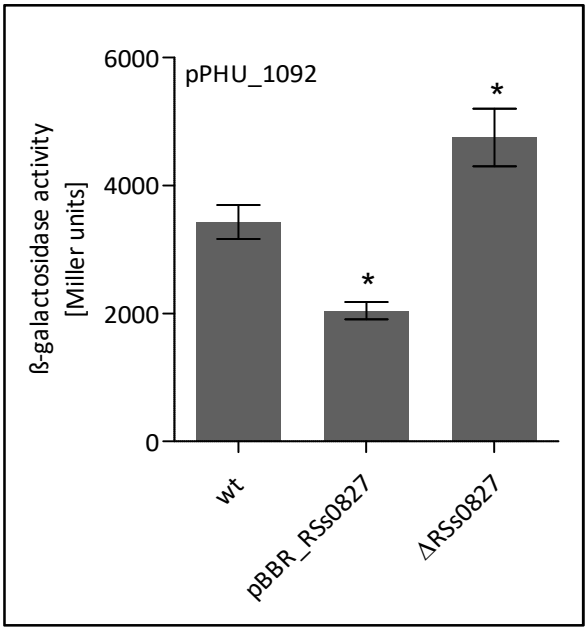

Figure 86: Effect of over-expression and deletion of RSs0827 on the translational *rpoE-lacZ* fusion. The reporter plasmid pPHU_1092 was transferred to the *R. sphaeroides* wild-type (wt), the RSs0827 over-expression strain (pBBR_RSs0827) and the RSs0827 knockout mutant (ΔRSs0827). The ß-galactosidase activity is depicted in Miller Units and represents the mean of biological triplicates measured in technical duplicates, shown with the standard error of the mean. The level of significance compared to the wild-type (wt) is indicated († 0.05 < p < 0.1 and * p < 0.05). Adapted from S. Martin, Bachelorthesis 2015.

Table 55: Raw data of the ß-galactosidase activity assay using the reporter plasmid pPHU_1092*lacZ*. The measured values are listed in Miller Units with the standard error of the mean (SEM) as well as percent (wt set 100%) with the relative error in percent.

Background strain	Miller Units	SEM	Percent	rel. error [%]
pBBR (EVC)	3432	265	100.0	7.7
pBBR_RSs0827	2047	134	59.6	6.5
ΔRSs0827	4752	450	138.5	9.5

3.3.2 *RpoE* as RSs0827 target

On the basis of the above-presented knowledge, the interaction of the RSs0827 sRNA and its potential target *rpoE* was to be further elucidated and verified.

As a first approach compensatory mutations as described for the Pos19 (3.1.8) and PcrX (3.2.7.1) project were tested. Therefor the interaction (seed region) between RSs0827 and the *rpoE* mRNA was predicted using the IntaRNA webtool (Wright *et al*., 2014; Busch *et al*., 2008) (Fig. 87). The prediction varies a little from the previous one (M. Späth, Tab. 54) since the algorithms of the webtool are updated and changed frequently. According to this predicted interaction, three (M3) and four (M4) nucleotides of the *rpoE* sequence were chosen and mutated as indicated in figure 87.

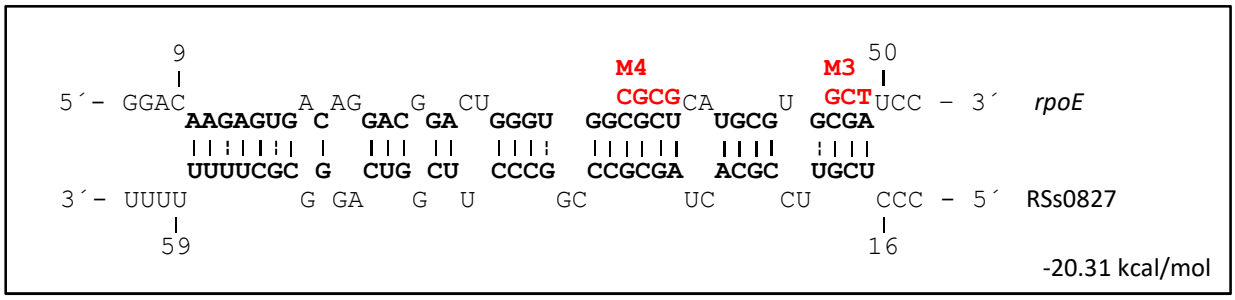

Figure 87: Predicted interaction site of RSs0827 and the *rpoE* mRNA. Numbers refer to the position of the 5' end (RSs0827) or start codon (*rpoE*). The mutations (M3 and M4) chosen for the *lacZ*-based *in vivo* reporter system are indicated in red. The interaction and free hybridisation energy (lower right) is depicted as predicted with IntaRNA webtool (Wright *et al*., 2014; Busch *et al*., 2008).

The mutations were inserted via a site-directed mutagenesis PCR (2.4.3.2) using the primer pairs rpoE_M3_fw / rpoE_M3_rev and rpoE_M4_fw / rpoE_M4_rev (Tab. 3). The pDrpoE (3.3.1) served as template hence the mutated fragments could be ligated (2.4.4.2) into the pPHU4352 after restriction with XbaI and HindIII as described above. After transferring the resulting reporter plasmids pPHU_1092M3 and pPHU_1092M4 to the RSs0827 over-expression strain (pBBR_RSs0827) and the corresponding EVC (pBBR) via conjugation, cells could be harvested for a ß-galactosidase activity assay. This assay revealed that the mutations were not sufficient to affect the regulatory potential of RSs0827 on the *rpoE-lacZ* fusion (Fig. 88 and Tab. 56). But it also showed that the mutated reporter plasmids pPHU_1092M3 and pPHU_1092M4 exhibit a stongly reduced activity (~162 and 17 MUs in the EVC background) compared to the unmutated reporter plasmid (3432 MUs, see Tab. 55).

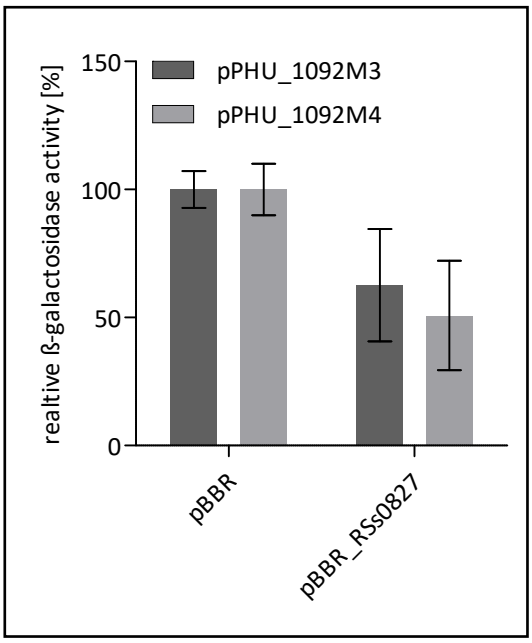

Figure 88: Effect of RSs0827 over-expression on the mutated *rpoE-lacZ* reporter fusions. The reporter plasmids containing the mutated *rpoE* fragments (pPHU_1092M3 and pPHU_1092M4) were transferred to the RSs0827 over-expression strain (pBBR_RSs0827) and the corresponding EVC (pBBR) via conjugation. The results of the subsequent ß-galactosidase activity assay are depicted in Miller Units as mean (with standard error of the mean) of biological triplicates and technical duplicates.

Table 56: Raw data of the ß-galactosidase activity assay using the mutated 1092-*lacZ* reporter plasmids. The RSs0827 over-expression strain is abbreviated as pRSs0827. The measured values are listed in Miller Units with the standard error of the mean (SEM) as well as percent with the relative error.

Background strain/ reporter plasmid	Miller Units	SEM [MUs]	Percent	rel. error [%]
pBBR / 1092M3	162.6	11.7	100.0	7.2
pRSs0827/ 1092M3	101.8	22.4	62.6	22.0
pBBR / 1092M4	17.7	1.8	100.0	10.1
pRSs0827 / 1092M3	9.0	1.9	50.8	21.4

Since the mutations in the *rpoE* sequence did not alter the regulation entailed by the RSs0827 over-expression, the compensatory mutations in the RSs0827 sequence were so far not approached.

Instead, an EMSA set-up was prepared to verify the interaction between the two RNAs. The RSs0827 sequence, as well as a 156 nt part (-19 – +134 nt from the start codon) of the *rpoE* sequence, were amplified to serve as templates for *in vitro* transcription. The amplification (2.4.3) was performed using the primer pairs T7_0827_fw / T7_0827_rev and T7_rpoE_fw / T7_rpoE_rev (Tab. 3). RSs0827 was prepared as a radio-labelled transcript (T70827*; 2.4.7.3) while *rpoE* was prepared as cold *in vitro* transcript (T7rpoE; 2.4.5). The first EMSA was carried out as described in 2.4.13, using a 0.25x TB gel containing 10 mM $MgCl_2$ and structure buffer in a final concentration of 1x per sample. 150 fmol of T70827* each was mixed with increasing amounts of T7rpoE after the de- and re-naturing steps. As a negative control T70827* was mixed with a 100-fold excess of cold T70557 transcript (3.1.9). The T70827* transcript alone, as well as de- and renatured together with a 100-fold excess of T7rpoE, were prepared as well. The EMSA showed an interaction between

T70827* and T7rpoE and the resulting band shift, which increases with increasing amount of T7rpoE (Fig. 89).

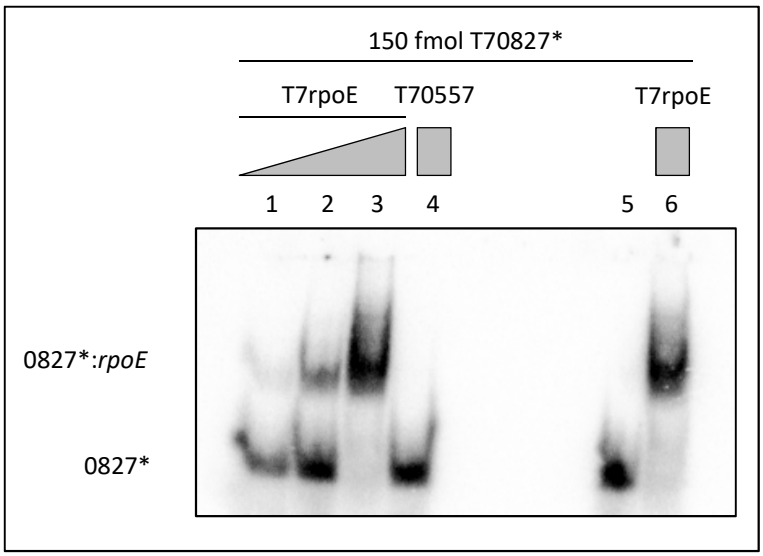

Figure 89: Testing the interaction between RSs0827 and *rpoE* using an EMSA. The radio-labelled RSs0827* *in vitro* transcript (T70827*) was de- and re-natured together with a 100-fold excess of cold *rpoE* transcript (T7rpoE; 6), loaded alone (5), and incubated with increasing amounts (150 – 15000 fmol) of cold *rpoE* transcript (1-3) after the renaturing step. As a negative control, T70827* was incubated with a 100-fold excess of cold T70557 transcript (4).

In a second EMSA, the interaction between the hot RSs0827 transcript and the cold *rpoE* transcript was competed by the addition of cold RSs0827 transcript. As shown for the PcrX*:*pufX* interaction (3.2.7.2), the addition of cold sRNA transcript (T70827) impairs the sRNA*:mRNA interaction (Fig. 90).

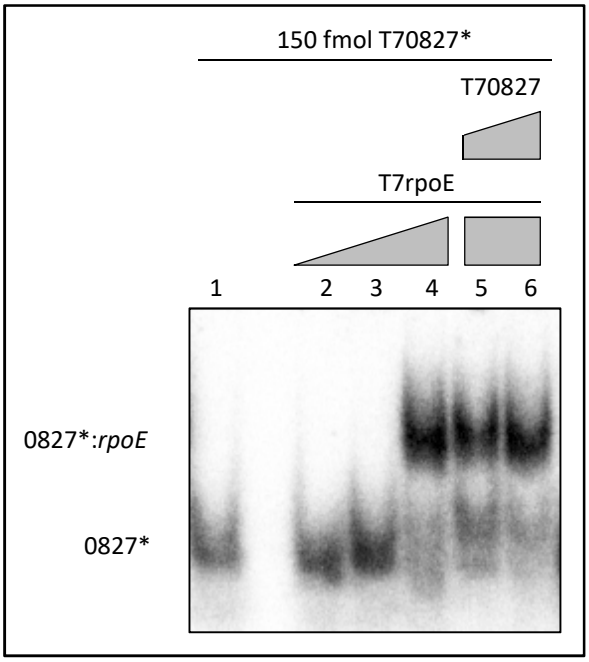

Figure 90: Competing the RSs0827*:*rpoE* interaction by adding cold RSs0827 *in vitro* transcript. Radio-labelled RSs0827* transcript was loaded alone (1) and mixed with increasing amounts (150 – 15000 fmol) of cold *rpoE* transcript (2-4). 10- or 100-fold excess of cold RSs0827 transcript over radio-labelled RSs0827* transcript were added to reactions containing 0827*:*rpoE* (150:15000 fmol) (5 and 6).

4. Discussion

The here investigated microorganism *R. sphaeroides* is a well-established model to study the bacterial response to oxidative stress and, due to its great metabolic versatility, the diverse mechanisms to adapt to varying environmental conditions. The presented work focussed on the involvement of three sRNAs in this response and adaptation.

4.1 Characterisation of the sRNA Pos19

4.1.1 Regulation and phenotype

The first and most intensively investigated sRNA in this work was named Pos19, for Photo-oxidative stress induced sRNA 19 (Müller *et al*., 2016). The sRNA Pos19 was found to have a distinct expression pattern (Fig. 23) which is defined by its RpoE-dependent promoter (3.1.1). The lack of Pos19 expression in the TF18 strain, in which the *rpoE-chrR* locus is deleted, has clearly verified this promoter dependency (Fig. 23). Interestingly, the Pos19 expression pattern further supported first evidence (Nuss *et al*., 2013; Hendrischk *et al*., 2007) that RpoE, the major regulator of the response to photo-oxidative stress in *R. sphaeroides*, is in addition to $^1O_2$ triggered by peroxides, including H_2O_2 and tBOOH. Since $^1O_2$ is known to cause the generation of, for example, histidine peroxides during the so-called indirect photo-oxidation (1.3), it is not surprising that parts of the RpoE regulon seemingly can also play a role in the defence against peroxide stress.

Besides the strong induction due to photo-oxidative and oxidative stress, Pos19 was found to be as strongly up-regulated upon iron starvation (Fig. 23). This was to be expected, since in addition to enhanced ROS formation via the Fenton reaction when iron is present, also iron limitation was shown to increase the cellular ROS level and moreover to activate the expression of *rpoE* (Peuser *et al*., 2011). Interestingly, already in 2005 studies had shown that iron starvation increases the intracellular ROS level in *Anabaena* sp. strain PCC 7120 and *Synechocystis* sp. strain PCC 6803, but not in *E. coli* or *B. subtilis.* It was therefore proposed that the ROS formation and subsequent damage induced by iron limitation could be a trait of photosynthetic organisms only (Latifi *et al*., 2005). This potential connection between iron starvation, ROS, and photosynthesis is also implied in the presented Pos19 data: a strain lacking Pos19 shows a significantly increased ROS level (Fig. 30) accompanied by slight growth impairments under iron-limiting and photosynthetic conditions (Fig. 33 and 34) compared to the wild-type.

Besides this more speculative connection to the iron metabolism, the presented data provide evidence for an involvement of Pos19 in the connection between oxidative stress and the modulation of the glutathione (GSH) metabolism. This modulation is likely to be entailed by the regulation of a set of sulphur genes, which also affect the cysteine and methionine pathway (Fig. 26), with cysteine being one of the main GSH components (Masip *et al*., 2006). The tripeptide GSH is

described as being one of the most prevalent cellular thiols and it has been known for several decades now that it protects the cell against oxygen toxicity (Meister and Anderson, 1983). In the defence against ROS, GSH acts as electron donor to maintain the reducing environment in the cell (1.7). Therefore a decrease or increase in the intracellular GSH level, as found in the strains constitutively overexpressing or lacking Pos19 (Fig. 30), was assumed to affect the resistance of the cells towards oxidative stress. Surprisingly, no difference in resistance was observable for either of the Pos19 strains in comparison to a control strain, as tested by a zone of inhibition assay (Fig. 30). Instead, the increased GSH level in the Pos19 knockout mutant (ΔPos19) even came along with a great increase of the intracellular ROS level (Fig. 30). Intuitively one would think that Pos19, which is induced during ROS-enhancing conditions, should rather positively affect the cysteine synthesis to maximize the GSH pool (Masharov *et al*., 2000) and thereby the ability to defend against oxidative stress. This view is supported by the finding that under stress conditions the sulphur genes are clearly induced in the EVC strain (Fig. 27). A possible explanation for the, on the first glance, counterproductive expression of Pos19 during oxidative and photo-oxidative stress is that the role of Pos19 is to counterbalance the induction of the sulphur genes and thereby the over-production of the sulphur-containing amino acids cysteine and methionine. This fine-tuning of the sulphur metabolism could have different beneficial roles in the cell. On the one hand cysteine, as well as methionine, are susceptible to direct oxidative damage (Pattison *et al*., 2011; Schöneich, 2005). On the other hand, cysteines can reduce ferric iron with exceptional speed, resulting in free iron which can drive the generation of hydroxyl radicals in the Fenton reaction (Park and Imlay, 2003). So the reason underlying the sulphur gene regulation might be rather to avoid too much cysteine over having not enough GSH. *De facto*, the reduced GSH level in the strain constitutively over-expression Pos19 did not lead to a higher sensitivity towards oxidative and photo-oxidative stress (Fig. 30). An additional explanation for the repression of the sulphur genes more generally addresses the cellular resources. All in all the stress defence systems, such as the GSH synthesis, have to be carefully regulated in order to avoid unnecessarily high expression. To put it more plainly: while maximizing the chances to survive, the expenses for the stress defence should be minimised (Guo and Gross, 2014).

Several results obtained in this work indicate that there are redundant systems, which can compensate both, a lack as well as a constitutive presence of Pos19. In the strain lacking the gene encoding Pos19 (ΔPos19), the induction of the selected genes, other than expected, did not reach higher levels than in the wild-type after 7 min of $^1O_2$ stress (Fig. 34). Accordingly, constitutively over-expressing Pos19 under non-stress conditions did not affect the sulphur genes in comparison to the EVC strain (Fig. 35). Redundant regulatory systems enabling a tight and precisely tuned regulation are commonly known in bacteria, as can be for example seen in the photosynthesis gene regulation of *R. sphaeroides* (Fig. 14). Further examples for regulatory redundancy, even highly identical down to the nucleotide level, can also be found in the sRNA field. For instance, the so-called sibling sRNAs AbcR1

and AbcR2 found in many *Rhizobiales* (Caswell *et al*., 2014). They negatively affect the ABC transport in *Sinorhizobium meliloti* by canonical targeting of the 5' regions of two of the ABC transporter mRNAs (Torres-Quesada *et al*., 2014). A second reason for the missing regulation of the potential targets in the knockout mutant and constitutive over-expression strains can be found in the experimental procedure. Most sRNAs are only expressed under very specific conditions and directly target one or multiple mRNAs to adapt to these conditions. So in general, the regulation via an sRNA happens rapidly and only for the time the cells need to adapt or the condition is prevailing. When permanently deleting or constitutively expressing the sRNA already under non-stress conditions instead, the resulting miss-regulation will be compensated, which in turn will mask direct regulatory effects. Therefore, a favoured setup is to use pulse expression of an sRNA, as was provided for Pos19 by stress exposure, to investigate potential targets (Sharma and Vogel, 2009). Moreover, it was purposed that sRNAs do not function in isolation, and therefore high levels of expression, often at times or conditions when the endogenous sRNA is normally not expressed, may have unintended consequences that complicate interpretation of the results (Storz *et al*., 2011).

Nevertheless there is one observation that is still conflicting: the slightly increased GSH level in the Pos19 knockout mutant (Fig. 30) cannot be explained by regulation, or in this case rather missing regulation, of the sulphur genes (Fig. 34). Alternative sources for the altered GSH biosynthesis might be the regulation of the *cox* operon and RSP_6037. The former was found to be up-regulated while the latter to be down-regulated in the Pos19 over-expression strain after $^1O_2$ stress, according to the microarray data (Tab. 48). From a study investigating the CcsR 1-4 sRNAs (1.9.5), that are co-transcribed together with RSP_6037, it is known that the CcsR sRNAs affect the *cox* genes. In turn the *cox* genes were found to influence the GSH level (Billenkamp *et al*., 2015). Yet a changed expression of the *cox* genes, RSP_6037 and the sRNAs CcsR 1-4 in the Pos19 knockout mutant remains to be confirmed. Considering the elevated amounts of ROS and GSH in the Pos19 knockout mutant contrasted by the unchanged resistance towards oxidative stress (Fig. 30), and accompanied by the slight growth phenotype under iron limitation and phototrophic growth (Fig. 32 and 33), a more complex role than only regulating the sulphur genes can be assumed for Pos19. Moreover, some mechanisms of sRNA entailed regulation do not result in altered mRNA levels, and changes in mRNA levels may not always be reflected as altered protein synthesis or activity (Storz *et al*., 2011). Therefore, for example, additional translatome and proteome studies could help to sharpen the knowledge about the Pos19 function.

4.1.2 Pos19 sORF

Another intriguing detail that was studied regarding the sRNA Pos19 is the sORF that was found within the sRNA's sequence (Fig. 36). Interestingly enough, the Pos19 sequence including this sORF could not be identified in bacteria related to *R. sphaeroides*, but was found to be quite conserved in four different *R. sphaeroides* strains (Fig. 38). Depending on the two start codons found in frame with

the stop codon, the sORF exhibits a length of 150 or 135 nt. To study the translation and properties of the sORF, a *lacZ*-based *in vivo* reporter system was utilised for translational fusions (3.1.5.1). Those studies showed that the sORF is truly translated *in vivo*, from the first of the two start codons (ATG1). As shown for the sRNA, also the peptide expression is dependent on RpoE, verified by testing for translation of the Pos19-*lacZ* fusion in the TF18 (Δ*rpoE-chrR*) background. The Pos19 translation was abolished when inserting internal stop codons at the position of the second start codon or codon 16. In contrast, mutating the SD-like sequence found upstream of Pos19 did not fully inhibit the translation (Fig. 37). When four of the eight nucleotides of the SD-like sequence were exchanged, after 60 min of $^1O_2$ 32% of translation compared to the wt sORF remained, and exchanging the full SD-like sequence only lowered the translation to 16%. Similar findings were reported for *Haloferax volcanii*, were the full replacement of the *sod* gene's SD motif did not even affect the translation rate at all. Additionally, in Haloarchea only 20-30% of all genes were bioinformatically predicted to be preceded by a SD motif (Kramer *et al*., 2014). Taken together, these findings support the growing evidence that in prokaryotes the SD sequence is not as important for translation initiation as previously thought (Omotajo *et al*., 2015). In addition to the characterisation of the Pos19 sORF properties, the *in vivo* translation of the Pos19 peptide was verified using a CFP-fusion and subsequent Western blot analysis (Fig. 41). This experiment also verified the induction of the peptide translation upon $^1O_2$ stress, already seen in the *lacZ*-based reporter studies.

Unfortunately the function of the small Pos19 peptide still remains enigmatic. Well studied members of peptides encoded by sRNAs are the δ-hemolysin from *Staphylococcus aureus*, SR1P from *B. subtilis* and SgrT from *E. coli* (1.1.1) (Vanderpool *et al*., 2011). The latter was shown to enhance the effect of its parental sRNA SgrS by inhibiting the activity of the glucose PTS transporter, whose mRNA is a target of the base-pairing SgrS (Wadler and Vanderpool, 2007). A cumulative role for the Pos19 peptide in the regulation of the sulphur metabolism was an appealing idea. But when introducing the mutations that were shown to abolish the peptide translation into the Pos19 sequence used for over-expression, the regulation entailed by those over-expressions was identical to the native Pos19 over-expression (Fig. 43). An involvement of the peptide in the regulation of the sulphur metabolism, for example via interaction with a protein from this metabolism, can not be ruled out completely, but at least the tested genes affected by Pos19 over-expression are regulated independently of the peptide. When using the BLASTP webtool (Altschul *et al*., 1997) an amino acid identity of 65% to the Pos19 peptide was only found for two hypothetical proteins with similar lengths from *Rhodovulum sulfidophilum* and *Roseibacterium elongatum*. Further analysis using the Phyre2 web portal (Kelley *et al*., 2015) to model the structure of the Pos19 peptide and to predict any protein homology or analogy did not give any exploitable results.

4.1.2 Target verification

The effect of Pos19 on potential target genes was further characterised using a second *lacZ*-based *in vivo* reporter system. In this system sequence parts of interest, here the predicted binding sites for Pos19 on the target sequence, are translationally fused to a promoterless *lacZ* gene under the control of a constitutive promoter. Using this system, a strong negative effect of the Pos19 over-expression on the translation of RSP_0557 was found, whose activity was reduced to 35% in the Pos19 over-expression background compared to the EVC strain (Fig. 44 A). This reduction was again observed when over-expressing the three mutated Pos19 variants which do not allow peptide translation. An effect of Pos19 on the RSP_0557 transcription was later excluded, by utilising a transcriptional fusion of the RSP_0557 promoter to the *lacZ* gene (Fig. 50). When testing a second potential target, *cysH*, a decrease of ß-galactosidase activity to around 75% was determined in the Pos19 over-expression strain. Surprisingly, this was also true for two reporter fusions chosen as controls, *bchN* (encoding a subunit of the light-independent protochlorophyllide reductase) and *puc2A* (encoding a ß-subunit of LHC II). When testing a third control fusion, namely *takP-lacZ*, no effect of the Pos19 over-expression was found, confirming that the effect measured for *cysH*, *bchN*, and *puc2A* is no general effect on the translation from the reporter plasmid (Fig. 44 A). When repeating the measurements in the Δ*hfq* background, the decreased activity found for the RSP_0557, *cysH*, *bchN*, and *puc2A* reporter fusion in wild-type background vanished (Fig. 44 B). This was rather surprising since in a previous study (Berghoff *et al*., 2011) Pos19 was not detected among the sRNAs found to interact with Hfq. Thus the coIP with 3xFLAG-tagged Hfq was repeated, using RNA from the strain over-expression Pos19 as input. This experiment clearly showed that Pos19 interacts with Hfq when present in elevated amounts (Fig. 45). That justifies the Hfq-dependent regulation of the *lacZ* reporter fusion after Pos19 induction upon $^1O_2$ stress described above.

The regulation of the *bchN* and *puc2A* reporter fusions via Pos19 again emphasises the connection between the photosynthesis gene regulation and photo-oxidative stress. Due to the weak level of regulation and absence of predicted binding sites for Pos19 in their sequence, the regulation of the two photosynthesis genes is assumed to be indirect. These findings lead to the presumption that the induction of Pos19 triggers subsequent steps in the defence against photo-oxidative and oxidative stress, which include suppressing the expression of the photosynthetic apparatus. This suppression is favourable for the cell to avoid further $^1O_2$ generation via photosensitisation reactions (1.2). Overall, it gets more and more evident that many sRNAs exhibit vast and diverse regulons, just like some transcription factors or miRNAs in eukaryotes, that do not solely depend on base-pairing interactions but also on secondary effects (Storz *et al*., 2011).

To demonstrate the direct interaction of Pos19 with the RSP_0557 mRNA, a compensatory mutant analysis was carried out (3.1.8). Unfortunately, with none of the six tested mutations a direct sRNA-mRNA interaction could be verified. Even though these kind of analyses continue to be the gold

standard for validation of direct targets, often the mutation in one RNA partner abolishes the regulation but the regulation cannot be restored by compensation of the complementarity (Adnan *et al*., 2015; Desnoyers *et al*., 2009), as seen for Pos19 M1 and M3 mutations (Fig. 48). Moreover, not every mutation is sufficient to affect the interaction, for example in the predicted 23 base pair interaction between *E. coli* SgrS and the *ptsG* mRNA, only four single mutations did show a significant change in regulation (Kawamoto *et al*., 2006). To verify the Pos19-RSP_0557 RNA interaction some further mutations could be tested or a more extended region (> 4 bp) could be mutated. A second attempt to show a direct binding between Pos19 and the RSP_0557 mRNA was undertaken with the help of EMSA experiments (3.1.9). Again no direct interaction could be detected.

Further experiments to emphasise the effect of Pos19 on the RSP_0557 mRNA were undertaken to determine the half-life of RSP_0557. These indicated that the RSP_0557 mRNA is more stable in the Pos19 knockout mutant (9.2 min) than in the wild-type (3.1 min; Fig. 52). For this experiment, the expression of RSP_0557 had to be induced prior to the rifampicin addition since the mRNA is otherwise not reliably detectable on a Northern blot membrane. Unfortunately, the H_2O_2 apparently oxidises the rifampicin, as also previously described (Finkel *et al*., 1971), resulting in falsified results. This especially becomes evident when calculating the Pos19 half-life from this experiment (13.9 min), which greatly differs from previously obtained data without H_2O_2 (5 min) (Berghoff *et al*., 2009). Trying to take advantage of the short half-life of H_2O_2 which, for example, is only 3.5 min in an *E. coli* culture with moderate density (Seaver and Imlay, 2001), one could repeat the experiment while adding the rifampicin later after the H_2O_2 addition (> 10 min). As second alternative would be to use heat stress to induce the RSP_0557 expression, still a known RNA half-life should be determined from the same experiment to exclude side effects of the heat to the rifampicin.

4.1.3 Properties and function of RSP_0557

Although a direct interaction between Pos19 and the RSP_0557 mRNA was not verified, the mRNA encoding a hypothetical protein remained in the focus of interest, due to the strong, Hfq-dependent regulation via Pos19. To investigate the function of RSP_0557 a constitutive over-expression and a chromosomal deletion (knockout) were constructed (3.1.11). The expression of RSP_0557, which was meanwhile known to be induced upon $^1O_2$ und heat stress, was found to be dependent on the alternative sigma factors RpoHI and RpoHII (Fig. 54). To clarify the role of RSP_0557 in the stress response, similar phenotypic charaterisations as for the Pos19 strains were conducted. Those assays revealed that the RSP_0557 knockout mutant, as well as the constitutive RSP_0557 over-expression, show a slight growth impairment compared to the wild-type during microaerobic growth (Fig. 55). In addition both strains were found to be more resistant towards $^1O_2$ and H_2O_2 than the wild-type (Fig. 66), which correlates with the increased GSH levels in the knockout mutant (128%) and the constitutive over-expression of RSP_0557 (127%; Fig. 57). This similar tendency of the two opposing

RSP_0557 strains was rather surprising and led to the assumption that the balanced expression of RSP_0557 is necessary for a balanced GSH level. Despite the beneficial effect of the increased GSH on the resistance of the two strains towards oxidative stress, this uncontrolled GSH synthesis goes to the cost of growth. Thereupon it was tested whether RSP_0557 represents the missing link between Pos19 and the regulation of the sulphur genes and the thereby influenced GSH level. When analysing the regulatory potential of Pos19 in the RSP_0557 knockout background, no significant difference compared to the regulation of the sulphur genes in the wild-type background was observable (Fig. 58). Based on these data no precise function for RSP_0557 could be assumed.

RSP_0557 is homologous to RSP_6037, a conserved hypothetical protein that is cotranscribed together with the four sRNAs CcsR1-4 (Billenkamp *et al*., 2015; Berghoff *et al*., 2009). Intriguingly, RSP_6037 was also found among the genes down-regulated upon Pos19 over-expression (log_2 ratio -1; Tab. 48). Both, RSP_0557 and RSP_6037, contain a domain of unknown function (DUF1127) that, according to the Pfam database (Finn *et al*., 2016), is found in several hypothetical bacterial proteins, where in some cases it represents the C-terminal region whereas in others it represents the whole sequence. Protein BLAST searches (Altschul *et al*., 1997) revealed that RSP_0557 is quite conserved among the *Rhodobacteracea* (49-97% identity), which is also true for its synteny (gene order) according to the SyntTax web server (Oberto, 2013). The BLAST searches also identified the primosomal protein DnaI from *Roseobacter* to be 55% identical to RSP_0557. Not described in *Roseobacter* but in *B. subtilis*, DnaI was shown to harbour a DNA-binding activity and to be one of the proteins loading the replicative ring helicase DnaC onto DNA during priming of DNA replication (Ioannou *et al*., 2006). Moreover, secondary structure prediction and comparisons by the Phyre2 web portal (Kelley *et al*., 2015) revealed that RSP_0557 shows similarity to the RNA-binding protein Smaug with a confidence of 54.6%. Smaug is known to bind RNA via the sterile-alpha motif (SAM) domain and is needed for the anteroposterior patterning in *Drosophila melanogaster* (Aviv *et al*., 2003). These last findings strongly imply a nucleic acid binding activity for RSP_0557, and potentially also for RSP_6037, which would be intriguing to test. This could be done using a coIP experiment as it was applied to detect sRNAs interacting with Hfq (Berghoff *et al*., 2011). First known sRNAs could be tested for binding to RSP_0557 using the coIP RNA for Northern blot, before sequencing the RNA if appropriate.

In summary, this work identified Pos19 to be an sRNA regulator of sulphur genes that contributes to GSH homoeostasis upon oxidative stress in *R. sphaeroides*. The remodelling of metabolic processes upon environmental changes is a mode of action becoming more and more prevalent for studied sRNAs (Gottesman and Storz, 2011). Pos19 depicts, besides SorY (Adnan *et al*., 2015), CcsR1-4 (Billenkamp *et al*., 2015), and SorX (Peng *et al*., 2016), the fourth *R. sphaeroides* sRNA altering metabolic processes while adapting to stress conditions. One of the potential main targets negatively affected by Pos19, namely RSP_0557, is seemingly involved in alteration the GSH metabolism and is

supposed to have a nucleic acid binding activity. To further define the function of Pos19 the direct interaction between the sRNA and its target mRNAs, especially RSP_0557, needs to be further examined or the interposed regulatory factor needs to be determined. The model presented below (Fig. 91) summarises the described parts of the Pos19 function.

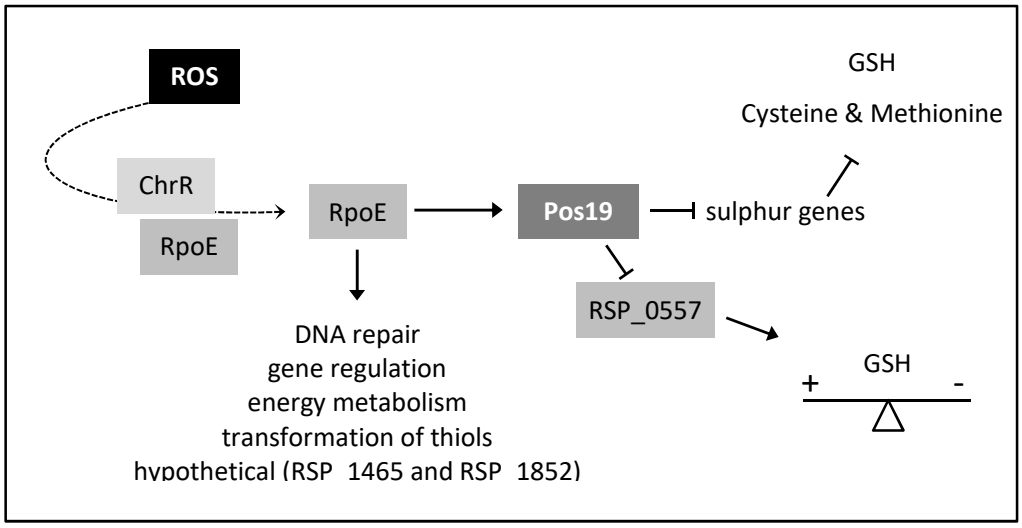

Figure 91: Model of effects entailed by Pos19 upon oxidative stress. The alternative sigma factor RpoE is released from its anti-sigma factor upon oxidative stress, and the expression of Pos19 is stress induced in a RpoE-dependent manner. RpoE additionally induces a set of genes needed for the stress defence. Pos19, in turn, represses a set of sulphur genes and thereby affects the cysteine and methionine synthesis pathway leading to alterations of the GSH level. Moreover, Pos19 represses RSP_0557, whose balanced expression is needed to maintain a balanced GSH level (lower right).

4.2 Characterisation of PcrX

4.2.1 Expression profile

PcrX, temporarily named as photosynthesis controlling sRNA X (previously RSspufX), was found to be co-transcribed together (3.2.4) and to share a terminator (Fig. 60) with the *R. sphaeroides puf* mRNA. Therefore PcrX exhibits an expression pattern similar to the *puf* mRNA, more precisely the sRNA is very weakly expressed during aerobic growth and induced upon a drop of the oxygen tension, reaching its highest expression under phototrophic conditions (Fig. 59 B). This expression is dependent on the two transcription factors PrrA and FnrL (Fig. 59 A and Fig. 14). As a 3'-UTR derived sRNA PcrX belongs to a more and more emerging new class of regulatory sRNAs. Those sRNAs were divided into two types: Type I sRNAs that are derived from an own promoter within the upstream gene or Type II sRNAs that originate via processing of the paternal mRNA (reviewed in Miyakoshi *et al.*, 2015). Moreover, the cotranscription together with the *puf* mRNA emphasises the already

presumed role of PcrX in the photosynthesis gene regulation. Besides the data verifying the co-transcription (3.2.4), a promoter study using two sequence fragments upstream of PcrX for transcriptional fusions gave a weak activity, 12 – 32 MUs and 20 – 54 MUs compared an average of ~5 MUs for the insert-less reporter plasmid, for both of the tested fragments (Tab. 53). Nevertheless, using the BPROM web tool (Solovyev and Salamov, 2011) no promoter motif was found in those fragments and the tendency found for those two fusions, subsiding with a drop of oxygen tension, does not fit in with the PcrX expression profile. Additionally, the activity of the 16S rRNA promoter (~1300 MUs) during microaerobic growth seemingly results in a 21-fold upregulation of PcrX compared to the EVC strain (calculated from signals shown in figure 68), which makes it implausible that an activity of 12-20 MUs measured for the PcrX upstream fragments (Tab. 53) should result in a 5-fold upregulation of PcrX upon a shift from aerobic to microaerobic growth (calculated from signals shown in figure 68). Taken toghether the presence of a promoter upstream of PcrX is assumed to be very unlikely.

4.2.2 Processing of the *puf* mRNA

To further characterise the generation of PcrX, the RNase responsible for the *puf* mRNA 3'UTR processing was sought. This search was started using available RNase knockout mutants, namely Δ*rnr,* Δ*rnc,* Δ*rnj,* Δ*rnc*/*rnj,* Δ*rppH*, and Δ*ybeY* (3.2.5). RNase R (*rnr*) is a 3'-5' exoribonuclease that acts on many different RNA substrates including ribosomal, transfer, messenger and sRNAs (reviewed in Domingues *et al*., 2015). RNase III (*rnc*) and RNase J (*rnj*) act as endoribonucleases, known for their role in tRNA and rRNA maturation in *E. coli* (reviewed in Lim *et al*., 2015) and specific RNA processing and degradation steps in *R. sphaeroides* (Rische-Grahl *et al*., 2014), respectively. The RNA pyrophosphohydrolase RppH is responsible for the conversion of the 5'-terminal triphosphate to a monophosphate to allow 5'-end-dependent access of RNase E (Deana *et al*., 2008; Celesnik *et al*., 2007). As one of the 206 genes comprising the postulated minimal bacterial genome set (Gil *et al*., 2004), YbeY is described as ssRNA-specific endoribonuclease involved in 16S rRNA 3' end maturation and quality control, as well as acting as co-endoribonuclease working with RNase R in the NCBI BioSystems Database (Geer *et al*., 2010). Moreover, YbeY was defined to play a major role in bacterial sRNA regulation in *Sinorhizobium meliloti*, even comparable to Hfq (Pandey *et al*., 2011; Pandey *et al*., 2014). In all of the tested RNase knockout mutants, induction of PcrX upon a shift from aerobic to microaerobic growth was detectable (Fig. 65). This led to the assumption that none of the tested RNases is, at least not solely, responsible for the processing of PcrX from the *puf* 3'UTR.

Another promising candidate for the processing is RNase E which is an essential bacterial endonuclease with a strong preference for single-stranded cleavage that is known to be involved in all parts of RNA metabolism (reviewed in Mackie, 2013). Instead of a classical knockout mutant a mutant carrying a thermosensitive variant of the *E. coli* RNase E replaced for the endogenous RNase E was used, since RNase E is essential in *R. sphaeroides* and can therefore not be deleted. When

shifting this strain, and as a control the wild-type, for 15 min to 42°C during microaerobic growth – which heat-inactivates the thermosensitive RNase E - no change in the PcrX level is observable in either strain (Fig. 66). But the overall level of PcrX before shifting to 42°C is reduced to the 0.42-fold in the RNase E mutant strain compared to the wild-type. In contrast to other *R. sphaeroides* sRNAs with half-lives between ~5 and 18 min (Berghoff *et al*., 2009), PcrX exhibits an extremely long half-life of around 290 min (3.2.2). By means of this finding, it was suspected that the unchanged level of PcrX before and after the 42°C shift is rather due to its stability under microaerobic conditions than due to affected processing and thereby missing additional "synthesis". To test this hypothesis, the experiment was repeated starting with aerobic cultivation, a condition where the PcrX level is very low, and shifting the cultures simultaneously to microaerobic growth to induce PcrX and 42°C to heat-inactivate the RNase E. However, weak PcrX expression in comparison to oxygen shift at 32°C was still found at 42°C in both strains (Fig. 67). A third set-up could be carried out shifting the cultures to 42°C for at least 10 min before also shifting to microaerobic growth, to exclude falsified results due to the strong induction of PcrX, which might be faster than the heat-inactivation of RNase E during a simultaneous shift. Additionally, a gene encoding a potential RNase G (RNase E/G family, RSP_0624) can be found in the *R. sphaeroides* genome. This RNase could display a surrogate for the studied RNase E, as it was found in *E. coli* (Lee *at al*., 2002), so that with a double-mutant of both RNases (in construction) better results would be achieved. Moreover, a recent RNAseq study in our group using the thermosensitive RNase E mutant indicated an RNase E cleavage site at the position that is assumed to be the processing site. Altogether the potentially RNase E-dependent processing of the *puf* 3'UTR should be further investigated.

4.2.3 Phenotype and targets of PcrX

When studying an sRNA, it is most important to reveal its mRNA targets. To study the effect of PcrX on chosen genes, an over-expression of PcrX was constructed. Although PcrX is induced when shifting the growth condition, during cultivation under the respective condition the PcrX level differs only slightly (Fig. 59), which is also true for the potentially targeted photosynthesis genes. Therefore a strong, constitutive over-expression was chosen over an inducible one and PcrX was over-expressed under the control of the 16S rRNA promoter. The over-expression works fine under all three tested growth conditions but is less pronounced during phototrophic growth compared to aerobic and microaerobic conditions (Fig. 68). The latter observation led to the, so far not tested, assumption that the turnover of PcrX is higher when the cells are grown phototrophically, which would again support the idea of PcrX acting in photosynthesis gene regulation. When cultivating the newly constructed PcrX over-expression strain for different experiments, it became obvious that it shows a lighter pigmentation than the corresponding EVC strain (Fig. 69). This lighter pigmentation was analysed using different assays such as BChl measurement and recording of full cell spectra. The BChl content, the overall LHC amount, as well as the full cell spectrum, was found to be strongly

reduced in the PcrX over-expression strain compared to the corresponding EVC strain (Fig. 70). Similar results were obtained when withdrawing samples during a growth curve performed during phototrophic conditions. Moreover, this growth curve revealed the impaired growth of the PcrX over-expression strain during phototrophic conditions (Fig. 71). Again the role of PcrX in the photosynthesis gene regulation was supported and PcrX, besides PcrZ (Mank *et al*., 2012), could be characterised as the second sRNA in *R. sphaeroides* strongly affecting the cells pigmentation when present in elevated amounts.

In addition to targets with a role in photosynthesis that were assumed to be affected by PcrX, a target prediction using the IntaRNA web tool (Wright *et al*., 2014; Busch *et al*., 2008) was performed to find additional potential candidates (3.2.7). The effect of the over-expression on the chosen potential target mRNAs was tested via an RT-PCR analysis (Fig. 72). The *pufBA* part of the *puf* mRNA, RSP_0290 (encoding a protein from the LHC I assembly), RSP_1945 (encoding a transcriptional regulator, *AscN* family), and RSP_2376 (encoding the 2-amino-3-ketobutyrate coenzyme a ligase, *kbl*) were found to be unaffected by PcrX. In contrast, the levels of *bchN* and *bchY* were slightly affected; they especially showed up-regulation in the PcrX over-expression strain during aerobic growth. The latter finding was also observed for *pufX* and is rather puzzling since up-regulation of the bacteriochlorophyll synthesis and LHC during aerobic conditions is needless. One possible explanation for this observation might be found in the mode of action of PcrX: assuming that the sRNA acts via base-pairing and recruitment of degradation factors such as RNases on the photosynthesis genes, those degradation factors or a factor linking those two actions could be absent during aerobic conditions. This could rather result in stabilisation instead of destabilisation of the mRNAs bound by PcrX during these usually “PcrX-free” conditions. This quite hypothetical idea remains to be tested. Nevertheless, down-regulation of two of the affected mRNAs, *bchY* and *pufX*, is found during microaerobic conditions which would argue for a negative regulation of photosynthesis genes via PcrX. This also fits for the finding that *bchY* is also down-regulated during phototrophic growth. In contrast, *pufX* is found to be strongly up-regulated in the PcrX over-expression strain during phototrophic conditions according to the RT-PCR data. Such a strong and antithetic regulation during conditions (microaerobic and phototrophic) where the photosynthesis genes normally show similar expression trends was rather surprising but make *pufX* an even more interesting target candidate.

4.2.4 *PufX* as a PcrX target

Due to the above-described findings of controversial regulation of *pufX* in the PcrX over-expression strain, the connection between PcrX and *pufX* was to be further characterised. Therefore again a translational fusion with the *lacZ* gene was constructed. The activity measured from this plasmid was reduced by at least 46% (lo and po, 68% for ho) in the PcrX over-expression strain under all three tested growth conditions (Fig. 73). This is not fully in line with the observations from the RT-PCR

analysis (4.2.3) but still shows the regulation of *pufX* entailed by PcrX. In further experiments, the same plasmid combination (pPHU_pufX-lacZ / pPcrX) was tested in the *hfq* knockout mutant (Δ*hfq*) which revealed that the regulation seen on the translational fusion is independent of Hfq (Fig. 73). As further steps to qualify the interaction, mutations were inserted into the predicted seed region of *pufX* and PcrX (M3 and M4, Fig. 74). As outlined for the compensatory mutation analyses for Pos19 and RSP_0557 (4.1.2), also the direct interaction between PcrX and *pufX* could not be verified using this set-up. The mutated *pufX-lacZ* fusion (M3) was down-regulated by the PcrX over-expression to the same extent as the unmutated fusion and even showed a stronger translation overall (Fig. 75). The second tested mutation (M4) resulted in a lack of PcrX over-expression (Fig. 76).

So instead of further compensatory mutant analysis, EMSA experiments were chosen to support the interaction of the two RNAs. For the EMSAs, the full PcrX sequence and a 134 nt part of *pufX* were amplified as templates for th*e in vitro* transcription (3.2.8.2). Using those transcripts it was possible to show the direct interaction resulting in a band shift (Fig. 77). The interaction between the radio-labelled PcrX transcript and the un-labelled *pufX* transcript could be diminished by adding an excess of cold PcrX transcript as a competitor (Fig. 78). Again mutations in the predicted seed region, this time on the *in vitro* transcripts (Fig. 79), were tested but were not sufficient to abolish the interaction between the PcrX and the *pufX* transcript (Fig. 80 and 81). Nine of the thirteen nucleotides predicted to interact were mutated so far, without finally proving the direct interaction. The remaining four nucleotides could be mutated, but a more comprehensive mutation of the seed region might be more successful. Altogether the mutational analysis showed the same problems due to the same reasons as the interaction study of Pos19 and RSP_0557 (4.1.2).

Besides the interaction between the sRNA PcrX and the *pufX* part of the *puf* mRNA also the results of this interaction were analysed. When determining the *puf* mRNA levels via Northern blot it became obvious that PcrX reduces the *puf* mRNA levels under microaerobic and phototrophic growth conditions (Fig. 82). In comparison to the RT-PCR analysis were the mRNA part amplified by the corresponding primer pair is examined, using the Northern blot technique one gets an impression of the full *puf* mRNA, which appears to be more reliable and convincing. The reduction of the mRNA level holds true for both detectable *puf* mRNA parts, the *pufBALMX* and the *pufBA* fragment, even though it is more pronounced for the *pufBALMX* part, especially under phototrophic conditions. The reduction of the *pufBA* fragment, even without a verified binding by PcrX, is not surprising since the reduction of the *pufBALMX* precursor fragment will inevitably affect the abundance of the *pufBA* fragment. Under phototrophic conditions, the *pufBA*/*pufBALMX* ratio of 0.6 in the EVC was shifted to 1.2 by the over-expression of PcrX (calculated according to the signal intensities in Fig. 82). Besides the overall abundance of the *puf* mRNA also the half-life of the *pufBALMX* segment was negatively affected in the PcrX over-expression strain (Fig. 83). The unchanged half-life of the *pufBA* part in these experiments additionally argues for an indirect effect of PcrX on the *pufBA* abundance as seen in figure 82, most likely by affecting the *pufBALMX* precursor.

Taken together PcrX negatively affects the abundance and half-life of its paternal mRNA *pufBALMX* and thereby allows the presumption that the *puf* mRNA carries its own translational regulator ensuring the needed ratio of *puBALMX* and *pufBA* that results in the needed stoichiometric amount of the encoded proteins (Fig. 16). The effect of the PcrX over-expression on further genes such as *bchN* and *bchY* and PcrX's long half-life moreover lead to the hypothesis that PcrX entails additional functions besides balancing the *puf* mRNA levels. The hypothesised model of PcrX's mode of action is summarised in figure 92 below.

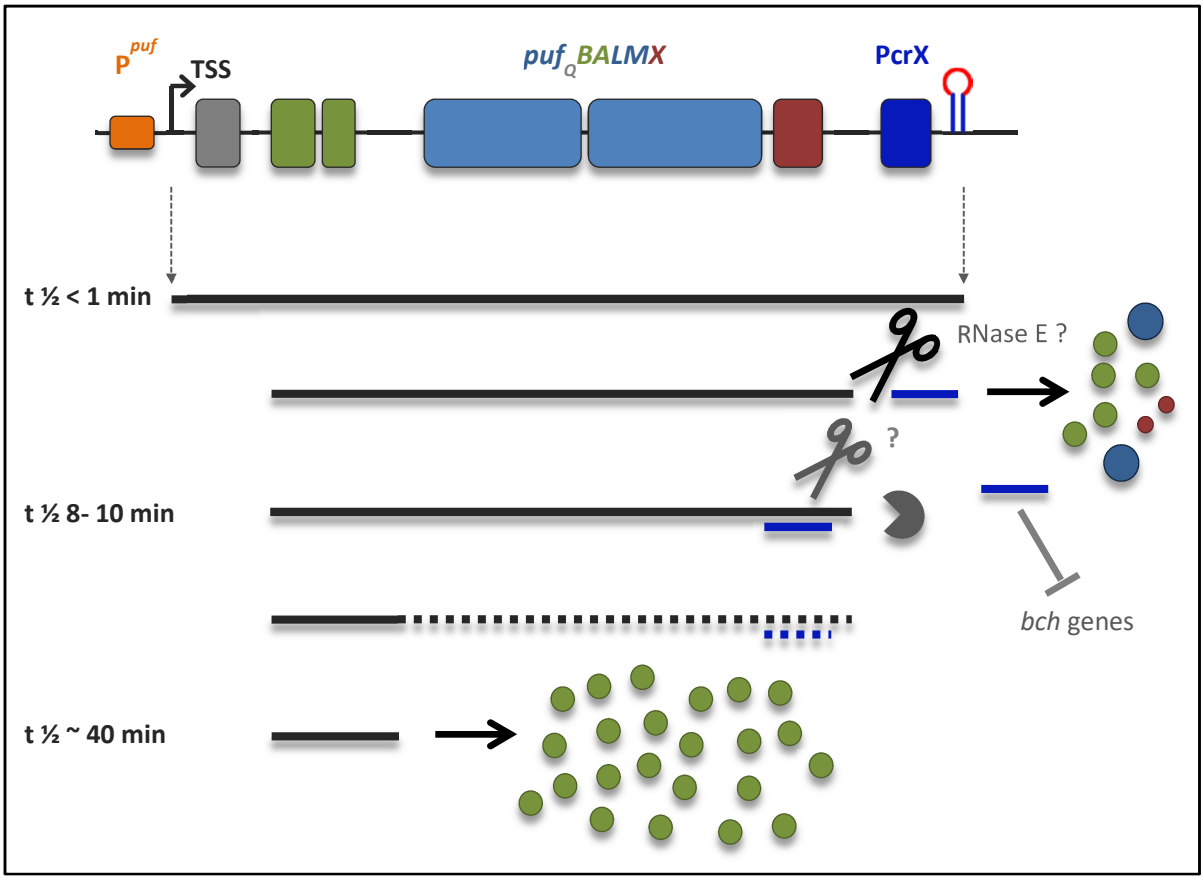

Figure 92: Model of the involvement of PcrX in the maintenance of the stoichiometric amount of the LHC I and RC components. After being processed from the *puf* mRNA, PcrX (dark blue) binds the *pufX* part leading to degradation of *pufBALMX*, resulting in the more stable *pufBA* fragment. The half-lives of the two main *puf* mRNA segments (depicted in minutes on the left) result in a stoichiometric amount (28:2:2) of reaction centre proteins (green), LHC I proteins (blue) and PufX (red). PcrX additionally seems to repress genes from the BChl synthesis (*bch* genes). All hypothetical steps are depicted in grey.

4.2.4 Additional perspectives

In addition to the above-discussed data on the sRNA PcrX, some preliminary data were obtained in the last weeks, and further hypotheses remain to be tested. The data obtained especially concern a newly constructed PcrX knockout strain, for which 37 nucleotides (3 – 39 nt from TSS) of the PcrX sequence were deleted without inserting a resistance cassette (pLO1 protocol Supp. 2). The success

of the deletion was verified via Northern blot, and first growth analyses comparing the knockout mutant to the wild-type revealed a slightly enhanced growth of the mutant. The next steps using this strain will be to analyse the *puf* mRNA level. If the *puf* mRNA level is found be altered in the PcrX knockout strain, the knockout should be compensated by inserting a plasmid reintroducing PcrX. Using this complementation to potentially restore the wild-type situation will give an idea whether observed effects on the *puf* mRNA are solely due to the lack of the sRNA or due to changes in the genomic context of the *puf* operon by deleting the 37 nucleotides. For this purpose, a plasmid carrying an IPTG-inducible promoter (pSRK) is currently tested in *R. sphaeroides*. This plasmid could allow expression of PcrX in the knockout mutant to similar levels as in the wild-type. Having confirmed that the deletion of PcrX affects the photosynthesis genes on the posttranscriptional level and not by disturbing the genomic context, further potential targets such as *bchY* could be investigated in the new PcrX knockout mutant. Regarding additional PcrX targets, there is one previous finding to consider. In a study in 2011 by Berghoff and colleagues, PcrX was shown to be among the sRNAs bound to Hfq (Fig. 93). Even though a dependency on Hfq to bind the *pufX* mRNA part was not confirmed (Fig. 73), PcrX might be dependent on Hfq to bind other target mRNAs.

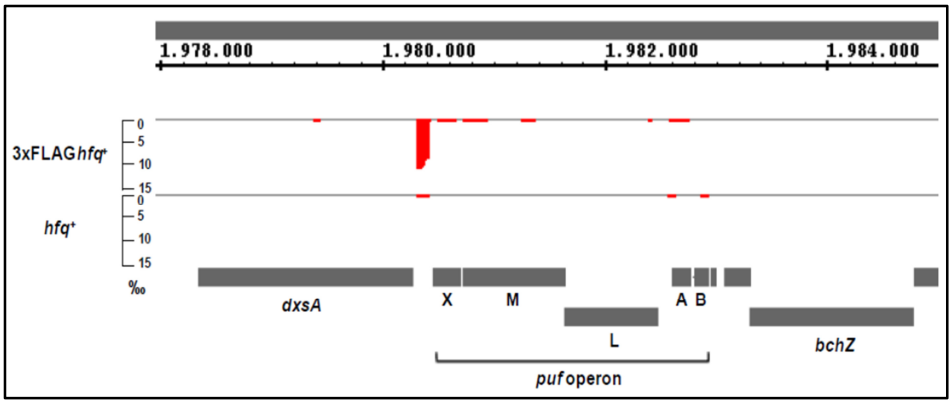

Figure 93: Interaction of PcrX with Hfq. The figure depicts a screenshot from the Integrated Genome Browser (IGB), showing the genetic context of the *puf* operon. Grey bars at the bottom represent ORFs on the (-) strand and running numbers at the top reflect the nucleotide position on the chromosome 1. Libraries for control coIP (2.4.1 hfq+) and for Hfq coIP (2.4.1 -3xFLAGhfq+) were loaded with cDNA reads visualised by red peaks. The scale on the left applies to normalised read numbers in ‰. The peak found in the IGR between *pufX* and *dxsA* corresponds to the PcrX sequence. Adapted from Berghoff *et al*., 2011.

4.3 Characterisation of the sRNA RSs0827

As summarised in the introduction to chapter 3.3 in the results part, RSs0827 was found to be induced upon iron limitation and later on was described to be expressed upon $^1O_2$ and heat stress from a RpoHI/HII-dependent promoter (Fig. 85).

4.3.1 Regulation of *rpoE* entailed by RSs0827

A microarray analysis comparing the RNA levels in the RSs0827 knockout mutant to those in the wild-type revealed several genes to be up- or down-regulated upon deletion of the RSs0827 gene (Fig. 84). Three of these genes were chosen as target candidates on the basis of their predicted interaction site (Tab. 54). So far the regulation of one of those target genes, *rpoE*, could be further characterised. An *in vivo* reporter assay using a translational *rpoE-lacZ* fusion showed a decrease of the fusions activity when RSs0827 was over-expressed, while in the RSs0827 knockout mutant the fusion showed increased activity (Fig. 86). Unfortunately, a compensatory mutant assay was again not successful to prove the direct interaction of RSs0827 and the *rpoE* mRNA. Reasons for the missing success with this kind of set-up are outlined in chapter 4.1.2 on the interaction study of Pos19 with RSP_0557. Once more an EMSA set-up was utilised to further verify the potential interaction between sRNA and mRNA. Incubating radio-labelled RSs0827 transcript with increasing amounts of cold *rpoE* transcript showed the assumed interaction resulting in a band shift (Fig. 89). The interaction was also weakened by adding cold RSs0827 transcript as a competitor (Fig. 90). Thereafter the direct interaction should be further proven by introducing mutations in the *in vitro* transcripts that disrupt the predicted binding site between RSs0827 and the *rpoE* mRNA.

Besides the three sRNAs DsrA, RprA, and ArcZ in *E. coli* positively affecting the translation of the alternative sigma factor RpoS, RSs0827 would represent one of the rare examples of sRNAs regulating an alternative sigma factor. The regulation of *rpoE* via RSs0827 could be valuable to keep the stress response from getting too exaggerated, especially under conditions where it is important to save cellular resources. It seems valid to have a fast and rather inexpensive regulatory factor that interferes with *rpoE*, in addition to the alternative sigma factor ChrR which depends on cost-intensive protein translation. One condition shown to harbour increased RSs0827 levels is the stationary phase, a condition also known to be characterised by increased ROS levels. During this phase, the *rpoE* expression is only slightly increased in the wild-type unless RSs0827 is deleted. In the RSs0827 knockout mutant, *rpoE* and consequently Pos19 were found to be up-regulated during the stationary phase (unpublished data of our group). Surprisingly a secondary effect upon changes in the RSs0827 level on Pos19 was not found during photo-oxidative stress. The only slight increase of *rpoE* and thereby no or only a mild stress response as seen in the wild-type seems to be favourable during the stationary phase, were cells starve and therefore cease growth and division. When increased ROS levels induce the expression of RSs0827 and simultaneously activate RpoE, while RSs0827 represses

rpoE, this regulatory circuit displays an incoherent feed-forward loop regarding the RpoE-dependent stress response. Moreover, the presence of ROS activates the alternative sigma factors RpoHI and RpoHII which in turn increase RSs0827 transcription (summarised in Fig. 94). In recent years many sRNAs were identified to act in regulatory coherent and incoherent feed-forward loops (Mank *et al*., 2013), such as PcrZ being activated by positive regulators of the photosynthesis genes (PrrA and FnrL) and in turn negatively affecting the photosynthesis genes (Mank *et al*., 2012). Or the sRNA RybB that is induced in a RpoE-dependent manner but negatively affects other RpoE-dependent genes in *E. coli* (Gogol *et al*., 2011). Taken together RSs0827 could display an additional regulatory factor in the cellular response to oxidative stress which especially acts during stationary phase, a condition that was in our group recently found to be quite heterogeneous and versatile in *R. sphaeroides*.

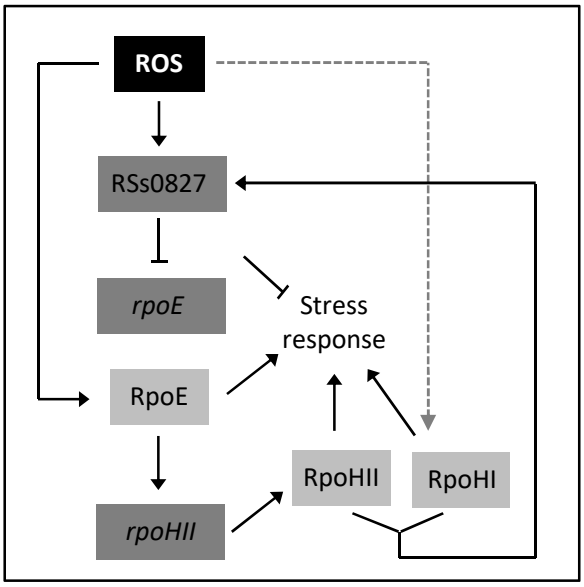

Figure 94: The incoherent feed-forward loop of RpoE regulation. The induction and activation of RSs0827 and RpoE via ROS and the resulting repression and activation of the stress defence are depicted. In addition the respective activation of RpoHII and RpoHI – the latter so far not elucidated as dotted grey arrow - via RpoE and ROS and the resulting activation of RSs0827 are shown. Genes are shown in dark grey, while the alternative sigma factors are shown in light grey.

5. Summary

The data obtained in the presented work again emphasise the importance of bacterial sRNA as regulators that fine-tune the metabolism and promote the stress defence upon changes in the environment (reviewed in Wagner and Romby, 2015). For the investigated model *R. sphaeroides*, a microorganism displaying a great metabolic versatility, many proteinaceous factors in the adaptation and response to environmental stimuli are known which mainly comprise receptors, transcription factors, and alternative sigma factors (described in 1.4, 1.6, 1.9.2, and 1.9.4). Since the discovery of a vast set of sRNAs in 2009 (Berghoff *et al*., 2009), the function of four of these sRNAs, namely PcrZ, CcsR1-4, SorY, and SorX, has been described (1.9.5), giving an even more detailed overview of the adaptation abilities of *R. sphaeroides*. In line with these descriptions, **the here investigated sRNAs Pos19, PcrX, and RSs0827** affect adaptive metabolic changes as well as the cells response in the defence against oxidative stress.

The sRNA Pos19 was found to affect pathways in the sulphur- and following glutathione (GSH) synthesis, by repressing a set of sulphur genes and the hypothetical protein RSP_0557. For the latter, a balanced expression seems to be required for a balanced cellular GSH pool. By means of these fine-tuning aspects of the sulphur metabolism that result in balanced cysteine and GSH levels, the RpoE-dependent sRNA Pos19 contributes to the refined response to oxidative stress. Additionally, Pos19 encodes a small peptide whose function so far remains enigmatic. Still, the survey concerning the peptide translation indicated that in *R. sphaeroides* the Shine-Dalgarno sequence is not essential for translation initiation, as it is known for other prokaryotes (Omotajo *et al*., 2015).

The sRNA PcrX was found to be encoded in and processed from the 3'UTR of the *puf* mRNA. In the last years more and more focus was put on 3'UTR derived sRNAs (reviewed in Miyakoshi *et al*., 2015). Interestingly, PcrX was found to regulate its parental mRNA via binding to the *pufX* part of the polycistronic mRNA. The obtained data hint towards the hypothesis that PcrX is involved in the segmental stability of the *puf* mRNA which is needed to ensure the translation of the encoded photosynthetic components in a stoichiometric amount. Another facet of the sRNA besides the "self-control" of its parental mRNA could be the regulation of additional genes. This idea is supported by the findings that the PcrX over-expression affects the mRNA levels of *bchN* and *bchY*, and that PcrX was found to be Hfq-bound, even though the effect on *pufX* seems to be independent of Hfq. Taken together, PcrX displays the second sRNA involved in the photosynthesis gene regulation of *R. sphaeroides* besides PcrZ.

Regarding the sRNA RSs0827, the newly obtained data strongly support the finding that the sRNA interacts with and thereby regulates the *rpoE* mRNA. Therefore RSs0827 could display a potential regulator that ensures the attenuation of the RpoE-dependent stress response under certain conditions. So far an effect of RSs0827 on the RpoE-dependent sRNA Pos19 could only be found during the stationary phase, but not during conditions of photo-oxidative stress.

6. Zusammenfassung

Die hier präsentierte Arbeit betont erneut die bereits häufig beschrieben Bedeutung von bakteriellen sRNAs als regulatorische Faktoren in der Stressantwort und der Adaption an Umwelteinflüsse (besprochen in Wagner and Romby, 2015). In dem betrachteten Modellorganismus *R. sphaeroides* sind in diesem Zusammenhang bisher vor allem Proteine mit regulatorischer Funktion bekannt. Diese umfassen Rezeptoren, Transkriptionsfaktoren, sowie alternative Sigma-Faktoren (beschrieben in 1.4, 1.6, 1.9.2 und 1.9.4). Seitdem im Jahr 2009 von Berghoff und Kollegen (Berghoff *et al*., 2009) eine Reihe von sRNAs in *R. sphaeroides* identifiziert wurden, konnte bereits für vier dieser sRNAs eine Funktion belegt werden (1.9.5). Darauf aufbauend konnten für die drei hier untersuchten sRNAs **Pos19, PcrX, und RSs0827**, Funktionen in der Regulation des Metabolismus und der oxidativen Stressantwort beschrieben werden.

Die sRNA Pos19 beeinflusst den Schwefel- und den darauf folgenden Glutathion (GSH) Metabolismus indem sie reprimierend auf eine Reihe von Genen aus den entsprechenden Stoffwechselwegen, sowie auf das hypothetische Protein RSP_0557, wirkt. Für letzteres scheint eine genau definierte Expression die Voraussetzung für ein ausgeglichenes GSH Level zu sein. Durch den Einfluss auf den Schwefel-, Cystein- und GSH-Metabolismus trägt die RpoE-abhängig exprimierte sRNA Pos19 so zur ausbalancierten Antwort auf oxidativen Stress bei. Des Weiteren kodiert Pos19 ein kleines Peptid, dessen Funktion bisher noch unbekannt bleibt. Die Untersuchungen bezüglich des Peptids haben allerdings gezeigt, dass in *R. sphaeroides* die Shine-Dalgarno Sequenz für die Initiation der Translation nicht zwingend notwendig ist. Ähnliche Beobachtungen sind bereits für weitere Prokaryoten beschrieben (Omotajo *et al*., 2015).

Die sRNA PcrX ist im 3'UTR der *puf* mRNA kodiert und wird aus der parentalen mRNA heraus prozessiert. In den letzten Jahren ist das Interesse an solchen in 3'- und 5'-UTRs kodierten sRNAs stetig gewachsen (besprochen in Miyakoshi *et al*., 2015). Bemerkenswerterweise deuten die gezeigten Daten darauf hin, dass PcrX den *pufX* Bereich der parentalen mRNA bindet und für die Prozessierung der *puf* mRNA eine Rolle spielt. Diese Prozessierung ist notwendig, um das stöchiometrische Verhältnis der durch die *puf* Gene kodierten Bestandteile des Photosyntheseappartes sicherzustellen. Neben dieser „Selbstkontrolle", scheint die Regulation weiterer Gene durch PcrX möglich zu sein, da die Überexpression von PcrX neben *pufX* auch weitere Gene wie *bchN* und *bchY* stark beeinflusst. Und obwohl die Regulation von *pufX* durch PcrX Hfq-unabhängig ist, wurde PcrX unter den sRNAs gefunden, die eine Bindung an Hfq aufgewiesen haben.

Für die sRNA RSs0827 konnten die gewonnen Daten die bereits vermutete Interaktion mit der *rpoE* mRNA nachweisen. Durch diese Interaktion könnte RSs0827 die RpoE-induzierte Stressantwort unter ausgewählten Bedingungen abschwächen. Ein Effekt von RSs0827 auf die RpoE-abhängige sRNA Pos19 wurde bisher aber lediglich in der stationären Phase gefunden.

References

Adnan, F, Weber, L, and Klug, G (2015) The sRNA SorY confers resistance during photo-oxidative stress by affecting a metabolite transporter in *Rhodobacter sphaeroides*. *RNA Biol*. **12(5):** 569-577

Altschul, SF, Madden, TL, Schäffer, AA, Zhang, J, Zhang, Z, Miller, W, and Lipman, DJ (1997) Gapped BLAST and PSI-BLAST: a new generation of protein database search programs. *Nucleic Acids Res*. **25:** 3389-3402

Alwine, JC, Kemp, DJ, and Stark, GR (1977) Method for detection of specific RNAs in agarose gels by transfer to diazobenzyloxymethyl-paper and hybridization with DNA probes. *Proc Natl Acad Sci USA.* **74(12):** 5350-5354

Andrews, SC, Robinson, AK, and Rodríguez-Quinones, F (2003) Bacterial iron homeostasis. *FEMS Microbiol Rev*. **27:** 215-237

Antelmann, H and Helmann, JD (2011) Thiol-Based Redox Switches and Gene Regulation. *Antioxid Redox Signal*. **14(6):** 1049–1063.

Anthony, JR, Warczak, KL, and Donohue, TJ (2004) A transcriptional response to singlet oxygen, a toxic byproduct of photosynthesis. *Proc Natl Acad Sci USA*. **102(18):** 6502-6507

Anthony, JR, Newman, JD, and Donohue, TJ (2005) Interactions Between the *Rhodobacter sphaeroides* ECF Sigma Factor, σE, and its Anti-sigma Factor ChrR. *J Mol Biol*. **341(2):** 345-360

Appleby, JL, Parkinso, JS and Bourret, RB (1996) Signal Transduction via the Multi-Step Phosphorelay: Not Necessarily a Road Less Traveled. *Cell*. **86(6):** 845–848

Aviv, T, Lin, Z, Lau, S, Rendl, LM, Sicheri, F, and Smibert, CA (2003) The RNA-binding SAM domain of Smaug defines a new family of post-transcriptional regulators. *Nat Struct Biol*. **10(8):** 614-621

Bagg, A, and Neilands, JB (1987) Ferric uptake regulation protein acts as a repressor, employing iron(II) as a cofactor to bind the operator of an iron transport operon in *Escherichia coli*. *Biochemistry.* **26:** 5471-5477

Bai, L, Xie, T, Hu, Q, Deng, C, Zheng, R, and Chen, W (2015) Genome-wide comparison of ferritin family from Archea, Bacteria, Eukarya, and Viruses: its distribution, characteristic motifs, and phylogenetic relationship. *Sci Nat*. **102:** 64. doi:10.1007/s00114-015-1314-3

Bateman, A, Coin, L, Durbin, R, Finn, RD, Hollich, V, *et al*. (2004) The Pfam protein families database. *Nucleic Acids Res*. **32:** D138–141

Béjà, O, Aravind, L, Koonin, EV, Suzuk, MT, Hadd, A, Nguyen, LP, Jovanovich, SB, Gates, CM, Feldman, RA, Spudich, JL, Spudich, EN and DeLong, EF (2000) Bacterial Rhodopsin: Evidence for a New Type of Phototrophy in the Sea. *Science*. **289(5486):** 1902-1906

Belasco, JG, Beatty, JT, Adams, CW, von Gabain, A, and Cohen, SN (1985) Differential expression of photosynthesis genes in *R. capsulata* results from segmental differences in stability within the polycistronic *rxcA* transcript. *Cell*. **40(1):** 171-181

Berghoff, BA, Glaeser, J, Sharma, CM, Vogel, J, and Klug, G (2009) Photooxidative stress-induced and abundant small RNAs in Rhodobacter sphaeroides.*Mol Microbiol*. **74(6):** 1497-1512

Berghoff, BA, Glaeser, J, Sharma, CM, Zobawa, M, Lottspeich, F, Vogel, J, and Klug, G (2011) Contribution of Hfq to photooxidative stress resistance and global regulation in *Rhodobacter sphaeroides*. *Mol Microbiol*. **80(6):** 1479-1495

Betteridge, DJ (2000) What is oxidative stress? *Metabolism* **49:** 3-8

Bignucolo, A, Appanna, VP, Thomas, SC, Auger, C, Han, S, Omri, A, and Appanna, VD (2013) Hydrogen peroxide stress provokes a metabolic reprogramming in *Pseudomonas fluorescens*: enhanced production of pyruvate. *J Biotechnol*. **167:** 309-315

Billenkamp, F, Peng, T, Berghoff, BA, and Klug, G (2015) A cluster of four homologous small RNAs modulates C1 metabolism and the pyruvate dehydrogenase complex in *Rhodobacter sphaeroides* under various stress conditions. *J Bacteriol*. **197(10):** 1839-1852

Birnboim HC, and Doly, J (1979) A rapid alkaline extraction procedure for screening recombinant plasmid DNA. *Nucleic Acids Res*. **7(6):** 1513-1523

Bradford, MM (1976) A Rapid and Sensitive Method for the Quantitation of Microgram Quantities of Protein Utilizing the Principle of Protein-Dye Binding. *Analytical Biochemistry*. **72:** 248-254

Brantl, S (2007) Metal sensing by RNA in bacteria: exception or rule? *ACS Chem Biol*. **2(10):** 656-660

Briggs, WR, Beck, CF, Cashmore, AR, Christie, JM, Hughes, J, Jarillo, JA, Kagawa, T, Kanegae, H, Liscum, E, Nagatani, A, Okada, K, Salomon, M, Rudiger, W, Sakai, T, Takano, M, Wada, M and Watson, JC (2001) The phototropin family of photoreceptors. *Plant Cell*. **13:** 993–997

Bryant, DA and Frigaard, N (2006) Prokaryotic photosynthesis and phototrophy illuminated. *Trends in Microbiology*. **14(11):** 488-496

Busch, A, Richter, AS, and Backofen, R (2008) IntaRNA: efficient prediction of bacterial sRNA targets incorporating target site accessibility and seed regions. *Bioinformatics*. **24(24):** 2849-2856

Cabiscol, E, Tamarit, J, and Ros, J (2000) Oxidative stress in bacteria and protein damage by reactive oxygen species*. Int Microbiol*. **3(1):** 3-8

Cadet, J (1994) DNA damage caused by oxidation, deamination, ultraviolet radiation and photoexcited psoralens. *IARC Sci Publ*. **125:** 245-276

Cadet, J, Berger, M, Douki, T, and Ravanat, JL (1997) Oxidative damage to DNA: formation, measurement, and biological significance. *Rev Physiol Biochem Pharmacol*. **131:** 1-87

Cadet, J, Delatour, T, Douki, T, Gasparutto, D, Pouget, JP, Ravanat, JL, and Sauvaigo, S (1999) Hydroxyl radicals and DNA base damage. *Mutat Res*. **424(1-2):** 9-21

Cartron, ML, Olsen, JD, Sener, M, Jackson, PJ, Brindley, AA, Qian, P, Dickman, MJ, Leggett, GL, Schulten, K, and Hunter, CN (2014) Integration of energy and electron transfer processes in the photosynthetic membrane of *Rhodobacter sphaeroides*. *Biochimica et Biophysica Acta*. **1837:** 1769-1780

Caron, MP, Bastet, L, Lussier, A, Simoneau-Roy, M, Masse, E, and Lafontaine, DA (2012) Dual-acting riboswitch control of translation initiation and mRNA decay. *Proc Natl Acad Sci USA*. **109:** E3444–E3453

Castenholz, RW and Garcia-Pichel, F (2000) Cyanobacterial responses to UV-radiation. In "The ecology of cyanobacteria". Kluwer Academic Publishers, Boston, Mass. 591-611

Caswell, CC, Oglesby-Sherrouse, AG, and Murphy, ER (2014) Sibling rivalry: related bacterial small RNAs and their redundant and non-redundant roles. *Front Cell Infect Microbiol*. doi: 10.3389/fcimb.2014.00151.

Celesnik, H, Deana, A, and Belasco, JG (2007) Initiation of RNA decay in *Escherichia coli* by 5' pyrophosphate removal. *Mol Cell*. **27(1):** 79-90

Chen, CY, Beatty, JT, Cohen, SN, and Belasco, JG (1988) An intercistronic stem-loop structure functions as an mRNA decay terminator necessary but insufficient for *puf* mRNA stability. *Cell*. **52(4): 609-619**

Cheng, Z, Wu, J, Setterdahl, A, Reddie, K, Carroll, K, Hammad, LA, Karty, JA and Bauer, CE (2012) Activity of the tetrapyrrole regulator CrtJ is controlled by oxidation of a redox active cysteine located in the DNA binding domain. *Mol Microbiol*. **85(4):**734-46

Cheng, Z, Li, K, Hammad, LA, Karty, JA, and Bauer, CE (2014) Vitamin B12 regulates photosystem gene expression via the CrtJ antirepressor AerR in *Rhodobacter capsulatus*. *Mol Microbiol.* **91:** 649–664

Cho, HS, Schotte, F, Dashdorj, N, Kyndt, J, Henning, R, and Anfinrud, PA (2016) Picosecond Photobiology: Watching a Signaling Protein Function in Real Time via Time-Resolved Small- and Wide-Angle X-ray Scattering. *J Am Chem Soc*. **138(28):** 8815-8823

Choudhary, M, and Kaplan, S (2000) DNA sequence analysis of the photosynthesis region of *Rhodobacter sphaeroides* 2.4.1. *Nucleic Acids Res*. **28(4):** 862-867

Choudhary, M, Fu, YX, Mackenzie, C, and Kaplan, S (2004) DNA sequence duplication in *Rhodobacter sphaeroides* 2.4.1: evidence of an ancient partnership between chromosomes I and II. *J Bacteriol.* **186(7):** 2019-2027

Clayton, RK (1966) The bacterial photosynthetic reaction center. *Brookhaven Symp Biol*. **19:** 62-70

Cogdell, RJ, Howard, TD, Bittl, R, Schlodder, E, Geisenheimer, I, and Lubitz, W (2000) How carotenoids protect bacterial photosynthesis. *Philos Trans R Soc Lond B Biol Sci*. **355(1402):** 1345-1349

Cogdell, RJ and Roszak, AW (2014) Structural biology: The purple heart of photosynthesis. *Nature*. **508:** 196-197

Comayras, F, Jungas, C and Lavergne, J (2005) Functional Consequences of the organization of the Photosynthetic Aparatus in *Rhodobacter sphaeroides* II. A Study of PufX$^-$ Membranes. *The Journal of Biological Chemistry*. **280:** 11214-11223

Condon, C (2007) Maturation and degradation of RNA in bacteria. *Current Opinion Microbiol* **10(3):** 271-278

Crack, JC, Green, J, Thomson, AJ and Le Brun, NE (2014): Iron-Sulfur Clusters as Biological Sensors: The Chemistry of Reactions with Molecular Oxygen and Nitric Oxide. *Acc. Chem. Res.* **47(10):** 3196–3205

Crofts, AR and Wraight, CA (1983) The electrochemical domain of photosynthesis. Biochim Biophys Acta. **726:** 149–186

Damm, K, Bach, S, Müller, KM, Klug, G, Burenina, OY, Kubareva, EA, Grünweller, A, and Hartmann, RK (2015) Impact of RNA isolation protocols on RNA detection by Northern blotting. *Methods Mol Biol*. **1296:** 29-38

Dangel, AW, and Tabita, FR (2009) Protein-protein interactions between CbbR and RegA (PrrA), transcriptional regulators of the cbb operons of *Rhodobacter sphaeroides*. *Mol Microbiol.* **71(3):** 717-729

De Grey, A and Rae, M (2007) Ending Aging, St. Martin's Griffin, New York, NY, USA, 2007

Deana, A and Belasco, JG (2005) Lost in translation: the influence of ribosomes on bacterial mRNA decay. *Genes Dev* **19(21):** 2526-2533

Deana, A, Celesnik, H, and Belasco, JG (2008) The bacterial enzyme RppH triggers messenger RNA degradation by 5' pyrophosphate removal. *Nature*. **451(7176):** 355-358

Demple, B and Harrison, L (1994) Repair of oxidative damage to DNA: enzymology and biology. *Annu Rev Biochem*. **63:** 915-948

Desnoyers, G, Morissette, A, Prévost, K, and Massé, E (2009) Small RNA-induced differential degradation of the polycistronic mRNA *iscRSUA*. *EMBO J*. **28(11):** 1551–1561

Desnoyers, G, Bouchard, M and Massé, E (2013) New insights into small RNA-dependent translational regulation in prokaryotes. *Trends Genet* **29(2):** 92-98

Devasagayam, TPA and Kamat, JP (2002) Biological significance of singlet oxygen. Indian Journal of Experimental Biology. **40:** 680-692

Di Mascio, P, Kaiser, S and Sies, H (1989) Lycopene as the Most Efficient Biological Carotenoid Singelt Oxygen Quencher. *Biochem and Biophys.* **274(2):** 532-538

Domingues, S, Moreira, RN, Andrade, JM, Dos Santos, RF, Bária, C, Viegas, SC, and Arraiano, CM (2015) The role of RNase R in trans-translation and ribosomal quality control. *Biochimie*. **114:** 113-118

Drews, G, and Golecki, JR (1995) in *The Anoxygenic Photosynthetic Bacteria* (Blankenship, RE, Madigan, MT, and Bauer, CE, eds), **pp.** 231–257, Kluwer Press

Dufour, YS, Landick, R, and Donohue, TJ (2008) Organization and Evolution of the Biological Response to Singlet Oxygen Stress. *J Mol Biol*. **383(3):** 713-730

Dufour, YS, Kiley, PJ, and Donohue, TJ (2010) Reconstruction of the core and extended regulons of global transcription factors. *PLoS Genet*. **6(7):** e1001027

Dühring, U, Axmann, IM, Hess, WR, and Wilde, A (2006) An internal antisense RNA regulates expression of the photosynthesis gene isiA. Proc Natl Acad Sci USA. **103(18):** 7054–7058

Dunlap, PV (1999) Quorum sensing of Luminescence in *Vibrio fisheri. J Molec Micobiol Biotechnol* **1(1)**: 5-12

Eggenhofer, F, Tafer, H, Stadler, PF, and Hofacker, IL (2011) RNApredator: fast accessibility-based prediction of sRNA targets. *Nucl Acids Res*. doi:10.1093/nar/gkr467

Ellman, GL (1959) Tissue Sulfhydryl Groups. *Archives of Biochemistry and Biophysics*. **82:** 70-77

Elsen, S, Ponnampalam, SN, and Bauer, CE (1998) CrtJ bound to distant binding sites interacts cooperatively to aerobically repress photopigment biosynthesis and light harvesting II gene expression in *Rhodobacter capsulatus*. *J Biol Chem.* **273:** 30762–30769

Emery, P, So, WV, Kaneko, M, Hall, JC and Rosbash, M (1998) CRY, a Drosophila Clock and Light-Regulated Cryptochrome, Is a Major Contributor to Circadian Rhythm Resetting and Photosensitivity. *Cell*. **95(5):** 669-679

Eraso, JM, and Kaplan, S (1995) Oxygen-insensitive synthesis of the photosynthetic membranes of *Rhodobacter sphaeroides*: a mutant histidine kinase. *J Bacteriol*. **177(10):** 2695-2706

Eraso, JM, Roh, JH, Zeng, X, Callister, SJ, Lipton, MS, and Kaplan, S (2008) Role of the global transcriptional regulator PrrA in *Rhodobacter sphaeroides* 2.4.1: combined transcriptome and proteome analysis. *J Bacteriol.* **190(14):** 4831-4848

Fantappie, L, Metruccio, MM, Seib, KL, Oriente, F, Cartocci, E, Ferlicca, F, Giuliani, MM, Scarlato, V, and Delany, I (2009) The RNA chaperone Hfq is involved in stress response and virulence in *Neisseria* menengitidis and is a pleiotropic regulator of gene expression. *Infect Immun*. **77:** 1842-1853

Farchaus, JW, Barz, WP, Grünberg, H and Oesterhelt, D (1992) Studies on the expression of the pufX polypeptide and its requirement for photoheterotrophic growth in *Rhodobacter sphaeroides*. *EMBO J*. **11:** 2779–2788

Fenton, HJH (1894). Oxidation of tartaric acid in presence of iron. *J. Chem. Soc*., Trans. **65(65):** 899–911

Finkel, JM, Pittillo, RF, and Mellett, LB (1971) Fluorometric and Microbiological Assays for Rifampicin and the Determination of Serum Levels in the Dog. *Chemotherapy*. **16:** 380–388

Finn, RD, Coggill, P, Eberhardt, RY, Eddy, SR, Mistry, J, Mitchell, AL, Potter, SC, Punta,M, Qureshi, M, Sangrador-Vegas, A, Salazar,GA, Tate, J, and Bateman, A (2016) The Pfam protein families database: towards a more sustainable future. *Nucleic Acids Res*. Database Issue **44:** D279-D285

Flint, DH, Tumninello, JF and Emptage, MH (1993) The inactivation of Fe-S cluster containing hydro-lyases by superoxide*. J. Biol. Chem*. **268:** 22369-22376

Fozo, EM (2012) New type I toxin-antitoxin families from "wild" and laboratory strains of *E. coli*: Ibs-Sib, ShoB-OhsC and Zor-Orz. *RNA Biol*. **9(12):** 1504-1512

Francia, F, Wang, J, Venturoli, G, Melandri, BA, Barz, WP, and Oesterhelt, D (1999) The reaction center-LH1 antenna complex of *Rhodobacter sphaeroides* contains one PufX molecule which is involved in dimerization of this complex. *Biochemistry*. **38(21):** 6834-6845

Frank, HA and Christensen, RL (1995) Singlet Energy Transfer from Carotenoids to Bacteriochlorophylls. *Anoxygenic Photosynthetic Bacteria.* Kluwer Academic Publisher pp. 373- 384

Frank, HA, Young, AJ, Britton, G, and Cogdell, RJ (1999) The Photochemistry of Carotenoids. *Advances in Photosynthesis and Respiration*. **Vol. 8**

Franze de Fernandez, MT, Eoyang, L, and Auguts, JT (1986) Factor fraction required for the synthesis of bacteriophage Qß-RNA. *Nature*. **219:** 588-590

Fried, L, Lassak, J, and Jung, K (2012) A comprehensive toolbox for the rapid construction of *lacZ* fusion reporters. *J Microbiol Methods*. **91(3):** 537-543

Frigaard, N, Gomez Maqueo Chew, A, Li, H, Maresca, JA and Bryant, DA (2003) Chlorobium tepidum : insights into the structure, physiology, and metabolism of a green sulfur bacterium derived from the complete genome sequence. *Photosynth Research.* **78:** 93–117

Fritsch, J, Rothfuchs, R, Rauhut, R, and Klug, G (1995) Identification of an mRNA element promoting rate-limiting cleavage of the polycistronic puf mRNA in Rhodobacter capsulatus by an enzyme similar to RNase E. *Molecular Microbiology*. **15:** 1017-1029

Gautheret D, Lambert A. (2001) Direct RNA Motif Definition and Identification from Multiple Sequence Alignments using Secondary Structure Profiles. *J Mol Biol.* **313**:1003–11

Geer, LY, Marchler-Bauer, A, Geer, RC, Han, L, He, J, He, S, Liu, C, Shi, W, and Bryant, SH (2010) The NCBI BioSystems database. *Nucleic Acids Res*. **38**(Database issue): D492-496

Geisselbrecht, Y, Frühwirth, S, Schröder, C, Pierik, AJ, Klug, G, and Essen, LO (2012) CryB from *Rhodobacter sphaeroides*: a unique class of cryptochromes with novel cofactors. *EMBO Rep*. **13:** 223–229

Geng, J, Song, Y, Yang, L, Qiu, Y, Li, G, Guo, J, Bi, Y, Qu, Y, Wang, W, Wnag, X, Guo, Z, Yang, R, and Han, Y (2009) Involvement of the post-transcriptional regulator Hfq in *Yerinsia pestis* virulence. *Plos One*. **4:** e6213

Gil, R, Silva, FJ, Peretó, J, and Moya, A (2004) Determination of the core of a minimal bacterial gene set. *Microbiol Mol Biol Rev*. **68(3):** 518-537

Gimpel, M, and Brantl, S (2016) Dual-function sRNA encoded peptide SR1P modulates moonlighting activity of *B. subtilis* GapA. *RNA Biol*. **13(9):** 916-926

Glaeser, J, Zobawa, M, Lottspeich, F, and Klug, G (2007) Protein synthesis patterns reveal a complex regulatory response to singlet oxygen in *Rhodobacter*. *J Proteome Res.* **6(7):** 2460-2471

Glaeser, J, Nuss, AM, Berghoff, BA, and Klug, G (2011) Singlet oxygen stress in microorganisms. *Adv Microb Physiol*. **58:** 141-173

Gomelsky, M and Klug, G (2002) BLUF: a novel FAD-binding domain involved in sensory transduction in microorganisms. *Trends Biochem Sci.* **27(10):** 497-500

Gomelsky, L, Moskvin, OV, Stenzel, RA, Jones, DF, Donohue, TJ, and Gomelsky, M (2008) Hierarchical regulation of photosynthesis gene expression by the oxygen-responsive PrrBA and AppA-PpsR systems of *Rhodobacter sphaeroides*. *J Bacteriol*. **190:** 8106–8114

Gogol, EB, Rhodius, VA, Papenfort, K, Vogel, J, and Gross, CA (2011) Small RNAs endow a transcriptional activator with essential repressor functions for single-tier control of a global stress regulon. *Proc Natl Acad Sci USA*. **108(31):** 12875-12880

Göpel, Y, Khan, MA, and Görke, B (2014) Ménage à trois: post-transcriptional control of the key enzyme for cell envelope synthesis by a base-pairing small RNA, an RNase adaptor protein, and a small RNA mimic. *RNA Biol*. **11(5):** 433-442

Gottesman, S (2005) Micros for microbes: non-coding regulatory RNAs in bacteria. *Trends Genet*. **21:** 399–404

Gottesman, S, and Storz, G (2011) Bacterial small RNA regulators: versatile roles and rapidly evolving variations. *Cold Spring Harb Perspect Biol*. **3(12)**

Guo, MS, and Gross, CA (2014) Stress-induced remodeling of the bacterial proteome. *Curr Biol*. **24(10):** R424-434

Gough, SP, Petersen, BO, and Duus, JO (2000) Anaerobic chlorophyll isocyclic ring formation in *Rhodobacter capsulatus* requires a cobalamin cofactor. *Proc Natl Acad Sci USA***. 97(12):** 6908-6913

Green, J and Paget, MS (2004) Bacterial redox sensors. *Nature Reviews Microbiology.* **2:** 954-966
Green, HA, and Donohue, TJ (2006) Activity of *Rhodobacter sphaeroides* RpoHII, a second member of the heat shock sigma factor family. *J Bacteriol*. **188(16):** 5712-5721

Gregor, J and Klug, G (1999) Regulation of bacterial photosynthesis genes by oxygen and light. *FEMS Microbiol Lett*. **179:** 1–9

Griffiths, M, Sistrom, WR, Cohen-Bazire, G, and Stanier, RY (1955) Function of carotenoids in photosynthesis. *Nature*. **176:** 1211-1214

Han, Y, Braatsch, S, Osterloh, L, and Klug, G (2004) A eukaryotic BLUF domain mediates light-dependent gene expression in the purple bacterium *Rhodobacter sphaeroides* 2.4.1. *Proc Natl Acad Sci U S A.* **101(33):** 12306-12311

Han, Y, Meyer, MH, Keusgen, M and Klug G (2007) A haem cofactor is required for redox and light signalling by the AppA protein of *Rhodobacter sphaeroides*. *Mol Microbiol.* **64(4):** 1090-1104

Hartmann, G, Honikel, KO, Knüsel, F, and Nüesch, J (1967) The specific inhibition of the DNA-directed RNA synthesis by rifamycin. *Biochim Biophys Acta*. **145(3):** 843-844

Heck, C, Rothfuchs, R, Jäger, A, Rauhut, R, and Klug, G (1996) Effect of the *pufQ-pufB* intercistronic region on *puf* mRNA stability in *Rhodobacter capsulatus*. *Molecular Microbiology*. **20:** 1165-1178

Heck, C, Balzer, A, Fuhrmann, O, and Klug, G (2000) Initial events in the degradation of the polycistronic *puf* mRNA in *Rhodobacter capsulatus* and consequences for further processing steps. *Molecular Microbiology*. **35:** 90-100

Hendrischk, AK, Braatsch, S, Glaeser, J, and Klug, G (2007) The *phrA* gene of *Rhodobacter sphaeroides* encodes a photolyase and is regulated by singlet oxygen and peroxide in a sigma(E)-dependent manner. *Microbiology*. **153(Pt 6):** 1842-1851

Heym, B, Zhang, Y, Poulet, S, Young, D and Cole, ST (1993) Characterization of the katG gene encoding a catalase-peroxidase required for the isoniazid susceptibility of Mycobacterium tuberculosis. *J Bacteriol.* **175(13):** 4255-4259

Hillion, M and Antelmann, H (2015) Thiol-based redox switches in prokaryotes. *Biol Chem.* **396(5):** 415–444.

Hoch, PG, Burenina, OY, Weber, MH, Elkina, DA, Nesterchuk, MV, Sergiev, PV, Hartmann, RK, and Kubareva, EA (2015) Phenotypic characterization and complementation analysis of Bacillus subtilis 6S RNA single and double deletion mutants. *Biochimie*. **117:** 87-99

Hoch, PG, Schlereth, J, Lechner, M, and Hartmann, RK (2016) *Bacillus subtilis* 6S-2 RNA serves as a template for short transcripts *in vivo*. *RNA*. **22(4):** 614-622

Hofacker IL, Fontana W, Stadler PF, Bonhoeffer LS, Tacker M and Schuster P. (1994) Fast Folding and comparison of RNA secondary structures. *Monastch. Chem.*, **125**:167-188

Holden-Dye, K, Crouch, LI and Michael, RJ (2008) Structure, function and interactions of the PufX protein. *Biochimica et Biophysica Acta (BBA) – Bioenergetics*. **1777(7–8):** 613–630

Hollands, K, Proshkin, S, Sklyarova, S, Epshtein, V, Mironov, A, Nudler, E, and Groisman, EA (2012) Riboswitch control of Rho-dependent transcription termination. *Proc Natl Acad Sci USA*. **109:** 5376–5381

Hübner, P, Willison, JC, Vignais, PM, and Bickle, TA (1991) Expression of regulatory *nif* genes in *Rhodobacter capsulatus*. *J Bacteriol*. **173(9):** 2993-2999

Hughes, J, Lamparte, T, Mittmann, F, Hartmann, E, Gärtner, W, Wilde, A and Börner, T(1997) A prokaryotic phytochrome. *Nature*. **386:** 663

Hunter, N, Daldal, F, Thurnauer, MC, Beatty, JT, Willows, RD, and Kriegel, AM (2009) Biosynthesis of bacteriochlorophylls in purple bacteria. In *The Purple Phototrophic Bacteria, advances in photosynthesis and respiration* (eds Hunter, N, Daldal, F, Thurnauer, MC, Beatty, JT), pp. 57–79 Berlin, Germany: Springer Science+Business Media BV

Halliwell, B, and Gutteridge, JMC (2006) Free Radicals in Biology and Medicine. Oxford University Press

Imam, S, Noguera, DR, and Donohue, TJ (2014) Global Analysis of Photosynthesis Transcriptional Regulatory Networks. *PLoS Genet*. **10(12):** e1004837

Imhoff, J (2001) The phototrophic alpha-proteobacteria. The prokaryotes: An evolving electronic resource for the microbiological community. M. Dwerkins

Imlay, JA and Linn, S (1988) DNA damage and Oxygen Radical Toxicity. *Science*. **240(4852):**640-642

Imlay, JA (2003) Pathways of oxidative damage. *Annu. Rev. Microbiol*. **57:** 395–418

Imlay, JA (2008) Cellular defenses against superoxide and hydrogen peroxide. *Annu Rev Biochem.* **77:** 755–776

Ioannou, C, Schaeffer, PM, Dixon, NE, and Soultanas, P (2006) Helicase binding to DnaI exposes a cryptic DNA-binding site during helicase loading in Bacillus subtilis. *Nucleic Acids Res*. **34(18):** 5247-5258

Irazusta, V, Cabiscol, E, Reverter-Branchat, G, Ros, J, and Tamarit, J (2006) Manganese is the link between frataxin and iron-sulfur deficiency in the yeast model of Friedreich ataxia. *J Biol Chem*. **281(18):** 12227-12232

Iseki, M, Matsunaga, S, Murakami, A, Ohno, K, Shiga, K, Yoshida, K, Sugai, M, Takahashi, T, Hori, T and Watanabe, M (2002) A blue-light-activated adenylyl cyclase mediates photoavoidance in *Euglena gracilis*. *Nature*. **415(6875):** 1047-1051

Jacobs, AT and Marnett, LJ (2010) Systems analysis of protein modification and cellular responses induced by electrophile stress. *Acc Chem Res*. **43(5):** 673-683

Jaubert, M, Zappa, S, Fardoux, J, Adriano, JM, Hannibal, L, Elsen, S, Lavergne, J, Verméglio, A, Giraud, E, and Pignol, D (2004) Light and redox control of photosynthesis gene expression in *Bradyrhizobium*: dual roles of two PpsR. *J Biol Chem*. **279:** 44407–44416

Jensen, RB, Wang, SC and Shapiro, L (2002) Dynamic localization of proteins and DNA during a bacterial cell cycle. *Nature Reviews Molecular Cell Biology*. **(3):** 167-176

Jimenez, RM, Polanco, JA, and Lupták, A (2015) Chemistry and Biology of Self-Cleaving Ribozymes. *Trends in Biochemical Science*. **40(11):** 648-661

Casal, JJ (2013) Photoreceptor Signaling Networks in Plant Response to Shade. *Annu. Rev. Plant Biol*. **64:** 403–27

Kammler, M, Schon, C, and Hantke, K (1993) Characterization of the ferrous iron uptake system of *Escherichia coli*. *J Bacteriol*. **175:** 6212-6219

Kawamoto, H, Koide, Y, Morita, T, and Aiba, H (2006) Base-pairing requirement for RNA silencing by a bacterial small RNA and acceleration of duplex formation by Hfq. *Mol Microbiol*. **61(4):** 1013-1022

Kawano, M, Reynolds, AA, Miranda-Rios, J, and Storz,G (2005) Detection of 5'- and 3'-UTR-derived small RNAs and cis-encoded antisense RNAs in *Escherichia coli*. *Nucleic Acids Res*. **33(3):** 1040–1050

Kehrer, JP (2000) The Haber–Weiss reaction and mechanisms of toxicity. *Toxicology*. **149(1):** 43–50

Keen, NT, Tamaki, S, Kobayashi, D, and Trollinger, D (1988) Improved broad-host-range plasmids for DNA cloning in gram-negative bacteria. *Gene*. **70:** 191–197

Kelley, LA, Mezulis, S, Yates, CM, Wass, MN, and Sternberg, MJE (2015) The Phyre2 web portal for protein modeling, prediction and analysis. *Nature Protocols*. **10:** 845-858

Kim, MJ, Ciani, S, and Schachtman, DP (2010) A peroxidase contributes to ROS production during Arabidopsis root response to potassium deficiency. *Mol Plant.* **3(2):** 420-427

Kingsford, C, Ayanbule, K, and and Salzberg, SL (2007) Rapid, accurate, computational discovery of Rho-independent transcription terminators illuminates their relationship to DNA uptake. *Genome Biology*. **8:** R22

Klug, G, Adams, CW, Belasco, J, Doerge, B, and Cohen, SN (1987) Biological consequences of segmental alterations in mRNA stability: effects of deletion of the intercistronic hairpin loop region of the *Rhodobacter capsulatus puf* operon. *The EMBO Journ*. **6:** 3515-3520

Klug, G, and Cohen, SN (1990) Combined actions of multiple hairpin loop structures and sites of rate-limiting endonucleolytic cleavage determine differential degradation rates of indicidual segments within polycistronic *puf* operon mRNA. *JBac*. **172:** 5140-5146

Klug, G (1991) Endonucleolytic cleavage of puf mRNA in Rhodobacter capsulatus is influenced by oxygen. *Proc Acad Natl Science USA*. **88:** 1765-1769

Köster, W (2001) ABC transporter-mediated uptake of iron, siderophores, heme and vitamin B_{12}. *Res Microbol*. **152:** 291-301

Kovach, ME, Elzer, PH, Hill, DS, Robertson, GT, Farris, MA, Roop, RM, *et al*. (1995) Four new derivatives of the broad-host-range cloning vector pBBR1MCS, carrying different antibiotic-resistance cassettes. *Gene*. **166(1):** 175-176

Kramer, P, Gabel, K, Pfeiffer, F, and Soppa, J (2014) Haloferax volcanii, a prokaryotic species that does not use the Shine Dalgarno mechanism for translation initiation at 5'-UTRs. *PLoS One*. **9(4):** e94979

Laguri, C, Phillips-Jones, MK and Williamson, MP (2003) Solution structure and DNA binding of the effector domain from the global regulator PrrA (RegA) from *Rhodobacter sphaeroides*: insights into DNA binding specificity. *Nucleic Acids Res*. **31(23):** 6778–6787

Laemmli, UK (1970) Cleavage of structural proteins during the assembly of the head of bacteriophage T4. Nature. **227:** 680–68

Lalaouna, D, Simoneau-Roya, M, Lafontaine, D and Massé, E (2013) Regulatory RNAs and target mRNA decay in prokaryotes. *Biochimica et Biophysica Acta - Gene Regulatory Mechanisms*. **1829(6–7):** 742–747

Lane, N (2002) Oxygen, the Molecule That Made the World. Oxford University Press, Oxford

Lanyi, JK (2004) Bacteriorhodopsin. *Annual Review of Physiology*. **66:** 665-688

Lascelles, J, and Hatch, TP (1969) Bacteriochlorophyll and heme synthesis in *Rhodopseudomonas spheroides*: possible role of heme in regulation of the branched biosynthetic pathway. *J Bacteriol*. **98(2):** 712-720

Latifi, A, Jeanjean, R, Lemeille, S, Havaux, M, and Zhang, CC (2005) Iron starvation leads to oxidative stress in *Anabaena sp*. strain PCC 7120. *J Bacteriol*. **187:** 6596–6598

Lee, JK, DeHoff, BS, Donohue, TJ, Gumport, RI, and Kaplan, S (1989) Transcriptional analysis of *puf* operon expression in *Rhodobacter sphaeroides* 2.4.1 and an intercistronic transcription terminator mutant. *J Biol Chem*. **264(32):** 19354-19365

Lee, K, Bernstein, JA, and Cohen, SN (2002) RNase G complementation of rne null mutation identifies functional interrelationships with RNase E in *Escherichia coli*. *Mol Microbiol*. **43:** 1445–1456

Lemire, JA, Harrison, JJ, and Turner, RJ (2013) Antimicrobial activity of metals: mechanisms, molecular targets and applications. *Nature Reviews Microbiology*. Published online: 13 May 2013

Lenz, O, Schwartz, E, Dernedde, J, Eitinger, M, and Friedrich, B (1994) The *Alcaligenes eutrophus* H16 *hoxX* Gene Participates in Hydrogenase Regulation. *J Bacteriol*. **176(14):** 4385-4393

Lesnik EA et al. (2001) Prediction of rho-independent transcriptional terminators in Escherichia coli. *Nucleic Acids Research*, **29:** 3583-3594

Li, W, Bottrill, AR, Bibb, MJ, Buttner, MJ, Paget, MS and Kleanthous, C (2003) The Role of zinc in the disulphide stress-regulated anti-sigma factor RsrA from *Streptomyces coelicolor. J Mol Biol.* **333(2):** 461-472

Lilburn, TG, Haith, CE, Prince, RC and Beatty, JT (1992) Pleiotropic effects of pufX gene deletion on the structure and function of the photosynthetic apparatus of *Rhodobacter capsulatus*. *Biochim Biophys Acta.* **1100:** 160–170

Lill, R (2009) Function and biogenesis of iron-sulphur proteins. *Nature* **460**: 831-838

Lim, B, Minji, S, Lee, H, Hyun, S, Lee, Y, Hahn, Y, Shin, E, and Lee, K (2015) Regulation of *Escherichia coli* RNase III activity. *Journ of Microbiol*. **53(8):** 487-494

Lin, C (2002) Blue Light Receptors and Signal Transduction. *Plant Cell*. **14**(Suppl): s207–s225

Liu, MY, Gui, G, Wei, B, Preston, JF 3rd, Oakford, L, Yüksel, U, Giedroc, DP, and Romeo, T (1997) The RNA molecule CsrB binds to the global regulatory protein CsrA and antagonizes its activity in Escherichia coli. *J Biol Chem*. **272(28):** 17502-17510

Lloyd, DR, Phillips, DH and Carmichael, PL (1997) Generation of putative intrastrand cross-links and strand breaks in DNA by transition metal ion-mediated oxygen radical attack. *Chem. Res. Toxicol.,* **10:** 393–400

Lloyd, DR and Phillips, DH (1999) Oxidative DNA damage mediated by copper(II), iron(II) and nickel(II) Fenton reactions: evidence for site-specific mechanisms in the formation of double-strand breaks, 8-hydroxydeoxyguanosine and putative intrastrand cross-links. *Mutation Research/Fundamental and Molecular Mechanisms of Mutagenesis.* **424(1-2):** 23-36

Loh, E, Dussurget, O, Gripenland, J, Vaitkevicius, K, Tiensuu, T, Mandin, P, Repoila, F, Buchrieser, C, Cossart, P, and Johansson, J (2009) A trans-acting riboswitch controls expression of the virulence regulator PrfA in *Listeria monocytogenes*. *Cell*. **139:** 770-779

Losi, A, Polverini, E, Quest, B, and Gärtner, W (2002) First evidence for phototropin-related blue-light receptors in prokaryotes. *Biophys J*. **82(5):** 2627-2634

Macalady, JL, Hamilton, TL, Grettenberger, CL, Jones, DS, Tsao, LE, and Burgos, WD (2013) Energy, ecology and the distribution of microbial life. *Phil Trans R Soc B*. **368:** 20120383

Macke T, Ecker D, Gutell R, Gautheret D, Case DA and Sampath R. (2001) RNAMotif – A new RNA secondary structure definition and discovery algorithm. *Nucleic Acids Res.* **29**: 4724–4735

Mackie, GA (2013) RNase E: at the interface of bacterial RNA processing and decay. *Nature Reviews Microbiology*. **11:** 45-57

Mank, NN, Berghoff, BA, Hermanns, YN and Klug, G (2012) Regulation of bacterial photosynthesis genes by the small non-coding RNA PcrZ. *Proc Natl Acad Sci U S A*. **109:** 16306–16311

Mank, NN, Berghoff, BA, and Klug, G (2013) A mixed incoherent feed-forward loop contributes to the regulation of bacterial photosynthesis genes. *RNA Biol.* **10(3):** 347-352

Marchesi, E, Rota, C, Fann, YC, Chignell, CF, and Mason, RP (1999) Photoreduction of the fluorescent dye 2'-7'-dichlorofluorescein: a spin trapping and direct electron spin resonance study with implications for oxidative stress measurements. *Free Radic Biol Med*. **26(1-2):** 148-161

Marnett, LJ, Riggins, JN and West, JD (2003) Endogenous generation of reactive oxidants and electrophiles and their reactions with DNA and protein. *J Clin Invest.* **111(5):** 583-593

Mars, RA, Mendonça, K, Denham, EL, and van Dijl, JM (2015) The reduction in small ribosomal subunit abundance in ethanol-stressed cells of Bacillus subtilis is mediated by a SigB-dependent antisense RNA. *Biochim Biophys Acta.* **1853:** 2553-2559.

Martinovich, GG, Cherenkevich, SN and Sauer H (2005) Intracellular redox state: towards quantitative description. *Eur Biophys J.* **34:** 937–942

Masharov, E, Cranford, MR, and Banerjee, R (2000) The Quantitatively Important Relationship between Homocysteine Metabolism and Glutathione Synthesis by the Transsulfuration Pathway and Its Regulation by Redox Changes. *Biochemistry*. **39(42):** 13005–13011

Masip, L, Veeravalli, K and Georgiou, G (2006) The many faces of glutathione in bacteria. *Antioxid Redox Signal.* **8(5-6):** 753-62.

Massé, E, and Gottesman, S (2002) A small RNA regulates the expression of genes involved in iron metabolism in *Escherichia coli*. *Proc Natl Acad Sci USA*. **99:** 4620–4625

Massé, E, Vanderpool, CK, and Gottesman, S (2005) Effect of RyhB small RNA on global iron use in *Escherichia coli*. *J Bacteriol*. **187:** 6962–6971

Masuda, S, and Bauer, CE (2002) AppA is a blue light photoreceptor that antirepresses photosynthesis gene expression in *Rhodobacter sphaeroides*. *Cell*. **110(5):** 613-623

Mao, L, Mackenzie, C, Roh, JH, Eraso, M, Kaplan, S, and Resat, H (2005) Combining microarray and genomic data to predict DNA binding motifs. *Microbiology*. **151(10):** 3197-3213

McEwan, AG (1994): Photosynthetic electron transport and aerobic metabolism in purple non—sulfur photortrophic bacteria. *Antonie Van Leeuwenhoek.* **66:** 151–164

McRee, DE, Tainer, JA, Meyer, TE, Van Beeumen, J, Cusanovich, MA, and Getzoff, ED (1989) Crystallographic structure of a photoreceptor protein at 2.4 A resolution. *Proc Natl Acad Sci U S A*. **86(17):** 6533-6537

Meister, A, and Anderson, ME (1983) Glutathione. *Ann Rev Biochem*. **52:** 711-760

Metz, S, Haberzettl, K, Frühwirth, S, Teich, K, Hasewinkel, C, and Klug, G (2012) Interaction of two photoreceptors in the regulation of bacterial photosynthesis genes. *Nucleic Acids Res*. **40(13):** 5901-5909

Meyer, TE (1985) Isolation and characterization of soluble cytochromes, ferredoxins and other chromophoric proteins from the halophilic phototrophic bacterium Ectothiorhodospira halophila. Biochim Biophys Acta. **806:** 175–183

Miller, JH (1972) Experiments in Molecular Genetics. *Cold Spring Harbor Laboratory Press*.

Miyakoshi, M, Chao, Y, and Vogel, J (2015) Regulatory small RNAs from the 3' regions of bacterial mRNAs. *Curr Opin in Microbiol.* **24:** 132-139

Moskvin, OV, Gomelsky, L, and Gomelsky, M (2005) Transcriptome analysis of the *Rhodobacter sphaeroides* PpsR regulon: PpsR as a master regulator of photosystem development. *J Bacteriol*. **187(6):** 2148-2156

Moskvin, OV, Kaplan, S, Gilles-Gonzalez, MA and Gomelsky, M (2007) Novel heme-based oxygen sensor with a revealing evolutionary history. *J Biol Chem.* **282(39):** 28740-28748

Morgan, JW and Anders, E (1980) Chemical Composition of Earth, Venus and Mercury. *PNAS.* **77(12):** 6973–6977

Mühlhardt, C (2009) Der Experimentator. *Springer Spektrum Verlag*

Müller, KM, Berghoff, BA, Eisenhardt, BD, Remes, B, and Klug, G (2016) Characteristics of Pos19 - A Small Coding RNA in the Oxidative Stress Response of *Rhodobacter sphaeroides. Plos One*. **11(9):** e0163425

Müller, P, Jahn, N, Ring, C, Maiwald, C, Neubert, R, Meißner, C, and Brantl, S (2016) A multistress responsive type I toxin-antitoxin system: bsrE/SR5 from the *B. subtilis* chromosome. *RNA Biol*. **13(5):** 511-523

Nahvi, A, Barrick, JE, and Breaker, RR (2004) Coenzyme B12 riboswitches are widespread genetic control elements in prokaryotes. *Nucleic Acid Res*. **32(1):** 143-150

Newman, JD, Falkowski, MJ, Schilke, BA, Anthony, LC, and Donohue, TJ (1999) The Rhodobacter sphaeroides ECF sigma factor, sigma(E), and the target promoters cycA P3 and rpoE P1. *J Mol Biol*. **294(2):** 307-320

Niwa, S,Yu, LJ, Takeda, K, Hirano, Y, Kawakami, T, Wang-Otomo, ZY and Miki, K (2014) Structure of the LH1–RC complex from *Thermochromatium tepidum* at 3.0 Å. *Nature*. **508:** 228-232

Nuss, AM, Glaeser, J, and Klug, G (2009) $RpoH_{II}$ Activates Oxidative-Stress Defense Systems and Is Controlled by RpoE in the Singlet Oxygen-Dependent Response in *Rhodobacter sphaeroides*. *J Bacteriol*. **191(1):** 220-230

Nuss, AM, Glaeser, J, Berghoff, BA, and Klug, G (2010) Overlapping alternative sigma factor regulons in the response to singlet oxygen in Rhodobacter sphaeroides. *J Bacteriol.* **192(10):** 2613-2623

Nuss, AM, Adnan, F, Weber, L, Berghoff, BA, Glaeser, J, and Klug, G (2013) DegS and RseP homologous proteases are involved in singlet oxygen dependent activation of RpoE in Rhodobacter sphaeroides. *Plos One*. **8(11):** e79520

Oberto, J (2013) SyntTax: a web server linking synteny to prokaryotic taxonomy. *BMC Bioinformatics*. **14:** 4

Oelze, J and Drews, G (1972) Membranes of Photosynthetic Bacteria. *Biochimica et Physica Acta.* **265(2):** 209-239

Oh, JI, and Kaplan, S (1998) The cbb_3 Terminal Oxidase of *Rhodobacter sphaeroides* 2.4.1: Structural and Functional Implications of Spectral Complex Formation. *Biochemistry*. **38:** 2688-2696

Okamura, MY, Paddock, ML, Graige, MS and Feher, G (2000) Proton and electron transfer in bacterial reaction centers. *Biochim Biophys Acta*. **1458:** 148–163.

Olsen, JD, Adams, PG, Jackson, PJ, Dickman, MJ, Qian, P and Hunter, CN (2014) Aberrant Assembly Complexes of the Reaction Center Light-harvesting 1 PufX (RC-LH1-PufX) Core Complex of *Rhodobacter sphaeroides* Imaged by Atomic Force Microscopy. *The Journal of Biological Chemistry*. **289:** 29927-29936

Omotajo, D, Tate, T, Cho, H, and Choudhary, M (2015) Distribution and diversity of ribosome binding sites in prokaryotic genomes. *BMC Genomics*. **16:** 604

Opdyke, JA, Kang, J, and Storz, G (2004) GadY, a Small-RNA Regulator of Acid Response Genes in *Escherichia coli*. *J Bacteriol*. **186(20):** 6698–6705

Outten, FW and Theil, EC (2009): Iron-based Redox Switches in Biology. *Antioxid Redox Signal*. **11(5):** 1029–1046

Paget, MS (2015) Bacterial Sigma Factors and Anti-Sigma Factors: Structure, Function and Distribution. *Biomolecules.* **5(3):** 1245-1265

Pandey, SP, Minesinger, BK, Kumar, J, and Walker, GC (2011) A highly conserved protein of unknown function in Sinorhizobium meliloti affects sRNA regulation similar to Hfq. *Nucleic Acids Res*. **39(11):** 4691-4708

Pandey, SP, Winkler, JA, Li, H, Camacho, DM, Collins, JJ, and Walker, GC (2014) Central role for RNase YbeY in Hfq-dependent and Hfq-independent small-RNA regulation in bacteria. *BMC Genomics*. **15:** 121

Papenfort, K, and Vogel, J (2009) Multiple target regulation by small noncoding RNAs rewires gene expression at the post-transcriptional level. *Research in Microbiology*. **160(4):** 278–287

Papenfort, K, Pfeiffer, V, Mika, F, Lucchini, F , Hinton, JC and Vogel, J (2006) sigma(E)-dependent small RNAs of *Salmonella* respond to membrane stress by accelerating global *omp* mRNA decay. *Mol Microbiol.* **62:** 1674-1688

Park, S, and Imlay, JA (2003) High levels of intracellular cysteine promote oxidative DNA damage by driving the fenton reaction. *J Bacteriol*. **185(6):** 1942-1950.

Parkinson, JS, and Kofoid, EC (1992) Communication modules in bacterial signalling proteins. *Annu Rev Genet*. **26:** 71-112

Pattison, DI, Rahmanto, AS, and Davies, MJ (2011) Photo-oxidation of proteins. *Photochem Photobiol Sci*. **11(1):** 38-53

Peng, T, Berghoff, BA, Oh, JI, Weber, L, Schirmer, J, Schwarz, J, Glaeser, J, and Klug, G (2016) Regulation of a polyamine transporter by the conserved 3' UTR-derived sRNA SorX confers resistance to singlet oxygen and organic hydroperoxides in *Rhodobacter sphaeroides*. *RNA Biol*. **13(10):** 988-999

Pérez-Marín, MC, Padmanabhan, S, Polanco, MC, Murillo, FJ, and Elías-Arnanz, M (2008) Vitamin B12 partners the CarH repressor to downregulate a photoinducible promoter in *Myxococcus xanthus*. *Mol Microbiol*. **67(4):** 804-819

Persson, F, Lindén, M, Unoson, C, and Elf, J (2013) Extracting intracellular diffusive states and transition rates from single-molecule tracking data. *Nat Methods*. **10(3):** 265-269

Peuser, V, Metz, S, and Klug, G (2011) Response of the photosynthetic bacterium *Rhodobacter sphaeroides* to iron limitation and the role of a Fur orthologue in this response. *Environ Microbiol Rep*. **3(3):** 397-404

Peuser, V, Remes, B, and Klug, G (2012) Role of the Irr protein in the regulation of iron metabolism in Rhodobacter sphaeroides. *Plos One*. **7(8):** e42231.

Pfaffl, MW (2001) A new mathematical model for relative quantification in real-time RT-PCR. *Nucleic Acids Res.* **29(9):** e45

Poljsak, B, Milisav, I, Lampe, T, and Ostan, I (2011) Reproductive benefit of oxidative damage: an oxidative stress "malevolence"? *Oxid Med Cell Longev*. **2011**: 760978

Ponnampalam, SN, Buggy, JJ and Bauer, CE (1995) Characterization of an aerobic repressor that coordinately regulates bacteriochlorophyll, carotenoid, and light harvesting-II expression in *Rhodobacter capsulatus*. *J Bacteriol.* **177(11):** 2990-29997

Ponnampalam, SN, and Bauer, CE (1997) DNA binding characteristics of CrtJ. A redox-responding repressor of bacteriochlorophyll, carotenoid, and light harvesting-II gene expression in *Rhodobacter capsulatus. J Biol Chem.* **272:** 18391–18396

Qian, P, Bullough, P and Hunter, CN (2008) Three-dimensional reconstruction of a membrane-bending complex. *J Biol Chem*. **283:** 14002-14011

Qian, P, Papiz, MZ, Jackson, PJ, Brindley, AA, Ng, IW, Olsen, JD, Dickman, MJ, Bullough, PA, and Hunter, CN (2013) Three-dimensional structure of the *Rhodobacter sphaeroides* RC-LH1-PufX complex: dimerization and quinone channels promoted by PufX. *Biochemistry*. **52(43):** 7575-7585

Randerath, K, Randerath, E, Smith, CV and Chiang, J (1996) Structural origins of bulky oxidative DNA adducts (type II I-compounds) as deduced by oxidation of oligonucleotides of known sequence. *Chem. Res. Toxicol.,* **9**: 247–254

Ratcliffe, EC, Tunnicliffe, RB, Ng, IW, Adams, PG, Qian, P, Holden-Dye, K, Jones, MR, Williamson, MP, and Hunter, CN (2011) Experimental evidence that the membrane-spanning helix of PufX adopts a bent conformation that facilitates dimerisation of the Rhodobacter sphaeroides RC-LH1 complex through N-terminal interactions. *Biochim Biophys Acta*. **1807:** 95-107

Rauhut, R, and Klug, G (1999) mRNA degradation in bacteria. *FEMS Microbiol Rev*. **23(3):** 353-370

Remes, B, Eisenhardt, BD, Srinivasan, V, and Klug, G (2015) IscR of *Rhodobacter sphaeroides* functions as repressor of genes for iron-sulfur metabolism and represents a new type of iron-sulfur-binding protein. *Microbiologyopen*. **4(5):** 790-802

Reisfeld, RA, Lewis, UJ, and Williams, DE (1962) Disc electrophoresis of basic proteins and peptides on polyacrylamide gels. *Nature*. **195(4838):** 281-283

Rhee, SG (1999) Redox signaling: hydrogen peroxide as intracellular messenger. *Experimental and Molecular Medicine,* **31(2):** 53–59

Rische-Grahl, T, Weber, L, Remes, B, Förstner, KU, and Klug, G (2014) RNase J is required for processing of a small number of RNAs in *Rhodobacter sphaeroides*. *RNA Biol*. **11(7):** 855–864

Roeder, B (1990) Tetrapyrroles: A chemical class of potent photosensitizers for the photodynamic treatment of tumours. *Lasers in Medical Science.* **5(2):** 99-106

Roh, JH, Smith, WE, and Kaplan, S (2004) Effects of oxygen and light intensity on transcriptome expression in *Rhodobacter sphaeroides* 2.4.1. Redox active gene expression profile. *J Biol Chem.* **279(10):** 9146-9155

Roszak, AW, Howard, TD, Southall, J, Gardiner, AT, Law, CJ, Isaacs, NW and Cogdell, RJ (2003) Crystal structure of the RC–LH1 core complex from *Rhodopseudomonas palustris*. *Science*. **302:** 1969-1972

Rui, B, Shen, T, Zhou, H, Liu, J, Chen, J, Pan, X, Liu, H, Wu, J, Zheng, H, and Shi, Y (2010) A systematic investigation of *Escherichia coli* central carbon metabolism in response to superoxide stress. *BMC Syst Biol*. **4:** 122

Sagawa, S, Shin, JE, Hussein, R, and Lim, HM (2015) Paradoxical suppression of small RNA actvivity at high Hfq concentrations due to random-order binding. *Nucleic Acids Res*. **43:** 8502-8515

Sasakura, Y, Hirata, S, Sugiyama, S, Suzuki, S, Taguchi, S, Watanabe, M, Matsui, T, Sagami, I, and Shimizu, T (2002) Characterization of a direct oxygen sensor heme protein from *Escherichia coli.* Effects of the heme redox states and mutations at the heme-binding site on catalysis and structure. *J Biol Chem*. **277(26):** 23821-23827

Schägger, H, Link, TA, Engel, WD and von Jagow, G (1986) in *Methods of Enzymology*. **126:** 224-237

Schägger, H and von Jagow, G (1987) Tricine–sodium dodecyl sulfate polyacrylamide gel electrophoresis for the separation of proteins in the range from 1–100 kDalton. *Anal. Biochem*. **166:** 368-379

Schägger, H (2006) Tricine-SDS-PAGE. *Nature Portocols*. **1(1):** 16-23

Scherrer, K, and Darnell, JE (1962) Sedimentation characteristics of rapidly labelled RNA from HeLa cells. *Biochem Biophys Res Commun*. **7:** 486-490

Scheuring, S, Seguin, J, Marco, S, Lévy, D, Robert, B and Rigaud, JL (2003) Nanodissection and high-resolution imaging of the *Rhodopseudomonas viridis* photosynthetic core complex in native membranes by AFM. *PNAS*. **100:** 1690–1693

Scheuring, S (2006) AFM studies of the supramolecular assembly of bacterial photosynthetic core-complexes. *Current Opinion in Chemical Biology*. **10(5):** 387-393

Schilke, BA, and Donohue, TJ (1995) ChrR positively regulates transcription of the *Rhodobacter sphaeroides* cytochrome c2 gene*. J Bacteriol*. **177(8):** 1929-1937

Schmidt, M, Zheng, P, and Delihas, N (1995) Secondary structures of *Escherichia coli* antisense *micF* RNA, the 5'-end of the target ompF mRNA, and the RNA/RNA duplex. *Biochemistry*. **34:** 3621–3631

Schöneich, C (2005) Methionine oxidation by reactive oxygen species: reaction mechanisms and relevance to Alzheimer's disease. *Biochim Biophys Acta*. **1703(2):** 111-119

Seaver, LC, and Imlay, JA (2001) Hydrogen peroxide fluxes and compartmentalization inside growing Escherichia coli. *J Bacteriol*. **183(24):** 7182-7189

Seaver, LC and Imlay, JA (2004) Are respiratory enzymes the primary sources of intracellular hydrogen peroxide? *J Biol Chem.* **279(47):** 48742-50

Serganov, A, and Nudler, E (2013) A decade of riboswitches. *Cell*. **152:** 17–24

Sharma, CM, and Vogel, J (2009) Experimental approaches for the discovery and characterization of regulatory small RNA. *Curr Opin Microbiol*. **12(5):** 536-546

Shimoni, Y, Friedlander, G, Hetzroni, G, Niv, G, Altuvia, S, Biham, O, and Margalit, H (2007) Regulation of gene expression by small non-coding RNAs: a quantative view. *Mol Syst Biol*. **3:** 138

Shpakov, AO and Pertseva, MN (2008) Signal transduction in prokaryotes. *Journal of Evolutionary Biochemistry and Physiology* **44**:129-150

Silvaggi, JM, Perkins, JB, and Losick, R (2005) Small Untranslated RNA Antitoxin in *Bacillus subtilis*. *J Bacteriol.* **187(19):** 6641–6650

Simon, LD, Randolph, B, Irwin, N, and Binkowski, G (1983) Stabilization of proteins by a bacteriophage T4 gene cloned in *Escherichia coli*. *Proc Natl Acad Sci USA*. **80(7):** 2059-2062

Smart, JL, and Bauer, CE (2006) Tetrapyrrole Biosynthesis in *Rhodobacter capsulatus* Is Transcriptionally Regulated by the Heme-Binding Regulatory Protein, HbrL. *J Bacteriol*. **188(4):** 1567-1576

Sobrero, P, and Valverde, C (2012) The bacterial protein Hfq: much more than a mere RNA-binding factor. *Crit Rev Microbiol*. **38(4):** 276-299

Solovyev, V, and Salamov, A (2011) Automatic Annotation of Microbial Genomes and Metagenomic Sequences. *Metagenomics and its Applications in Agriculture, Biomedicine and Environmental Studies*, Nova Science Publishers. p. 61-78

Sousa, SA, Ramos, CG, Moreira, LM, and Leitão, JH (2010) The *hfq* gene is required for stress resistance and full virulence of *Burkholderia cepacia* to the nematode *Caenorhabditis elegans*. *Microbiology*. **156:** 896-908

Sprenger, WW, Hoff, WD, Armitage, JP, and Hellingwerf, KJ (1993) *J Bacteriol*. **175:** 3096

Storz, G, Vogel, J, and Wassarman, KM (2011) Regulation by Small RNAs in Bacteria: Expanding Frontiers. *Mol Cell*. **43(6):** 880–891

Straight, R and Spikes, J (1985) Photosensitized oxidation of biomolecules.In: Frimer, A., ed. *Singlet O_2: volume 4: polymers and biomolecules*. Boca Raton, FL: CRC Press. **1985:** 91–143

Stougaard, P, Molin, S, and Nordström, K (1981) RNAs involved in copy-number control and incompatibility of plasmid R1. *Proc Natl Acad Sci USA*. **78:** 6008–6012

Swartz, TE, Tseng, T, Frederickson, MA, Paris, G, Comerci, DJ, Rajashekara, G, Kim, J, Mudgett, MB, Splitter, GA, Ugalde, RA, Goldbaum, FA, Briggs, WR and Bogomolni, RA (2007) Blue-Light-Activated Histidine Kinases: Two-Component Sensors in Bacteria. *Science*. **317(5841):** 1090-1093

Swem, LR, Kraft, BJ, Swem, DL, Setterdahl, AT, Masuda, S, Knaff, DB, Zaleski, JM, and Bauer, CE (2003) Signal transduction by the global regulator RegB is mediated by a redox-active cysteine. *EMBO J*. **22(18):** 4699-4708

Tabita, FR (1995) The biochemistry and metabolic regulation of carbon metabolism and CO_2 fixation in purple bacteria. *The Purple Phototrophic Bacteria*. **28:** 885–914

Toledano, MB, Kullik, I, Trinh, F, Baird, PT, Schneider, TD and Storz, G (1994) Redox-dependent shift of OxyR-DNA contacts along an extended DNA-binding site: a mechanism for differential promoter selection. *Cell.* **78(5):**897-909

Toledo-Arana, A, Repoila, F, and Cossart, P (2007) Small non-coding RNAs controlling pathogenesis. *Current Opinion in Microbiology*. **10:** 182–188

Tomizawa J, Itoh, T, Selzer, G, and Som, T (1981) Inhibition of ColE1 RNA primer formation by a plasmidspecified small RNA. *Proc Natl Acad Sci USA*. **78:** 1421-1415

Torres-Quesada, O, Reinkensmeier, J, Schlüter, JP , Robledo, M, Peregrina, A, Giegerich, R, Toro, N, Becker, A, and Jiménez-Zurdo, JI (2014) Genome-wide profiling of Hfq-binding RNAs uncovers extensive post-transcriptional rewiring of major stress response and symbiotic regulons in *Sinorhizobium meliloti*. *RNA Biol*. **11(5):** 563–579

Trotochaud, AE, and Wassarman, KM (2005) A highly conserved 6S RNA structure is required for regulation of transcription. *Nat Struct Mol Biol*. **12(4):** 313-319

Tuckerman, JR, Gonzalez, G and Gilles-Gonzalez, MA (2001) Complexation precedes phosphorylation for two-component regulatory system FixL/FixJ of *Sinorhizobium meliloti*. *Journal of Molecular Biology.* **308(3):** 449-455

Tsai, C,Liao, R, Chou, B, Palumbo, M, and Contreras, LM (2015) Genome-Wide Analyses in Bacteria Show Small-RNA Enrichment for Long and Conserved Intergenic Regions*. J Bacteriol*. **197(1):** 40–50

Tsukatani, Y, Matsuura, K, Masuda, S, Shimada, K, Hiraishi, A and Nagashima, KVP (2004) Phylogenetic distribution of unusual triheme to tetraheme cytochrome subunit in the reaction center complex of purple photosynthetic bacteria. *Photosynth. Res.* **79:** 83–91

Updegrove, TB, Zhang, A, and Storz, G (2016) Hfq: the flexible RNA matchmaker. *Curr Opin Microbiol*. **30:** 133-138

Vakulskas, CA, Leng, Y, Abe, H, Amaki, T, Okayama, A, Babitzke, P, Suzuki, K, and Romeo, T (2016) Antagonistic control of the turnover pathway for the global regulatory sRNA CsrB by the CsrA and CsrD proteins. *Nucleic Acids Res*. **44(16):** 7896-7910

Van Assche, E, Van Puyvelde, S, Vanderleyden J and Steenackers ,HP (2015) RNA-binding proteins involved in post-transcriptional regulation in bacteria. *Front Microbiol* eCollection 2015: doi: 10.3389/fmicb.2015.00141

Vanderpool, CK, Balasubramanian, D, and Lloyd, CR (2011) Dual-function RNA regulators in bacteria. *Biochimie*. **93(11):** 1943-1949

van Niel, CB (1944) The culture, general physiology, morphology, and classification of the non-sulfur purple and brown bacteria. *Bacteriol Rev*. **8:** 1-118

Vasilyeva, L, Miyake, M, Khatipov, E, Wakayama, T, Sekine, M, Hara, M, Nakada, E, Asada, Y, and Miyake, J (1999) Enhanced hydrogen production by a mutant of *Rhodobacter sphaeroides* having an altered light-harvesting system. *J Biosci Bioeng*. **87(5):** 619-624

Vermeulen, AJ, and Bauer, CE (2015) Members Of The PpaA/AerR Antirepressor Family Bind Cobalamin. *J Bacteriol.* doi: 10.1128/JB.00374-15

Vieira, J, and Messing, J (1982) The pUC plasmids, an M13mp7-derived system for insertion mutagenesis and sequencing with synthetic universal primers. *Gene.* **19(3):** 259-268

Vitreschak, AG, Rodionov, DA, Mironov, AA, and Gelfand, MS (2003) Regulation of the vitamin B12 metabolism and transport in bacteria by a conserved RNA structural element. *RNA*. **9(9):** 1084-1097

Vogel, J, and Luisi, BF (2011) Hfq and its constellation of RNA. *Nat Rev Microbiol*. **9(8):** 578-589

Wadler, CS, and Vanderpool, CK (2007) A dual function for a bacterial small RNA: SgrS performs base pairing-dependent regulation and encodes a functional polypeptide. *Proc Natl Acad Sci USA*. **104(51):** 20454-20459

Wagner,EG, and Unoson, C (2012) The toxin-antitoxin system *tisB-istR1*: Expression, regulation, and biological role in persister phenotypes. *RNA Biol*. **9(12):** 1513-1519

Wagner, EG, and Romby, P (2015) Small RNAs in bacteria and archaea: who they are, what they do, and how they do it. *Adv Genet*. **90:** 133-208

Wassarman, KM (2007) 6S RNA: a regulator of transcription. *Mol Microbiol*. **65(6):** 1425-1431

Wassarman, KM, Repoila, F, Rosenow, C, Storz, G and Gottesman, S (2016) Identification of novel small RNAs using comparative genomics and microarrays. *Genes and Development.* **15:** 1637–16

Waters, LS, and Storz, G (2009) Regulatory RNAs in bacteria. *Cell*. **136(4):** 615-628

Wilusz, Cj, and Wilusz, J (2005) Eukaryotic Lsm proteins: lessons from bacteria. *Nature Structural and Molecular Biology.* **12:** 1031 - 1036

Winkler, WC, Nahvi, A,Roth, A, Collins, JA, and Breaker, RR (2004) Control of gene expression by a natural metabolite-responsive ribozyme. *Nature*. **428:** 281-286

Wright, PR, Georg, J, Mann, M, Sorescu, DA, Richter, AS, Lott, S, Kleinkauf, R, Hess, WR, and Backofen, R (2014) CopraRNA and IntaRNA: predicting small RNA targets, networks and interaction domains. *Nucl Acids Res*. **42(W1):** W119-W123

Yanisch-Perron, C, Vieira, C, and Messing, J (1985) Improved M13 phage cloning vectors and host strains: nucleotide sequences of the M13mp18 and pUC19 vectors. *Gene*. **33:** 103-19

Yeh, K, Wu, S, Murphy, JT and Lagarias, JC (1997): A Cyanobacterial Phytochrome Two-Component Light Sensory System. *Science*. **277(5331):** 1505-1508

Yin, L, Dragnea, V, and Bauer, CE (2012) PpsR, a regulator of heme and bacteriochlorophyll biosynthesis, is a heme-sensing protein. *J Biol Chem*. **287(17):** 13850-13858

Yin, L, Dragnea, V, Feldman, G, Hammad, LA, Karty, JA, Dann, CE, and Bauer, CE (2013) Redox and Light Control the Heme-Sensing Activity of AppA. *mBio*. **4(5):** e00563-13

Yin, L, and Bauer, CE (2013) Controlling the delicate balance of tetrapyrrole biosynthesis. *Phil Trans R Soc B*. **368:** 20120262

Youvan, DC, Bylina, EJ, Alberti, M, Begusch, H and Hearst, JE (1984) Nucleotide and deduced polypeptide sequences of the photosynthetic reaction center, B870 antenna, and flanking polypeptides from *R. capsulata*. *Cell*. **37:** 949-957

Zappa, S, Li, K, and Bauer, CE (2010) The tetrapyrrole biosynthetic pathway and its regulation in *Rhodobacter capsulatus*. *Adv Exp Med Biol.* **675:** 229–250

Zeilstra-Ryalls, JH, and Kaplan, S (1995) Aerobic and anaerobic regulation in *Rhodobacter sphaeroides* 2.4.1: the role of the fnrL gene. *J Bacteriol*.**177(22):** 6422-6431

Zeilstra-Ryalls, J, Gomelsky, M, Eraso, J, Yeliseev, A, O'Gara, J, and Kaplan, S (1998) Control of photosystem formation in *Rhodobacter sphaeroides*. *J Bacteriol.* **180:** 2801–2809

Zepp, RG, Wolfe, NL, Baughman, GL, and Hollis, RC (1977) Singlet oxygen in natural waters. *Nature*. **267:** 421–423

Zhart, TC and Deretic, V (2002) Reactive Nitrogen and Oxygen Intermediates and Bacterial Defense: Unusual Adaptations in Mycobacterium tuberculosis. *Antioxidants and Redox Signaling*. **4(1):** 141-159

Zheng, M, Aslund, F, and Storz, G (1998) Activation of the OxyR transcription factor by reversible disulfide bond formation. *Science*. **279(5357):** 1718-1721

Zheng, M, and Storz, G (2000) Redox sensing by prokaryotic transcription factors. *Biochemical Pharmacology*. **59(1):** 1-6

Degree theses:

Yannick Hermanns (2014) Die Auswirkung von Umwelteinflüssen auf die mRNA Stabilitäten in Rhodobacter sphaeroides. Globale Untersuchungen der mRNA Halbwertszeiten unter aeroben, microaeroben und phototrophen Wachstumsbedingungen. JLU Gießen

Janis Kiebel (2013) Funktionsanalyse der sRNA RSs0827 im Eisenstoffwechsel von *Rhodobacter sphaeroides*. JLU Gießen

Markus Späth (2014) Analysis of RSs0827 - a small RNA in *Rhodobacter sphaeroides* with an unknown function. JLU Gießen

Sabine Martini (2015) The Role of Small Noncoding RNA RSs0827 in Iron Dependent Gene Regulation in *Rhodobacter sphaeroides*. JLU Gießen / University of Apllied Science Bonn-Rhein-Sieg

Daniel Scheller (2016) Analyse einer kleinen RNA in Rhodobacter sphaeroides. JLU Gießen

Websources:

Oleinick, NL (2011) Basic Photosensitization. Photobiology.info/Oleinick.html

Own publications and scientific contributions:

Damm, K, Bach, S, **Müller, KM**, Klug, G, Burenina, OY, Kubareva, EA, Grünweller, A, and Hartmann, RK (2015) Improved Northern blot detection of small RNAs using EDC crosslinking and DNA/LNA probes. *Methods Mol Biol*. **1296:** 41-51

Damm, K, Bach, S, **Müller, KM**, Klug, G, Burenina, OY, Kubareva, EA, Grünweller, A, and Hartmann, RK (2015) Impact of RNA isolation protocols on RNA detection by Northern blotting. *Methods Mol Biol.* **1296:** 29-38

Müller, KM, Berghoff, BA, Eisenhardt, BD, Remes, B, and Klug, G (2016) Characteristics of Pos19 – a Small Coding RNA in the Oxidative Stress Response of *Rhodobacter sphaeroides*. *Plos One*. **11(9):** e0163425

Fine-tuning of sulfur metabolism by a dual-function RNA upon singlet oxygen stress in *Rhodobacter sphaeroides.* International Meeting on Sensory and regulatory RNAs in prokaryotes Würzburg, 2013 - Poster

Fine-tuning of sulfur metabolism by a dual-function RNA upon singlet oxygen stress in *Rhodobacter sphaeroides*. Meeting on Sensory and regulatory RNAs in prokaryotes Jena, 2014 –Talk

Fine-tuning of sulfur metabolism and glutathione levels by a small RNA upon singlet oxygen stress in *Rhodobacter sphaeroides*. VAAM Annual Meeting Dresden, 2014 - Poster

A small coding RNA regulates glutathione homeostasis upon singlet oxygen stress in *Rhodobacter sphaeroides*. VAAM Annual Meeting Marburg, 2015 – Poster

A small RNA involved in regulation of bacterial photosynthesis genes. Meeting on Sensory and regulatory RNAs in prokaryotes Braunschweig, 2015 – Talk

A small RNA involved in regulation of bacterial photosynthesis genes. VAAM Annual Meeting Jena, 2016 – Poster

Supplement

(**Supp. 1**) The microarray data employed in this work have been published (Müller *et al*., 2016) and have been deposited in NCBI's Gene Expression Omnibus, they are accessible through GEO Series accession number **GSE59046**.

(**Supp. 2**) pLO1 protocol

Construction of a deletion (insertion) mutant of *Rhodobacter sphaeroides* using pLO1 suicide vector

1. Clone the DNA fragment, which is designed to construct a mutant strain of *R. sphaeroides*, into the suicide vector pLO1 (the DNA fragment which is to clone must have more than 200 bp on both sides of the deletion site to guarantee the efficient homologous recombination).

2. Introduce the constructed suicide plasmid into *R. sphaeroides* by conjugation

3. Transconjugants (single crossover strains) are selected for Km resistance

4. The colonies of the single crossover strains are restreaked on the RÄ-agar plates containing Km to purify the strains.

5. RÄ liquid medium without Km is inoculated with the purified single crossover strain, and the strain is cultured to OD_{660} of 0.4-0.5.

6. 10-, 20-, 30- µl of the liquid culture of the single crossover strain is spread onto RÄ medium (agar Platten) containing 10% (w/v) sucrose (preparation see below)

7. The double crossover strains are selected for sucrose resistance.

8. Pick both small and large colonies of the double crossover strains and restreak them on RÄ medium (with 10% sucrose) to purify the strain.

9. The deletion of the target gene is verified by means of PCR or Nouthern blotting analysis.

Preparation of the solid RÄ plates containing 10% sucrose

1. Prepare 100 ml of 2X RÄ-agar solution containing the double concentration of RÄ components and agar and autoclave it.

2. Add 4 ml of phosphate solution and 1.6 ml of vitamin solution for RÄ to 2X RÄ-agar solution (das sind auch jeweils doppelte Mengen)

3. Keep the 2X RÄ-agar medium in the water bath at 60-65°C to prevent solidification of the medium.

4. Prepare 100 ml of 20% sucrose solution in water and warm it to 60-65°C in the water bath, which faciliates the filtration of the viscous sucrose solution.

5. Filter the warmed 20% sucrose solution using a syringe filter (0.4 µm) to sterilize the solution

6. Mix 100 ml of 20% sucrose solution with 100 ml of 2X-agar medium to make 10% sucrose RÄ-agar medium.

7. Pour the mixed medium into the plates

Danksagung

Mein besonderer Dank gilt Prof. Dr. Gabriele Klug, für die stete Unterstüzung und ihr Vertrauen, aber besonders für ihre Hilfsbereitschaft und den wissenschaftlichen *input*.

Danke, an Prof. Dr. Roland Hartmann für die Begutachtung meiner Arbeit und die Betreuung im IRTG. Und vielen Dank an PD Dr. Elena Evguenieva-Hackenberg und Prof. Dr. Katja Becker für die Teilnahme an meiner Prüfungskomission.

Dankbar bin ich vor allem allen Kollegen und Studenten die mich in den letzten Jahren praktisch, theoretisch und freundschaftlich begleitet haben.

Und zu guter Letzt, DANKE an meine ganze Familie – besonders an Benni, Mama, Papa, Julia, Stefan, Marius, Carolina und Lea – dafür, dass ihr immer für mich da wart. Ich liebe euch.